A Failure Analysis of Small-Diameter Cast Iron Pipes in Reactive Soil Zones of Melbourne

By

Darshana Rasika Weerasinghe

BSc.Eng (Civil)

A thesis submitted for the degree of Doctor of Philosophy at Monash University in 2018

Department of Civil Engineering

Monash University

Australia

COPYRIGHT NOTICE

To My Late Parents

ABSTRACT

The work presented in this thesis started in May 2014 as part of the Smart Water Fund project: An Innovative Integrated Algorithm for Cost-Effective Management of Water Pipe Networks. The aim of the overall project was to develop integrated algorithms and modules using a Global Information System (GIS) framework to assist the scoping and timing of the replacement and rehabilitation of small- (reticulation) and large-diameter (critical) water pipes. Among these modules, the development of a reactive soil module to incorporate the influence of climate-induced reactive soil on buried pipes was achieved, and this is the subject of this thesis.

The effect of seasonal climate-induced reactive ground movements has been recognised as a severe problem for small-diameter (less than 300mm), old and brittle (especially cast iron) pipes that are buried in reactive soil zones in Melbourne. It has been established that most small-diameter pipes fail by circumferential cracks (broken back) due to bending stresses caused by ground movement. Apart from observations, measurements and data analyses, a comprehensive pipe failure analysis has not been carried out previously in relation to this problem. Therefore, the present work was started with the objectives of developing a GIS-applicable engineering methodology to estimate reactive ground movement-induced longitudinal pipe stresses for pipe failure analysis.

In this study, the finite element method was initially used to study the seasonal behaviour of buried pipes in reactive soil environments under drying and wetting conditions, and the pipe bending patterns and pipe failure mechanisms at critical locations such as driveways, elevated bedrocks, trees, soil boundaries and locally wet areas. A small-diameter pipe failure case study was carried out to find field evidence to verify the theoretical explanations of the pipe failure mechanisms at critical locations (stress hotspots). The all the knowledge gathered from these studies was then combined to develop a set of analytical equations to estimate pipe-bending stresses for different soil moisture changes and different conditions. Finally, the

applicability of these simplified equations was verified by comparing the results with past pipe failures in different regions.

The methodology used for the finite element modelling of reactive soil and pipe deformation produced reasonable results that were then compared with available field pipe deformation data. Three-dimensional simulations of moisture-governed reactive soil-pipe interactions showed critical stress accumulations at different parts of the pipe at different hotspot locations and explained the seasonal variations of pipe failure. These estimated failure mechanisms were reasonably consistent with the field observations of broken back failures at driveways, roads, trees and possible water leaks. The analytical equations for pipe stress estimation showed that the maximum bending stresses are in the range of 20 to 30 MPa. After incorporating corrosion effects, this analytical model was completed for further applications in GIS.

DECLARATION

I hereby declare that this thesis contains no material which has been accepted for the award of any other degree or diploma at any university or equivalent institution and that, to the best of my knowledge and belief, this thesis contains no material previously published or written by another person, except where due reference is made in the text of the thesis.

Signature: [redacted]..

Name: Darshana Rasika Weerasinghe

Date: 01/03/2018

PUBLICATIONS DURING ENROLMENT

- WEERASINGHE, D., KODIKARA, J. & BUI, H. 2015. Impact of Seasonal Swell/Shrink Behavior of Soil on Buried Water Pipe Failures. *In:* KULATHILAKA, A., SENANAYAKE, K., RATHNAWEERA, P., NAWAGAMUWA, U., FOWZE, J. S. M., PRIYANKARA, N. & DE SILVA, N., eds. Proceedings of the International Conference on Geotechnical Engineering ICGE-Colombo-2015, 10-11 August 2015 Colombo, Sri Lanaka. Sri Lankan Geotechnical Society,pp. 101-104.

- WEERASINGHE, D., KODIKARA, J. & BUI, H. 2016. Numerical modelling of swelling/shrinkage behaviour of unsaturated soils for buried pipe stress analysis. *In:* CHEN, Z., WEI, C., SUN, D. A. & XU, Y., eds. Unsaturated Soil Mechanics - from Theory to Practice: Proceedings of the 6th Asia Pacific Conference on Unsaturated Soils- 2015, Guilin , China. CRC Press/Balkema,pp. 615-620.

- WEERASINGHE, D., ANDERSON, M., KODIKARA, J. & BUI, H. 2016. The Effect of Basalt Rock Profile in Reactive Soil Zones in Melbourne on Pipe Failures in summer. Ozwater'16, 10-12 May 2016 Melbourne, Australia.

- WEERASINGHE, D., KODIKARA, J. & BUI, H. 2017. A study of reactive soil influence on small diameter pipe failures in Melbourne. AGS VIC Symposium 2017: Reactive Clays and Light Structures, 25 October 2017 Melbourne, Australia.

- JIANG, R., WEERASINGHE, D., ZHANG, C., ZHAO, X. L., KODIKARA, J. & HUTCHINSON, C. R. 2017. Leak-before-break (LBB) analysis and failure processes for small-diameter cast iron pipes. *In:* HEIDARPOUR, A. & ZHAO, X.-L., eds. Tubular Structures XVI: Proceedings of the 16th International Symposium on Tubular Structures, 4-6 December 2017 Melbourne, Australia. CRC Press/Balkema,pp. 625-630.

- WEERASINGHE, D., KODIKARA, J. & BUI, H. Use of finite element modelling for estimating reactive soil induced stresses in small diameter pipes (Journal paper, *in-preparation*).

- WEERASINGHE, D., KODIKARA, J. & BUI, H. Critical stress hotspots for circumferential (broken-back) failure analyses of small diameter cast iron water pipes in Melbourne: Finite element analyses and field observations (Journal paper, *in-preparation*).

- WEERASINGHE, D., KODIKARA, J. & BUI, H. A simple analytical model to estimate bending stress in small diameter cast iron pipes in reactive soil zones (Journal paper, *in-preparation*).

ACKNOWLEDGEMENTS

I would first like to express my sincere gratitude and thankfulness to my main supervisor, Professor Jayantha Kodikara, for his outstanding guidance and support throughout the past four years. His encouraging advice, feedback, motivation and immense knowledge and experience in this research area provided me with great insights into my research and kept me on the right track to achieve my goals. I would also like to acknowledge my second supervisor, Dr. Ha Bui, for his regular feedback to improve my research progress. I would like to extend my further thanks to research assistants Dr. Derek Chan, Dr. Ben Shannon, Dr. Gift Dumedah, Dr. Ivan Zhang, Dr. Ravin Deo, Dr. Suranji Rathnayake and Dr. Jian Ji, who offered their friendly support for my fieldwork, laboratory experiments and computer analyses. Dr. Alex McKnight assisted by proofreading the final draft for grammatical and stylistic errors.

I would like to heartily remember my late parents who brought me up, educated me, and showed me the way to reach this height of my life. I believe their blessings from heaven gave me the strength and courage to come through all the hard times during the past few years. I would also like to thank my loving sister for supporting me in many situations during my research. Many thanks to my all high school and university teachers for teaching and guiding me towards higher studies.

This research was funded by the Smart Water Fund Project: an innovative integrated algorithm for cost-effective management of water pipe networks. I would like to express my sincere gratefulness to all partners: Melbourne Water, City West Water, South East Water and Yarra Valley Water, for their financial support. Without these highly supportive partners, this research could not have been accomplished. I would like to express my special gratitude to the asset management team members of City West Water; Nishanthie Ratnayaka, Michael Velasquez and Jason Kennett, for supporting and facilitating my field studies.

I would also like to acknowledge the support from all the academic, research, administration and laboratory staff members of the Department of Civil Engineering, Monash University during my research period. Also, I extend my thanks to all my fellow PhD students and office-mates for sharing a memorable and joyful time and making the past four years unforgettable. It was a great experience for me to work with all these brilliant people.

Finally, but no less importantly, I would like to express my heartiest thankfulness to all my friends who have supported, motivated, encouraged, and cheered me up and been with me as a family during the past few years. I could not imagine a better four years without their love, care and companionship. Thank you for the awesome time!

NOTATIONS

b	Circumferential width of the corrosion patch
C_s	Intersection of the steady-state corrosion line with the pit depth axis
D	Pipe diameter (internal)
d	Depth of the corrosion patch
d_{eff}	Effective depth of the corrosion patch
d_{pipe}	Pipe depth
d_{rock}	Rock depth
E	Young's modulus of the pipe material
e	Void ratio
e_0	Initial void ratio
e_d	Edge distance of slab mounds on reactive grounds
e_N	Natural logarithm
e_w	Moisture ratio
f	Corrosion patch size factor
G_s	Specific gravity of the soil
H_s	Suction change depth (reactive depth)
h	Thickness of the soil layer
I	Second moment of the area of pipe section
I_{pt}	Instability index
I_{ss}	Shrink-swell index
I_{θ_v}	Soil strain index

i	Characteristic length of the differential ground movement curvature
K	Soil subgrade modulus
M_G	Flexible pipe bending moment
$M_{G,max}$	Maximum flexible pipe bending moment
M_{norm}	Bending moment normalising factor
M_P	Pipe bending moment
$M_{p,max}$	Maximum pipe bending moment
$M_{s,a}$	Mass of the soil sample in air
$M_{s,a0}$	Initial mass of the soil sample in air
$M_{s,dry}$	Dry mass of the soil sample
$M_{s,w}$	Mass of the soil sample in water
P_w	Water pressure in pipe
p	Net stress
$p_{equivalent}$	Equivalent all round pressure
$p_{equivalent,0}$	Initial equivalent all round pressure
q	External loads on the pipe
r_s	Steady-state (long-term) corrosion rate
S_{max}	Maximum differential soil moment
S_r	Degree of saturation
$S_{reduced}$	Reduced tensile strength of due to corrosion
$S_{tensile,CI}$	Tensile strength of cast iron
S_v	Free vertical soil movement
s	Soil suction

T_{years} Exposure time (age) of the pipe

t Pipe wall thickness

u_a Pore air pressure

u_w Pore water pressure

V_s Volume of the soil sample

v Vertical pipe movement

w Gravimetric moisture content

w_0 Initial gravimetric moisture content

x Distance along the pipe

x_0 Mean ordinate of the bending curvature

y_m Differential movements of slab mounds on reactive grounds

y_s Characteristic surface movement

z Vertical depth from the ground surface

α One dimensional soil expansion coefficient

α^* Gradient of the void ratio – moisture ratio line

ΔH Free ground movement at pipe depth

Δu Suction change

Δw Gravimetric moisture content change

$\Delta\varepsilon_{sh}$ Linear shrinkage of the soil

$\Delta\theta_v$ Volumetric moisture content change

$\Delta\theta_{v,pipe}$ Volumetric moisture content change at pipe depth

ε_{bottom} Longitudinal strain at pipe bottom

ε_{eff} Strain due to effective stress change in the porous medium

ε_f	Flexible strain in the pipe
ε^{ms}	Saturation driven moisture swelling in the porous medium
ε_{top}	Longitudinal strain at pipe top
ε_{Total}	Total strain in the porous medium
ε_v	Volumetric soil strain
ε_z	Vertical soil strain
$\theta_{Available,\%}$	Percentage available moisture content
θ_{FC}	Volumetric moisture content at field capacity
θ_{PWP}	Volumetric moisture content at permeant wilting point
θ_v	Volumetric moisture content
$\theta_{v,mean}$	Mean volumetric moisture content
κ	Logarithmic elastic constant
μ	Mean of a normal distribution
$\rho_{s,dry}$	Dry density of the soil sample
ρ_w	Density of water
σ	Total stress in soil
$\sigma_{hoop,w}$	Pipe hoop stress due to water pressure
σ_P	Pipe bending stress
$\sigma_{p,max}$	Maximum pipe bending stress
σ^*	Standard deviation of a normal distribution
σ'	Effective stress in soil skeleton
σ'_{xx}	Effective stress in x direction
σ'_{yy}	Effective stress in y direction

σ'_{zz}	Effective stress in z direction
χ	Chi parameter in effective stress equation

TABLE OF CONTENT

LIST OF FIGURES

LIST OF TABLES

CHAPTER 1: INTRODUCTION

1.1 Research Background

Melbourne's water reticulation network is one of the oldest pipe systems in Australia. It has been functioning for more than 100 years to distribute drinking water to some 4 million people in Melbourne. Most of the old pipes are made of cast iron and they have been subjected to various external and internal loads throughout their lifetime. As pipes age, the strength to bear these loads is gradually decreased by natural material deteriorations such as corrosion. As a result, pipes fail when the loads exceed the remaining strength of the pipe. In the ageing pipe network of Melbourne, about 4000 failures are reported annually (Gould, 2011), creating difficulties for both water suppliers and consumers. Due to limited knowledge, these failures have been recognised as random events in both space and time over the past decades. Therefore, asset management has become a cost factor for water service providers, as unscheduled pipe repairs cost a significant amount of money each year.

To understand these pipe failures, researchers have worked to find possible reasons for the extensive pipe failures in Melbourne. Both statistical and engineering methods have been adopted to identify the most influential factors responsible for these frequent pipe failures. For instance, statistical analyses of Melbourne's past pipe failure data (Chan et al., 2007; Gould and Kodikara, 2008; Gould, 2011) have shown that the influence of reactive ground movements is a critical factor for circumferential crack failures (also known as broken-back failures) in small-diameter (less than

300mm) pipes in reactive soil zones in Melbourne. Reactive zones are defined as the layers of soil close to the surface that directly interact with the atmosphere. Soils can display varying degrees of reactivity to moisture change depending on their properties, including their mineralogy. It has been established that reactive soils show significant volume changes when the soil moisture content changes and enforces vertical movements on adjacent structures, such as footings, pipes, and road pavement. These movements create additional bending stresses in the structures that can lead to structural failures. This effect of reactive ground movements on buried pipes has been shown by monitoring the pipe movement and deformations of an in-service pipe in a reactive clay zone in Melbourne (in Altona North). It has been shown that the pipe longitudinal stresses that are generated due to pipe bending are the result of movement of the surrounding soil (Chan et al., 2015). These observations have provided a conceptual understanding of the interaction between broken-back pipe failures and seasonal ground movements in reactive soil zones.

However, the absence of an analytical methodology to determine these reactive ground movement-induced pipe stresses has been identified as a major knowledge gap for failure analyses of broken-back failures of small-diameter pipes. For another predominant pipe failure type, longitudinal split failure, this requirement has been significantly advanced by recent research at Monash University (Rajeev et al., 2014; Rathnayaka et al., 2016; Rathnayaka et al., 2017). Therefore, the present work was initiated with the main objective of filling this knowledge gap by proposing a detailed methodology to quantify pipe-bending stresses due to reactive soil movements in small-diameter pipes buried in reactive soils.

The research report in this thesis was started in May 2014, as part of the Smart Water Fund Project for An Innovative Integrated Algorithm for Cost-Effective Management of Water Pipe Networks.

1.1.1 Smart Water Fund Project - An Innovative Integrated Algorithm for Cost-Effective Management of Water Pipe Networks

This Smart Water Fund project commenced in March 2014 with a specific focus on the development of integrated algorithms and modules using a GIS framework to help undertake effective scoping and timing of the replacement and rehabilitation of small- (reticulation) and large-diameter (critical) water pipes, on the basis of the improved understanding of the operating requirements and asset deterioration mechanisms of the pipe networks of project partner utilities (Smart Water Fund, 2017b). This project was partnered by Melbourne Water, City West Water Ltd., South East Water and Yarra Valley Water.

The overall project was divided into five different modules as listed below:

1) Reactive soil module
2) Pipe failure prediction module
3) Pipe failure consequence module
4) Pipe risk ranking module
5) Pressure transient module

Each module is to be integrated with the GIS layers of pipe asset information, past failure records, soil properties, topological information, road and traffic data, water pressure data (static and pressure transient), and soil moisture data. The ultimate use of each module is an advanced contribution towards pipe-risk ranking, and selection for condition assessment, renewal and replacement planning. This includes the use of statistical methods for analysing past data especially applicable to small- diameter pipes and the use of the external and internal factors associated with each pipeline segment to make estimates of remaining pipe life and the likelihood of failure, mainly applicable to large-diameter critical pipes. The framework will define the risk profiles of pipelines on the basis of the probability of failure against the consequences of failure. On the basis of levels of uncertainty in decision making, appropriate condition assessments to improve decision making will be provided (Smart Water Fund, 2017b).

The work presented in this thesis is aligned with the reactive soil module which is mainly concerned with small-diameter pipe failures in reactive soil zones in Melbourne. The relevance of this module to the other modules in the project is shown in Figure 1.1.

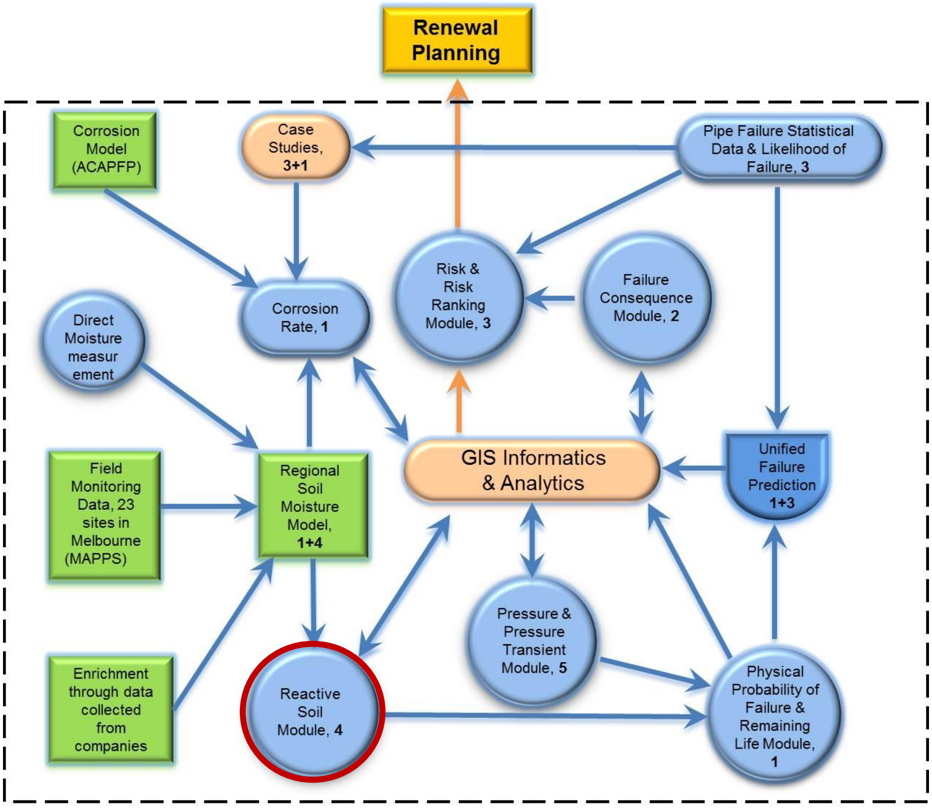

Figure 1.1. The interrelation of five modules in overall project (Smart Water Fund, 2015)

1.2 Research Objectives

Based on the identified knowledge gaps in the current literature on reactive soil-induced circumferential pipe failure analyses of small-diameter pipes, this research was started with the following objectives:

Objective 1:

Development of a methodology to estimate longitudinal pipe stresses due to swelling/shrinking behaviour of reactive soils using both analytical and numerical models. Numerical models are preferred at the early stage and simplified analytical methods are preferred for the final stress estimation models.

Objective 2:

Investigation of the failure mechanisms of small-diameter pipes at different locations such as driveways, nature strips, roads, and trees under different conditions (soil drying and soil wetting) and explanations of the seasonal variations of pipe failure rates (observation of more failures in summer).

Objective 3:

Utilisation of the findings of research on pipe failure prediction models by integrating the pipe stress estimation methods with the soil, soil moisture and pipe network data available in GIS platforms.

1.3 Thesis Structure

Chapter 1: Introduction

This chapter presents the background, initiation and the research objectives of the current study, which is part of the Smart Water Fund Project for An Innovative Integrated Algorithm for Cost-Effective Management of Water Pipe Networks.

Chapter 2: Literature Review

This chapter provides a comprehensive review of previous studies of pipe failure and reactive soil behaviour was carried out prior to the research with the purpose of providing a basis for the current work. The review focuses on past studies of Melbourne's pipe network and pipe failures, fundamentals and problematic behaviour of reactive clays, reactive soil-induced pipe movements and pipe deformation and stress analyses. Since random failures in old pipe networks are a globally-recognised problem, a wide range of research is available on general pipe failure studies.

Chapter 3: Development of a Finite Element Model for Pipe Stress Analysis

This chapter presents the initial work carried out to develop a numerical simulation methodology to estimate pipe stresses due to reactive soil movements. A commercial software package is used to develop a finite element model to simulate reactive soil behaviour and its interaction with pipes to determine the resultant flexural stresses in the pipe wall. Laboratory experiments to determine soil properties for modelling are also discussed in this chapter. The results of the analyses are compared with measurements of field pipe movements at the Altona North monitoring site to verify the model.

Chapter 4: Stress Hotspots of Circumferential Failure Analyses

This chapter presents the analysis of potential locations of circumferential failures that are likely to occur due to reactive ground movements. Therefore, the identification and comprehensive analysis of these locations are an important step in understanding and predicting the failure mechanisms of small-diameter pipes in reactive soil zones. This chapter focuses on field scenarios that can locally affect pipe stress and cause broken-back failure. The study includes field observations of such hot spots, detailed studies of the factors that create hotspots, and finite element simulations to visualise the effects of surrounding features on pipe bending.

Chapter 5: Small-diameter Pipe Failure Case Studies

This chapter presents the observations of field pipe case studies which evaluate the field evidence for pipe failures at hypothetical stress hotspots. The aim of these case studies was to gather detailed information about cast iron pipe failures due to ground movement and identify their relevance to stress hotspots. Therefore, cast iron pipe failures in severely reactive soil zones of Melbourne are the focus of these case studies. Visual inspections of the pipe failure environment and the failure crack orientation were used to identify the causes of and categorise the failures. This chapter explains all the findings of 21 cases studied during the 13-month study.

Chapter 6: An Analytical Model to Estimate Pipe Stresses

This chapter presents the methodology for the development of an analytical method of estimating reactive soil-induced pipe stresses. This analytical method provides a set of mathematical equations to analyse longitudinal pipe stresses for different pipe-bending scenarios. These equations are derived according to the pipe bending patterns and the equations are calibrated and verified using finite element simulations. The main purpose of developing this analytical method is to utilise the findings of the research for use in a wide range of applications. Since these analytical equations are programmable in simple computer applications, these stress estimations can be efficiently integrated with any pipe failure assessment models.

Chapter 7: Application of Pipe Stress Estimation Model to Field Pipe Failure Analyses

This chapter presents the application of pipe stress estimations in field pipe analyses and other pipe failure prediction models, including the contribution to the Smart Water Fund project: "An Innovative Integrated Algorithm for Cost-Effective Management of Water Pipe Networks". The estimations of pipe bending stresses due to seasonal soil moisture variations are integrated with the broken-back failure predictions of the Monash Pipe-failure Prediction (MPP) model. The stress estimations are verified by comparing the seasonal variations of the estimated stresses with past pipe failure records. Before the stress estimations are applied to the failure predictions, the effects of corrosion patches are included as a reduction of the nominal strength of the pipe material (cast iron).

Chapter 8: Conclusions and Recommendations

The last chapter presents the major results of this PhD research and outlines recommendations for future research.

CHAPTER 2: LITERATURE REVIEW

2.1 Overview

A comprehensive review of previous studies of pipe failures and reactive soil behaviours was undertaken in the initial phase of this research. The review focuses on past studies of Melbourne's pipe network and pipe failures, the fundamentals and problematic behaviour of reactive clays, reactive soil-induced pipe movements and pipe deformation and stress analyses. Since random failures in old pipe networks are recognised as a global problem, a wide range of literature is available on general pipe failure studies. However, the mechanisms of reactive ground movement-induced pipe failures have generally received little attention globally. Due to the importance of this issue for Melbourne pipe networks, some research has been conducted at Monash University in the past few years. These studies have provided the basis for the current study.

2.2 Melbourne's Water Reticulation System

Melbourne's water reticulation system is one of the oldest pipe networks in Australia and provides drinking water to about 4.7 million people in the metropolitan area. The total length of the assets in this network has been estimated to be over 12000 km (Gould, 2011). The first part of the literature review focuses on the basic characteristics of Melbourne's water system.

2.2.1 History and administration of the pipe network

Urban development of the city of Melbourne and its metropolitan area started in the 1830s with European settlement in Australia (City of Melbourne, 2017). With the rapid population growth in the first 2 to 3 decades of urbanisation, the requirement of a systematic water supply system arose. Initially, the Metropolitan Board of Works (MMBW) became the responsible governing body for supplying water to this growing population and the initiation of Melbourne's water supply system (Melbourne Water, 2017). Therefore, the current water reticulation system has a history of at least 150 years.

Currently, the governing structure of this water reticulation system consists of one wholesale water supplier and three retail water corporations. The wholesale water authority, Melbourne Water, maintains the upstream reservoirs and supplies wholesale water to the retail water corporations. The three retailers, City West Water, South East Water and Yarra Valley Water distribute the water to households across the metropolitan area (Melbourne Water, 2017). Therefore, the operations and maintenance of the reticulation water system are mostly undertaken by these three retailers. Figure 2.1 shows the map of the service area of the retail water authorities.

Consideration of the retail water authorities and their service areas is important in this study since the presence of reactive soil and its properties varies spatially. In addition, communication with the water authorities has been important for all past pipe failure analyses, which are referred to in this literature review, in order to obtain the asset information and the historical pipe failure data for their service areas.

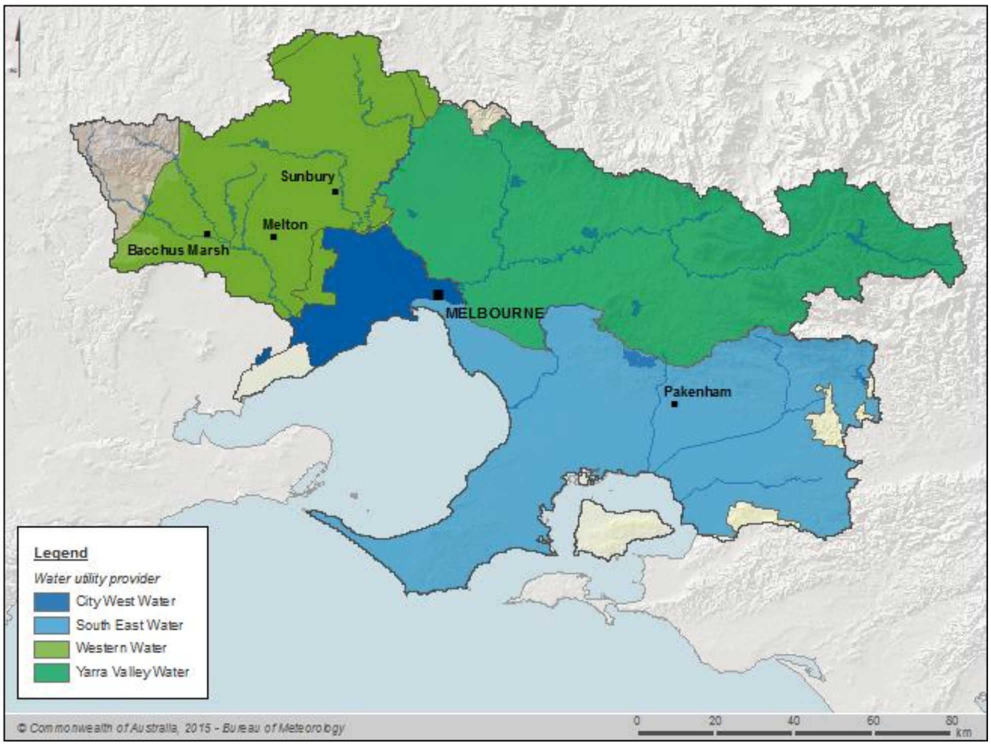

Figure 2.1. Service areas of the water retail authorities in Melbourne (Bureau of Meteorology, 2017a)

2.2.2 Pipe manufacturing materials

In a detailed study of the pipe network, knowledge of the properties of the pipes and their manufacturing materials is important, as the mechanical behaviour of the pipes is dependent on their material properties. A detailed study of Melbourne's water reticulation system (Gould, 2011) identified that the pipe network is composed of both metallic and non-metallic materials, as reported in Table 2.1.

Table 2.1. Manufacturing materials of Melbourne water pipes (Gould, 2011)

Metallic materials	Non-metallic materials
Cast iron (CI), Ductile iron (DI, Copper (CU), Galvanised wrought iron (GWI) and Steel (S)	Asbestos cement (AC), Reinforced concrete (RC), Polyvinyl chloride (PVC), Polyethylene (PE) and Glass reinforced plastic (GRP)

An assessment of the individual pipe asset data of City West Water and South East Water (Gould, 2011) showed that the highest proportion of pipes are made of cast iron. Therefore, from here onwards, this literature review focuses on a discussion of the properties of cast iron pipes. The distribution of all different pipe materials in the networks is shown in Figure 2.2.

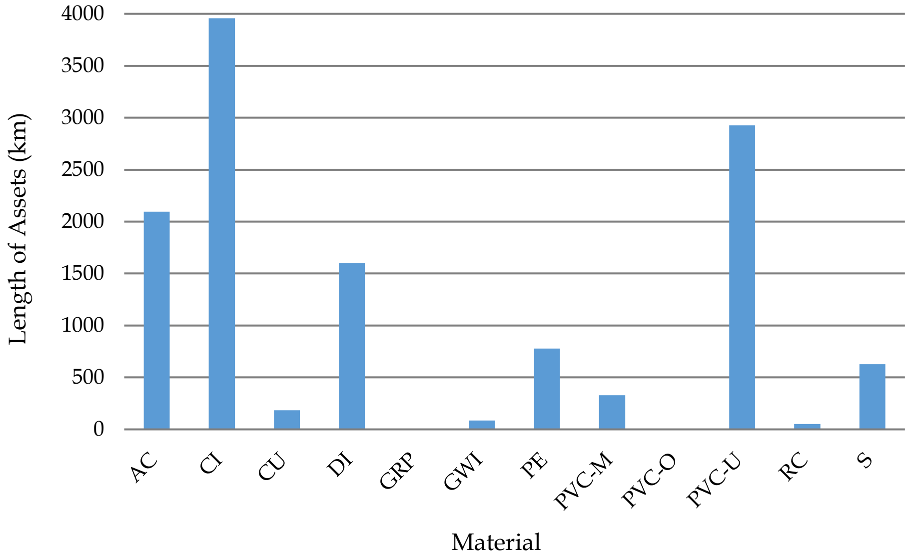

Figure 2.2. Distribution of different pipe materials (Gould, 2011)

2.2.2.1 Methods of manufacture of cast iron pipes

The method of manufacture of cast pipes has varied over the years of their installation from the 1850s to the 1980s (Scott, 1990; Rathnayaka, 2016; Shannon et al., 2016a). A timeline of the different manufacturing techniques of eastern Australian metallic pipes is shown in Figure 2.3.

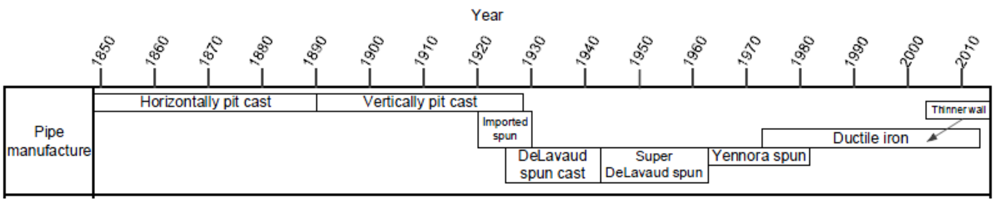

Figure 2.3. Timeline of manufacturing methods of Eastern Australian pipes (Shannon et al., 2016a)

As previous studies have shown, horizontally and vertically pit (or static) cast iron was the major pipe material from the 1850s to the 1920s. Then it changed to spun cast iron until ductile iron became popular in the 1970s. Pit and spun casting are two major pipe manufacturing methods where the casting is done using sand moulds assembled in pits for pit cast and spinning moulds for spun cast (Cast Iron Pipe Research Association, 1952). These pipes were imported from the United Kingdom in the early years until the 1890s and Australian manufacturers started producing pipes after the 1890s (Jiang et al., 2017b).

It has also been identified that the metallurgy and hence the mechanical properties of the cast iron varied as the casting techniques changed (Makar and Rajani, 2000; Shannon et al., 2016a).

2.2.2.2 Mechanical properties of cast iron pipes

Cast iron is a ternary alloy with 92 to 95% iron, 2 to 4% carbon and 0.5 to 3% silicon with traces of manganese, sulphur and phosphorus (Leedom, 1946). Cast iron is a brittle material with a limited elastic range (Crossland and Dearden, 1958). Therefore, knowledge of the basic mechanical properties such as elastic modulus and ultimate tensile strength is important for a mechanistic study of cast iron pipes. As shown in Table 2.2, different researchers have published these basic properties based on laboratory tests of cast iron samples obtained from cast iron pipes of different ages.

Table 2.2. Basic material properties of cast iron pipes (Rathnayaka, 2016)

Casting type	Reference	Secant elastic modulus (GPa)	Tensile strength (MPa)	Description of test sample
Pit	(Rajani, 2000)	38 - 168	33 - 267	With corrosion pits
Spun	(Rajani, 2000)	43 - 159	135-305	
Pit and spun	(Seica and Packer, 2004)	23 -150	47 - 297	
Spun	(Yamamoto et al., 1983)		100 - 150	
Pit and spun	(Gould, 2011)	10 -215	10.5 - 249	
Pit and spun	(Colin and Baker, 1991)		137 - 212	No information

Note that these mechanical properties have been reported either using pristine material (after removing any corrosion products and machining to flat surfaces) or with corrosion products (keeping the corrosion profile after grit-blasting). The variations of mechanical properties presented in Table 2.2 were explained as a result of the variable corrosion in test samples, since the tests were conducted on samples with corrosion pits. However, the tensile strength of spun cast iron pipes manufactured in the 1900s is considerably higher than that of early manufactured pit cast pipes (Rajani, 2000).

2.2.3 Pipe sizes

As a pipe network is designed to carry water from major reservoirs to individual premises, it has to be composed of different pipe sizes to efficiently transport the required water quantity. For City West Water, (Gould, 2011) reported that the reticulation network consists of pipes with diameters from 25mm to 400mm, and the distribution of these pipe sizes among different pipe materials is shown in Figure 2.4.

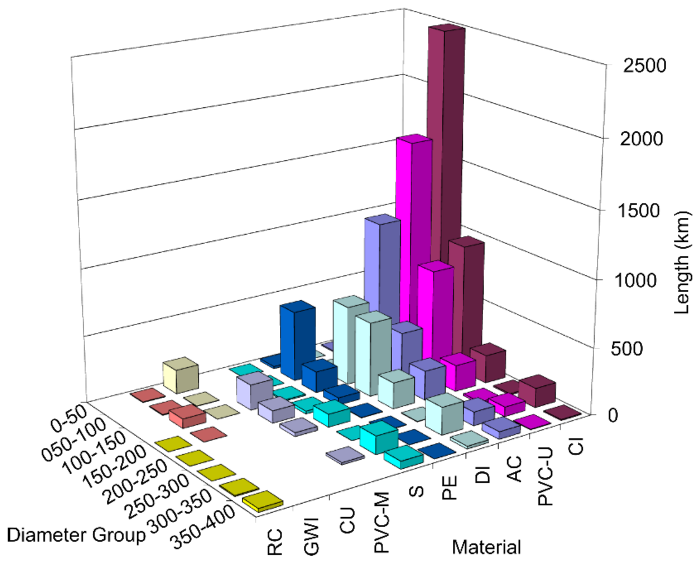

Figure 2.4. Different pipe sizes and materials of City West Water and South East Water pipe networks (Gould, 2011)

It is evident that the highest portions of the pipes belong to the 100-150mm diameter cast iron pipe group. Similarly, the diameter group 100-150mm has the highest percentage of pipes in most of the other materials. This pipe diameter group analysis indicates that pipe diameters smaller than 300mm are the most common pipe diameters in the reticulation pipe network. In other studies (Gould and Kodikara, 2008; Gould, 2011; Chan, 2013; Rathnayaka, 2016), 300mm diameter has been used as the boundary to differentiate large- and small-diameter pipes. Therefore, for the purposes of the present research, small-diameter pipes are defined as pipes with pipe diameters less than 300mm.

In addition to the pipe diameter, pipe wall thickness is an important parameter to express the size of the pipe. Figure 2.5. Relationship between pipe diameter and wall thickness (Shannon et al., 2016a) presents the relationships between pipe diameter and pipe wall thickness on the basis of data gathered from Australian pipe manufacturing standards (AIS, 1941) and reported in past research (Shannon et al., 2016a; Ji et al., 2017; Jiang et al., 2017b).

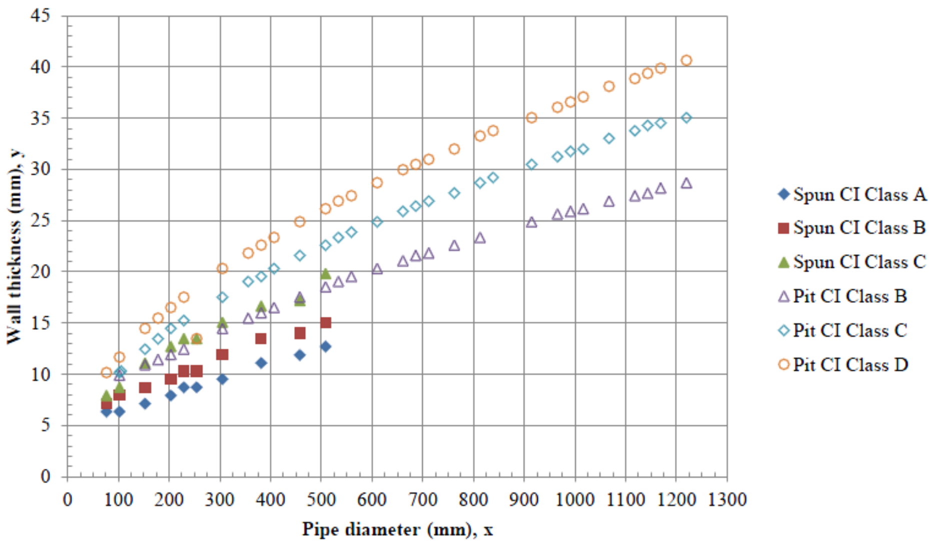

Figure 2.5. Relationship between pipe diameter and wall thickness (Shannon et al., 2016a)

Classes A, B, C of spun cast iron and classes B, C, D of pit cast iron represent the different pipe classes which were used in pipeline design to withstand different internal water pressures (Jiang et al., 2017b). An overall evaluation of pipe wall thickness data highlights that the wall thickness of pit cast pipes is generally higher than that of spun cast iron pipes and the wall thickness increases as the pipe class is raised.

2.2.4 Pipe burial information

In the City West Water (CWW) pipe network, the reticulation pipes are usually buried under grass-covered nature strips between streets and houses. In some cases, the pipes are buried under local roads and parking areas. To some extent, this situation is common for other utilities. However, the burial process of these pipes has changed over the past decades. Therefore, this section of the literature review concerns the burial information of both older and newer pipes.

Trenching, pipe laying and back-filling are the main steps in the pipe burial process. Trenching is undertaken according to the pre-defined burial depth. As general information about pipe burial depths in Melbourne is not available in published literature, the information in Table 2.3 was collected by personally communicating with asset management personnel in CWW (Rivette and Moore, 2015).

Table 2.3. Pipe burial depth information for Melbourne pipes. (Rivette and Moore, 2015)

Construction time	Pipe Diameter	Soil Cover
1850 - 1920	4″ – 12″ (100 – 300mm)	1′6″ to 1′9″ (450-525mm)
	> 12″ (>300mm)	3′6″ to 4′0″ (1050-1200mm)
1920 - 1980	4″ (100mm)	2′ 0″ (600mm) (extra 150mm under roads)
	6″ (150mm)	2′ 6″ (750mm)
	9″ (225mm)	3′ 0″ (900mm)
	12″ (300mm)	3′ 0″ – 3′ 6″ (900 – 1050mm)
1980 - Present	100 – 300 mm	450 mm (extra 150 mm under roads)
	> 300 mm	1000mm

The pipe burial depth is a variable of both construction time and the pipe size. Small-diameter pipes are buried at shallower depths while large pipes are buried deeper. In addition, the burial depths have become slightly shallower over time. Overall, all pipe burial depths are in the first 1.2m from the ground surface. This is shallower than the common pipe depths used in other countries such as Canada (typically 1.2 to 2.4m deep), where the pipe depths are designed to avoid the ground freezing zone (Rajani et al., 2012).

In the context of Melbourne's climate, the identified pipe burial region is within the seasonal soil moisture variation zone or reactive zone, specified as the first 2.3m from the ground surface for western Melbourne (Australian Standards, 2011). This region is considered to be mostly unsaturated, being subjected to seasonal moisture variations and ground movements.

In addition to the specified soil covers above the pipe, 150mm of minimum soil support is maintained below the pipe at locations where the bedrock is close to the surface (see Figure 2.6. Soil cover and the minimum soil support at the bottom of the pipe (Rivette and Moore, 2015)). The purpose of this minimum soil support at the bottom of the pipe is to protect the pipe from possible damage due to direct contact with the rock. As the information provided by asset management personnel at CWW indicates (Rivette and Moore, 2015), this minimum soil support at the bottom is provided by breaking the rock and filling with soil materials.

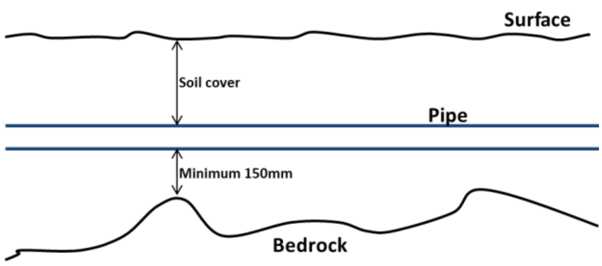

Figure 2.6. Soil cover and the minimum soil support at the bottom of the pipe (Rivette and Moore, 2015)

Back-filling is also an important step in the pipe burial process. For present pipe installation and repair, specific guidelines and recommendations for back-filling materials, compaction methods and compaction levels have been developed by the water authorities (MRWA, 2013) to enhance pipe safety under both trafficable and non-trafficable areas. The backfill materials are selected on the basis of the compaction requirements, such as particle size gradations and fraction of rock particles.

However, the natural soil at the trenching site was used as the back-fill material before specified back-fills started to be used in the 1960s (Jiang et al., 2017b). Therefore, the natural soil can be identified as the surrounding soil material for many old cast iron pipes. This is an important fact for the current work, as the reactive soil environment of old cast iron pipes is the main objective of the investigation.

2.2.5 Current condition of old metallic pipes (corrosion defects)

As the pipe network has been in service for up to about 150 years, knowledge of the current condition of pipe assets is essential for pipe failure analysis. It has been identified that underground metallic pipes, which have been exposed to different environmental conditions throughout their lifetime, are severely affected by material deterioration such as electro-chemical corrosion (Rajani and Kleiner, 2001; Petersen and Melchers, 2012; Cole and Marney, 2012; Ji et al., 2017). Underground corrosion is a complex time-dependent process that is influenced by many factors, such as the dynamics of moisture and oxygen and other environment facts (Cole and Marney, 2012).

2.2.5.1 Pipe wall corrosion

In previous studies, overall pipe corrosion deterioration has been investigated as two separate components: internal and external pipe corrosion (Rathnayaka, 2016; Jiang et al., 2017b). Internal pipe corrosion gained more attention in the early years due to public health concerns (Rathnayaka, 2016). As a mitigation step, in the 1920s, cement linings were introduced to the internal surface of cast iron and ductile iron pipes to prevent internal corrosion and to improve water flow (Jiang et al., 2017b). It has been reported that these cement linings effectively restricted internal corrosion (Jones, 1941).

Therefore, the effects of pipe internal corrosion became insignificant compared with the effects of external corrosion, and external corrosion has been recognised as the main factor causing most pipe failures (Yamamoto et al., 1983; Ji et al., 2015; Ji et al., 2017).

The reduction of pipe wall thickness is the main weakening factor due to corrosion (Ji et al., 2017). This reduction in wall thickness is considered to be a result of cast iron graphitisation, where iron is lost from the metal matrix as iron salt, which is later transformed into ferric hydroxide. This salt leaves the matrix, rendering the remaining carbon a weak porous mass (Leedom, 1946). In field pipes, this graphitisation is observed in two different degrees: uniform corrosion and pitting corrosion, which can also manifest in clusters or patches (Rajeev et al., 2014). The uniform corrosion results an all-round thickness reduction in the cast iron pipe wall, whereas pitting corrosion results localised thickness reductions (pitting) of the cast iron pipe wall. These two different corrosion patterns are illustrated in Figure 2.7.

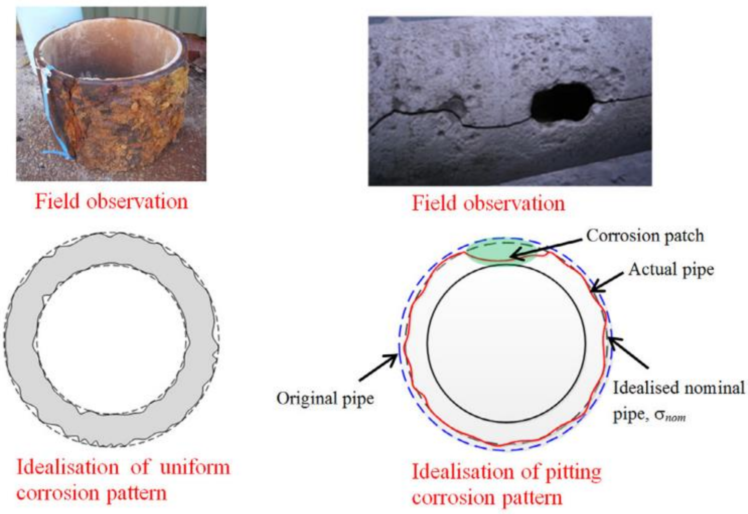

Figure 2.7. Difference between uniform and pitting corrosion (Ji et al., 2017)

The consequences of pitting corrosion for pipe failure have gained more attention than uniform corrosion, as the most pipe failures examined have been observed at large corrosion patches (Makar, 2000; Kodikara et al., 2012) (see examples in Figure 2.8.

Examples of failures at corrosion patches (Rathnayaka, 2016)). Therefore, the effects of these corrosion pits (patches) on pipe failures have been an intense topic in global pipe failure research.

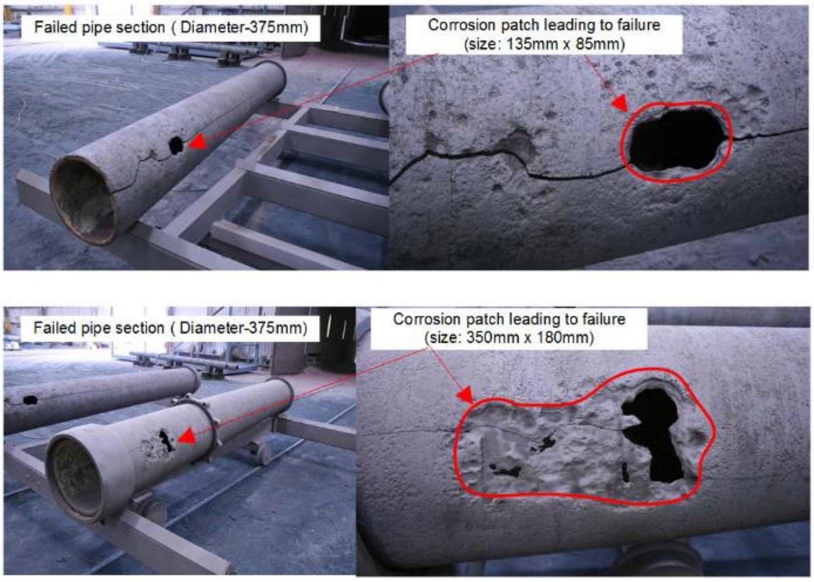

Figure 2.8. Examples of failures at corrosion patches (Rathnayaka, 2016)

2.2.5.2 Effects of corrosion patches

The effects of these corrosion patches on the current condition of pipes have been considered in two different ways.

The consideration of the reduction in the structural capacity or the strength of the pipe (load that needs to break the original pipe section including the graphitised section represented as an equivalent stress) due to pipe wall graphitisation (corrosion) has been the first approach and is the most commonly used. Empirically-developed cast iron pipe strength reduction models have been reported in various parts of the world, including the United Kingdom (Atkinson et al., 2002), Canada (Rajani, 2000) and Japan (Yamamoto et al., 1983). All these methods have shown an inversely proportional linear relationship between tensile strength of cast iron pipe sections and corrosion pit depth. The relationship for Australian cast iron pipes (Gould, 2011) is shown in Figure 2.9. Cast iron pipe strength deterioration with graphitisation (Gould, 2011), which indicates the strength of both pit and spun cast iron pipes gradually decreases to 0 from the initial strength of 200 – 250MPa as the corrosion (graphitisation) depth to original wall thickness ratio approaches unity. This well-established empirical relationship implies that the loss of load bearing cast iron from the pipe section weakens the section strength as the pipe tends to fail at lower stresses. In addition, mathematical representations of these strength reductions are available in pipeline engineering handbooks (Antaki, 2003).

The second method is a more mechanistic approach of incorporating corrosion defects in pipe failure analyses. In this technique, stress concentration at corrosion patches has been considered as the major factor affecting pipe failure and the stress concentration factors for such corrosion patches have been defined according to the corrosion patch dimensions (Ji et al., 2015; Rathnayaka, 2016). This analytical method is mainly based on finite element simulations and an example of stress concentration at a corrosion patch is shown in Figure 2.10. Finite element analysis of stress concentration at a corrosion patch (Ji et al., 2015). The figure explains the tensile stress variation around a corrosion pit on a pressurised pipe. It shows a significant stress increase at the bottom of the pit (red coloured area) when compared to the unaffected area of the pipe (blue coloured area). Therefore, this pit geometry based stress concentration brings up the stress in the pipe wall closer to the material strength of the cast iron and eventually causes the breakage. This method has been successfully applied and validated with large-diameter pipe longitudinal failure analyses (Rathnayaka, 2016).

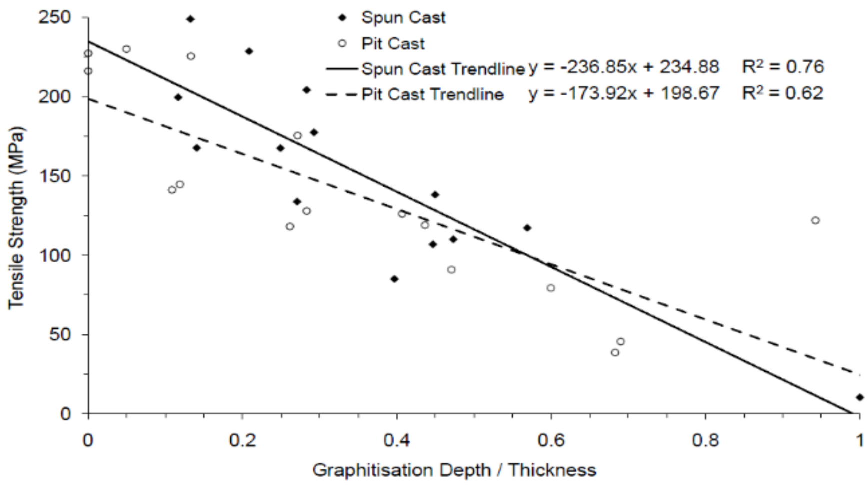

Figure 2.9. Cast iron pipe strength deterioration with graphitisation (Gould, 2011)

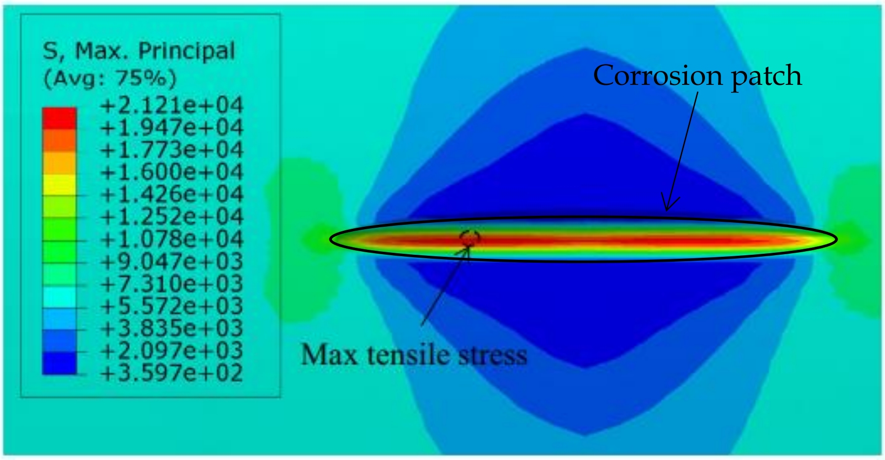

Figure 2.10. Finite element analysis of stress concentration at a corrosion patch (Ji et al., 2015)

The both methods can capture the possibility of pipe failure at corrosion pits, in the first, by means of lower strength and, in the second, by means of elevated stresses. As both methods involve the corrosion patch dimensions (width, length and/or patch depth), it is important to know the current corrosion damage in the pipe network.

2.2.5.3 Field methods to identify current condition of pipes

Since the literature has clearly stated that the consideration of current corrosion or the material deterioration level of old metallic pipes are essential for failure studies, it is important to study practical methods of assessing current pipe condition. A broad range of condition assessment techniques in practice and under investigation by water utilities have been reported by previous researchers (Costello et al., 2007; Rathnayaka, 2016).

These methods include the use of closed-circuit television (CCTV) cameras to visually identify the defects on pipe interior (suitable for large pipes), sonar or laser surveys to identify pipe wall thickness variations due to corrosion losses, and electromagnetic methods such as magnetic flux leakage (MFL) and broadband electromagnetic (BEM) surveys to characterise metal losses on pipe walls. The applicability and limitations of these methods vary with the pipe material (including coatings), pipe size, accessibility of the pipe etc. (Table 2.4).

Table 2.4. Applicability and limitations of pipe condition assessment methods (Costello et al., 2007).

Method	Applicability and limitations
CCTV	• Real time assessment necessary • Some progress has been made to overcome this issue by automated processing techniques • Subjective, as inspector has to identify and categorise defects in image • Can be time intensive, depending on number of defects per km pipe
Sonar / laser surveys	• Determines internal profile of the pipe along its length • Can measure pipe wall deflection, corrosion loss and volume of debris in invert • Can be operated in air or water, but not both simultaneously If pipe partially filled with water, only part of the pipe can be assessed at any one time Therefore, surveys often carried out at night and at times of low flow
MFL and BEM	• Good for cast iron and steel pipes • Used in intelligent pigs for detection and characterisation of corrosion and circumferential and longitudinal cracks • Can be difficult to maintain close contact with the pipe and potentially result in damage to the lining of the pipe • Thus often limited to cleaned and unlined pipes • Can detect small defects, but has difficulties detecting short and shallow defects • Data therefore contain a degree of uncertainty

The applicability of electromagnetic methods (MFL and BEM) for Australian cast iron pipes (large-diameter pipes) has been broadly investigated as a part of the advanced condition assessment and pipe failure prediction (ACAPFP) project that involved surveying a 1km long in-service cast iron pipe and developing algorithms to match the scanned pipe wall shapes (Miro et al., 2013). However, the applicability of these techniques into a large pipe network can be a costly effort.

2.3 Pipe Failure

The structural failure of a water pipe is generally defined as a breakage due to the ultimate inability to withstand internal and external forces on the pipe. Although these pipes have been primarily installed to distribute water to required destinations, they are also subjected to various forces throughout their lifetime. Therefore, the applied forces on the pipe and the decaying structural capacity of the pipe have been highlighted as two important factors for pipe failure studies.

The high factor of safety against failure (a ratio given by the structural capacity divided by stresses due to applied loads) at the time of pipe installation continuously declines during the pipe's lifetime as the structural capacity of the pipe deteriorates for several reasons, including corrosion pitting, degradation, fracture, creep and material softening (Rajani and Kleiner, 2004; Rajeev et al., 2014). Failure occurs when the factor of safety reaches the critical value of 1. The most possible timeline of this decline is explained in Figure 2.11. Time dependent reduction of the factor of safety: Source (Rajani and Kleiner, 2004), but has been recently modified by the leak- before-break concept (Rathnayaka et al., 2017).

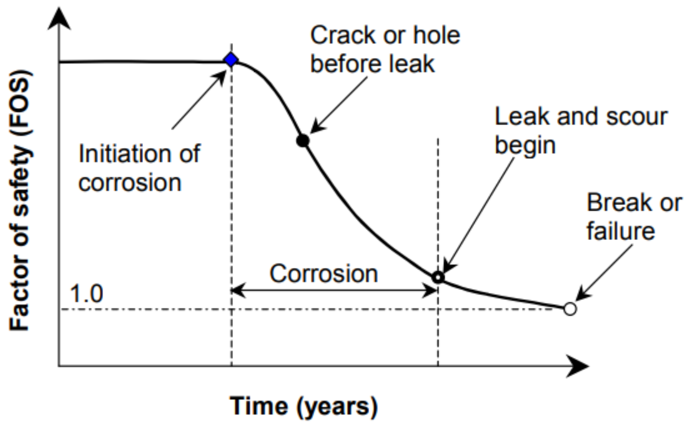

Figure 2.11. Time dependent reduction of the factor of safety: Source (Rajani and Kleiner, 2004)

2.3.1 Forces on pipes

The critical forces which are generally imposed on a buried pipeline have been identified as those produced by internal water pressure, bending forces, crushing forces, soil movement-induced tensile forces and temperature-induced expansive forces, whereas only water pressure and crushing forces have been considered for pipe designs (Makar et al., 2001). Further details of these forces can be found in the literature, as summarised in Table 2.5.

Table 2.5. Typical forces on buried pipes

Force type	Description	References
Internal water pressure	Categorised as two components: static water pressure that is the normal operational pressure, and transient pressure that is created due to changes in pressurised water system. Transient events create more problems and can generate elevated hoop stresses.	(Rathnayaka et al., 2016; Rathnayaka, 2016)
Bending forces	Create axial stresses. Generated due to forces in transverse direction to the pipe such as traffic loads and other overburdens. Forces vary with burial depth.	(Rajani et al., 1996; Rajani and Tesfamariam, 2004; Robert et al., 2016b; Chan et al., 2016)
Crushing forces	Create hoop stresses. Generated due to forces in transverse direction to the pipe such as traffic loads and other overburdens. Forces vary with burial depth.	
Ground movement-induced forces	Create pipe bending and axial stresses. Ground movement can be caused by several reasons such as ground settlement, freezing and thawing, and volume changes of reactive soils. Generally depend on environmental, climatic and soil conditions.	(Rajani and Zhan, 1996; Rajani and Kleiner, 2001; Chan et al., 2015; Gould, 2011)
Temperature-induced forces	Create axial stresses due to thermal expansion and contraction of metallic pipes. Critical in environments where the seasonal temperature variations are significant.	(Habibian, 1994; Rajani et al., 1996; Rajani et al., 2012)

The relevance and the importance of some of these forces for pipe failure analyses has been considered to varying degrees. For instance, studies of temperature- induced forces and frost loads on pipes have gained more attention in the northern hemisphere in countries such as Canada (Rajani and Kleiner, 2001; Rajani et al., 2012). In contrast, factors such as water pressure have been a common consideration worldwide in pipe failure studies.

Temperature effects and crushing forces such as traffic loads have been considered as insignificant in past studies of Australian water pipe failures (Chan et al., 2015; Chan et al., 2016). The main reasons are the relatively low temperature variations and the sufficient burial depths under road pavements to withstand surface loads. However, the forces induced by ground movements have been considered in detail, especially for the reactive soil zones in Melbourne (Chan et al., 2007; Gould and Kodikara, 2008; Gould, 2011; Chan, 2013). Table 2.6 shows the available calculation methods to determine the effects of some of these loads on buried pipes.

Table 2.6. Calculation methods of some forces / stresses on pipes

Force on pipe	Calculation method
Hoop stresses due to internal water pressure	$\sigma_{hoop,w} = \frac{P_w D}{2t}$ (Wiggin et al., 1939) where, $\sigma_{hoop,w}$ is the pipe hoop stress, P_w is the internal water pressure (steady-state & transient), D is the pipe diameter and t is the pipe wall thickness.
Forces due to traffic loads	$W_t = \frac{CR_x FP}{D}$ (AWWA C101–67, 1977) where, W_t is the load on pipe per unit length, P is the traffic load at the surface, D is the pipe diameter, F is a unit-less impact factor that characterizes the dynamic effect of vehicles (a function of burial depth), R_x is a reduction factor that accounts for 2 or more adjacent axles (unit-less), and C is an unit-less surface load factor that depends on pavement type.
Axial effect due to temperature changes	$\varepsilon_{x,T} = \alpha_p \, \Delta T$ (Rajani et al., 1996) where, $\varepsilon_{x,T}$ is the axial strain due to temperature change, α_p is the expansion coefficient of pipe material and ΔT is the temperature change.

2.3.2 Failure types

Depending on the dominant stress acting in the pipe wall at the time of failure and the location of the breakage, different types of failures have been identified based on field pipe failures. The location of the failure has been divided into two categories: failures in the pipe barrel (the pipe section with uniform diameter) and failures at pipe joints (bell-shaped connection). As reported in the research literature, failures in pipe barrels have been categorised as blowout holes, circumferential cracking (broken back) due to excessive axial stresses, longitudinal cracking due to excessive hoop stresses and spiral cracking (which can be due to a combination of hoop and longitudinal stresses), whereas the failure modes in joints have been categorised as bell splitting and bell shearing (Makar et al., 2001; Rajeev et al., 2014). The causes of each failure type have been identified and are summarised in Table 2.7.

As the explanations given for different pipe failure types show, these failures have been identified as directly influenced by the condition of the pipe section, which is dominated by the corrosion level and the pipe size. The present work places more focus on circumferential crack (broken back) failures in pipe barrels.

Table 2.7. Main reasons for different pipe failure types (Makar et al., 2001)

Failure type	Reason	Visual failure
	Pipe barrel failures	
Blowout holes	This failure occurs as the water pressure blows the thinned remaining pipe wall due to corrosion pitting. Damage can vary from a very small hole to a large one, depending on how localised the corrosion was.	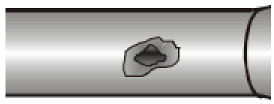
Circumferential cracking (broken back),	This failure type is mainly caused by axial stresses due to bending forces. Common in small pipes.	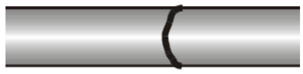
Longitudinal cracking	Hoop stresses due to internal water pressure and external crushing loads are the main causes.	
Spiral cracking	This failure type is caused by combination of axial and hoop stresses. Not very common.	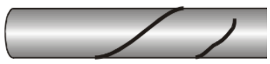
	Pipe joint failures	
Bell splitting	Main reason has been identified as hoop stresses due to different thermal expansion properties of pipe metal and joint fastening material (lead).	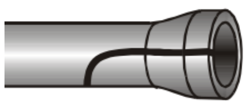
Bell shearing	Bending forces have been identified as the most likely reason for this failure type. Commonly observed in large pipes.	

2.3.3 Factors affecting pipe failures and failure rates

It was stated above that pipe failure is defined as an event associated with the applied forces on pipes and the weakened structural capacities of pipes. However, these two main contributors have been identified as being influenced by several physical and environmental factors. A comprehensive study of these influencing factors reported them in three different categories: static factors (non-variable factors), dynamic factors (time-dependent variables) and operational factors (responsibility of water utilities) (Kleiner and Rajani, 2002). The factors identified in this work are listed in Table 2.8.

Table 2.8. Factors influencing pipe failures: Source (Kleiner and Rajani, 2002)

Static	Dynamic	Operational
Material Diameter Wall thickness (initial) Soil (back-fill) properties Installation	Age Temperature (soil, water) Soil moisture Soil electrical resistivity Bedding conditions Dynamic loading	Replacement rate Cathodic protection Water pressure

The table shows that static factors are constants throughout a pipe's lifetime and also applicable in global pipe failure analyses, whereas the dynamic factors are time- and location-dependent. In contrast, operational factors such as replacement rate, cathodic protection against corrosion and operational water pressure are dependent on the requirements of the water utilities.

The relevance of these factors for Australian (especially Melbourne's) pipe failures have been studied by some researchers (Gould, 2011; Rajeev et al., 2014). In these studies, pipe material, pipe diameter, soil properties, pipe age and soil moisture are highlighted as the major factors affecting local pipe failure rates. In these studies, the pipe failure rate is defined as the number of pipe failures per 100 kilometres of pipe per year. The major observations of these studies are outlined in the following sections.

2.3.3.1 Influence of pipe diameter and material on Melbourne's pipe failures

Studies of Melbourne's past pipe failures have shown that small-diameter cast iron pipes are the most frequently failed (Gould, 2011). This pipe failure rate variation can be seen in Figure 2.12. Pipe failure rate variation with different materials and diameters (Gould, 2011). As the reported number of circumferential crack (broken back) failures in the pipe network are significantly higher than the longitudinal crack failures, the majority of these failures are expected to be broken-back failures. Therefore, the bending forces on pipes are the major reason for this observed failure pattern, as small-diameter pipes show smaller inertia to bending and the brittle properties of cast iron show lower resistance to bending stresses. This trend has been reported for other cities in the world (Kettler and Goulter, 1985; Vloerbergh and Blokker, 2009).

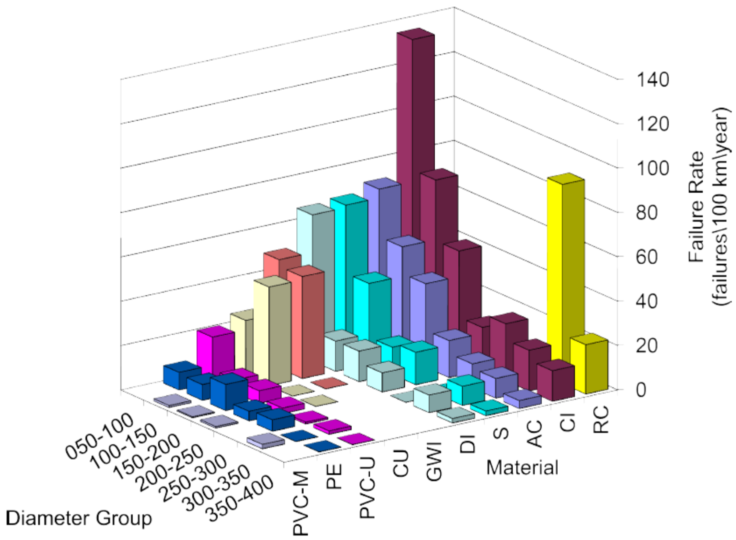

Figure 2.12. Pipe failure rate variation with different materials and diameters (Gould, 2011)

2.3.3.2 Influence of soil and environmental conditions on Melbourne's pipe failures

The influence of the environment and the soil are critical factors for Melbourne pipe failures, mainly due to the reactive soil environments around Melbourne (Gould, 2011;

Chan, 2013). Comparisons of pipe failure rates with different expansive soil environments (very expansive-VE, moderately expansive-ME, slightly expansive-SE and stable soil-ST) show that the failure rates are significant in very expansive soil environments (Gould, 2011). These failure rates are also influenced by the pipe diameter and pipe material, and dominated by brittle materials like cast iron. These observations are shown in Figure 2.13. Influence of soil type on Melbourne's pipe failure rates (Gould, 2011).

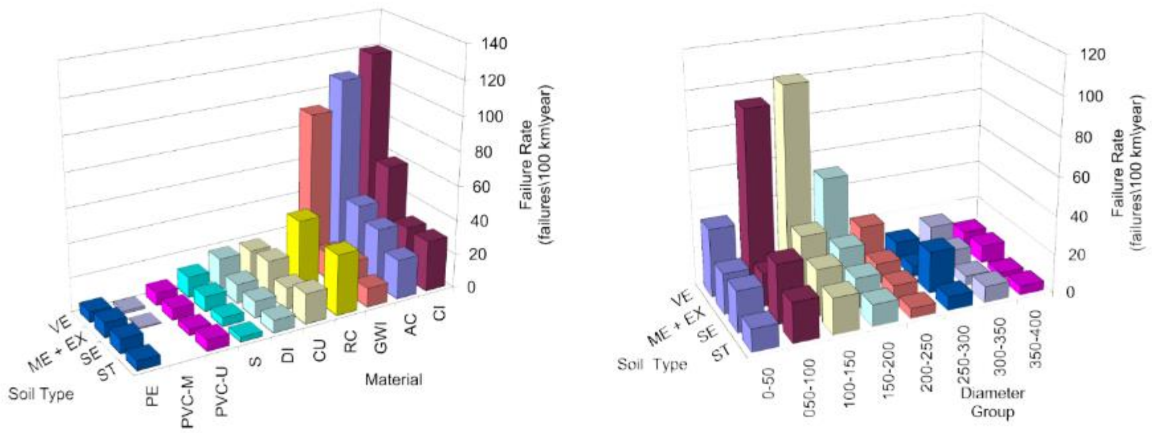

a) Pipe failure rate variations with pipe material and soil type

b) Pipe failure rate variations with pipe diameter and soil type

Figure 2.13. Influence of soil type on Melbourne's pipe failure rates (Gould, 2011)

The higher failure rates of small-diameter cast iron and asbestos cement pipes (both brittle materials) in very expansive soil environments are considered to be a result of pipe bending in reactive soil environments.

In addition to variations with soil types, Melbourne's intra-year pipe failure rate variations show that pipe failure rates are significantly high in drier months (December to March) of the year (Chan et al., 2007; Ibrahimi, 2005; Gould, 2011; Gould et al., 2011a) (see Figure 2.14. Intra year variation of Melbourne's pipe failure rates (Gould, 2011)). This observation has led researchers to conclude that the failure rates are influenced more by dry environmental conditions than wet conditions.

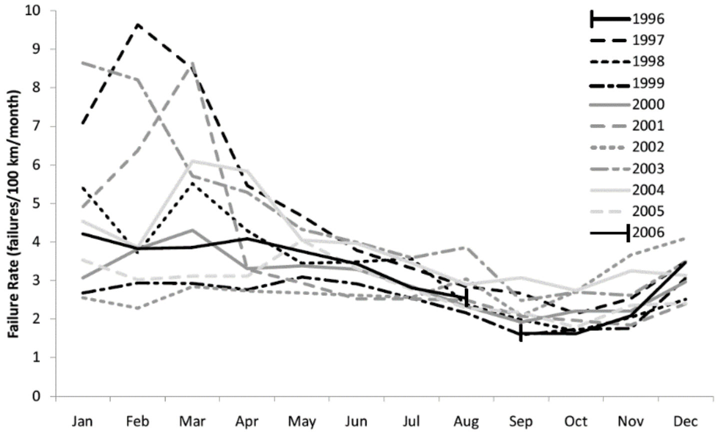

Figure 2.14. Intra year variation of Melbourne's pipe failure rates (Gould, 2011)

This trend (higher failures in dry summers) has been similarly observed for pipe failures in Texas, USA where many high plasticity clays are present (Hudak et al., 1998). However, an opposite trend has been observed in cities where the ground freezing is being a critical fact (Habibian, 1994; Rajani et al., 1996). The higher failure rates during winters are considered to be the result of frost loads (Rajani and Zhan, 1996).

With the above observations of pipe failure rate variations with pipe size, material and surrounding soils, it has been established that the small diameter pipe failures in Melbourne are influenced by the seasonal changes in reactive soil grounds. Further discussion of this issue is included in Section 2.6.

2.4 Reactive (Expansive) Soils

Reactive soils (also known as expansive or swelling soils) are soils that show significant volume changes and cause vertical ground movements (shrinking and swelling) as the water content changes (Cameron and Walsh, 1984; Dif and Bluemel, 1991; Nelson and Miller, 1997). The problematic behaviour of these soils has been recognised worldwide, as the ground swelling and shrinkage induced by soil reactivity cause structural damage to many man-made structures, including buildings, pavements and pipelines (Cameron and Walsh, 1984; Jones and Jefferson, 2012).

2.4.1 Characteristics of soil reactivity

The reactivity of the soil is characterised as the amount of swell-shrink movement that is produced by the soil in response to the soil moisture change. This shrink–swell potential of expansive soils is mainly determined by its mineral and chemical composition, initial water content, void ratio and soil structure, vertical stress, particle size distribution and soil profile (Cameron and Walsh, 1984; Bell and Culshaw, 2001; Jones and Jefferson, 2012; Nelson et al., 2015).

2.4.1.1 Mineral and chemical composition

Generally, clay minerals are silicates of aluminium and/or iron and magnesium and basically consist of silicon tetrahedron and alumino-magnesium octahedron units (Grim, 1953; Nelson et al., 2015). Depending on the orientation and strength of the interlayer bonding between these units, these mineral structures are categorised into the following groups:

- Kaolinite group
- Illite or mica-like group
- Montmorillonite or smectite group

The crystal structures of all these three groups are layered and the contribution to the reactiveness of the soil is determined by the characteristics of these layers (Nelson and Miller, 1997). The interlayer bonds in each mineral group are schematically presented in Figure 2.15.

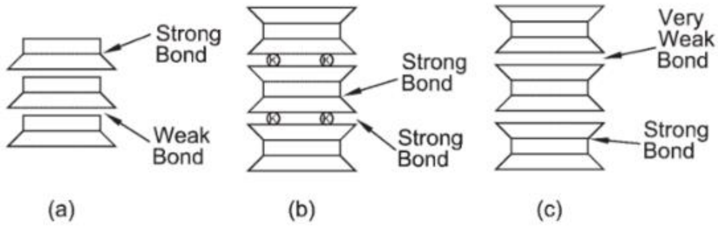

Kaolinite Illite Montmorillonite

Figure 2.15. Different interlayer bonds in clay mineral groups (Nelson et al., 2015)

Of these arrangements, the montmorillonite group, which has the weakest interlayer bonds, has been designated as the most expansive minerology compared with the less-expansive kaolinite and illite groups (Nelson and Miller, 1997; Nelson et al., 2015), mainly due to the weakness of the interlayer bonds and the imbalanced charges (positively charged at the edges and negatively charged on the surface). The montmorillonite platelets tend to attract water molecules in to the gaps between platelets to equilibrate the imbalanced charges (Nelson and Miller, 1997). This creates expansion in the clay particle and is responsible for the volume expansion. In general practice, these montmorillonite clays are commonly known as bentonite (Nelson et al., 2015).

However, depending on the water attraction and the expansion process, the swelling mechanism of these clays have been recognised as having two main components as follows (Barshad, 1955):

- The expansion of the crystal lattice itself, as found in montmorillonite.
- The increase in volume due to the adsorption of water molecules between individual clay particles

The individual clay particles are distinguished with respect to a unit known as a clay micelle (see Figure 2.16. A clay micelle: Source (Nelson et al., 2015)). A clay micelle is defined as a unit that contains a negatively-charged (on the surface) clay particle surrounded by positively-charged cations (sodium and/or calcium ions) and water (hydrated or osmotic water) (Nelson et al., 2015).

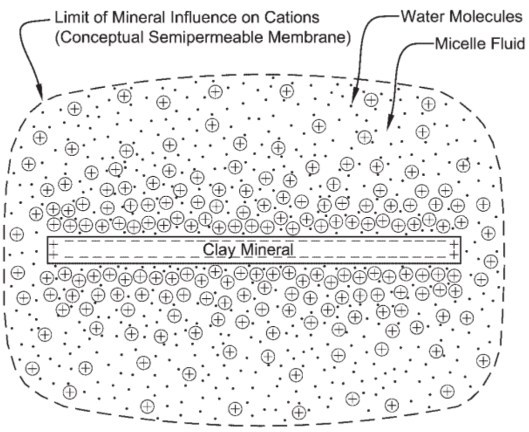

Figure 2.16. A clay micelle: Source (Nelson et al., 2015)

The expansion of the crystal lattice is identifiable and measurable by x-ray analyses while inter-micellar swelling is measurable from the total volume change of the sample. However, the significance of each component has been found to vary from soil to soil (Barshad, 1955).

In some studies, all the above swelling mechanisms involving the attraction of water molecules are categorised as a single swelling mechanism named physicochemical swelling (Terzaghi, 1931). In addition, another type of swelling mechanism is categorised as mechanical swelling, which involves the deformation of platy clay particles under suction loading and unloading (Terzaghi, 1931).

In summary, both the clay minerology and the characteristics of the clay micelles influence the swell potential of reactive clays, as the minerology defines the inter-platelet water attraction and the composition of the clay micelles (boundaries and type of ions dissolved) defines the expansion of the micelles (Nelson et al., 2015).

2.4.1.2 Structural composition

Under macro-structural composition, the initial condition (water content, void ratio and vertical stress), particle size and macro structure are considered, as these factors are easily determinable.

Since tight arrangements of reactive minerals produce higher reactive potentials, closer depositions of particles with more contact (at lower water contents and higher densities), referred to as dispersed or oriented structures, have been recognised to present higher reactive conditions than looser depositions (with higher water contents and lower densities), referred to as flocculated or random soil structures (Nelson et al., 2015). As shown in Figure 2.17. Variation of swelling properties with water content and dry density of soil (Chen, 1973), this has been experimentally observed by testing volume change properties at different water contents and densities (Chen, 1973).

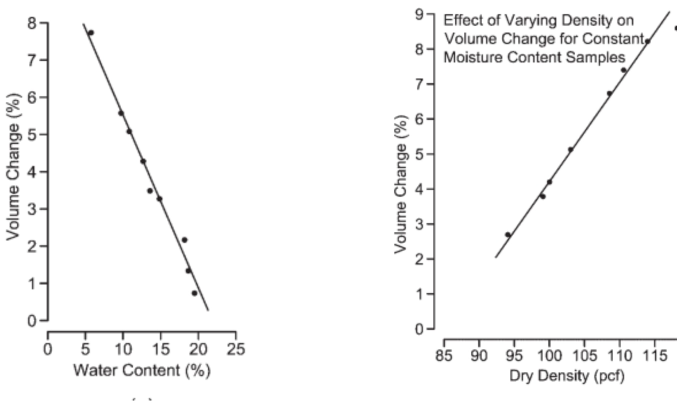

Figure 2.17. Variation of swelling properties with water content and dry density of soil (Chen, 1973)

2.4.2 Methods of identification of reactive clay soils

The identification of reactive clays generally relies on their micro- and macro-scale characteristics. These methods have been developed based on the following soil properties which are directly or indirectly influenced by the micro- and macro-scale aspects outlined in Section 2.4.1.

- Minerology
- Plasticity indices
- Soil suction characteristics
- Volume change indices

2.4.2.1 Mineralogical methods

Mineralogical methods of identifying reactive clays include X-ray diffraction (XRD), differential thermal analysis (DTA) and electron microscopy (Nelson et al., 2015). The principle of all these methods is to identify the clay minerals that cause soil reactivity (montmorillonite). The basis of each method is explained in Table 2.9.

Table 2.9. Mineralogical methods of identifying reactive clays (Nelson et al., 2015)

Method	Basis
XRD	Measuring basal plane spacing by the amount by which X-rays are diffracted around crystals
DTA	Heating the sample and thermograms are compared to those for pure minerals
Electron microscopy	Directly observing the clay particles. Qualitative identification is possible based on size and shape of the particles

Note that these mineralogical methods require special equipment and a robust knowledge of soil minerology, as identification is mainly based on visual comparison. An image of montmorillonite is shown in Figure 2.18. Electron micrograph of montmorillonite (Nelson et al., 2015).

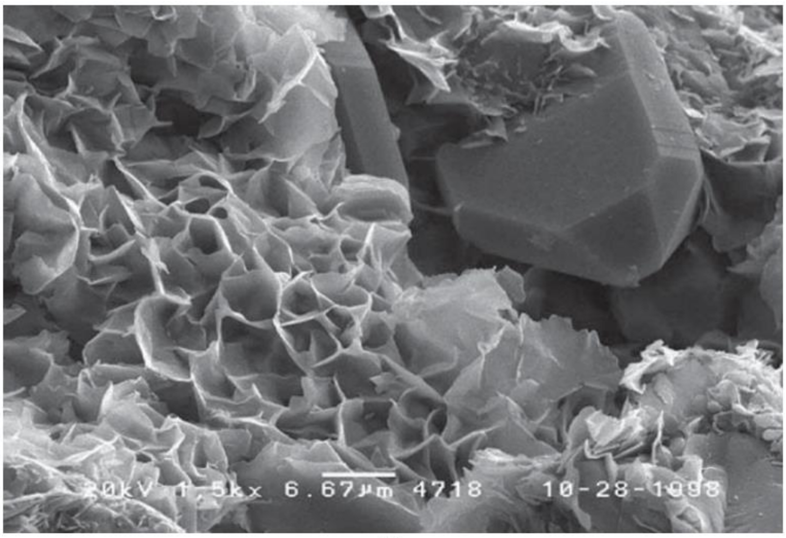

Figure 2.18. Electron micrograph of montmorillonite (Nelson et al., 2015)

2.4.2.2 Use of soil indices

Soil indices such as the plasticity index (PI), shrinkage indices and activity ratio (A_c) are relatively simple methods for the identification of reactive clays. The plasticity index is defined as the difference between the liquid limit and the plastic limit of the soil (Australian Standards, 2009b). Clay plasticity is dependent on the minerology as well as the composition of the clay micelles (Nelson et al., 2015). Therefore, the use of the plasticity index to indicate the reactivity of soil has been a successful method over many years (Holtz and Gibbs, 1956; Snethen et al., 1977; Covar and Lytton, 2001; Nelson et al., 2015). Table 2.10 compares the typical variations in measured plasticity indices of different expansive clays.

The table shows that the degree of expansion increases with higher plasticity indices, showing the higher reactiveness of high plasticity clays. This can be further explained by studying the presence of higher expansive clays (montmorillonite) at the higher plasticity end of the chart shown in Figure 2.19. Plasticity characteristics of clay minerals (Nelson et al., 2015).

Table 2.10. Variation of soil expansiveness with plasticity index

Degree of expansion	Plasticity index (%)	
	(Holtz and Gibbs, 1956)	(Snethen et al., 1977)
Very high	Greater than 35	
High	25 - 41	Greater than 35
Medium or Marginal	15 - 28	25 - 35
Low	Less than 18	Less than 25

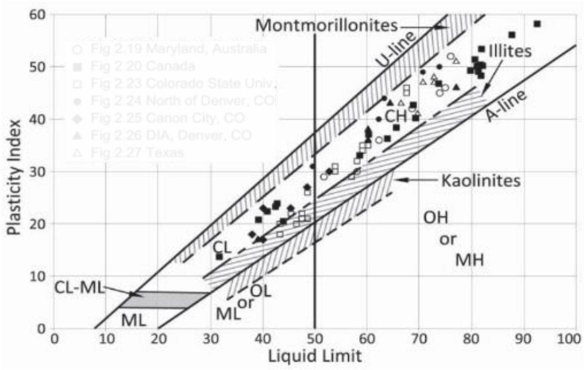

Figure 2.19. Plasticity characteristics of clay minerals (Nelson et al., 2015)

The activity ratio has been defined as the ratio between the plasticity index and the clay fraction of the soil (Skempton, 1953). Therefore, this can be thought of as a further extension of the previous classification system. As shown in Table 2.11, the activity ratio also shows an ascending trend with higher reactivity. The reported activity ratios of different minerals groups clearly show the influence of minerology on reactive behaviour.

Table 2.11. Activity ratios of different reactive soils (Skempton, 1953)

Soil classification	Activity Range	Typical clay minerals
Inactive (non-expansive)	Less than 0.75	Kaolinite
Normal	0.75 – 1.25	Illite
Active (higher reactive potential)	Greater than 1.25	Montmorillonite

2.4.2.3 Soil suction-based methods

In addition to the above methods, soil-suction characteristics have been also correlated with soil reactivity (Thompson and McKeen, 1995; Rao et al., 2011). As the soil suction governs water absorption and retention in the soil skeleton, comparisons of swelling parameters with suction at optimum moisture content of several soil samples have shown that the soil volume change due to its reactivity increases in samples with higher suctions (Rao et al., 2011) (see Figure 2.20. Variation of free swell index with soil suction at optimum moisture content (Rao et al., 2011)). However, this method has been identified as a time-consuming process from sample preparation to obtaining results.

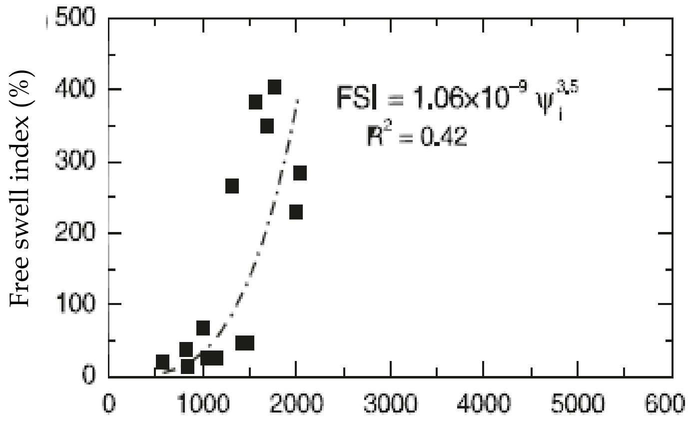

Figure 2.20. Variation of free swell index with soil suction at optimum moisture content (Rao et al., 2011)

2.4.2.4 Volume measurement-based methods

The other most common methods of identifying reactive soils are volume measurements and corresponding indices. Three common procedures are explained below.

- Shrink-swell index (I_{ss}) is a simple and common practice of identifying reactive potentials of expansive clays (Fityus et al., 2005; Jones and Jefferson, 2012). This index is calculated by measuring the swell component (one-dimensional swell inside a consolidation ring) and the shrinkage component (axial shrinkage of an unrestrained core shrink sample) of the soil separately. The calculation of I_{ss} , as given in AS1289.7.1.1 (Australian Standards, 2003a), is shown in Equation 2.1.

$$I_{ss} = \frac{\varepsilon_{sh} + \frac{\varepsilon_{sw}}{2}}{1.8} \qquad \text{Equation 2.1}$$

where, ε_{sh} is the axial shrinkage of the core (in %) and ε_{sw} is swell strain component (in %). Table 2.12 shows typical ranges of free swell indices in different reactive soils.

Table 2.12. Comparison of shrink-swell indices (in strain % per pF)

AS2870 Site classification	I_{ss} (Peck et al., 1992)	I_{ss} (Li et al., 2014)
Class S (slightly reactive)	0.8 – 1.7	
Class M (moderately reactive)	1.7 – 3.3	
Class H (highly reactive)	3.3 – 5.8	5 – 6
Class E (extremely reactive)	Greater than 5.8	6 - 8

- The free swell index (FSI) is another method used to classify reactive soils (Sridharan and Prakash, 2000; Nelson et al., 2015). FSI is defined by measuring the volume of a soil sample (dry sieved) in water and kerosene oil and calculating the ratio as shown in Equation 2.2 (Bureau of Indian Standards, 1977).

$$FSI = \frac{Volume\ in\ water - Volume\ in\ kerosene\ oil}{Volume\ in\ kerosene\ oil} \times 100 \qquad \text{Equation 2.2}$$

As the soil volume increases in water due to its reactiveness, the free swell index becomes higher for expansive soils. Table 2.13 shows typical ranges of free swell indices in different reactive soils.

Table 2.13. Typical FSI values of different reactive soils (Nelson et al., 2015)

Free Swell Index (FSI)	Expansion Potential
Less than 20	Low
20 – 35	Medium
35 – 50	High
Greater than 50	Very high

- The expansion index is another volume measuring method that involves monitoring the volume change (measured as the height change) of a wet soil specimen (degree of saturation 40 to 60%) placed in a metal ring under a small confining pressure (6.9 kPa) for about 24 hours (ASTM International, 2003a). The index is calculated as shown in Equation 2.3.

$$Expansion\ Index = \frac{Final\ thickness - Initial\ thickness}{Initial\ Thickness} \times 1000 \qquad \text{Equation 2.3}$$

The following table shows the typical ranges of expansion indices in different soils.

Table 2.14. Expansive index ranges for different reactive soils

Expansion Index	Expansion Potential
0 – 20	Very low
21 – 50	Low
51 – 90	Medium
91 – 130	High
Greater than 130	Very high

2.4.3 Constitutive behaviour of unsaturated expansive clays

The constitutive behaviour of any type of soil is important for the mechanical analysis of its behaviour under applied and natural loadings. Until the principle of effective stress was introduced (Terzaghi, 1936; Bishop, 1959), the use of an appropriate state variable(s) to explain constitutive behaviour was a challenging task in soil mechanics. Although the effective stress concept has been a significant achievement for the analysis of saturated soil (two-phase soil: solid skeleton and pore water), the most appropriate state variables to explain the behaviour of unsaturated soils (three-phase soil: solid skeleton, pore water and pore air) has been the subject of debate over the years and various approaches are used, as discussed below.

2.4.3.1 Nature of constitutive models available for unsaturated soils

In early stages, the effective stress was identified as the major state variable (similar to saturated soils) to explain the deformation of unsaturated soils (Bishop, 1959), as expressed in Equation 2.4.

$$\sigma' = \sigma - u_a - \chi(u_w - u_a) \qquad \text{Equation 2.4}$$

where, σ is the total stress, σ' is the effective stress and u_a and u_w are pore air and pore water pressure respectively. The range of the χ parameter has been considered as being from 0 to 1 ($\chi = 1$ for saturated soils). However, the use of effective stress as a single-state variable is controversial, as a unique relationship between soil deformation and effective stress has not been found for many unsaturated clayey soils, except soils with high degrees of saturation of 85% or above (Jennings and Burland, 1962). In recent years, the weaknesses of this approach have been redressed by considering the χ parameter as a function of suction $(u_w - u_a)$ and this has been verified by several experimental results (Khalili and Khabbaz, 2002; Loret and Khalili, 2002).

As an alternative to the above method, the use of two independent state variables, net stress $(\sigma - u_a)$ and matric suction $(u_w - u_a)$, has been also considered for unsaturated soils (Bishop and Blight, 1963; Fredlund and Morgenstern, 1976; Alonso et al., 1990). The proposed constitutive models have been tested with various clay samples and reasonable agreements have been found between predicted and measured deformations, and the methods have been further improved by considering non-linearities and hysteresis.

In addition to the above conventional methods of determining deformation of unsaturated soils, a novel method has been proposed with the new state variables of net stress $(\sigma - u_a)$ and moisture ratio (e_w), which the product of gravimetric moisture content and specific gravity (Kodikara, 2012). This method has been verified for experimental results of compacted unsaturated clays and the proposed state variables are conveniently measurable with simple laboratory tests (unlike suction measurements).

Since both net stress and suction (either combined or independently) are governing variables in all the above models, the constitutive behaviour (only volumetric behaviour is referred to here) has been mainly expressed in three-dimensional space. The volume change axis is usually represented by the void ratio (e). Net stress $(\sigma - u_a)$ is denoted as 'p'. The other axis is represented by suction $(u_w - u_a = s)$ in some models (Alonso et al., 1990), while it is used as moisture ratio (e_w) in the recent MPK framework (Kodikara, 2012). The constitutive behaviour is explained for both net stress changes (loading curves) and suction or moisture changes (drying-wetting cycles) and the loading paths are described in p - s space (Alonso et al., 1990; Loret and Khalili, 2002) or loading-wetting space (Kodikara, 2012).

2.4.3.2 Extension of unsaturated soil constitutive models for expansive soils

In addition to macro-structural deformation, which is considered in constitutive models for unsaturated soils, micro-structural deformations have been also considered in models for unsaturated expansive soils (Gens and Alonso, 1992; Alonso et al., 1999). It has been recognised that the micro-structural behaviour that is mainly due to the physicochemistry of clay minerals is independent of the macro-structural behaviour, but the reverse is not always true. Further, micro-structural volume change has been considered as reversible (elastic) for most cases (Alonso et al., 1990).

This micro- and macro-structural volume changes can be explained using the diagram in Figure 2.21. Micro- and macro-structural behaviour of expansive clays (Alonso et al., 1999) .

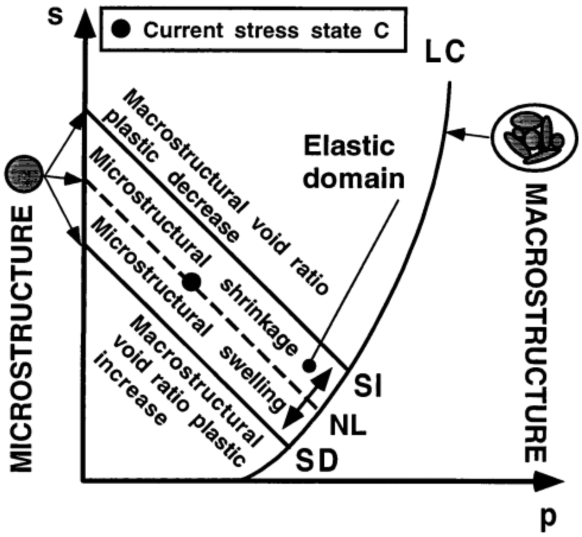

Figure 2.21. Micro- and macro-structural behaviour of expansive clays (Alonso et al., 1999)

In the above figure, s, p, NL, SD, SI and LC denote the suction, net stress, neutral line, suction decrease, suction increase and loading collapse yield curve, respectively. Micro-structural swelling has been identified as a function of the summation of suction and net stress ($s + p$) and the micro-structural strains are therefore zero along the neutral line (constant $s + p$ line) (Gens and Alonso, 1992). With a slight suction change (moisture change) the current micro-structural state can change to swelling or shrinkage (a reversible change) that affects the macro-structure, causing macro-structural deformation (an irreversible change). The starts of these irreversible deformations are represented by the SD and SI lines in Figure 2.21. Micro- and macro-structural behaviour of expansive clays (Alonso et al., 1999) . The LC line is the yield surface for increasing net stress (loading).

This concept can be further explained as shown in Figure 2.22. Total and micro-structural volume changes (Gens and Alonso, 1992) . As the suction decreases from the initial states (A, B, and C), the total volume change is equal to the reversible micro-structural change in the first phase (samples A and B). Then the irreversible macro-structural strain change starts when the suction decreases to the initial NL. From there, the total volume change is composed of both macro- and micro-structural changes (Gens and Alonso, 1992).

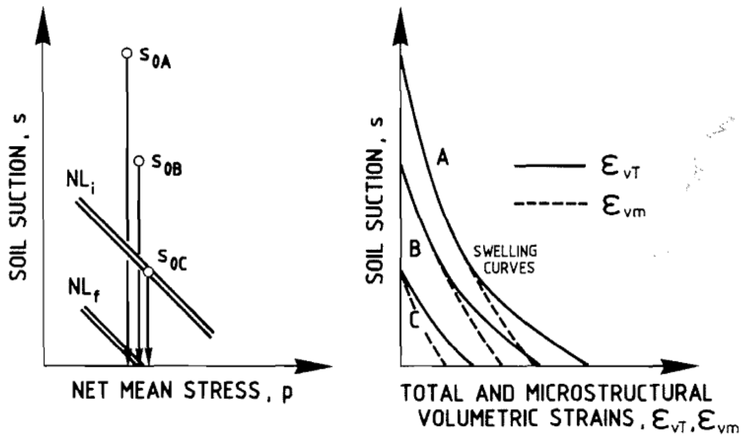

Figure 2.22. Total and micro-structural volume changes (Gens and Alonso, 1992)

2.4.3.3 Environmentally-stabilised expansive soil concept

As a further extension to the previously explained constitutive behaviour of expansive clays, the environmentally-stabilised expansive soil concept was established after observing fully reversible volume changes in the space of void ratio vs. water content after reaching a natural equilibrium (Tripathy et al., 2002; Gould et al., 2011b; Kodikara, 2012). It has been noted that the soil reaches this natural equilibrium state after undergoing several wet-dry cycles (about 4 cycles in some experiments).

Therefore, this concept is a convenient way of determining the volume changes of natural expansive soils that have undergone a number of wet-dry cycles. In addition, these equilibrium swell shrink paths have been found to be unaffected by the initial conditions (dry density and water content) of the soil, whilst they are affected only by the surcharge pressure (Tripathy et al., 2002). A set of example test results of naturally-stabilised soil volume changes is illustrated in Figure 2.23. It can be seen that since these equilibrium paths are nearly parallel to the saturated line, the gradient is similar to the gradient of the saturation line in the given space.

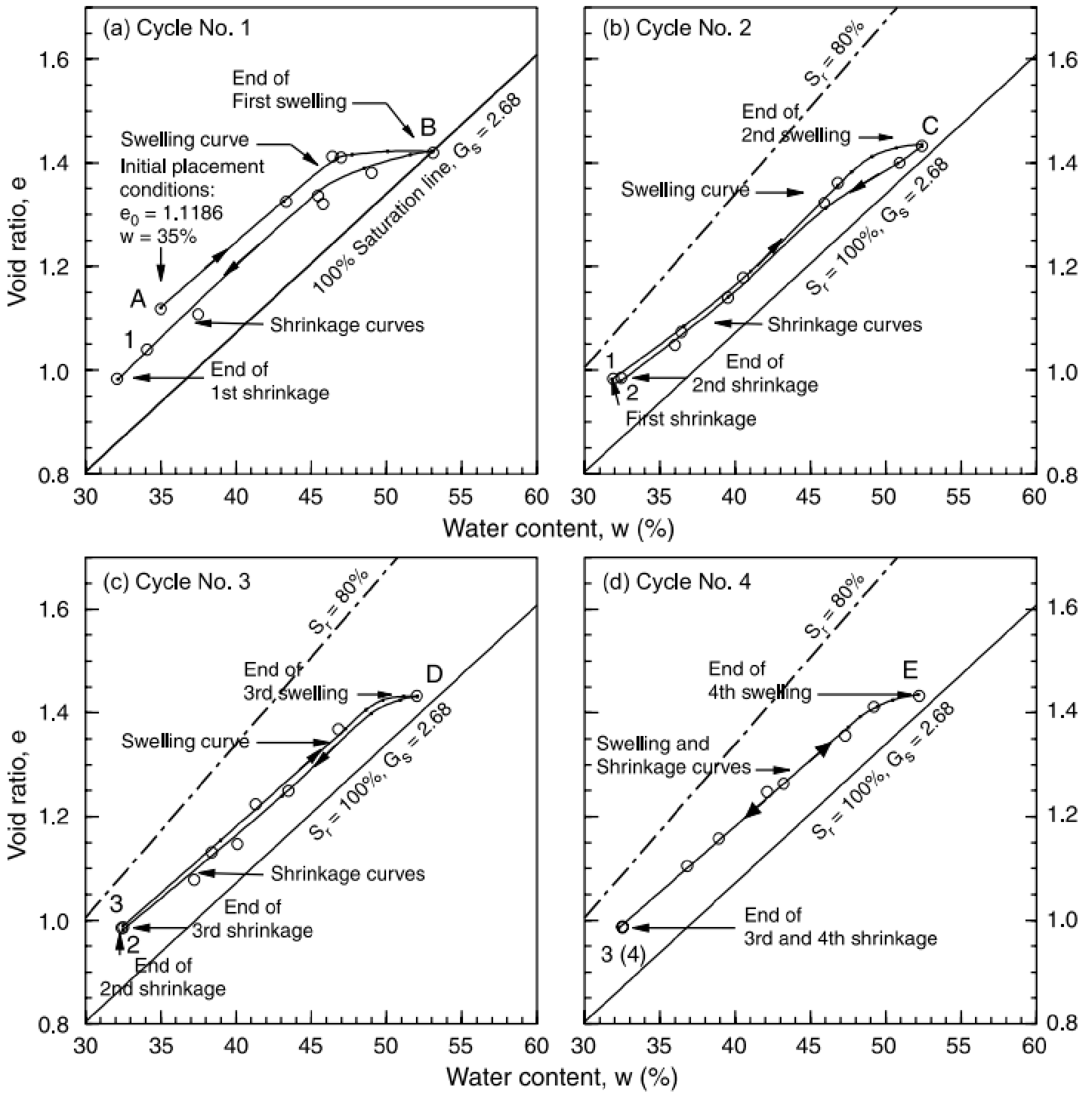

Figure 2.23. A set of test results of environmentally stabilised volume change curves: Source (Tripathy et al., 2002)

Later, this concept was further developed to a complete constitutive surface by considering the effect of net stress change (Gould et al., 2011b). In this model, the soil volume change is formulated into a surface which is dependent on both the water content and the net stress of the soil. This surface is shown in Figure 2.24. Void ratio (e) – water content (w) – net stress (σ) surface for environmentally stabilised expansive clays: Source (Gould et al., 2011b) . This environmentally-stabilised expansive soil concept has been used in numerical analyses of ground movements in natural expansive soil-related problems in the past (Gould, 2011). Therefore, this volumetric constitutive behaviour is used in the present study.

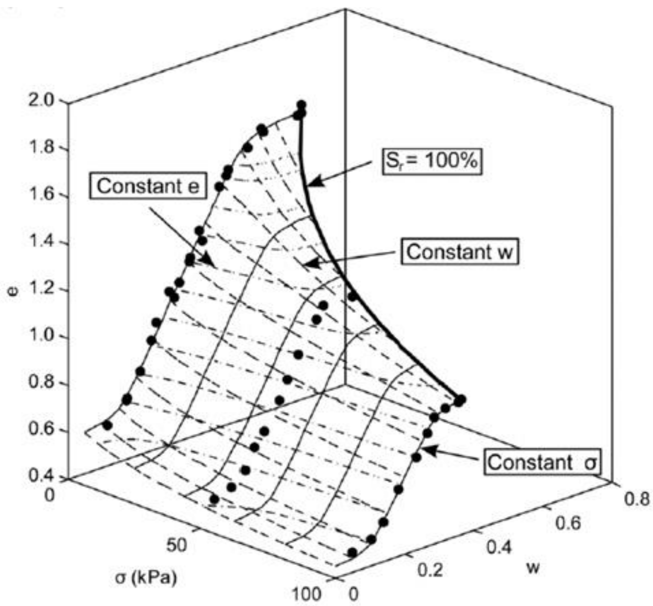

Figure 2.24. Void ratio (e) – water content (w) – net stress (σ) surface for environmentally stabilised expansive clays: Source (Gould et al., 2011b)

2.4.4 Reactive clay sites in Melbourne

The surface soil in a significant area in the northern and western suburbs of Melbourne has been identified as reactive basaltic clay weathered from basalt rock of newer volcanic formations (Peck et al., 1992; Srithar, 2014). The thickness of this reactive clay varies from a shallow depth to more than 10 m. Figure 2.25. Geology around Melbourne (Geological Survey of Victoria, 1974) shows the predominance of these newer volcanic formation soils in the western part of Melbourne.

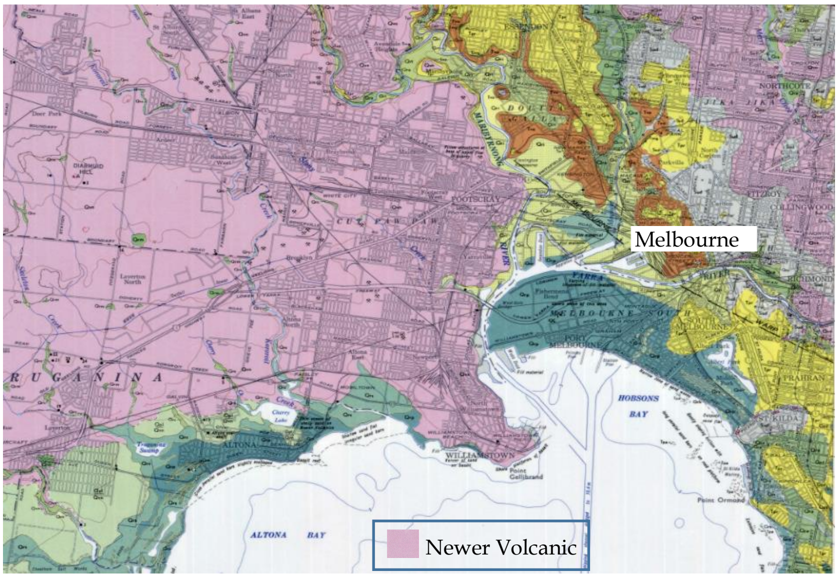

Figure 2.25. Geology around Melbourne (Geological Survey of Victoria, 1974)

These residual soils have been reported as grey or greyish-brown high plasticity heavy clays that mostly contain montmorillonite with relatively low kaolin and mica clay contents (Dahlhaus and O'Rourke, 1992). The basic engineering properties of these soils are shown in Table 2.15.

Table 2.15. Engineering properties of Melbourne's basaltic clays (Srithar, 2014)

Property	Typical Range	Comments
Liquid limit (%)	50 to 100	Typical ranges; some values may be outside these ranges
Plastic limit (%)	20 to 40	
Plasticity index (%)	30 to 80	
Linear shrinkage (%)	15 to 25	
Shrink-swell index (% strain/pF)	3 to 8	
Activity	0.8 to 0.9	Based on limited data
Optimum moisture content (%)	15 to 30	Standard Compaction test
Maximum dry density (t/m3)	1.4 to 1.8	
Undrained shear strength (kPa)	50 to 200	Strength and stiffness parameters are highly dependent on moisture content of the soil and the strength and stiffness can be lower if the soil is wet
Effective friction angle (deg)	25 to 28	
Effective cohesion (kPa)	5 to 20	
Young's modulus (MPa)	15 to 60	

A map prepared by analysing a number of borehole investigations (see Figure 2.26. Presence of reactive (expansive) soils around Melbourne (Gould, 2011)) over the service areas of City West Water and South East Water shows that about 60% of the soils in this region are either very expansive or expansive (Gould, 2011). The different expansive soils were classified according to the soil type and the Grant engineering classification codes (Grant codes) (Grant, 1972; Gould and Kodikara, 2008). The relationship between Grant cord description and soil classification in Figure 2.26 is explained in Table 2.16.

Table 2.16. Expansive soil classification from Grants codes (Gould, 2011)

Grant code description	Classification in Figure 2.26
Expansive soil	Very expansive (VE)
Mottled clay	Expansive (ME+EX)
Clay	
Silty soil	Slightly expansive (SE)
Sand	Stable (ST)

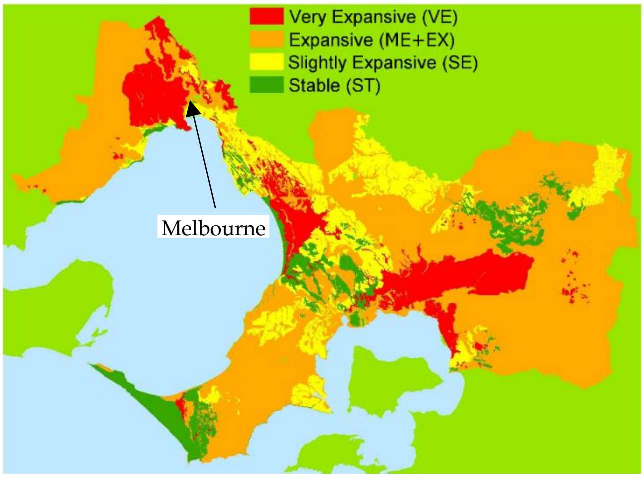

Figure 2.26. Presence of reactive (expansive) soils around Melbourne (Gould, 2011)

With the presence of reactive clays, property damage caused by reactive ground movements, including house wall cracks, road pavement damage and pipe failures are frequently reported in the western suburbs. Some examples can be seen in

Figure 2.27. Examples of structural damage due to reactive ground movement in Melbourne.

Figure 2.27. Examples of structural damage due to reactive ground movement in Melbourne

2.4.4.1 Reactive soil site classifications: AS2870

Because of this problematic behaviour of reactive soils, the identification and classification of building sites before construction begins is important. The most common way of classifying these sites is the recommendations given in the Australian standard for residential slabs and footings, AS2870 (Australian Standards, 2011).

One way of classifying a site is based on the calculated characteristic surface movement (y_s). The characteristic surface movement, y_s is defined in AS2870 as the movement of the surface of a reactive site caused by moisture changes from extreme dry to extreme wet condition in the absence of a building and without consideration of load effects (Australian Standards, 2011).

Equation 2.5 explains the y_s calculation:

$$y_s = \frac{1}{100}\sum_{n=1}^{N}\left(I_{pt}\,\Delta u\, h\right)_n$$ Equation 2.5

where, I_{pt} is the instability index in % per pF (pF is defined as log negative [hydraulic head in centimetres], or by 1.01 + log[suction in kPa] (Fityus et al., 2005)), Δu is the average soil suction change in the layer under consideration (in pF), h is the thickness of the layer under consideration and N is the number of layers within the design depth of suction change.

The soil reactivity is measured by the instability index, which gives the vertical strain (as a %) per unit suction change (in pF) and the soil moisture variation is used as the suction change. In this method, a linearly-varying suction change profile is considered with the possible effects of bedrock and the groundwater table (as shown in Figure 2.28. Linear suction profiles (Australian Standards, 2011) .

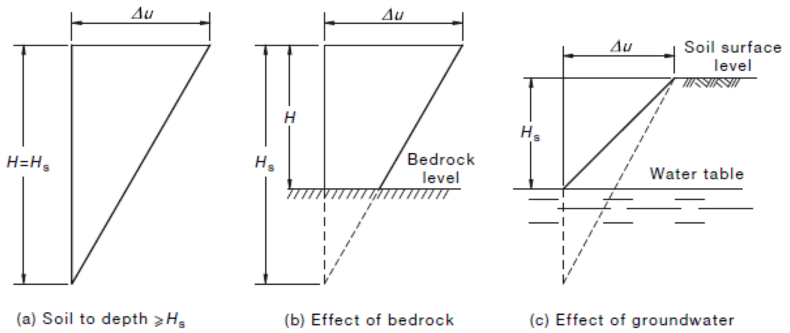

Figure 2.28. Linear suction profiles (Australian Standards, 2011)

As the figure indicates, the maximum depth of consideration is defined as the maximum depth of suction change (H_s) and when the bedrock or the water table is shallower than H_s, the soil above the bedrock is considered for the calculation. This maximum depth (H_s) is defined as 2.3m for temperate climate zones of Melbourne where most of the reactive soil regions are present. The instability index (I_{pt}) is recommended to be calculated from the shrink-swell index of the soil. The standard procedure of the shrink-swell index test is explained in AS1289.7.1.1 (Australian Standards, 2003a). The calculated y_s is used to classify the soils, as shown in Table 2.17.

Table 2.17. Expansive soil site classifications (Australian Standards, 2011)

y_s (mm)	Classification
$0 < y_s \leq 20$	S (slightly expansive)
$20 < y_s \leq 40$	M (moderately expansive)
$40 < y_s \leq 60$	H1 (highly expansive)
$60 < y_s \leq 75$	H2 (highly expansive)
$y_s > 75$	E (extremely expansive)

2.4.4.2 Ground movement observations

The characteristic surface ground movements that are used for classification purposes were discussed in the previous section. However, the actual ground movements and their seasonal variations can vary, as evident from the measured actual ground movements at different reactive soil regions in Melbourne (Holland and Walsh, 1980; Chan, 2013; Karunarathne et al., 2014; Srithar, 2014).

Ground movements measured by placing precise levelling points at an experimental slab monitoring site in Sunshine (H2 site with a seasonal heave of about 65mm) (Holland and Walsh, 1980) are shown in Figure 2.29. Seasonal ground movements at Sunshine (Holland and Walsh, 1980) . The figure shows that the seasonal swell soil movements (maximum of 20mm) start from the middle of the year and continue until the summer starts at the end of the year. Shrinkage (maximum of 30mm) movements start from the beginning of the summer. However, the seasonal movement changes yearly with the annual climatic conditions.

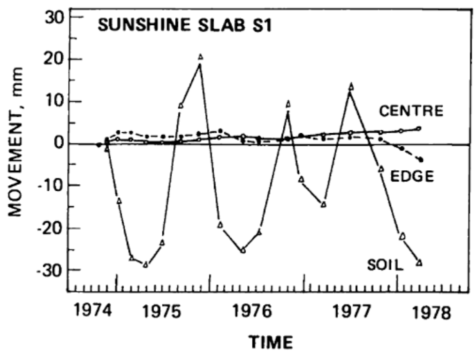

Figure 2.29. Seasonal ground movements at Sunshine (Holland and Walsh, 1980)

Another data set is presented in Table 2.18 which was measured using rod extensometers at another experimental site in Braybrook (Karunarathne et al., 2014). The seasonal variations show that the maximum swell and shrinkage movements at the ground surface are 26 and 19mm respectively. Showing a similar variation pattern to the previous dataset, the maximum swell movements are observed in the middle of the year (winter: June 2013) and the maximum shrinkages are in summer (January 2014)

Table 2.18. Seasonal ground movements at Braybrook (Karunarathne et al., 2014)

	Thickness change with respect to previous measurement (mm)							
Measured date	25 Mar 2013	20 Jun 2013	21 Aug 2013	21 Oct 2013	11 Dec 2013	29 Jan 2014	26 Feb 2014	01 Apr 2014
Total change (mm)	-1	26	-2	1	0	-19	-6	-3

The ground movements shown in Figure 2.30. Seasonal ground movements at Altona North (Chan, 2013) were measured using rod extensometers installed at a pipe monitoring site at Altona North (Chan, 2013). Seasonal ground movements at different depths show that the maximum movements near the ground surface (400mm depth) are in the range of 10 to 20mm during the period of measurement. The magnitude of the movements gradually decrease towards the deep layers.

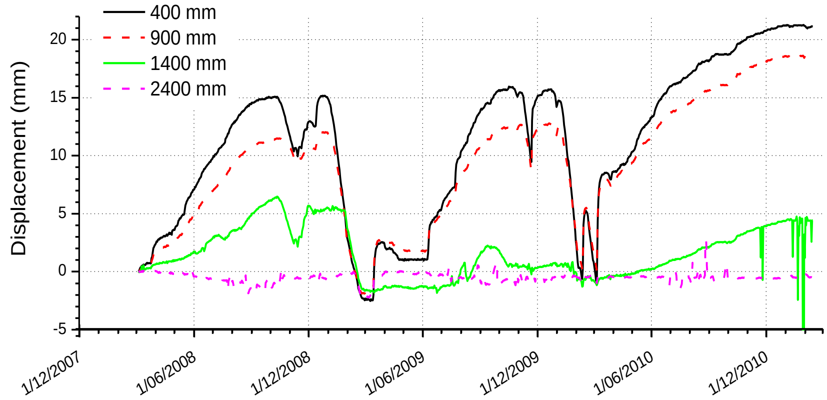

Figure 2.30. Seasonal ground movements at Altona North (Chan, 2013)

The depth variations of observed ground movements have been similarly presented by another researcher (Srithar, 2014) as shown in Table 2.19. These measurements are based on monitoring sites of residential slab experiments (Holland, 1978; Holland and Walsh, 1980). As these data show, the magnitude of seasonal movement is comparatively low below the 0.6m depth. This information is important for the present study as most pipes are buried in the zone from 0.6 to 1m deep (see Section 2.2.4). The movements are almost negligible after 1.2m.

Table 2.19. Seasonal swell measures at different Melbourne sites (Srithar, 2014)

Location	Seasonal heave (swell) (mm)			
	At surface	At 0.6m depth	At 1.2m depth	At 1.8m depth
Altona	31	3	0	Rock at 1.4m
Whittlesea	49	12	5	0
Broadmeadows	47	15	2	0
Keilor	24	0.3	0	0
Sunshine (middle)	54	10	0	0
Sunshine (east)	65	22	9	4
Sunshine (west)	47	12	2	0
Werribee	47	2	0	0

It is noticed that the swelling and shrinkage ground movement observations discussed in this section depend on the time at which the monitoring was begun. The observations started in dry periods (eg. Altona North observations) tend to show more swelling ground movements than shrinkage movements. However, all these data provide valuable information on the magnitude of seasonal ground movements (the difference between the minimum and maximum ground movement) in observed areas and depths

2.5 Soil Moisture Data and Availability

In addition to ground movement measurements, it is important to consider the variation in moisture content for the present research. In this section, the availability of moisture data and the nature of Melbourne's seasonal soil moisture variations are discussed. The soil moisture data are generally available in three categories: measured, estimated and remotely-sensed data.

2.5.1 Field measurements

Field measurements represent direct observations from field sites. Indirect ways of determining soil moisture contents, such as neutron scattering, gamma-ray attenuation, in-situ electromagnetic techniques and hygrometric techniques (Schmugge et al., 1980), are used in preference to direct measurement in laboratory measurements (Australian Standards, 2005). This is mainly due to the less work involved in indirect measurements as samples are not required. A summary of these indirect measurement methods are presented in Table 2.20.

Of these indirect methods, the neutron scattering method (using neutron probes) has been frequently used for moisture measurements in Australia (Li and Ren, 2010; Kodikara et al., 2013; Fityus et al., 2011). In this indirect method, calibration is required prior to obtaining soil moisture contents to correlate the raw measurement of the equipment (neutron count) with volumetric soil moisture contents (Kodikara et al., 2013). An example dataset of neutron probe soil moisture measurements is presented in Figure 2.31. The figure shows the average variation of continuous soil moisture measurements carried out at several sites in the western suburbs of Melbourne (Kodikara et al., 2013) from June 2009 to March 2014. Moisture data are presented for four different depth levels (0-250mm, 250-750mm, 750-1000mm and 1000-1400mm).

Table 2.20. Summary of indirect moisture-measurement techniques (Schmugge et al., 1980)

Method	Description
Neutron scattering	Moisture contents are determined by emitting neutrons with high energy and measuring the thermalised neutron density (neutron count) after collisions with nuclei of atoms and heating. Suitable for rapid and deep moisture variation measurements.
Gamma-ray attenuation	Moisture contents are determined considering the scattering and absorption of gamma-rays which are related to the density of matter in their path (density is a function of water content). Measurements can be taken without opening the soil. However, gamma-ray penetration is limited to a small distance (1 to 2cm).
In-situ electromagnetic techniques	Moisture contents are determined by considering the effect of moisture on electrical and magnetic properties of the soil. The dielectric properties can be measured as either soil resistivity or capacitance.
Hygrometric techniques	The relationship between moisture content and the relative humidity in the soil medium is used to determine the moisture content. Several types of hygrometers are used (electrical resistance, capacitance, piezoelectric sorption, infrared absorption etc.)

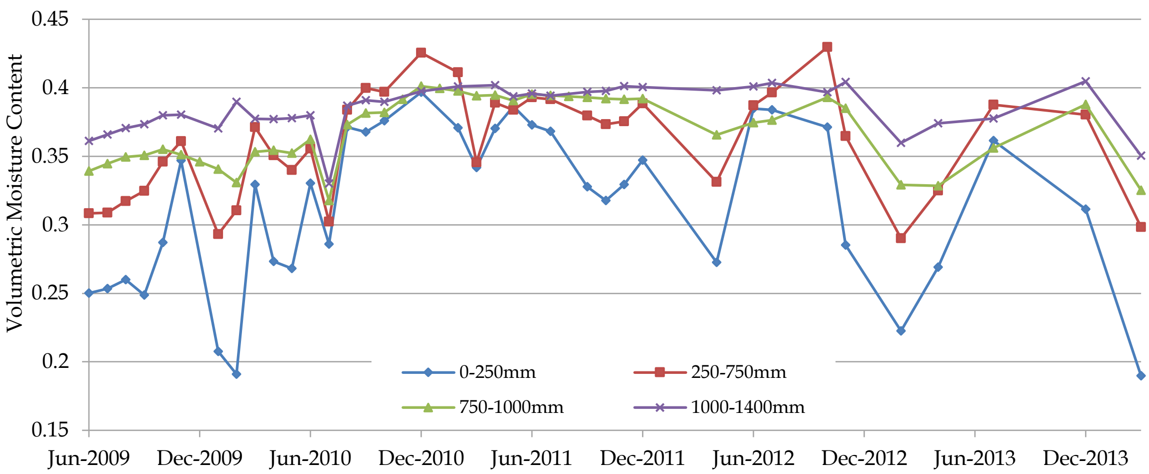

Figure 2.31. Average soil moisture variations of western suburbs of Melbourne (Kodikara et al., 2013)

As can be seen in Figure 2.31, the surface moisture fluctuation (0-250mm) is significantly higher than the deep moisture fluctuation (1000-1400mm). This is the reason for the lower swell-shrink movements at deeper levels. However, the pipe level (750-1000mm) moisture variation shows that the volumetric moisture contents vary between 0.31 and 0.41 (with a mean value of 0.36). Therefore, this limited measurements can be used to roughly estimate the maximum soil moisture changes at pipe level, which are generally about 0.05 (5%) around the mean value (this gives 5% drying and 5% wetting).

The above observation of 5% drying and 5% wetting moisture changes from the mean value at the pipe depth was also observed in another dataset obtained using neutron probe measurements (as shown in Figure 2.32. Neutron probe moisture measurements at Maryland site (Li and Ren, 2010)) in Maryland, Newcastle (Li and Ren, 2010). The wet and dry extreme moisture profiles (at an open grass area and near a tree) of the monthly measurements show about 10% moisture content change in the 0.75 to 1m depth range, which is similar to the Melbourne measurements. However, the mean moisture content appear to slightly vary compared with the Melbourne observations (0.36).

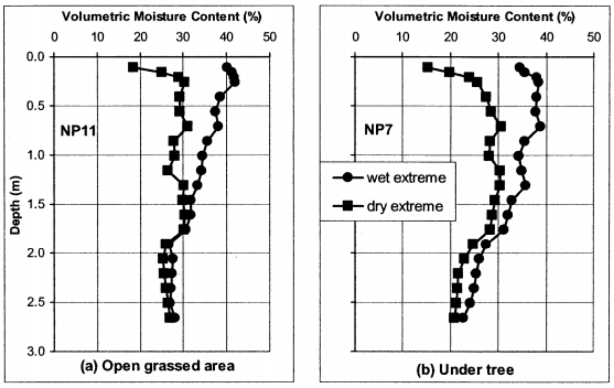

Figure 2.32. Neutron probe moisture measurements at Maryland site (Li and Ren, 2010)

The third set of neutron probe soil moisture measurements, which were measured in Braybrook, Victoria from 2013 to 2015 (Karunarathne, 2016), are shown in Figure 2.33. These data show that the moisture content around the pipe depth (0.75m) changes from 34% to 40%. In comparison to other two observations, this dataset shows a slightly less moisture content variation as 3% for wetting and 3% for drying around the mean volumetric moisture content, which is approximately 37% in this dataset.

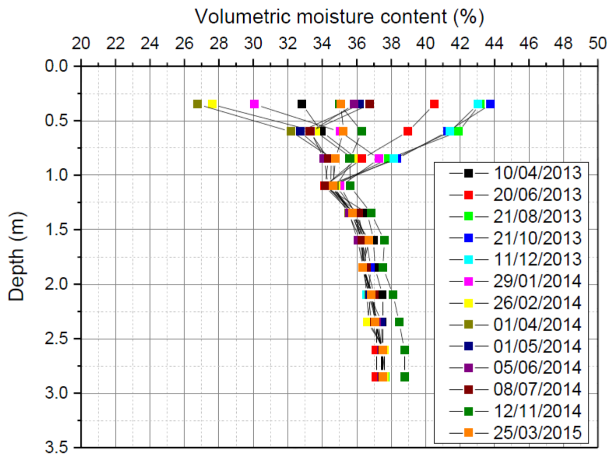

Figure 2.33. Soil moisture measurements at Braybrook (Karunarathne, 2016)

2.5.2 Soil-moisture estimation models

As the above field measuring methods require specialised equipment and regular measurements, they are costly for large-scale and long-term soil moisture observations. Therefore, soil water estimation models have been considered as a convenient method for large-scale moisture data. These models basically involve the mass or energy balance principle of a defined soil column, as the water content in the soil column is a function of precipitation, surface runoff, net lateral sub-surface flow, evaporation or condensation, transpiration, capillary rise from lower levels and percolation (Schmugge et al., 1980). Basically these parameters represent the water accumulation and dispersion of the defined soil column.

The above parameters have been incorporated in different models as either direct measurements or other environment /climate variables that affect these parameters. For example, the Joint UK Land Environment Simulator (JULES) model (Best et al., 2011; Clark et al., 2011) uses the following parameters to simulate the moisture content:

- Shortwave and longwave radiation at the surface
- Rainfall and snowfall

- Surface wind (vertical and horizontal components)
- Atmospheric temperature and specific humidity
- Surface pressure
- Surface type and vegetation

Based on the JULES model, a verified soil moisture estimation model has been developed at Monash University for the Melbourne metropolitan area as part of the Smart Water Fund Project (Smart Water Fund, 2015). This model has been prepared with a 1km x 1km grid (1km^2 resolution) and moisture contents are estimated on a daily basis. Figure 2.34Figure 2.34. A snapshot of the moisture model developed at Monash University (Smart Water Fund, 2015) shows a snapshot of the model which mostly shows drier moisture contents as the selected data are from late summer (March 2010).

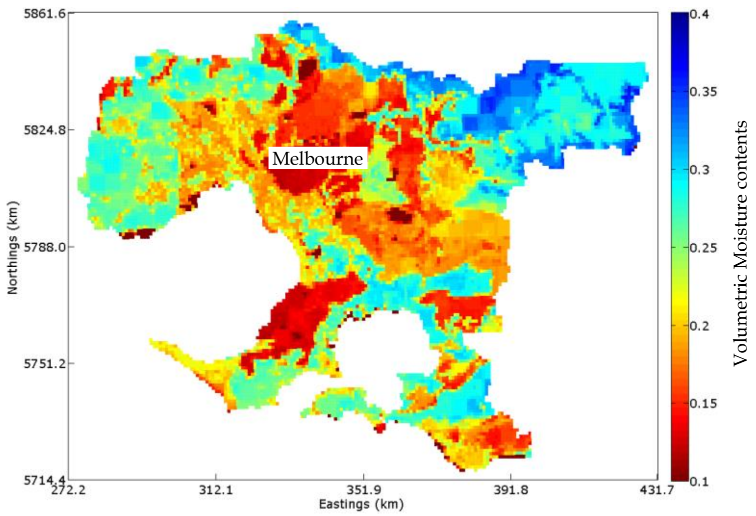

Figure 2.34. A snapshot of the moisture model developed at Monash University (Smart Water Fund, 2015)

A similar model has been published by the Bureau of Meteorology, Australia (BOM) for the whole of Australia based on a 5km x 5km grid (25km^2 resolution) (Bureau of Meteorology, 2017b). This model has been developed as the Australian Water Resources Assessment Landscape Model (AWRA-L) (Viney et al., 2014; Hafeez et al., 2015; Smith et al., 2015) and daily moisture data are produced based on soil cover, precipitation, air temperature and solar radiation data. Since the data are available and accessible online (Bureau of Meteorology, 2017b) a snapshot is shown in Figure 2.35. The moisture values are presented as percentages of 'available water content' and the applicability these data is discussed in Chapter 7.

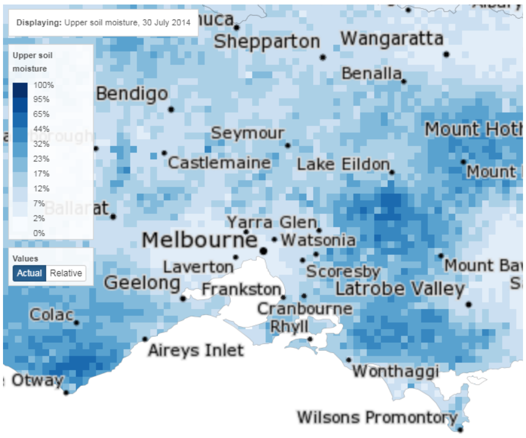

Figure 2.35. A snapshot from the BOM moisture model (Bureau of Meteorology, 2017b)

The availability of moisture data for different soil layers (at different depths) is another advantage of these models. However, the low resolution (single moisture values for large areas) is a disadvantage of such models.

In addition to the above large-scale models, some other numerical simulations have been reported in the literature, in which the soil-atmosphere interaction is modelled to determine the time variations of soil moisture contents (Rajeev et al., 2012; Karunarathne, 2016). As the model estimations have been verified with field moisture observations at Melbourne sites, these models are also available for the soil moisture estimation of Melbourne soils.

2.5.3 Remote-sensing method

This method is based on the measurement of the electromagnetic energy that is either reflected or emitted from the soil, as the intensity of this radiation is known to vary with soil moisture, depending on the dielectric properties or/and temperature of the soil (Schmugge et al., 1980). These radiations have been identified in different ranges (wave lengths), including reflected solar, thermal infrared, active and passive microwave. The advantages and disadvantages of this method depend on the resolution, scanning swath and the interaction with local vegetation and cloud cover (for satellites).

This type of remote sensing technique which is also being validated with Australian soil moisture data, is currently being developed as a global Soil Moisture Active–Passive (SMAP) satellite project (Kim et al., 2017; Yee et al., 2016).

2.6 Studies of Pipe Deformation in Reactive Soils

The influence of soil reactivity and seasonal climate variations on past pipe failure patterns was discussed in Section 2.3.3.2, based on previous statistical data analyses. This section reviews previous studies that provide physical evidence of the influence of reactive soil on pipes. Since some Melbourne pipes are buried at relatively shallow depths (see Section 2.2.4) in reactive soil zones and they are within the reactive zone depth (the active moisture zone) (see Section 2.4.4.1), the influence of reactive soil on pipes has been extensively considered for Melbourne pipes. Therefore, most of the recent studies are limited to Melbourne pipes, as discussed below.

2.6.1 Laboratory tests

As an initial attempt to physically observe the effects of reactive soil on a buried pipe, a laboratory model was developed at Monash University to measure the deformation of a buried pipe under soil swelling conditions (Chan, 2008; Gallage et al., 2011). In this test, a 2.18 m long polyethylene pipe with internal and outer diameters of 85 mm and 110 mm, respectively was buried in a box filled with expansive clay and the soil was subjected to progressive wetting. The wetting procedure involved applying water to the base of the box and allowing to raise the moisture content by the capillary effect. The pressure head at the base of the box has been gradually increased at certain time intervals to accelerate the wetting of soil. The measured pipe deflections are presented as in Figure 2.36, which clearly shows a parabolic pipe bending pattern as the ends are restrained at the edges of the box.

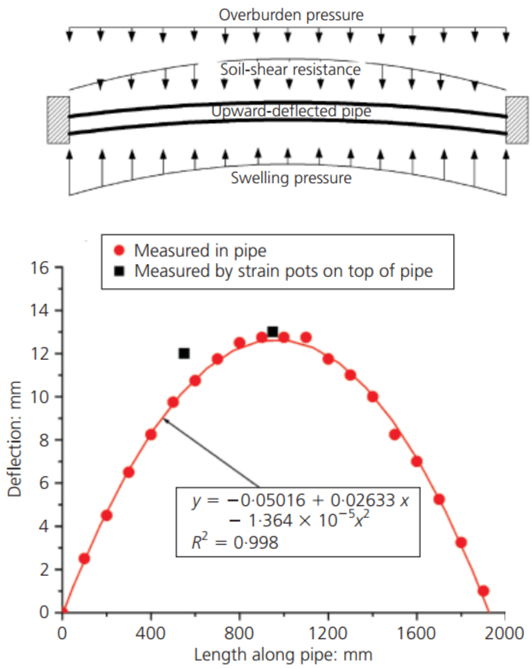

Figure 2.36. Observed pipe deflections in laboratory testing (Gallage et al., 2011)

The observed pipe deflection was explained as the result of swell pressures as the imposed swell pressure on pipes pushed the pipe upwards to create pipe bending.

This test result reflects the possible pipe deflections in reactive soil environments, as field pipes are generally under the same conditions with natural moisture variations and possible mechanical restraints. However, the deflections of cast iron pipes were expected to be lower than this, as cast iron is a less flexible material.

2.6.2 Field observations

The behaviour of buried pipes under reactive soil conditions was monitored by a research group at Monash University (Chan, 2013; Chan et al., 2015; Gould, 2011) in two reactive soil regions in Melbourne (Altona North and Fawkner). The deformation of a 100mm diameter cast iron cement-lined (CICL) pipe was monitored at Altona North and of a 150mm diameter cast iron gas pipe at Fawkner. These pipes were instrumented with thermocouples, thermal conductivity sensors, soil moisture sensors, strain gauges and earth pressure cells at different locations along the pipe at different depths. The Altona North pipe layout (a longitudinal section along the nature strip) is shown in Figure 2.37.

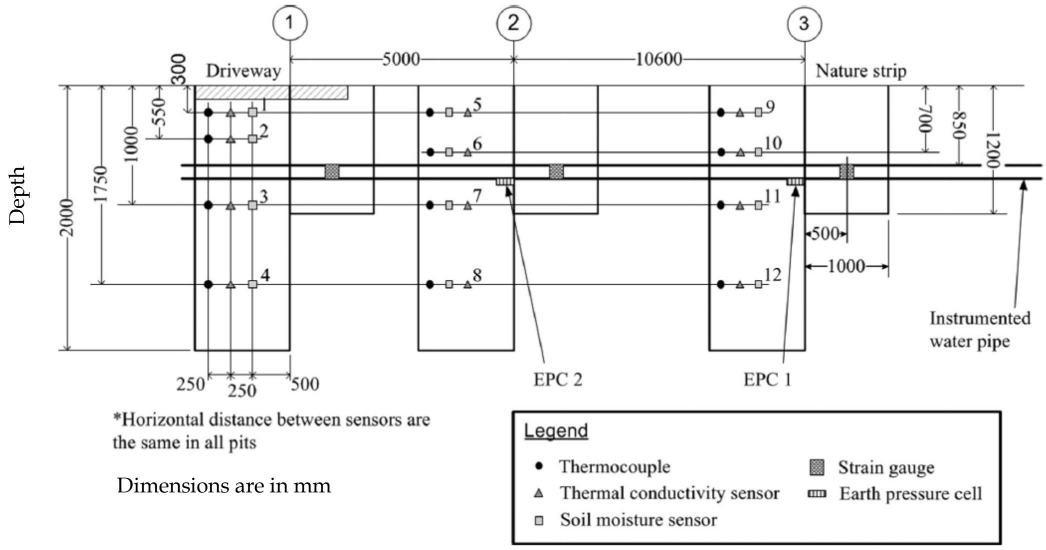

Figure 2.37. Pipe instrumentation section (along the nature strip) at Altona North (Chan et al., 2015)

At each measuring pit (①,② and ③ in Figure 2.37. Pipe instrumentation section (along the nature strip) at Altona North (Chan et al., 2015)), pipe strains (both longitudinal and hoop components), temperature, soil moisture and suction, and soil pressure were continuously monitored in addition to the climate measurements at each site. As the pipe strain observations at Altona North show in Figure 2.38, the pipe deformations at each measuring location demonstrate a clear relationship between soil moisture variations. The shown strains are in the form of flexural strains (difference of longitudinal strains at pipe top and bottom).

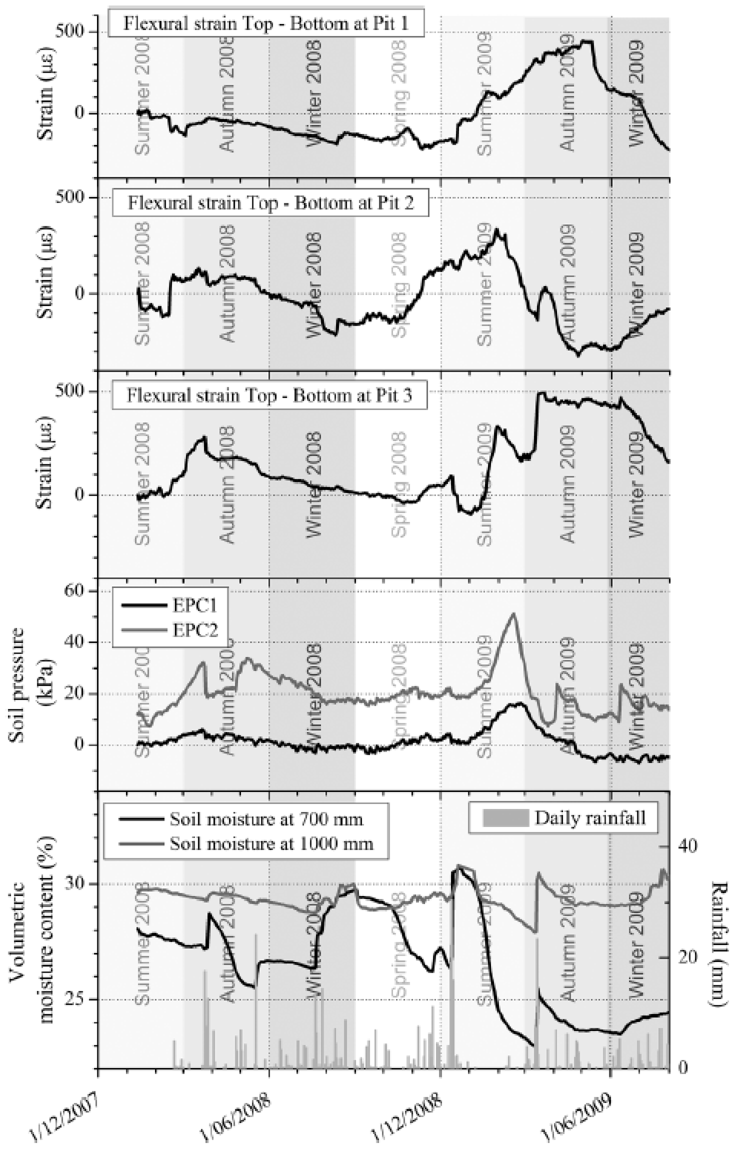

Figure 2.38. Pipe deformation, soil pressure and soil moisture content observations at Altona North (Chan et al., 2015)

Since pit ① is located under a driveway, it shows a different deformation pattern compared with the other two pits that are located under the grassed nature strip. This is possibly due to the restrictions under driveways, which are studied in detail in the present study (see Chapter 4). However, the accuracy of some of these measurements after April 2009 was doubted by the authors as some erratic data were observed (Chan et al., 2015).

The observed maximum strains are in the range of 500 $\mu\varepsilon$ (producing stresses around 20 MPa (Chan, 2013)), which are significantly lower than the strength of cast iron (Section 2.2.2.2). This is acceptable, as severe corrosion conditions were not observed on the tested pipes and a failure was not reported during the observation period.

2.7 Previous Attempts to Estimate Ground Movement-induced Pipe Stresses

Since the development of a comprehensive methodology to estimate longitudinal pipe stresses for broken back pipe failure analyses is the prime aim of the present study, previous studies related to the current work are discussed in this section. Both numerical and analytical methods have been used in stress determination.

2.7.1 Numerical models

In this section, numerical studies undertaken on simulated reactive soil and pipe interactions are discussed.

The laboratory experiment noted in Section 2.6.1 was modelled in a three-dimensional finite deference continuum program and the results were compared with experimental results (Rajeev and Kodikara, 2011). In this model, the reactivity of the soil was simulated by assuming a linear relationship between the linear shrinkage of the soil ($\Delta\varepsilon_{sh}$) and the gravimetric water content change (Δw) (Equation 2.6), and further assuming the soil moisture content change was the only factor affecting volume change.

$\Delta\varepsilon_{sh} = \alpha\, \Delta w$ Equation 2.6

The one-dimensional soil expansion coefficient (α) was calculated as in Equation 2.7 and used in the calculation of moisture change steps, as shown in Figure 2.39.

$\alpha = \frac{\alpha^* G_s}{3(1+e)}$ Equation 2.7

where, G_s is the soil specific gravity and e is the initial void ratio of the step. α^* is defined in Figure 2.39.

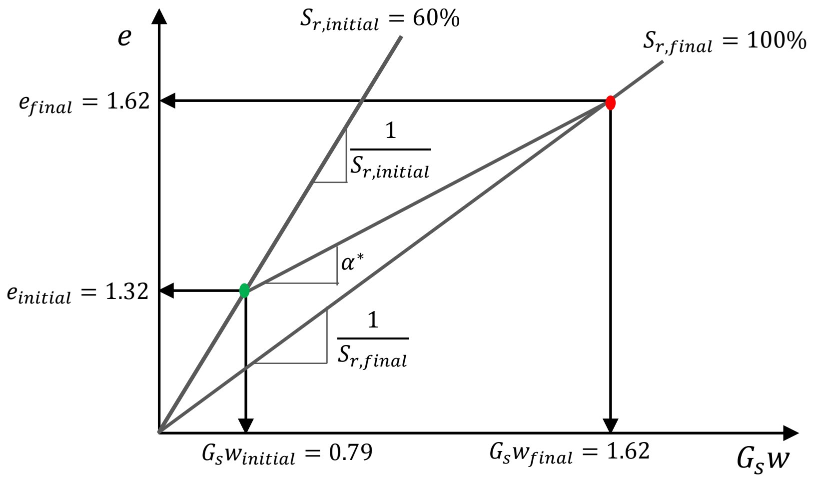

Figure 2.39. Calculation of soil expansion coefficient (Rajeev and Kodikara, 2011)

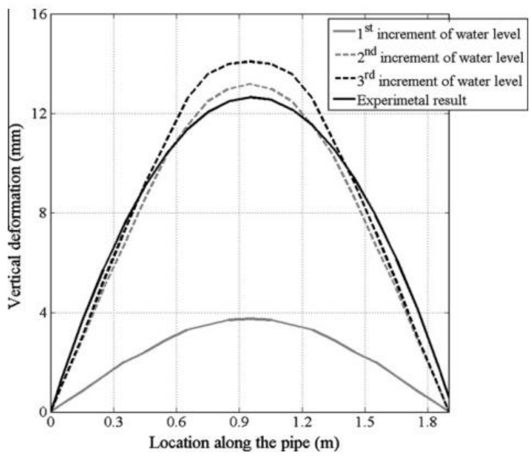

Figure 2.40. Comparison of experimentally and numerically observed pipe deformations: Source (Rajeev and Kodikara, 2011)

The interaction between the soil and the pipe was assumed to be a non-slip contact. Moisture increments were applied similarly to the laboratory experiments (Section 2.6.1) and the pipe deformations were compared, as illustrated in Figure 2.40.

The comparison in Figure 2.40 shows a good agreement between the numerical and experimental results. This result indicates the effectiveness of the selected linear relationship for soil volume changes, in addition to the simplicity of modelling controlled conditions of a laboratory test.

Another numerical simulation was found in the literature in an attempt to simulate the in situ pipe deformation monitored at the Altona North pipe site (Section 2.6.2) using a simplified method (Gould, 2011). In this model, the pipe-soil system was simplified into a problem of a beam on an elastic springs, as shown in Figure 2.41. This type of spring model has been used in other flexural analyses of buried pipes as a simplification (Rajani and Tesfamariam, 2004). The volumetric behaviour of soil was implemented in the springs by considering the behaviour of environmentally-stabilised soils (Gould et al., 2011b).

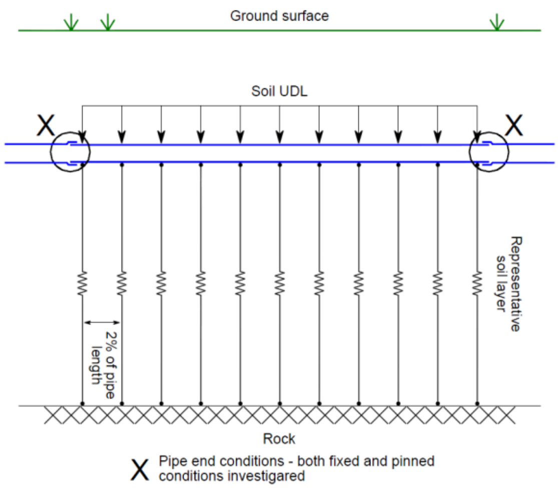

Figure 2.41. Simplified spring model (Gould, 2011)

The numerical simulation of a 20m long cast iron pipe section for field measured soil moisture variations showed significant over-estimations of the pipe stresses in comparison to the field values. The dependency of the results on the chosen boundary conditions was identified as the main reason for these pipe stress over-estimations.

Furthermore, the difficulty of defining true boundary conditions in the field was reported.

Both methods discussed in this section involve user-defined sub-routines available in commercial software for simulation of expansiveness of the soil. In addition, the simplifications made to the physical representations of pipe-soil system in these models were identified as a practical issue for further use of these models to simulate detailed field pipe problems.

2.7.2 Analytical models

Pipe stress estimation analytical models are useful in many applications, as the simplified stress calculation equations are programmable for practical uses. However, such equations to find pipe bending stresses have been found to be rare, whereas simplified equations are commonly used in practice for other pipe loads such as water pressure, thermal loads, soil overburden and surface loads (Rajani et al., 1996; Moser and Folkman, 2001).

The methodology presented in an analytical approach to simulate pipe stresses due to climate induced soil settlements (Wols and Thienen, 2014) was found to be an adoptable approach to the present work. In this method, the Euler beam theory is applied to the pipe by assuming the pipe is a beam on elastic springs. Therefore, the pipe deformation is expressed as in Equation 2.8.

$$\frac{d^2}{dx^2}\left(EI\frac{d^2u(x)}{dx^2}\right) + K\big(u(x) - S_v(x)\big) = q(x) \qquad \text{Equation 2.8}$$

where, $S_v(x)$ is the free vertical soil movement along the pipe direction (x) and $u(x)$ is the pipe movement function. For a fully flexible pipe, both these functions are assumed to be the same. For stiff pipes, the soil sub-grade modulus (K) is incorporated. The other loads on the pipe (example; traffic loads and other surcharge loads), are included as $q(x)$ and the pipe's Young's modulus and the second moment of area of the cross-section are used as E and I respectively.

By assuming the external loads on the pipe, $q(x)$, are zero the solutions are presented, as explained below.

After the settlement profile, $S_v(x)$, is determined, the pipe bending moments $M_g(x)$ are calculated by assuming the pipe is fully flexible and exactly follows the ground movement. The second derivative of $S_v(x)$ is used to calculate $M_g(x)$, as expressed in Equation 2.9.

$$M_g(x) = -EI\frac{d^2S_v(x)}{dx^2} \qquad \text{Equation 2.9}$$

This $M_g(x)$ is then related to the actual pipe bending moment $M_P(x)$ by multiplying by a normalising factor (M_{norm}) which depends on the soil-pipe interaction (stiffness) properties (Equation 2.10).

$$M_P(x) = M_{norm} \times M_g(x) \qquad \text{Equation 2.10}$$

As the last step, the pipe bending stress $\sigma_P(x)$ at the pipe wall (pipe with diameter D) is calculated, as expressed in Equation 2.11.

$$\sigma_P(x) = \frac{M_P(x)}{I} \times \frac{D}{2} \qquad \text{Equation 2.11}$$

The maximum stress in the pipe wall can be determined by considering the derivative of the above expression to find the maxima of the function.

In this methodology, the parameters required to estimate the pipe stress are as follows:

- The free ground movement function $S_v(x)$: a mathematical expression is required to determine the ground movement. This can be determined by calculating the uniform or differential ground movements along the pipe.
- The soil-pipe interaction (stiffness) factor (M_{norm}): this has been identified as a function of pipe section properties, material properties and soil stiffness (Wols and Thienen, 2014). The required fitting parameters can be determined from numerical models.
- The pipe parameters (E, I and D)

The applicability of this methodology to the current study is discussed in Chapter 6.

2.8 Conclusion

The literature review covered previous studies of Melbourne's pipe network and pipe failures, the fundamentals and problematic behaviour of reactive clays, soil moisture variations, and reactive soil-induced pipe movements and pipe deformation and stress analysis. The following conclusions were drawn from this literature review:

- Melbourne's water reticulation network is one of the oldest pipe networks in Australia, and consists of 12000 km of pipes made of different materials and of different sizes. Most of the old pipes are identified as small-diameter (100 to 300mm) cast iron pipes. As the pipes are decades old, these metallic pipes are corroded to different degrees.
- About 4000 pipe failures are reported annually in Melbourne. The most frequent failure type has been identified as circumferential cracking (broken-back) failures of small-diameter cast iron pipes. The higher failure rates observed in reactive soil regions and the greater number of summer failures indicate the effect of seasonal ground movements on these pipe failures.
- The behaviour of reactive (expansive) clays is basically determined by their minerology, as montmorillonite minerals are mostly responsible for the expansive behaviour of soils. In Melbourne, the basaltic residual soils in the western metropolitan area are identified as extremely expansive soils. Seasonal ground movements have been observed in the range of 60-70mm (for both swelling and wetting) at the surface, while they decrease as the depth increases.
- Soil moisture data available from different sources indicate that the seasonal moisture variations at deeper layers (around the pipe depth) are smaller than the surface moisture variations.
- The influence of reactive ground movements on buried pipes is confirmed by both laboratory and field experiments. These experiments clearly show that pipe bending occurs due to soil moisture variation-induced ground movement. However, the observed pipe deflection of the laboratory experiment, which is similar to the deflection of a simply supported beam, reflects the effect of end

supports provided to the pipe. Therefore, the monitored pipe deflection in the laboratory test may not be directly comparable to the results of field tests.

- Both numerical methods and analytical approaches have been used to estimate pipe stresses due to reactive soil movements. However, both methods involved some avoidable assumptions and limitations. The reliability of both methods can be limited due to these assumptions. The main advantage of the analytical approach, when compared with the numerical methods, was identified as the possibility of its application in pipe networks where thousands of pipes need to be analysed such as in GIS applications. In this context, the analytical method identified in this literature review is worth considering for providing solutions for the current work.

CHAPTER 3: DEVELOPMENT OF A FINITE ELEMENT MODEL FOR PIPE STRESS ANALYSIS AND ALTONA NORTH PIPE ANALYSIS

3.1 Overview

This chapter presents the initial work on the development of a numerical simulation methodology to estimate pipe stresses due to reactive soil movements. This work mainly consists of the use of a commercial software to develop a finite element model to simulate reactive soil behaviour and its interaction with pipes to determine the resultant flexural stresses in the pipe wall. Knowledge gained from the literature review in Chapter 2 was used to define the scope of the modelling process and its performance. The Altona North test pipe (Section 2.6.2) was selected for this initial simulation as the deformation/strains measured on the test pipe can be used to compare the model results. Therefore, the methodology presented in this case specific analysis explains the basic steps of developing the finite element model, including the constitutive relations, selection of the geometry of the model, the use of reactive soil properties and the incorporation of measured field soil moisture data obtained from the Altona North pipe observations.

3.2 Modelling Software

As the numerical simulation method was chosen for the basic studies, a suitable modelling software for the simulation process was considered according to the basic requirements of the study. The prime aim of this numerical simulation was to research the effects of reactive ground movements on buried small-diameter pipes and hence to estimate the resultant flexural stresses. Therefore, the ability to simulate fluid-induced volumetric changes of a medium was considered as the primary concern and the ability to simulate three-dimensional multi-material models was considered as the secondary requirement when selecting suitable modelling software.

For this study, the commercial finite element analysis software Abaqus (Dassault Systèmes, 2014) was selected. Abaqus is a general purpose finite element software that is applicable for many engineering analyses, including the coupled analyses of mechanical, thermal and hydraulic problems. The user-friendly features of three-dimensional modelling and the inbuilt analysis procedures for geotechnical problems also supported this selection. Specifically, the inbuilt procedure to model moisture swelling materials made this selection preferable. Since this approach is independent of user-defined codes, the model can be used widely without requiring any computer coding knowledge. This is an advantage of this procedure compared with previous attempts at the numerical simulation of reactive soil-pipe problems (Section 2.7.1).

This feature in Abaqus has been used simultaneously in reactive soil simulations in footing analyses of reactive soil regions (Shams et al., 2017). In addition, this software has been used widely in material capacity and pipe failure analyses in various applications (Robert et al., 2013; Robert et al., 2016a; Robert et al., 2016b; Zhang et al., 2017).

3.3 Selection of a Soil-pipe Segment for Modelling

This finite element model was developed for a selected soil-pipe section from Altona North pipe monitoring site. Initially, this selection was made by considering a representative unit for common soil-pipe environments. Since most small-diameter pipes (diameter < 300mm) are laid under grass-covered nature strips, along with other underground services, the nature of these nature strips was studied before making the selection. These visual inspections led to a number of hypotheses.

Direct exposure to the atmosphere makes the soil moisture content below these nature strips more subject to significant changes than the moisture content below impermeable concrete covers and road pavements. When a continuous pipeline lies under a number of nature strips and concrete driveways across the nature strip and road intersections, as shown in Figure 3.1, they create changing conditions for the soil-pipe environment. Therefore, a pipe segment between two driveways (or road intersections) can be treated as a repetitive unit of a long pipeline that goes through several nature strips, driveways and road intersections. Typically, these nature strips were observed as being 10 to 30m long and 1 to 4m wide grassed areas.

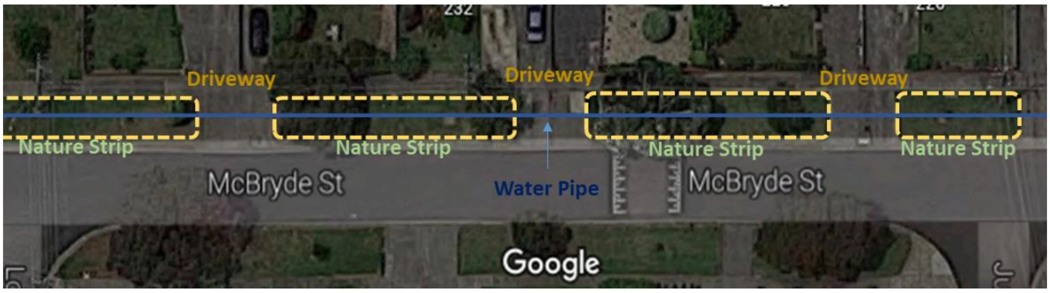

Figure 3.1. Appearance of nature strips and driveways along a pipe

These possible changes at driveways are discussed in detail under the model boundary conditions in Section 3.6. A sectional view of this selected soil-pipe segment is shown in Figure 3.2. Further, this selection of a pipe segment between two driveways for modelling made the comparisons and verifications of the finite element modelling results easier, as the field measurements of an in-service pipe in reactive clays were obtained from a similar section (Section 2.6.2).

Figure 3.2. A soil-pipe segment between two driveways

The horizontal dimensions of length and width were chosen to be similar to the field size of the nature strip. In relation to the vertical dimension, the depth of the section was selected according to the thickness of reactive clays below the surface. As the literature review showed, this thickness is determined by either the bedrock level or the moisture variation depth (Section 2.4.4.1).

This selected segment was then further broken down to a quarter of the section by considering the symmetry, as illustrated in Figure 3.3. The major assumption made in this quarter model was that similar conditions exist in other nature strips along the pipe. This assumption is acceptable when sufficient data (soil properties and moisture contents) at closer points is not available for detailed modelling. Data with fine resolutions are not available for large-scale modelling as the soil property and soil moisture data are only available for larger regions (Sections 2.4.4 and 2.5). However, the changes in the transverse direction of the pipe were not considered as the prime purpose of this simulation is to assess the longitudinal effects.

This basic geometry was implemented in Abaqus as a three-dimensional drawing. The pipe was placed at the relevant depth of the case for analysis as noted with respect to each analysis. Figure 3.3 shows that the final modelling assembly is a combination of a soil block to represent the reactive nature strip, a buried pipe segment and a driveway above the soil at one end. The model dimensions were determined according to the specific cases and the selected dimensions for Altona North pipe segment are described in Section 3.9.

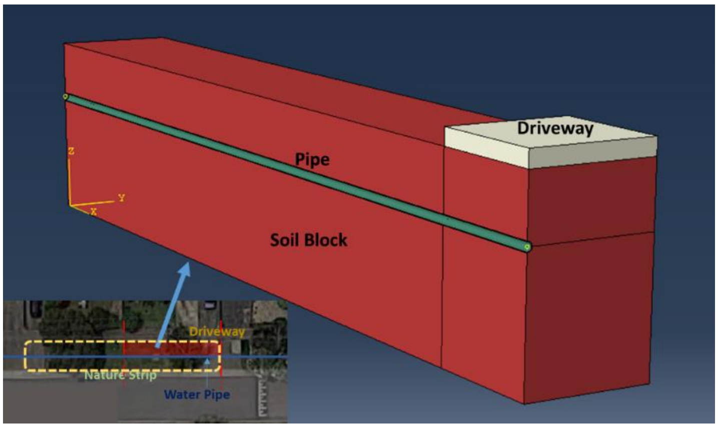

Figure 3.3. Modelling a quarter of the nature strip

3.4 Material Properties for the Model

After the model geometry was decided, the next step was to assign appropriate materials to the relevant parts in the model. Three distinguishable materials, reactive soil, cast iron (pipe) and concrete (driveway), are used in this model, as explained below.

3.4.1 Modelling reactive soil as a three-phase elastic material

In Abaqus, the inbuilt feature to simulate moisture swelling materials is to analyse a porous medium that consists of solid grains, a wetting fluid and a non-wetting fluid (Dassault Systèmes, 2014). The wetting fluid is pore water and the non-wetting fluid is pore air. The inclusion of pore air in the system makes the soil medium unsaturated and this condition is reasonably applicable to the soil near small- diameter pipes, as the literature review revealed (Section 2.2.4).

The total strain change in the soil medium due to external effects is determined by considering the following features (Dassault Systèmes, 2014):

- The compressibility of individual solid grains
- The compressibility of wetting fluid (pore water)
- The thermal response of solid grains and wetting fluid
- The saturation-driven moisture swelling
- The strain component that modifies the effective stress in the medium.

However, some of the above behaviours were ignored on reasonable grounds. For instance, the compressibility of individual soil grains and wetting fluid (pore water) was assumed to be negligible, as the bulk moduli of inorganic soil grains and water are significantly higher than the bulk modulus of the soil medium. The effect of temperature variations was not considered as the region for this research, Melbourne, does not experience considerable temperature variations causing soil particles and water to expand significantly, as the maximum monthly mean temperature changes are below 15^0C in Melbourne (Bureau of Meteorology, 2017c).

On the basis of the above assumptions, the final volumetric strain change of the medium was simplified, as shown in Equation 3.1:

$$\varepsilon_{Total} = \varepsilon_{eff} - \varepsilon^{ms} \qquad \text{Equation 3.1}$$

where, ε_{Total} is the total strain change in the medium, ε_{eff} is the strain change in the medium corresponding to effective stress change and ε^{ms} is the strain change due to saturation-driven moisture swelling. The sign convention is that compressive strains are positive.

The effective stress of the medium is calculated using Bishop's effective stress equation for unsaturated soils (Bishop, 1959) and substituting degree of saturation (S_r) and soil matric suction (s). This calculation is shown in Equation 3.2:

$$\sigma' = \sigma + S_r s \qquad \text{Equation 3.2}$$

where, σ' and σ are the effective and total stresses in the medium respectively, and these stresses are calculated for all three orthogonal directions.

The strain component due to the effective stress change in the medium is determined by the selected porous elastic constitutive behaviour for the soil. The soil near small-diameter pipes in Melbourne is most likely to show the properties of environmentally stabilised soils, since excavated and then re-compacted natural soil around the pipe has had a long time (over 50 years) to undergo wet/dry cycles (Gould et al., 2011b; Kodikara, 2012) (Section 2.4.3). Therefore, the strains are expected to be recoverable in subsequent wetting and drying cycles. This non-linear elastic behaviour is expressed in the following Equation 3.3:

$$\varepsilon_{eff} = \frac{\kappa}{1+e_0} ln\left(\frac{p}{p_0}\right) \qquad \text{Equation 3.3}$$

where, p and p_0 are the final and initial equivalent pressure components of three orthogonal effective stresses respectively, calculated as shown in following Equation 3.4:

$$p = \frac{1}{3}\left(\sigma_{xx} + \sigma_{yy} + \sigma_{zz}\right) \qquad \text{Equation 3.4}$$

The other parameters in Equation 3.3 are the logarithmic elastic constant, κ and the initial void ratio of the medium, e_0.

3.4.2 Parameters for soil modelling

The required input information for the soil model was identified as listed below:

- Soil suction vs. saturation curve (sorption curve)
- Moisture swelling vs. saturation curve (moisture swelling curve) and
- Logarithmic elastic constant

These necessary soil characteristics were determined for the Altona North clay as the results of the model were calibrated according to field measurements at Altona North.

The relationship between the soil's matrix suction and its degree of saturation was obtained from the soil water characteristic curves determined for Altona North reactive clays (Chan et al., 2015). These soil-water characteristic curves were developed by conducting filter paper tests (ASTM International, 2003b) for soil specimens from different depths. In the present study, the average soil-water characteristic curve for the pipe depth region (350 to 1000mm depth) was used for the analysis. This soil-water characteristic curve is illustrated in Figure 3.4.

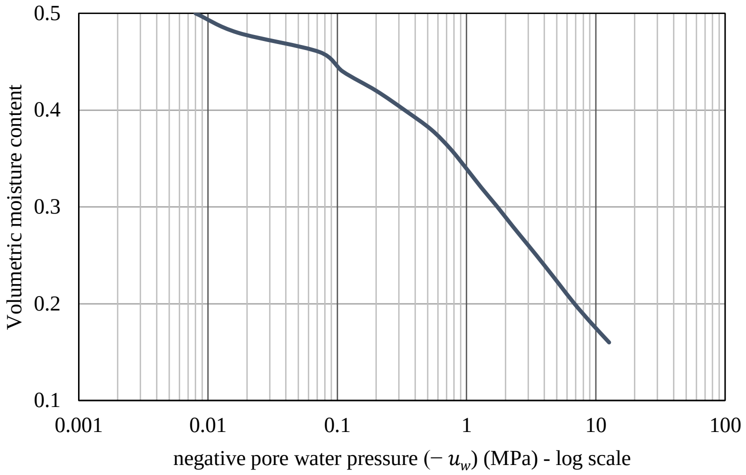

Figure 3.4. Soil water characteristic curve for soil at pipe depth in Altona North; after (Chan et al., 2015)

In the above figure, soil matric suction is denoted as negative pore water pressure $(-u_w)$ in the horizontal axis because of the zero pore air pressure (atmospheric pressure) in the medium ($u_a = 0$). For an unsaturated soil medium, the pore pressure (u_w) is a negative pressure (suction) and hence the negative pore water pressure $(-u_w)$ is a positive quantity. The volumetric water content in the vertical axis was converted to the degree of saturation, as explained in Section 3.4.4.

The relationship between moisture swelling and degree of saturation was determined by carrying out soil volume measurement tests for the soil specimens obtained from Altona North. The laboratory tests and the results of the soil volume measurements are explained in Section 3.4.3.

3.4.3 Laboratory testing of swelling properties of Altona North clay

The volumetric behaviour of Altona North clay was measured in the laboratory by measuring the volume of soil samples with different moisture contents. The undisturbed specimens were extracted from the old pipe-monitoring site located at McIntosh Road, Altona North. Undisturbed samples from the approximate pipe depth (600 to 1000mm) and below the pipe depth (1000-1400mm) were collected from boreholes. In addition, some disturbed soil samples were collected at various depths for preliminary classification tests.

Boreholes were drilled near the pipeline using an auger drilling machine and the samples were extracted using a 63mm diameter piston sampler (Australian Standards, 2015). Samples were collected from two boreholes (AL1 and AL2) within a 200m distance along the pipe (Table 3.1).

Table 3.1. Locations of soil sample collection

Sample ID	Sampling Location
AL 1	Corner of McIntosh Rd and Farrington Avenue, Altona North
AL 2	Corner of McIntosh Rd and Bright Avenue, Altona North

3.4.3.1 Preliminary tests

Disturbed soil samples collected from the AL 1 and AL 2 boreholes were used to determine the preliminary classification properties of the Altona North clay soil. These undisturbed samples were obtained from several depths from which undisturbed samples had not previously been collected. Samples from the surface and deeper soil (1.5m) were tested according to the Australian standard methods (Table 3.2) to determine in situ soil moisture content (gravimetric), Atterberg consistency limits, specific gravity, linear shrinkage and particle size distribution. The purpose of these tests was to compare the uniformity of the properties of soils above and below the pipe.

The results of laboratory soil sample tests and the results from previous researches (Chan, 2013) are shown in the Table 3.3. As can be seen from the results, significantly high clay contents and liquid limit and plasticity index values throughout the soil profile indicate the highly reactive properties of Altona North soil, according to the general classification methods (Section 2.4.2). This is an expected outcome, as Altona North is located in an identified reactive soil zone in Melbourne (Section 2.4.4).

Table 3.2. Standard methods used in preliminary tests

Soil Test	Test Method
Gravimetric Moisture Content, w	AS 1289 2.1.1 (Australian Standards, 2005)
Liquid Limit, LL	AS 1289 3.1.1 (Australian Standards, 2009c)
Plastic Limit, PL	AS 1289 3.2.1 (Australian Standards, 2009a)
Plasticity Index, PI	AS 1289 3.3.1 (Australian Standards, 2009b)
Specific Gravity of Soil, G_s	AS 1289 3.5.1 (Australian Standards, 2006)
Linear Shrinkage %	AS 1289 3.4.1 (Australian Standards, 2008)
Particle Size Distribution	AS 1289 3.6.3 (Australian Standards, 2003b)

Table 3.3. Altona North soil classification test results

Soil Property	Disturbed Soil Samples				Altona North soil at 0.85m depth (Chan, 2013)
	AL1 Surface	AL1 1.5m deep	AL2 Surface	AL2 1.5m deep	
Sample Moisture Content	21%	27%	20%	26%	
Liquid Limit	50%	111%	66%	87%	99%
Plastic Limit	27%	25%	24%	23%	29%
Plasticity Index	23%	86%	42%	64%	70%
Specific Gravity of Soil	2.68	2.68	2.67	2.66	
Linear Shrinkage %	14.6%	26.8%	21.2%	29.1%	21%
Clay %	42%	63%	61%	56%	60%
USCS classification (ASTM International, 2006)	High Plasticity Clay				

3.4.3.2 Volume measurements

Measurements of void ratio variations against the moisture content changes were analysed to establish a relationship between sample void ratio and moisture contents, accounting for possible hysteresis between wetting and drying paths. In the laboratory, the samples were removed from the tubes and cut into small pieces 20 to 30mm in length and width and 5 to 10mm thick for testing, as shown in Figure 3.5. Four samples were prepared for each specimen. Then the sample volumes and moisture contents were indirectly determined by following the method of submerged mass measurement of hand-sprayed plaster-coated soil samples (Liu and Buzzi, 2014).

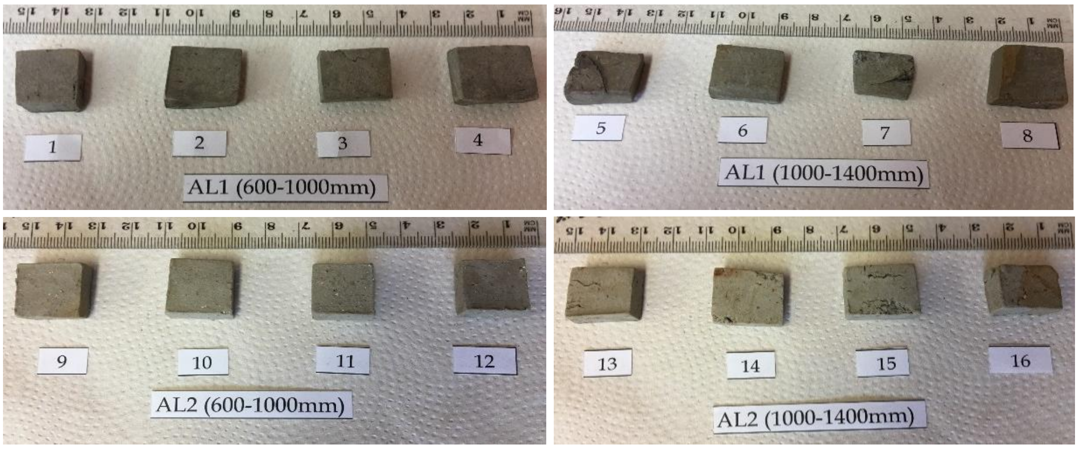

Figure 3.5. Soil samples for volume measurements

In this experiment, a thin spray of waterproof, breathable and transparent first aid spray plaster was used as the coating to cover the surface of each small sample. This breathable plaster allows the moisture to enter and leave the sample during wetting and drying whilst preventing particle erosion by water during the submerged mass measurements. Also, the coating protects the sample from rapid water intake during the submerged measurements and allows the measurements without affecting the sample moisture content.

Drying and wetting conditions were applied to the samples by storing samples in an enclosed environment, such as a sealable bag, under different humid conditions. In the wetting process, the samples were stored with a wet tissue paper (not in contact with the soil) to provide a humid environment inside the bag whereas a dry tissue paper was used to absorb the moisture in the drying process. In each process, a minimum of 48 hours was allowed to achieve moisture equilibrium between the sample and the air in the bag.

The experimental procedure is briefly summarised below.

- At the beginning of the test, the initial mass (in air) of each sample ($M_{s,a0}$) were measured. Separate similar samples from the same sample depths were used to determine the initial gravimetric moisture content (w_0) of each sample set (AL1 600-1000mm, AL1 1000-1400mm, AL2 600-1000mm and AL2 1000-1400mm), using the oven drying method (Australian Standards, 2005).
- After the coated samples were allowed to reach a certain moisture content inside an enclosed environment, mass (in air) of each sample ($M_{s,a}$) were measured using the balance. Then the simple apparatus assembled with a digital balance and water beaker with a sample hanger, as shown in Figure 3.6, was used to measure the buoyant mass on water ($M_{s,w}$) due to the submerged sample.
- After the measurements were taken, samples were restored in the same enclosed environment to achieve the next moisture content.

The methodology used to calculate the sample volumes, void ratios and moisture contents is explained below.

First, the bulk volume of the sample (V_s) was calculated using the measured buoyant mass on water due to the submerged sample ($M_{s,w}$) and the density of water (ρ_w) as given in Equation 3.5:

$$V_s = \frac{M_{s,w}}{\rho_w} \qquad \text{Equation 3.5}$$

The dry mass of each small sample ($M_{s,dry}$) was calculated as shown in Equation 3.6 using the mass in air ($M_{s,a0}$) and the gravimetric moisture content (w_0) of each sample at the test initiation. The initial moisture contents of both AL1 and AL2 soils shown in Table 3.4.

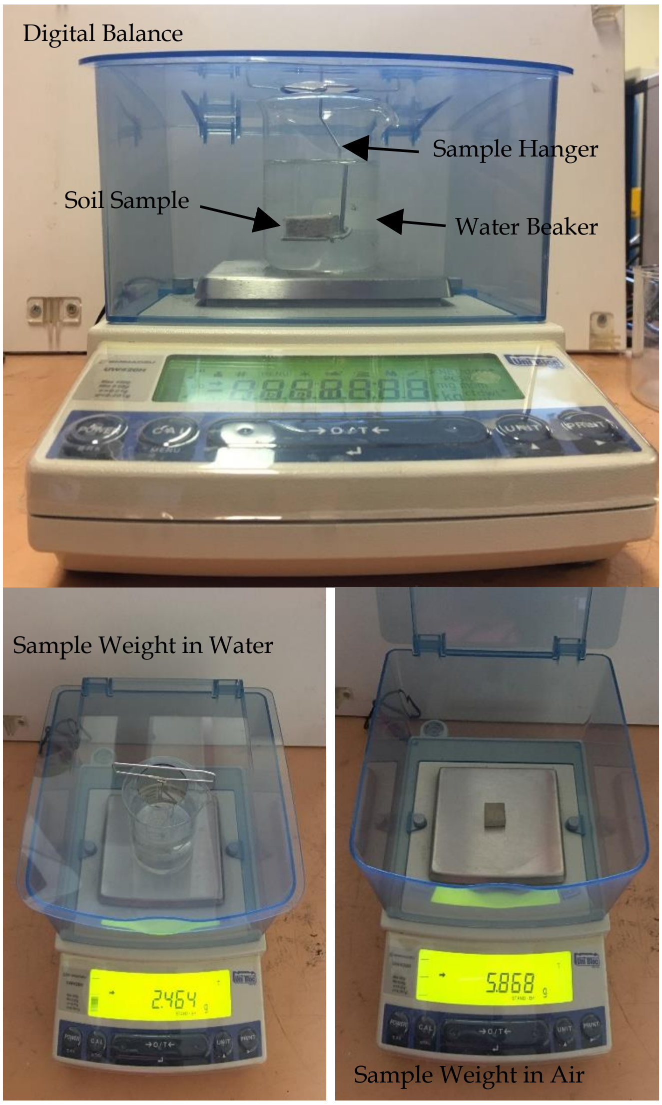

Figure 3.6. Sample mass measuring apparatus

$$M_{s,dry} = \frac{M_{s,a0}}{1+w_0} \qquad \text{Equation 3.6}$$

Table 3.4. Initial soil moisture contents of each volume measurement specimen

Soil Specimen	Initial Moisture Content (%)
AL 1 (600-1000mm)	23.4
AL 1 (1000-1400mm)	21.2
AL 2 (600-1000mm)	25.9
AL 2 (1000-1400mm)	22.3

Next, the gravimetric water content (w), volumetric water content (θ_v), dry density ($\rho_{s,dry}$) and void ratio (e) of each sample were calculated, as shown in the following Equations 3.7, 3.8, 3.9 and 3.10, respectively:

$$w = \frac{M_{s,a} - M_{s,dry}}{M_{s,dry}}$$ Equation 3.7

where, $M_{s,a}$ is the sample mass in air.

$$\theta_v = \frac{M_{s,a} - M_{s,dry}}{\rho_w V_s}$$ Equation 3.8

$$\rho_{s,dry} = \frac{M_{s,dry}}{V_s}$$ Equation 3.9

$$e = \frac{G_s \rho_w}{\rho_{s,dry}} - 1$$ Equation 3.10

Figure 3.7 shows the calculated volume changes of the tested soil samples as variations of void ratios with respect to volumetric moisture content changes. It can be observed that the initial four test points (2015-09-08, 2015-09-30, 2015-10-05 and 2015-10-08) follow a drying path (indicated in brown arrows) as the water content decreases. The remaining four test points (2015-10-20, 2015-10-30 and 2016-01-08) are on a wetting path (indicated in blue arrows) as the moisture content increases over time.

As Figure 3.7 indicates, a linear variation was observed between the void ratio (e) and gravimetric water content (w) of all tested samples. The figure also shows that the void ratio change follows the same straight-line path during wetting and drying moisture changes. This observation of recoverable volume changes confirms the applicability of the environmentally-stabilised soil concept for natural soils near pipes (Section 2.4.3).

These void ratio changes were considered for the volumetric strain calculation (Equation 3.11).

$$\varepsilon_{Total} = \frac{e - e_0}{1 + e_0}$$ Equation 3.11

where, e_0 is initial void ratio.

The average variations of the four samples were considered for this calculation (Figure 3.8):

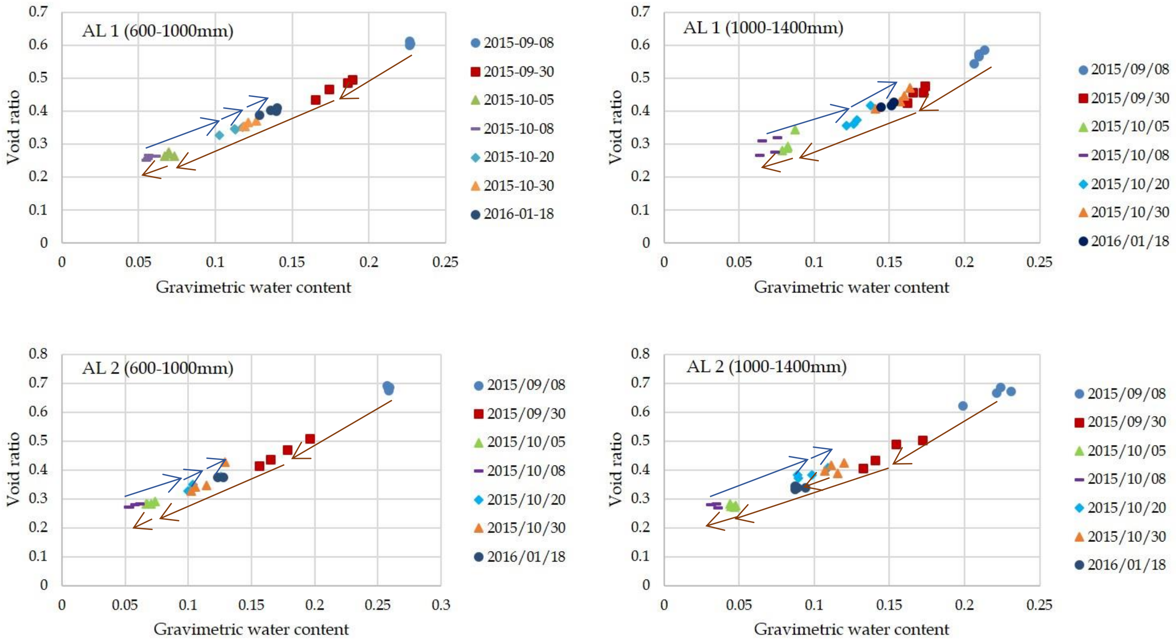

Figure 3.7. Void ratio vs. water content graphs for tested soil samples

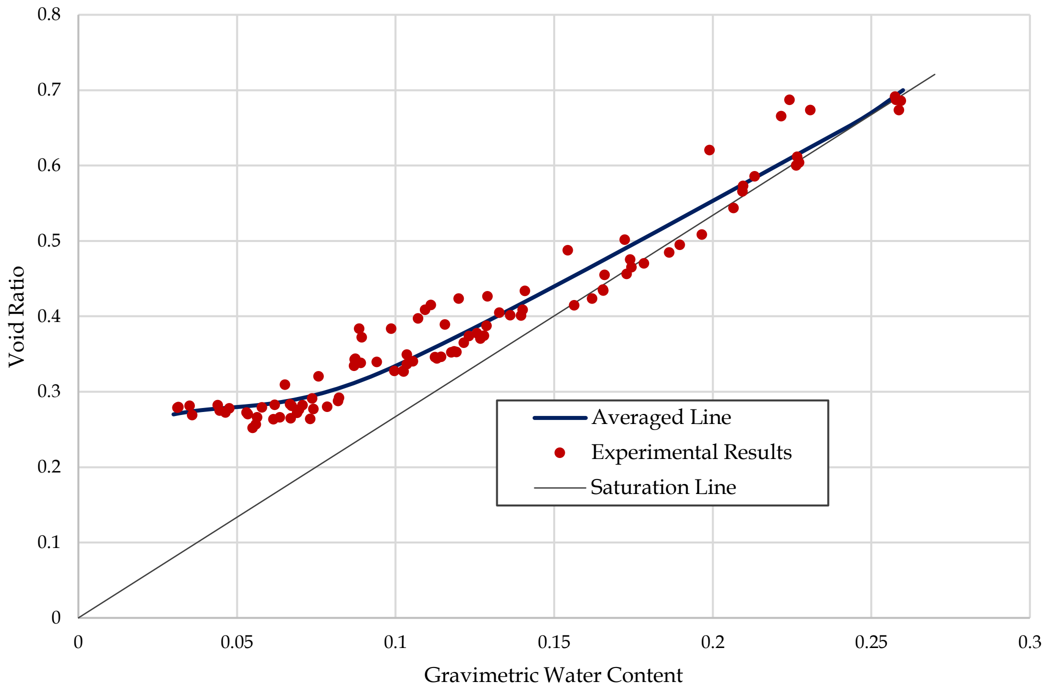

Figure 3.8. Average void ratio variation of all tests

In Figure 3.8, most points lie above the saturation line as the soil is in an unsaturated state. Unavoidable measurement and experimental errors were considered to be the primary reason for several points being plotted outside the saturation line. However, the average line is consistent with the idealised shrinkage curve practised for environmentally-stabilised soils (Gould et al., 2011b). Therefore, this average volume change path was used to define the soil model of Altona North clay for finite element modelling.

3.4.4 Summary of the input soil properties

The soil model was determined by considering a mean soil moisture content of 0.36 (volumetric). This mean moisture content value was selected paying attention to the soil moisture observation data of the Altona North pipe test-site (Section 2.5.1). Therefore, the volume change (strain) was assumed to be zero at this mean moisture content and the subsequent drying and wetting volume strains were calculated with respect to this mean value (Table 3.5).

The degree of saturation (S_r) of each drying and wetting step was calculated according to Equation 3.12:

$$S_r = \frac{G_s\, w}{e} \qquad \text{Equation 3.12}$$

In the calculation of the effective stress-induced strain component, the logarithmic elastic constant, κ was assumed to be 0.05. The assumed κ value can be justified as it is within the typical range for clayey soils (Schofield and Wroth, 1968), able to produce reliable ground movements to compare with field ground movements (see Section 3.9.3.1) and able to produce path (drying or wetting) independent ground movements as observed in environmentally stabilised soils. Then the moisture swelling strain (ε^{ms}) was determined, as defined in Equations 3.1, 3.2 and 3.3. The soil water characteristic curve (Figure 3.4) was used to relate the corresponding pore water pressures (u_w) of each moisture content.

Table 3.5. Input soil model of Altona North clay

State	θ_v	w	e	u_w (MPa)	S_r	ε_{Total}	ε^{ms}
Dry	0.26	0.14	0.40	-3.01	0.91	-0.15	-0.10
	0.28	0.15	0.44	-2.28	0.92	-0.12	-0.08
	0.30	0.17	0.48	-1.73	0.92	-0.09	-0.06
	0.32	0.18	0.52	-1.30	0.93	-0.06	-0.04
	0.34	0.20	0.57	-0.99	0.94	-0.03	-0.02
Mean Soil Moisture	0.36	0.22	0.62	-0.75	0.94	0	0
Wet	0.38	0.24	0.67	-0.53	0.95	0.03	0.02
	0.40	0.26	0.73	-0.33	0.95	0.06	0.04
	0.42	0.28	0.79	-0.20	0.95	0.10	0.06
	0.44	0.30	0.85	-0.11	0.96	0.13	0.08
	0.46	0.33	0.92	-0.07	0.96	0.17	0.10

Finally, the information in the above table was used in the software to define the required material characteristic relationships of S_r vs u_w and S_r vs ε^{ms}.

3.4.5 Cast iron material

A linear-elastic material model was assumed for the cast iron pipes. However, the non-linear behaviour of cast iron material was studied before assigning these linear parameters. The hyperbolic constitutive behaviour of cast iron has been extensively studied and used in large-diameter pipe failure analyses (Zhang et al., 2017).

This non-linear model has been effective for failure and crack propagation analyses, as material non-linearity is more significant in such analyses. Since the focus of the present study is to analyse the field pipe strains due to reactive ground movements and they are normally in the range of 500με, a linear tangential modulus was selected for this analysis. The corresponding parameters are shown in Table 3.6. A comparison of the deformation behaviours of selected linear modulus and the initial hyperbolic curve is shown in Figure 3.9.

Table 3.6. Material parameters for cast iron

Parameter	Value
Young's modulus, E_{CI}	83.4 GPa
Poisson's ratio, ν_{CI}	0.3

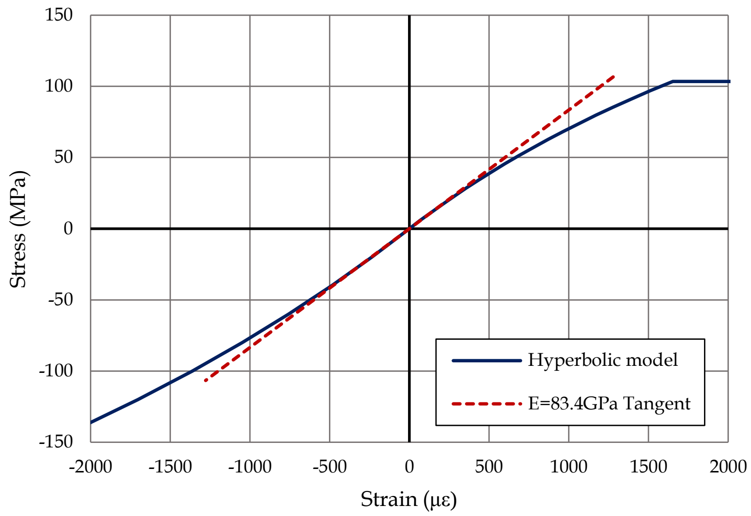

Figure 3.9. Comparison of constitutive models of cast iron

It can be seen that the selected linear Young's modulus is an ideally match with the hyperbolic model for smaller strains (less than 500με). In addition, the use of this linear behaviour reduces the computational time as it simplifies the models.

3.4.6 Concrete driveway

A portion of a concrete driveway was included in this model to maintain the rigid constraints to the upward surface movement of the soil at one end. This rigid constraint was assumed as the driveway is not flexible to differential soil movements. As observed in residential areas in Melbourne, a driveway is a 3 to 7m long (and wide) and about 200mm thick reinforced concrete structure. As the structural behaviour of driveways was not a concern in this analysis, the material properties of the concrete were considered as being not as significant as the other material properties. However, a general Young's modulus and a Poisson's ratio of concrete were assigned, as shown in Table 3.7, for modelling requirements.

Table 3.7. Material parameters for concrete

Parameter	Value
Young's modulus, E_{conc}	25 GPa
Poisson's ratio, ν_{conc}	0.2

3.5 Modelling of interaction interfaces

The interactions were defined for the interfaces between two different materials in the model. In this analysis, different materials were associated with the separate components, the soil, pipe and driveway, of the model assembly. Therefore, two interactions were defined to replicate the soil-pipe and soil-driveway interfaces, as explained in the following sections.

3.5.1 Soil-pipe interaction

The contact forces between the soil and the pipe were considered to be acting as both normal and tangential surface forces. Since the pipe is horizontally laid in a vertically moving soil, the normal contact forces are prominent at the top and the bottom of the pipe, whereas the tangential contact is significant at the sidewalls. Therefore, the interaction between the pipe and the soil was defined as a `hard contact' for normal contact and a linear friction interface for tangential contact.

The major properties of the hard contact of the normal contact are given below:

- No overlap between two materials
- No resistance to separation

These normal contact assignments can be justified, as the cast iron or soil particles are not penetrating into each other under compression loads and there is no appreciable tensile resistance between the soil and the pipe.

In this analysis, a friction coefficient of 0.35 was assigned to the tangential contact at the soil-pipe interface. This value was selected as the friction coefficients for steel/ductile iron pipes and fine-grained soil interfaces, which have been found to be in the range of 0.3 to 0.4 in the design guidelines (ASCE, 2014).

3.5.2 Soil-driveway interaction

The soil-driveway interaction was simply defined as a hard contact in the normal direction. Interaction properties for the transverse direction were not defined, since the response of the driveway was limited to the vertical direction. Properties of this hard contact are similar to the normal contact assigned for the soil-pipe interaction.

3.6 Boundary Conditions

Boundary conditions were applied to the model in accordance with the field conditions of the analysis. Since this analysis includes both mechanical and hydraulic boundaries, their natural field restraints were considered for the definition of boundary conditions. The application of these boundary conditions is explained in the following sections.

3.6.1 Mechanical boundary conditions

The mechanical boundary conditions of the model were applied to the outer surfaces of the model as shown in Figure 3.10. Since symmetry was considered in defining the model configurations, symmetric boundary conditions were applied to the vertical faces of the model. This means that the movement in the normal direction to the face was restrained while movements in transverse directions were allowed. For example, movements in y-direction (in Figure 3.10) are restrained in the y-direction while movements in x and z-directions are allowed. These boundary conditions were also applied to the corresponding faces of the pipe in a similar manner.

Since the bottom of the model represents the boundary of the reactive soil layer that is normally bordered by the bedrock or the end of the moisture variation depth, the soil at the bottom was assumed to be non-moving. Therefore, the vertical movement was restrained at the bottom of the model.

The top surface of the model that represents the nature strip was considered as a free surface that is able to move freely in all directions. However, the driveway was considered as a fixed driveway in this analysis to simulate the upward resistance to the vertical movement of the soil under the driveway. The direct effect of this fixed boundary condition on presented results is considered to be insignificant as the results are presented as relative strains and stresses with respect to the analysis Date 1 (see Section3.93.9.2). Figure 3.10 illustrates all the mechanical boundary conditions of the model. It should be noted that the restrictions of the hidden vertical faces are similar to those of the visible faces on the opposite sides.

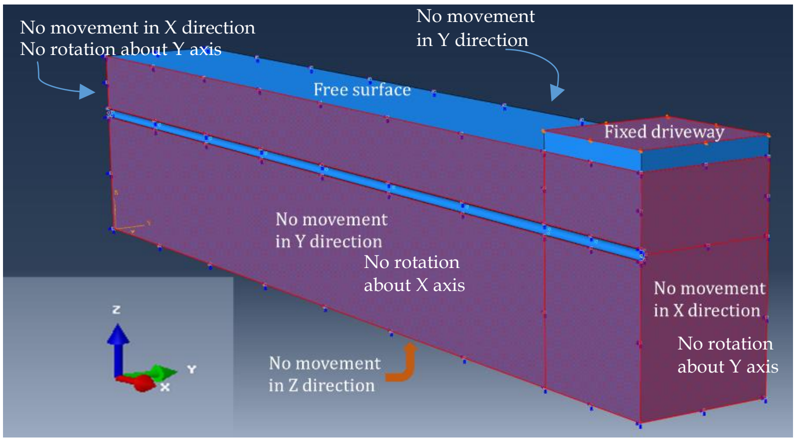

Figure 3.10. Mechanical boundary conditions of the model

3.6.2 Hydraulic boundary conditions

In Abaqus, hydraulic boundary conditions can be applied to the model as suction values as either constant or variable with time. There are two main approaches for specifying or commuting internal suction values. In the first, internal suction values are computed on the basis of specified boundary conditions through the coupled analyses. This approach is used in Chapter 4 and more details are presented therein. In the second, internal suction values can be specified (when they are known) and coupled analysis is not used. For the Altona North pipe analysis, the second approach was followed since internal measurements have been made and the focus was on the pipe deformations.

3.7 Application of Soil Moisture Variations

As the primary variable of the analysis, the field-observed moisture variations were applied to the model in each analysis. In the Abaqus model, pore water pressure is used as the major variable representing soil moisture. Therefore, the field moisture variations were assigned to the model as a change of pore water pressure on the basis of the soil water characteristics curve (Figure 3.4). In order to define the changes in conditions, it is necessary to define the initial state where the change starts and the final state at the end of a change. The procedure for defining initial and final states is explained in the following sections.

3.7.1 Initial state

The initial state of the model defines the conditions of the soil medium at the beginning of the analysis. If the initial conditions are not defined, the program assumes zero (or default) for the initial state parameters and analyses from zero to the defined final state (Dassault Systèmes, 2014). These initial conditions can be applied as external inputs as well as the adoption of the end state of a different analysis. Therefore, this initial condition can be a deformed or undeformed state for the present analysis.

However, in this analysis the initial state was considered as the undeformed state of the soil-pipe at a neutral soil moisture content that is neither dry nor wet. The mean soil moisture content of long-term soil moisture fluctuations was identified as the neutral moisture content that can be used to define the undeformed initial state of the pipe. This initial state of the soil medium was then defined in the model by assigning initial values for the following parameters:

- Pore water pressure
- Degree of saturation

- Void ratio
- Effective stress

It must be noted that all these parameters are interdependent. Therefore, they must be consistent with the definitions of the material properties.

3.7.2 Final state

After defining the initial state, the final pipe state comes from the change in the model considered for the analysis. As the soil moisture content is the major variable for the pipe stress/strain computations, the soil state at the final soil moisture content needed to be defined. The moisture changes were applied as pore pressure (hydraulic) boundary conditions.

In addition, the spatial variations of the soil moisture changes in horizontal and vertical directions were considered in the application of hydraulic boundary conditions. These spatial variations were determined based on observations of moisture changes at different soil depths (Section 2.5) and various other environments such as concrete covers. However, when the measured moisture changes were readily available with all the spatial variations, they were directly applied in the analysis.

3.8 Mesh Definition

Before the analysis, the finite element model was divided into a mesh of 100mm long cubic elements. However, a 25mm long refined mesh was considered for the pipe and the soil near the pipe, as this area is subjected to major deformations and deformation gradients during the analyses. The element types used for the different components of the model are listed in Table 3.8. Three dimensional elements were used to model all three components, the soil block, pipe and the driveway. The pipe was modelled as a solid body with the correct wall thickness.

Table 3.8. Element types in the model

Component	Element type	Reference
Soil	C3D8P: 8-node trilinear displacement and pore pressure element	(Dassault Systèmes, 2014)
Pipe	C3D8R: 8-node linear brick, reduced integration element	
Driveway		

3.9 Analysis and Results

As the Altona North test pipe was considered for this analysis (Section 2.6.2), the dimensions of the considered nature strip section were 30 long, 3m wide and 2m deep (the depth to the basaltic rock). Next, horizontal symmetry was used to reduce the original size to a quarter size with the dimensions of 15m long and 1.5m wide, as shown in Figure 3.11. Half of the 2.7m wide driveway was added to one end of the nature strip. The dimensions of the pipe were also selected according to the size of the test pipe (Table 3.9).

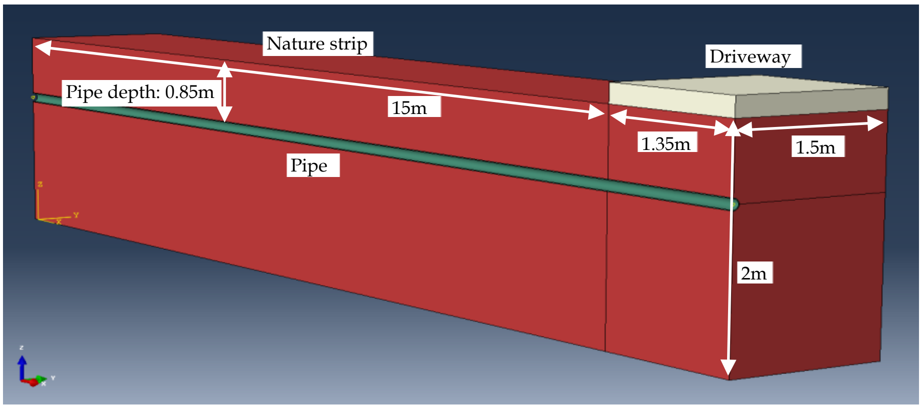

Figure 3.11. Dimensions of the finite element model

Table 3.9. Dimensions of Altona North pipe

Pipe Parameter	Value
Internal diameter	100mm
Wall thickness	8.5mm
Pipe length	16.35m
Burial depth	850mm

3.9.1 Analysed field soil moisture variations

Moisture variations were applied according to those observed during the monitored time. The initial date (12th January 2008) and three other specific dates with observations of significant moisture content changes were selected for this analysis (17th March 2008, 10th August 2008 and 30th January 2009). As the moisture contents were measured at three locations, Pit 1 (under the driveway), Pit 2 (5m away from driveway) and Pit 3 (15m away from driveway) are referred to as measurement locations. The moisture variation observations above the pipe (0.55 or 0.7m depth) and below the pipe (1 or 1.5m depth) at each pit location are illustrated in Figure 3.12.

In the analysis, the undeformed pipe state was considered corresponding to the first date of moisture monitoring (12th January 2008). Therefore, the results are relative to the results of the analysis date 1 (12-01-2008). In each analysis, the initial state was selected according to the long-term mean soil moisture content (0.36) and the final states were assigned according to the observed soil moisture contents of the selected dates. These moisture content values are given in Table 3.10.

Pit 1 - under the driveway; Pit 2 - 5m away from driveway; Pit 3 - 15m away from driveway

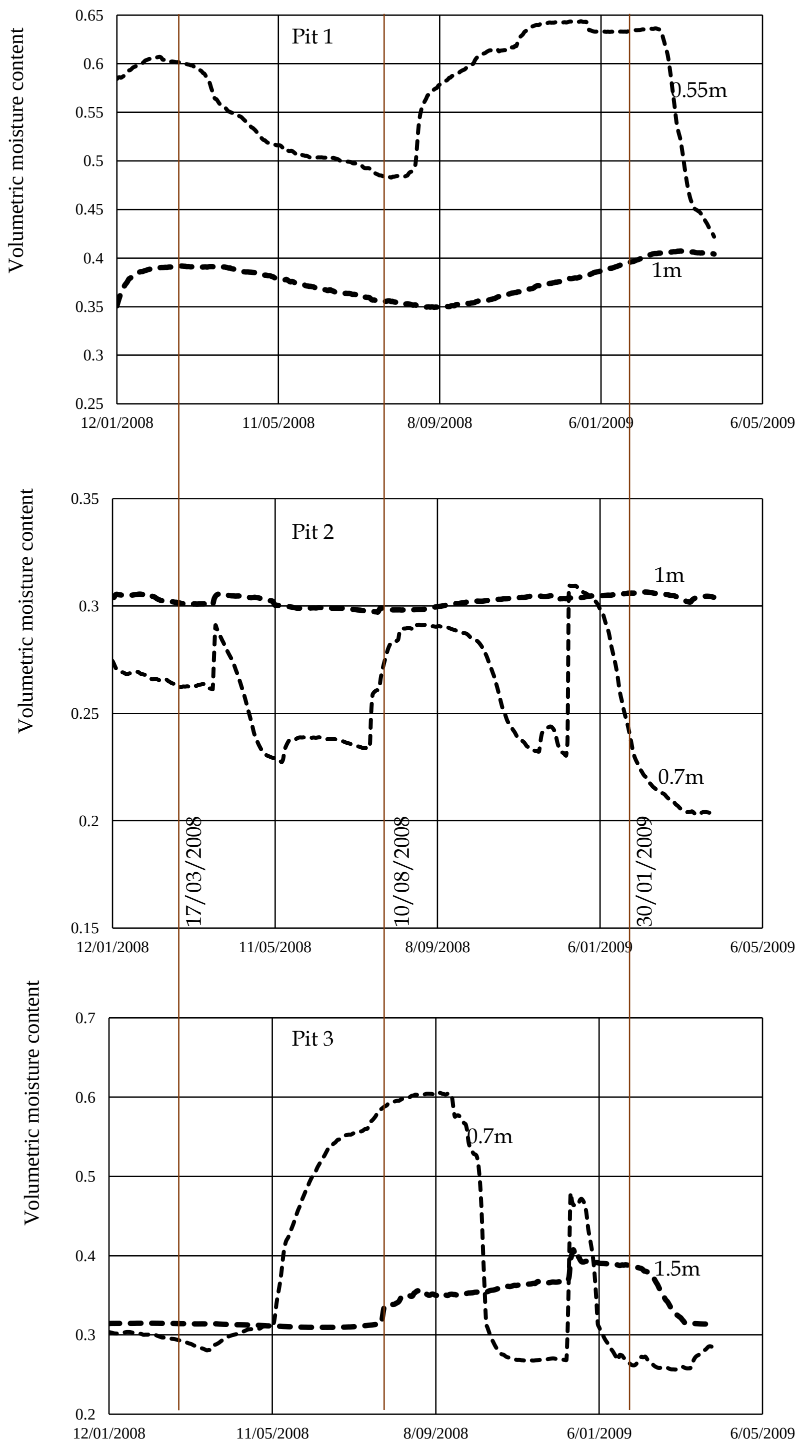

Figure 3.12. Monitored moisture variations at Altona North pipe (Chan et al., 2015)

Table 3.10. Soil moisture contents at three pits at selected dates

State of the analysis		Depth	Volumetric moisture content		
			Pit 1	Pit 2	Pit 3
Date 1	12-01-2008	Above the pipe	0.58	0.27	0.30
		Below the pipe	0.35	0.30	0.31
Date 2	17-03-2008	Above the pipe	0.59	0.26	0.28
		Below the pipe	0.39	0.30	0.31
Date 3	10-08-2008	Above the pipe	0.48	0.28	0.60
		Below the pipe	0.35	0.30	0.34
Date 4	30-01-2009	Above the pipe	0.63	0.23	0.26
		Below the pipe	0.40	0.31	0.39

The soil water characteristic curve corresponding to the Altona North site (Figure 3.4) was used to convert these moisture contents into pore pressure values. In addition to the initial pore pressure value, the corresponding initial void ratio and the initial degree of saturation were defined from the input soil properties of the Altona North clay (Table 3.5). Since the moisture values were not available for the intermediate space between adjacent pits, a linear horizontal variation of moisture contents was assumed in the horizontal space between adjacent pits (Figure 3.13).

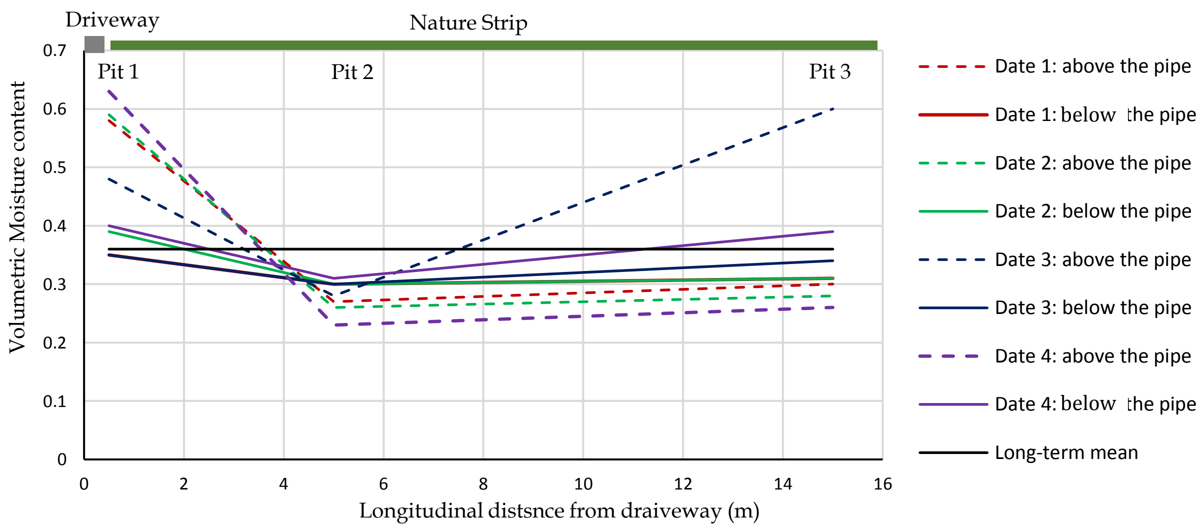

Figure 3.13. Longitudinal variation of applied moisture contents (above the pipe: 0.55 or 0.7m and below the pipe: 1.0 or 1.5m depths)

A uniform vertical moisture variation was assumed within the layers (above and below the pipe). Since the modelled soil depth (2.0m) is within the designated soil moisture variation depth (2.3m as explained in Section 2.4.4.1), the moisture change at the bottom of the model was not restrained.

3.9.2 Results

Pipe strains and stresses in the longitudinal direction were obtained as the major results of these analyses, as pipe bending was the major concern of this study. The pipe bending was then determined by calculating the flexural strains and flexural (bending) stresses along the pipe. The all presented strains and stresses are relative to the assumed undeformed pipe state for the Date 1 (12-01-2008). The relative results were calculated by deducting the results of Date 1 analysis from other analyses (Date 2, 3, and 4 in Table 3.10).

3.9.2.1 Flexural strains

Flexural strain (ε_f) in the pipe has been defined as the difference between the longitudinal strain at the pipe top (ε_{top})and bottom (ε_{bottom}) (Chan et al., 2015) (Equation 3.13). In this calculation, tensile strains were considered as positive and compressive strains were taken as negative.

$$\varepsilon_f = \varepsilon_{top} - \varepsilon_{bottom} \qquad \text{Equation 3.13}$$

The variation of calculated flexural strains (relative to 12-01-2008) along the pipe in each analysis are illustrated in Figure 3.14.

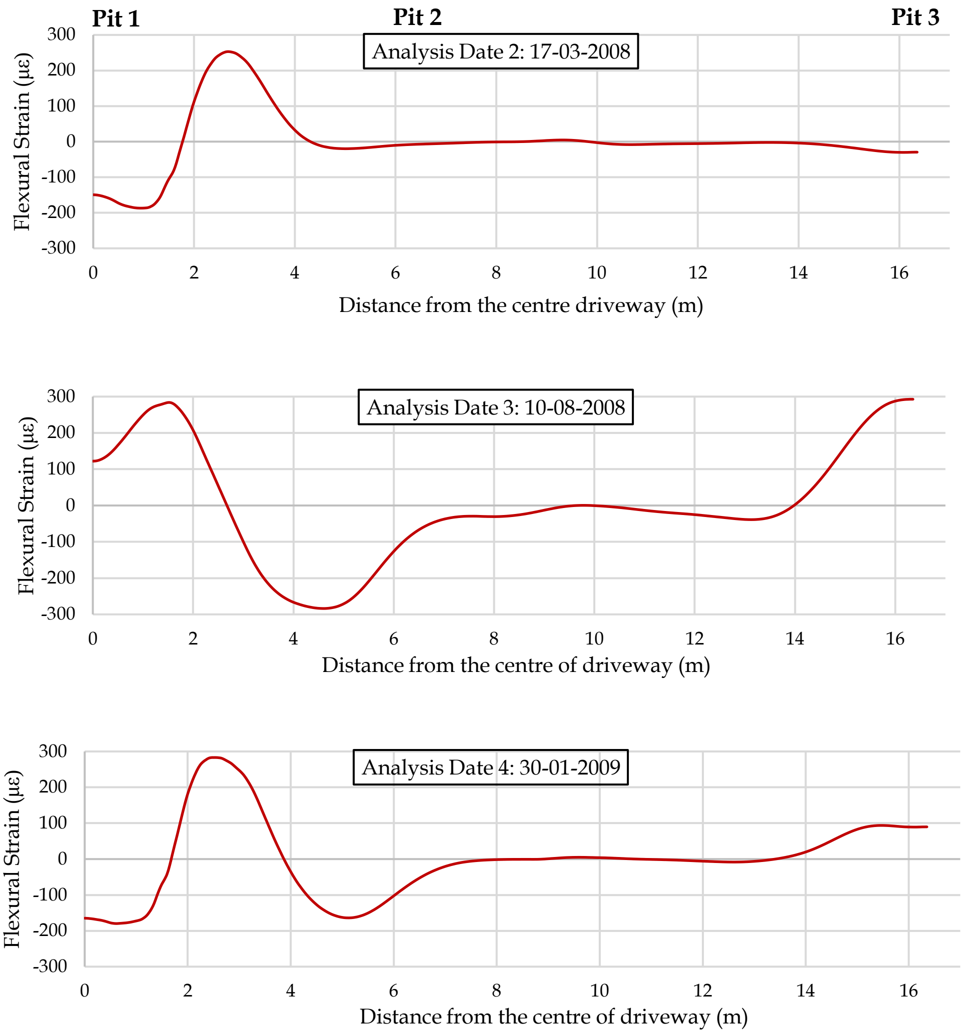

Figure 3.14. Calculated relative flexural strains along the pipe for each analysis

The corresponding monitoring pits were located at distances of 0.5m (Pit 1), 6.35m (Pit 2) and 16.35m (Pit 3) along the horizontal axes of Figure 3.14.

The following observations were made for the numerically-calculated flexural strain variations along the analysed pipe section (Figure 3.14).

- Flexural strains along the pipe are generally in the range of ±300με which is similar to the observed flexural strain variations of field measurements during the considered monitoring time (Section 2.6.2).
- In all three analyses, except the higher strains in analysis date 3 at 15-16m away from driveway, all significant strains occur near the driveway (0 to 2m from the centre of driveway) and at other pit locations. This is a reasonable observation, since the soil moisture variations were applied to the model at these pit

locations and the intermediate values were linearly interpolated between pit locations due to lack of information. Therefore, these calculated flexural strains reflect the pipe deformation according to the major moisture changes at pit locations. The anomaly in analysis date 3 can be explained as a result of higher moisture change. However, a further explanation to these observations is provided in this section.

- As discussed earlier, fixed driveway conditions were used in this analysis since the relative strains were calculated and its exact nature was unknown. This will be examined further and more refined analysis will be undertaken in Chapter 4.

The shape of the strain variation (Figure 3.14) represents the deformed shape of the pipe, which is governed by soil moisture-induced ground movement. Therefore, the above observations can be further explained by using the applied moisture variations to the model.

According to the definition of flexural strains (Equation 3.13), positive flexural strains indicate higher tensile strains at the pipe top associated with upward pipe bending (crest shape), and negative flexural strains are associated with downward pipe bending (trough shape) with higher tensile stresses at the pipe bottom. In terms of ground movement, it can be stated that positive flexural strains are correlated with ground swelling and negative flexural strains are associated with ground shrinking.

The ground movement results for analysis dates 17-03-2008, 10-08-2008 and 30-01-2009 (relative to the ground movement on 12-01-2008) at pipe depth are shown in Figure 3.15. Also, the potential ground swellings and shrinkages for applied moisture variations (with respect to 12-01-2008) of each analysis noted in Table 3.10 are evaluated in Table 3.11.

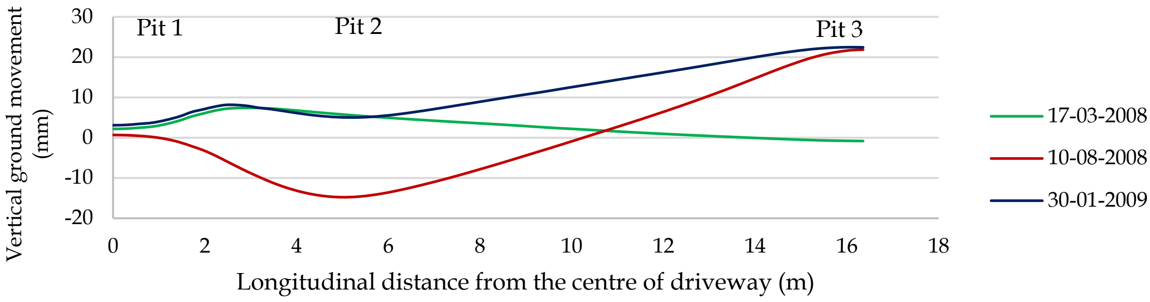

Figure 3.15. Vertical ground movements (relative to 12-01-2008) at pipe depth (0.85m)

Table 3.11. Evaluation of soil swell/shrink potential at each location

State of the analysis		Depth	Change in the soil		
			Pit 1	Pit 2	Pit 3
Date 2	17-03-2008	Above the pipe	Moisture increased (ground swelling)	Moisture decreased (ground shrinking)	Moisture decreased (ground shrinking)
		Below the pipe	Moisture increased (ground swelling)	No change	No change
Date 3	10-08-2008	Above the pipe	Moisture decreased (ground shrinking)	Moisture increased (ground swelling)	Moisture increased (ground swelling)
		Below the pipe	No change	No change	Moisture increased (ground swelling)
Date 4	30-01-2009	Above the pipe	Moisture increased (ground swelling)	Moisture decreased (ground shrinking)	Moisture decreased (ground shrinking)
		Below the pipe	Moisture increased (ground swelling)	Moisture increased (ground swelling)	Moisture increased (ground swelling)

The evaluations in Table 3.11 were then compared with the ground movement variations at pipe depth in Figure 3.15 and flexural strain variations in Figure 3.14 to make the following conclusions about the relationship between swell/shrink ground movements and pipe flexural strains:

- Flexural strains and pipe depth ground movements are very sensitive to soil moisture variations at the pipe bottom. Significant positive flexural strains are noticed when the bottom soil is swelling.

- Similarly, insignificant strains are noticed when the bottom soil is not subjected to moisture changes.
- However the pit 1 strains indicate the additional influence of the driveway, showing the sensitivity of flexural strains to the mechanical restraints in the model.

As the above conclusions indicate, the strain outputs of the analyses clearly replicate the effects of applied moisture variations. However, these strains were further verified using field measurements, as explained in Section 3.9.3.

3.9.2.2 Longitudinal pipe stress

In addition to the flexural strains, the results of longitudinal pipe stresses (relative to 12-01-2008) were also studied to identify the ultimate effects of ground movements on the pipe. The stresses presented in Figure 3.16 are relative longitudinal stresses along the pipe top and pipe bottom.

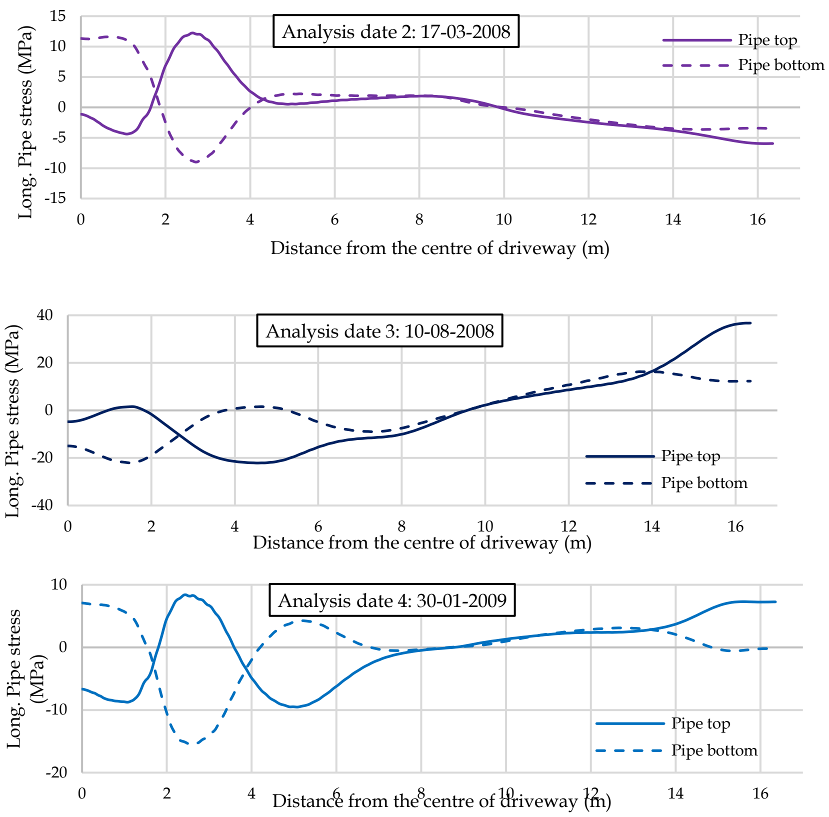

Figure 3.16. Longitudinal pipe stresses (relative to 12-01-2008) along the pipe

Note that the tensile stresses are positive and the longitudinal stresses are combined bending/flexural and axial stresses. However, it can be seen that the bending stresses are dominant along the pipe as the stresses at the pipe top and the pipe bottom are separated by considerable amounts.

The bending stresses are mainly generated by the differential pipe movements in the longitudinal direction. The minor component, the axial stresses, are generated by the minor swell/shrink movements in the longitudinal direction, through the frictional soil-pipe interface. The non-bending stress components are not discussed in the current work as the main focus of the current study is to investigate the bending stresses along the pipe.

Since these stress variations are correlated with the pipe strains, the locations of higher stresses are the same as the locations of higher flexural strains. The maximum stresses are in the range of 40 MPa, which is generally lower than the tensile strength of cast iron (Section 2.2.2). This estimation of lower stresses can be accepted, since no pipe failure was reported on this pipe during the monitored time period.

3.9.3 Comparison with field measurements

As the final verification step, the model outcomes were compared with the field measurements of Altona North pipe (Chan, 2013; Chan et al., 2015). The available field measurements of ground movements and pipe strains were considered for this verification.

3.9.3.1 Comparison of ground movements

Figure 3.17 shows the measured ground movements at 0.4m and 0.9m depths and the corresponding finite element results (relative to 12-01-2008) for the three analysis dates.

The upward ground movements were considered as positive and the measurements were taken at the middle of the nature strip. The comparison shows that the finite element results are reasonably consistent with the field measurements. However, some deviations between measured and numerical estimations are possibly due to minor variations of the field soil properties which were assumed to be uniform everywhere in the model. Therefore, the ground movement estimations of the model are considered as being acceptable for the purpose of this model.

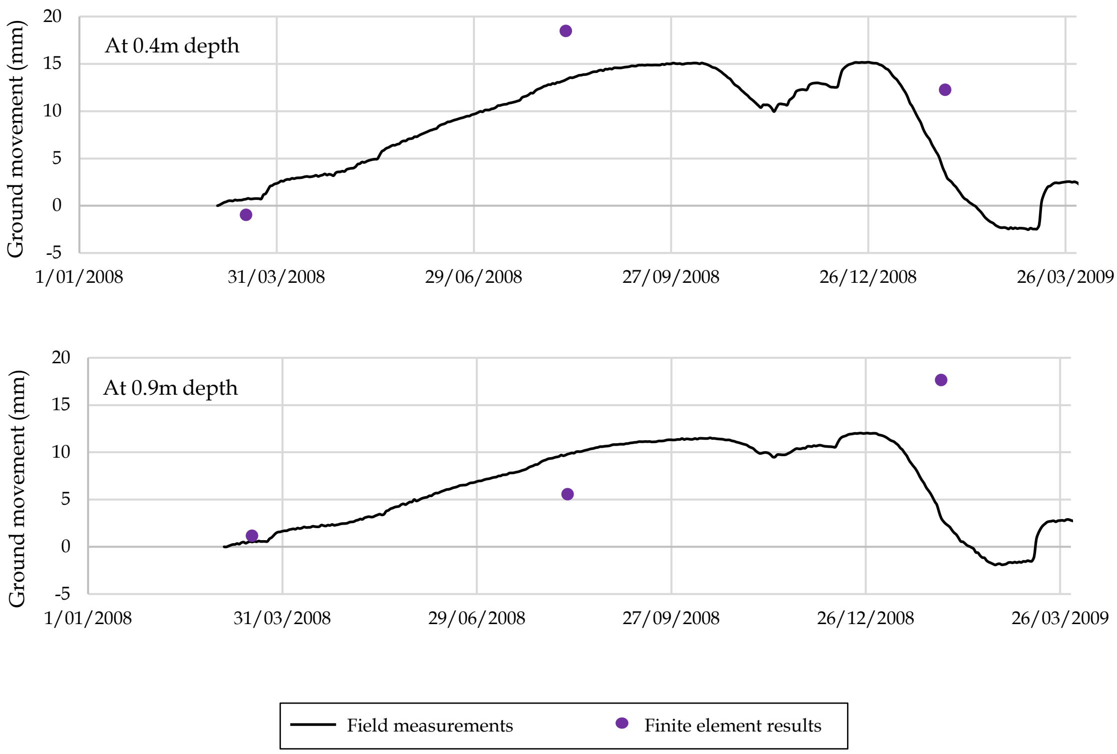

Figure 3.17. Comparison of ground movements

3.9.3.2 Comparison of pipe strains

The variations of field-observed pipe flexural strains were compared with the numerically-determined pipe flexural strains of each analysis, and the results are shown in Figure 3.18.

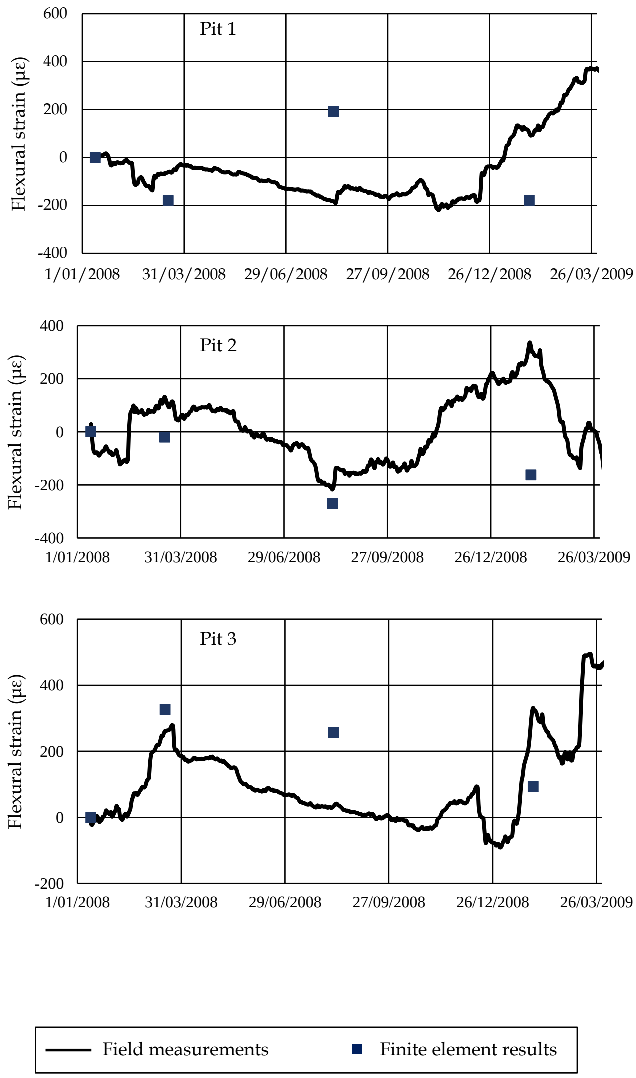

Figure 3.18. Comparison of pipe flexural strains

The comparison shows a reasonable qualitative agreement of strain variations between field measurements and finite element results. It can be seen that, both field measurements and finite element results converge in the similar strain range of ±400με. However, considerable discrepancies can be seen between two entities in some analyses. The possible reasons for these disagreements were considered to be the effects of some unavoidable modelling assumptions and possibly due to field measurement errors. An explanation is given below:

- Assumption of an undeformed pipe shape at the beginning of the measurements (12-01-2008). This assumption was made due to the lack of information about the initial deformation of the pipe. When the pipe is subjected to bending from a bent shape, the final results are not similar to the case of bending from an undeformed shape.

- Assumption of uniform soil properties. The possible presence of different soil properties affects strain measurements, as pipe deformation is associated with the vertical movement of the ground/pipe along the entire pipe length. However, this assumption is unavoidable as such fine soil property variations are not available for modelling.
- Use of linearly-interpolated moisture variations between measuring pits. The possible moisture variations between measuring pits, which are not considered here, affect the deformation of the pipe. Therefore, the pipe strain calculations may vary slightly from the field measurements.

Despite the variations in the modelling and the measured results in the field, it is quite evident that the proposed model captures the general behaviour of the field performance of the pipe during wetting and drying. Hence, the model is considered further in the analyses to be presented in the forthcoming chapters.

3.10 Conclusions

This chapter has presented the procedure for the development of a finite element model to simulate the interaction behaviour of reactive soil and small-diameter pipes. The soil-pipe model was developed for comparison with instrumentally-monitored pipe deformations at the Altona North reactive soil site. The results of this chapter can be summarised as follows:

- The finite element model shows the ability to reasonably estimate stresses and strains that may be used in pipe failure analyses. Despite some disagreements, mainly due to assumptions and limitations in the modelling method and possibly due to measurement errors, the finite element analyses provide satisfactory stress and strain estimations compared with the field observations.
- The pipe strain and stress estimations of the model show strong dependency on input soil properties and moisture variations. Therefore, the reliability of available input data is important for field pipe simulations.
- This method of simulating reactive soil movements is a relatively simple procedure as user-defined sub-routines are not involved. However it is theoretically justified on the basis of incremental non-linear elastic analysis applicable to environmentally-stabilised soils. This procedure is used for further analyses of critical pipe bending scenarios and stress estimations in the following chapters.

CHAPTER 4: STRESS HOTSPOTS FOR CIRCUMFERENTIAL FAILURE ANALYSIS

4.1 Overview

The previous chapter described the applicability of the finite element method for pipe stress/strain estimation for reactive soil environments. The chapter concluded that pipe-bending stresses were maximised at places where changes occur in the soil environment around the pipe. In addition, the uniform conditions along a pipeline created insignificant stresses as the bending is negligible under uniform pipe/ground movements. This observation provided an insight about the potential location of circumferential failures (broken-back failures) that are caused by reactive ground movements. Therefore, the identification and comprehensive analysis of such locations are an important step in understanding and predicting the failure mechanisms of small-diameter pipes in reactive soil zones. This chapter focuses on field scenarios that can locally affect pipe stress and cause circumferential failure. The study includes field observations of such hot spots, detailed studies of the factors that create hotspots, and finite element simulations to visualise the effects of surrounding features due to pipe bending.

4.2 Pipe Bending Characteristics

Circumferential failures of small-diameter pipes are generally caused by longitudinal pipe bending (Section 2.3.1). In reactive soil regions, the vertical ground movements induced by seasonal soil moisture variations are known to be the major reason for pipe bending (Section 2.3.2.2). However, the finite element simulations showed that if the ground/pipe movement is uniform along the pipeline, the pipe does not undergo significant bending or stresses. The uniform movement keeps the pipe axis straight as the original unbent position. When an external or internal factor affects this uniform ground/pipe movement, by creating changing conditions along the pipe, the pipe tends to undergo differential movements. This is where the bending is likely to occur along the pipe and bending stresses become significant. The pipe can experience mild, moderate or sharp bending patterns, depending on the severity of the differential movement, as illustrated in Figure 4.1.

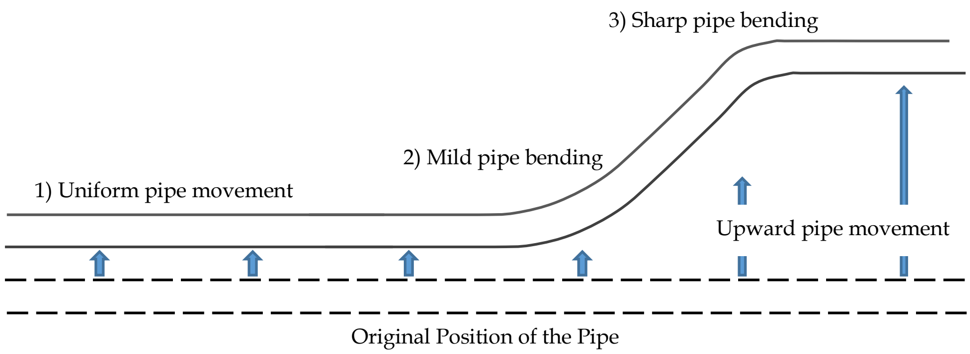

Figure 4.1. Illustration of pipe bending due to differential ground movement

In addition, it can be expected that bending stresses will become large when the pipe undergoes sharp bending, as the bending stress is proportional to the curvature of the bending shape.

This basic knowledge of possible pipe bending characteristics provides an insight into the identification of potential locations of high pipe failure risk of circumferential failure, if the locations with differential ground/pipe movements and their severities are known. In this study, such locations are referred as `stress hotspots' and a detailed investigation of field stress hotspots is presented in the following sections.

4.3 Stress Hotspots

The study of field stress hotspots began by observing the natural and man-made features that can create changing conditions to the surroundings of the pipe burial environment. Field visits, interactive maps and geotechnical databases were considered during the initial phase of field stress hotspot identification. Small-diameter water reticulation pipes are normally buried under the nature strip between roads and houses. Burial depth is variable, however, as an average value, it can be assumed to be about 750mm from the surface (Section 2.2.4). Figure 4.2 shows a view of a nature strip where a pipe is commonly buried.

Figure 4.2. Typical view of a pipe burial area; Image: Mills St. Altona North, VIC. (Google Maps, 2017)

It was observed that, these grass-covered nature strips are normally 2 to 5m wide and 20 to 30m long between concrete driveways. Concrete driveways connect individual households to the road. Large- to moderate-sized trees are frequently planted in the nature strip. These features that are observable at the ground surface were considered for further investigation of stress hotspots. In addition to these surface features, some possible sub-surface features were also considered.

Initially, some hotspots were conceptually identified and hypotheses were developed for further investigation. These are listed below and illustrated in Figure 4.3.

1. Driveways
2. Bedrock peaks near the pipe
3. Soil boundaries
4. Water leaks
5. Tree roots

Figure 4.3. Stress hotspots identified for detailed investigations

Possible primary and secondary effects of each of these hotspot features were considered in the analyses, and field measurements and available data were used to verify their existence. Finite element simulations were then carried out to determine the pipe bending behaviour for each feature.

4.4 Driveways

Driveways are frequently seen on nature strips where pipes are buried, connecting a building lot to the adjacent road. These driveways are from 2.5m to 7m wide, depending on the number of households or businesses that share the same driveway (the maximum is 2). Driveways can be considered as a strong, impermeable structure as they are normally constructed of about 200mm thick reinforced concrete slab. A section of a partially constructed driveway is shown in Figure 4.4.

Figure 4.4. Section of a reinforced concrete driveway

However, some old driveways are weaker in structural strength as they are cracked due to repetitive vehicle loads and swelling pressure from the sub-soil. Figure 4.5 shows such a cracked driveway and it can be seen that the cracked sections have undergone relative vertical movement of about 2 to 3cm.

Figure 4.5. Uncracked and cracked driveways

The effects of driveways on the soil-pipe environment were considered as being twofold: the effects on soil moisture variation; and the free soil movement under the driveway. However, the potentially weakened behaviour of cracked driveways was ignored in the present study since uncracked driveways create the maximum differential effects and provide a worst-case and arguably more general scenario.

4.4.1 Moisture variation under driveways

Moisture variation under driveways was considered to be similar to the moisture variations under concrete slabs. When an impermeable slab is placed on uncovered ground, the environmental exposure of the soil under the slab is directly affected. As soil moisture infiltration and evaporation are limited through the slab, the soil under the slab experiences much lower moisture changes than the surrounding uncovered soil. This observation has been simulated by various numerical models (Li et al., 1996; Fredlund and Vu, 2003) and Figure 4.6 shows the numerically-simulated seasonal surface suction variation under a 8.9m wide slab at different distances from the slab edge. It can be seen that the suction variation significantly reduces towards the centre of the slab and it becomes negligible when it reaches 1.7m from the edge of the slab. Such differential moisture varying conditions lead to differential ground movements under the slab and the nearby open field.

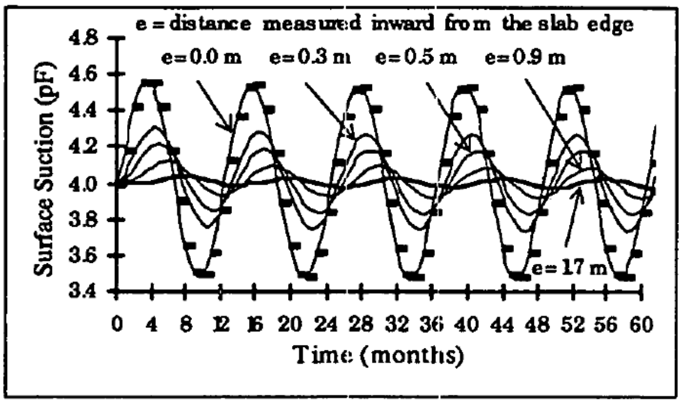

Figure 4.6. Seasonal surface suction variation under a slab (Li et al., 1996)

Further, this differential moisture variation has been observed to be distinctive in wetting and drying conditions. It has been observed that the differential downward movement during drying is considerably more significant than the differential upward movement during wetting (Hamilton, 1969; Sattler and Fredlund, 1991). The prime reason for this is explained as the drying of the open field is more dominated by the demands of the vegetation during dry periods. Therefore, the uncovered area tends to dry out more quickly than the covered soil, creating greater differential conditions. In contrast, soil wetting is not affected by vegetation very much, but can be accelerated by the presence of cracks and gaps in the soil and the soil/structure interfaces. Therefore, soil wetting under the driveway can be faster than the drying process.

As a further investigation, the field soil moisture variations observed at the Altona North pipe monitoring site (Chan et al., 2015) were closely studied to identify the soil moisture variation characteristics under driveways and nature strips. Figure 4.7 shows the pipe depth moisture variations under a 2.7m wide driveway and the adjacent nature strip (5m away from the driveway).

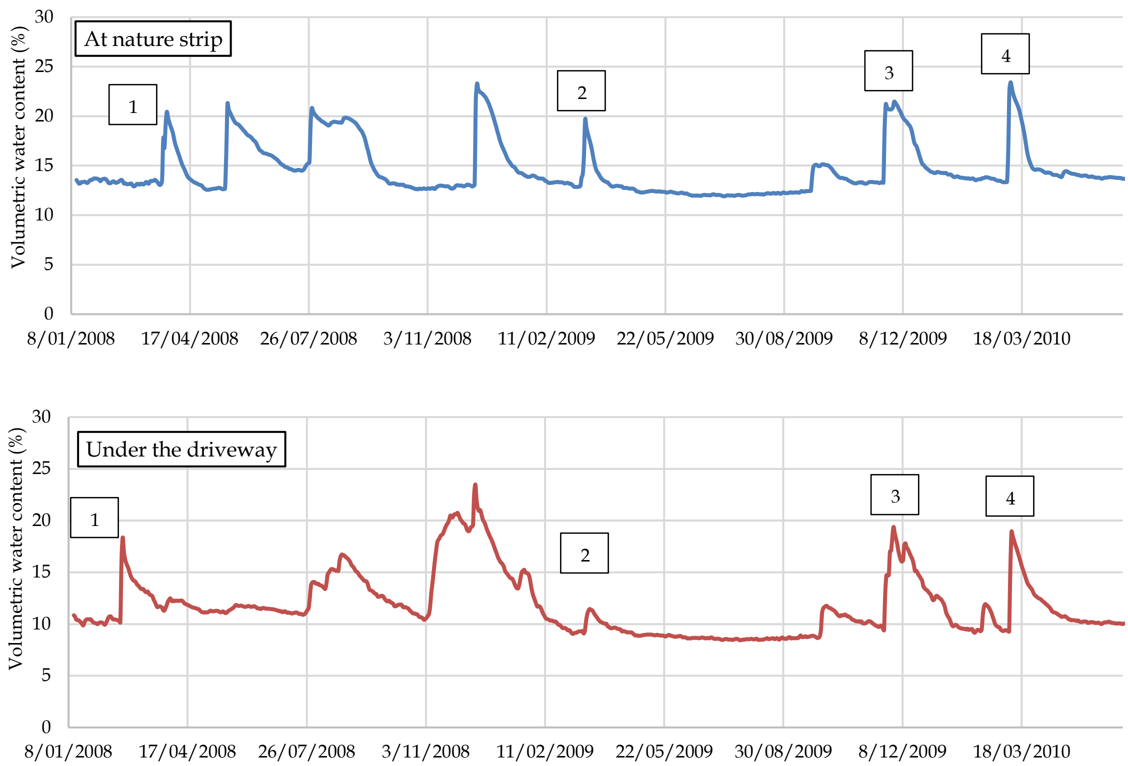

Figure 4.7. Soil moisture variations at pipe depth (Chan et al., 2015)

The figure shows that wetting and drying occur in narrow time frames at the nature strip whereas broader time frames are observed for the soil under driveways. This indicates the rapid response of the nature strip moisture contents to environmental changes. However, further observations show that the wetting moisture responses under the driveway are as fast (for the reasons noted above) as the nature strip moisture changes, while drying under the driveway takes longer than the nature strip. Table 4.1 shows an interpretation of Figure 4.7 data to explain the distinct behaviour of wetting and drying times near driveways.

Table 4.1. Altona North soil moisture changes under driveways and at nature strip

Moisture peak (Figure 4.7)	Month	Moisture change at nature strip	Moisture change under driveway	Soil wet / dry
1	February – May 2008	+7% change in 5 days	+8% change in 4 days	Wetting
		-7% change in 30 days	-7% change in 60 days	Drying
2	March – April 2009	+7% change in 5days	+4% change in 7 days	Wetting
		-7% change in 20 days	-4% change in 37 days	Drying
3	December – February 2009/10	+8% change in 3 days	+9% change in 6 days	Wetting
		-8% change in 31 days	-9% change in 72 days	Drying
4	March – May 2010	+10% change in 4 days	+13% change in 3 days	Wetting
		-10% change in 39 days	-10% change in 76 days	Drying

On the basis of these findings, the following conditions of differential moisture variations under driveways during wetting and drying seasons were used to determine possible differential ground movements near driveways:

- During the wet season, both the centre of the driveway and the open field (nature strip) gain soil moisture at similar rates and this creates less differential ground movement;
- During the dry season, the nature strip loses soil moisture at a faster rate than the soil underneath the centre of the driveway and this creates significant differential ground movement;
- Therefore, potential pipe bending is expected to be higher during dry seasons than during wet seasons.

In the finite element analysis (Section 4.4.3), different moisture variations at driveways and nature strips were configured on the basis of these observations (Figure 4.6 and Figure 4.7) as separate moisture analysis was not within the scope of the present study.

4.4.2 Mechanical restraints at driveways

In addition to the soil moisture restrictions, possible mechanical restraints at driveways were investigated to determine the ground movement controls near a driveway. Initially, these driveways were assumed to be fixed and negligible movements were considered in comparison to the soil at nature strips (Section 3.6.1 and Figure 3.10). The observed rigid (reinforced) connections between driveways and road edges were considered in this assumption. This assumption yields a fully restrained upward soil movement under the driveway as the fixed driveway prevents free swelling movement. However, downward movement is unrestricted, as the contact between the soil and the driveway does not show any split resistance. As this behaviour creates distinctive conditions during soil wetting (swelling) and drying (shrinking), potential pipe bending near driveways was assumed to be dissimilar for wetting and drying.

Since this assumption of fixed conditions at driveways was not verified by the field conditions, the measurement of the field behaviour of driveways was required to test the applicability of this assumption. Therefore, a levelling survey was carried out to measure the elevation changes of driveways and adjacent nature strips to investigate their relative movement.

4.4.2.1 Levelling survey to measure field driveway movements

As a relatively simple method of monitoring vertical movements of field driveways caused by seasonal ground movements, a levelling survey was started in April 2015 at McIntosh Road, Altona North. The purpose of this survey was to frequently measure the elevation of selected driveways with reference to a nearby fixed reference point. The elevation change was then calculated to determine the behaviour of driveways due to ground movement.

The selection of fixed reference points was an important step in this survey as these reference points needed to be stable against the surrounding ground movement. A building or a similar structure with deep foundations resting on bedrock was identified as an ideal reference point. However, due to the unavailability of such a structure, two reference points were established prior to the survey.

The two boreholes that were used to collect undisturbed samples (AL 1 and AL 2, Table 3.1) were utilized to establish these reference points. These locations are shown in Figure 4.8.

Figure 4.8. Locations of driveway movement measurements at McIntosh Rd. Altona North

These two reference points (RP 1 and RP2) were located near two sets of driveways selected for this survey. Each set of driveways comprised four driveways and three nature strips between them.

As shown in Figure 4.9, the reference points were made of 25mm diameter steel rods fixed into the bedrock (fixed at 3.1m depth at RP1 and at 2.5m depth at RP2). As a protective measure, a 50mm diameter PVC pipe was inserted around the steel rod and a cover was used at the surface.

a) Schematic diagram of reference points

b) Surface view of reference points (before

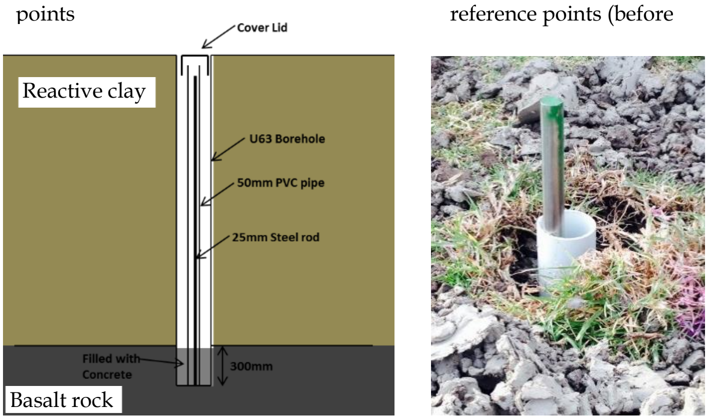

Figure 4.9. Establishment of reference points

In each measurement set, measuring started and finished at these reference points (started from RP1 and finished at RP2). The levelling measurements were taken using a dumpy level (model D10346) and a levelling staff with a least count of 5mm (see Figure 4.10).

Dumpy level

Levelling staff

Figure 4.10. Levelling instruments

The driveway and nature strip movement measurements indicated that the assumption of fixed driveways is not applicable to field driveways. It can be seen that both nature strips and driveways move vertically according to the soil moisture (rainfall) variations (Figure 4.11). This observation was acceptable as the entire area, including the driveway's connection with the road and footpath, is also subjected to moisture-induced ground movement.

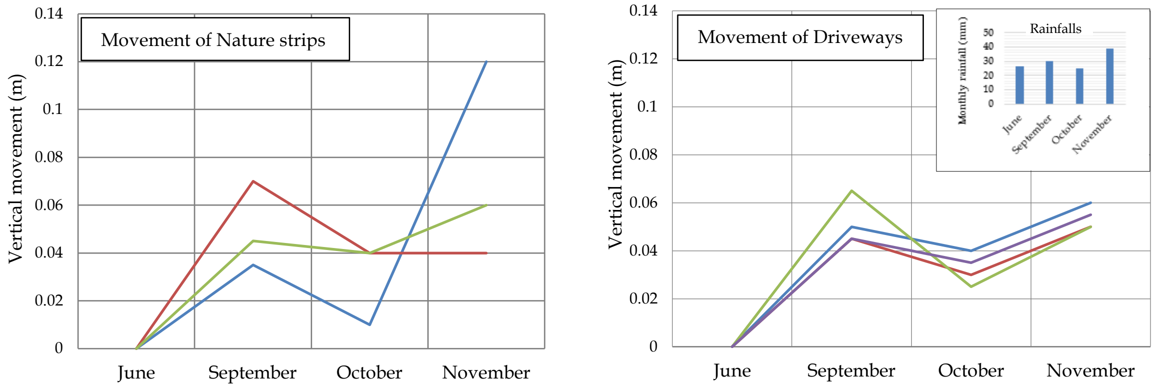

Figure 4.11. Relative movements of driveways and nature strips

After this observation, the previously restrained vertical movement was removed from the general finite element modelling of driveways in this chapter to allow vertical movement with the soil underneath. This new boundary condition at driveways was considered in further finite element analyses of pipe bending at driveways.

4.4.3 Finite element simulations of pipe deformation at driveways

The observations and the theoretical conclusions that were established about changing conditions at driveways were simulated in finite element modelling to observe the effect of these conditions on pipe deformation near driveways. A 10m long nature strip was modelled with a 1.5m wide driveway section (half of a 3m wide driveway). A 100mm cast iron pipe was placed at a depth of 0.75m and the total depth of the soil was considered as the maximum depth of soil moisture variations for Melbourne, 2.3m (Australian Standards, 2011). This model configuration is illustrated in Figure 4.12.

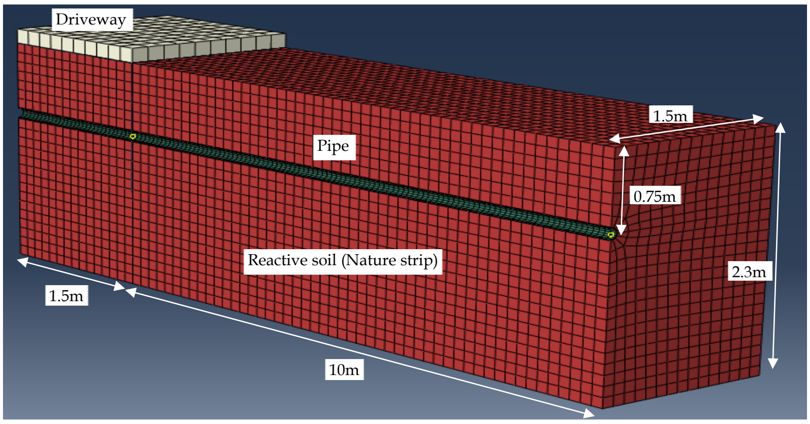

Figure 4.12. Finite element model dimensions

4.4.3.1 Soil moisture variations

Soil moisture variation in the uncovered nature strip area was considered to vary linearly in the vertical direction. This consideration of higher moisture variations near the surface and small variations at deeper depths has been similarly recognised in typical soil moisture profiles (Fityus, 1999; Australian Standards, 2011). In this analysis, three moisture changes $(\Delta\theta_v = \pm 0.01\ (= 1\%),\ 0.03\ (= 3\%),\ 0.05 (= 5\%))$ were applied to the pipe depth with the linear vertical variation, as shown in Figure 4.13.

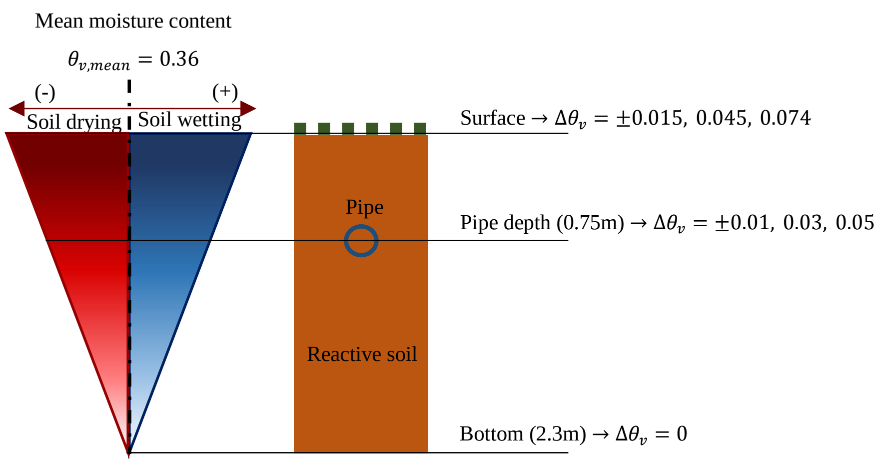

Figure 4.13. Linear moisture variation along the depth

The wetting moisture variations were considered as positive moisture changes and the drying variations as negative changes. The mean volumetric moisture content was assumed to be 0.36 similar to the observations (Section 2.5.1). For finite element modelling, these moisture changes were converted into pore-water pressure changes.

The moisture change under the driveway was considered separately according to the studies in Section 4.4.1. Considering both edge moisture variation (Figure 4.6) and drying/wetting rapidity (Figure 4.7, Table 4.1), changes were applied as shown in Table 4.2. Based on the observations, ratios of 0.1 and 0.6 were applied to the moisture variations between the driveway centre and the nature strip for drying and wetting, respectively.

Table 4.2. Defined soil moisture changes (at pipe depth) at driveway and nature strip

Soil Drying			Soil Wetting		
At nature strip (NS)	Under driveway centre (DW)	Ratio NS:DW	At nature strip	Under driveway centre	Ratio NS:DW
1%	0.1%	0.1	1%	0.6%	0.6
3%	0.3%		3%	1.8%	
5%	0.5%		5%	3%	

The above moisture changes were applied as the hydraulic (suction) boundary conditions at controlled boundaries of the model (under the driveway centre and uncovered area). The intermediate suction variations (the horizontal moisture gradient from driveway centre to edge) are calculated by the programme, according to the Darcy's flow equation and the continuity of the liquid phase (Dassault Systèmes, 2014). For this analysis, the hydraulic conductivity of the basaltic clay soil was assigned as 2.2×10^{-5} m/s (Chan, 2013).

Figure 4.14 shows the results of soil moisture variations under the covered area. A difference between drying and wetting can be seen as the moisture gradient (colour difference) for drying is higher along the pipe than that for wetting.

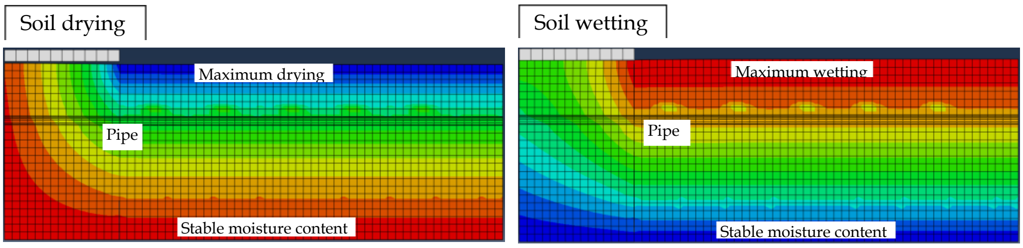

(Blue: minimum moisture content, Red: maximum moisture content)

Figure 4.14. Simulated moisture variations near driveways

4.4.3.2 Restraints on the driveway

As the fixed driveway conditions were found to be not realistic after the field observations, the vertical movement of the driveway was allowed in the general finite element simulations in Chapter 4. However, the rigidity of the driveway was observed to be a factor influencing upward soil movement, as the driveway does not bend with the soil pressure. The considerable thickness (200mm) and the comparatively short length gives this rigidity to the reinforced concrete driveway that has been designed to withstand vehicle loads. Therefore, the driveway slab was restrained from the rotation about its centreline. In comparison, this effect was not expected in soil drying as the soil moves downwards freely (away from the driveway).

4.4.3.3 Pipe stress variations

The longitudinal stress along the pipe was studied to identify the effects of driveways on pipes. Stress along the pipe top and bottom for soil drying and wetting were examined separately, as shown in Figure 4.15 and Figure 4.16 respectively.

The figure indicates that the maximum tensile stresses (positive stresses) occur on the pipe top at the centre of the driveway when the surrounding soil is drying (Figure 4.15). Therefore, according to these results, circumferential failures are likely to appear at the centre of the driveway with crack opening from the pipe top.

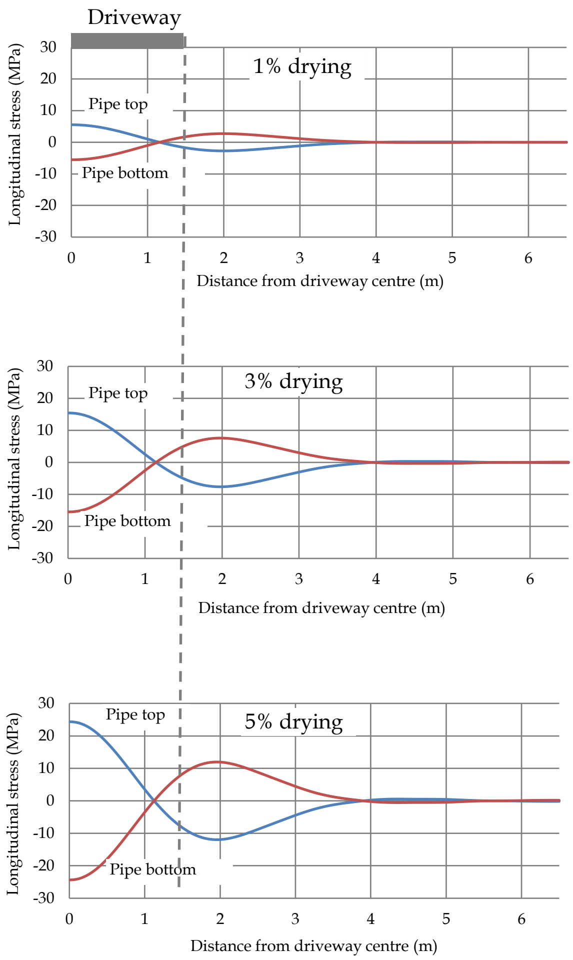

Figure 4.15. Longitudinal stress variation along the pipe – soil drying

In the case of soil wetting, the maximum tensile stresses (positive stresses) occur on the pipe bottom at the edge of the driveway (Figure 4.16). This indicates that failure is likely to occur at the edge of the driveway (1.5m from the centre) with cracking from the pipe bottom.

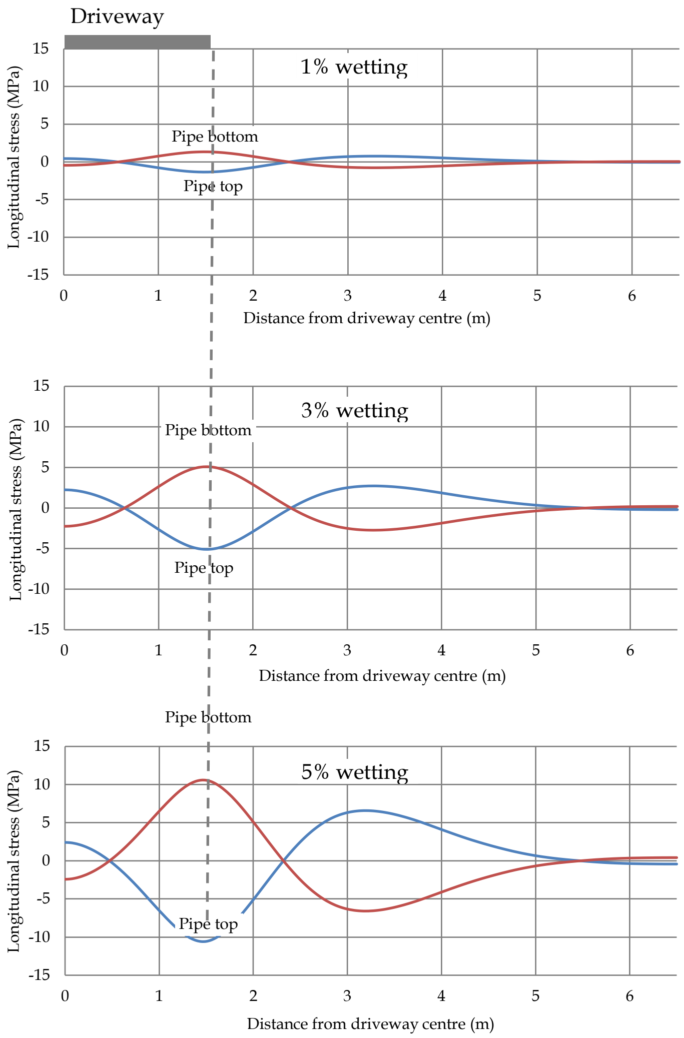

Figure 4.16. Longitudinal stress variation along the pipe – soil wetting

Further comparisons of longitudinal pipe stresses for soil wetting and drying showed that the stresses are more significant in soil drying than in soil wetting. A comparison of these observations is provided in Table 4.3. This observation of higher stress estimations in soil drying is a result of the greater differential conditions expected for soil drying near driveways (Section 4.4.1). This suggests that the failure potential is higher during dry seasons (summer) than during wet seasons (winter). To the author's knowledge, this is the first time a theoretical explanation has been given for this well-stablished observation (Figure 2.14).

Table 4.3. Comparison of pipe stress results near driveways

	Soil Drying	Soil Wetting
Highest tensile stress is at	Centre of the driveway, pipe top	Edge of the driveway, pipe bottom
Stress range (MPa) – for maximum of 5% moisture change	0 to 25	0 to 12
Failure potential	Circumferential failure at centre of the driveway with crack opening from top	Circumferential failure at edge of the driveway with crack opening from bottom

Furthermore the significant stresses only appear close to the driveway and the stresses becomes insignificant more than 4 to 5m from the driveway centre. The maximum stresses are in the range of 25 MPa and they are sufficient to break a corroded pipe with reduced strength (refer to Section 2.2.5.2).

All these observations are theoretically consistent with the hypothetical stress hotspots near driveways and the observation of more pipe failures in summer in Melbourne.

4.5 Bedrock underneath the pipe

The potential importance of the bedrock profile underneath the pipe for pipe stress analysis was considered after the changing depths of the shallow basalt rock profile at Altona North were noted. The available information on bedrock depth along McIntosh Road, Altona North (at borehole locations; AL1 and AL2 in Chapter 3 and BH1 at the instrumentation site (Chan et al., 2015)) shown in Figure 4.17 indicate the variability of the rock profile from 2m deep to more than 3m deep within a distance of less than 200m.

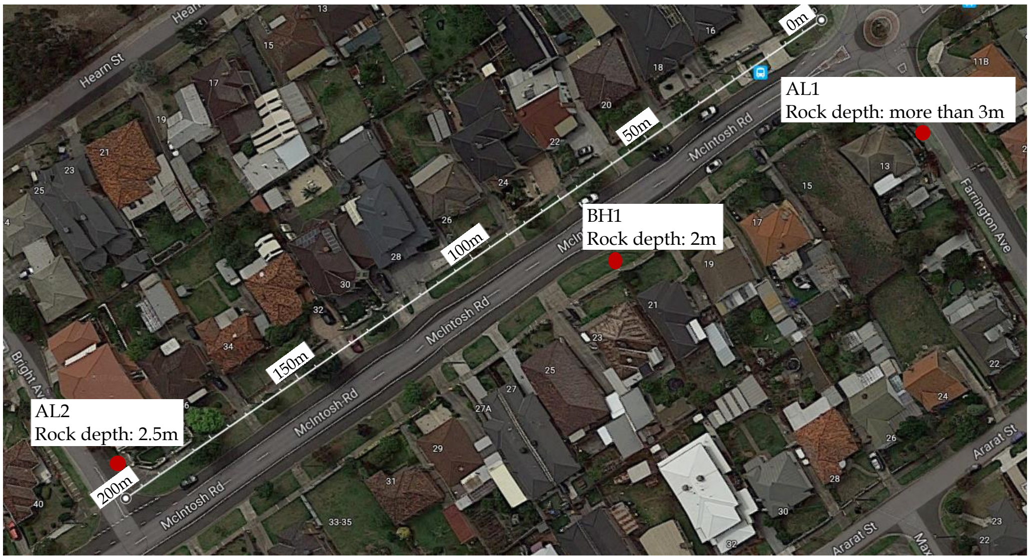

Figure 4.17. Bedrock depth variation observed at McIntosh Road, Altona North

According to geological maps, these reactive soil zones in Western Melbourne suburbs are underlain by variably weathered basalt rock layers formed by historical lava flows (Peck et al., 1992). Therefore, a waving rock profile is conceivable in this region. Furthermore, the rock layers have variably weathered since their original formation about a million years ago.

As illustrated in Figure 4.18, the potential effects of a varying rock profile on pipe deformation were determined as follows:

- A varying rock profile changes the thickness of the overlying clay layer;
- As the total ground movement at a certain depth (pipe depth in this study) is proportional to the thickness of the reactive clay layer (Fityus, 1999; Australian Standards, 2011), non-uniform ground movements take place along the profile;
- Therefore, the pipe may be subjected to differential movements, creating longitudinal bending stresses in the pipe wall; and
- When the rock is near the pipe, the rock peaks restrain downward pipe movement by acting as a mechanical restraint.

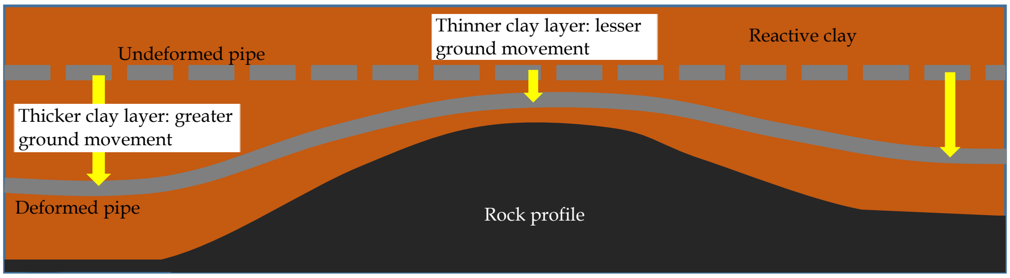

Figure 4.18. Effect of bedrock underneath the pipe on pipe bending

However, a substantial study of this basalt rock profile is required to enhance the applicability of this hypothesis as the primary rock depth information (Figure 4.17) is not sufficient to draw strong conclusions. Therefore, a detailed investigation was initiated to study the true nature of the basalt rock profile of the western suburbs of Melbourne.

4.5.1 Study of basaltic rock surface profile

A comprehensive study of basalt rock depth variations was carried out in the western suburbs of Melbourne where basaltic reactive clays are commonly present. All accessible rock depth information on the area and other possible techniques of measuring rock depth were considered during the initial stage of the study. The selected methods included the evaluation of borehole information and the use of indirect geophysical methods to measure the rock depth.

4.5.1.1 Borehole information – set 1

An extensive borehole dataset of geotechnical investigations in the western suburbs of Melbourne undertaken during sewer pipe construction was obtained from City West Water Ltd. for this study. This dataset contains approximately 75,000 borehole logs along sewer pipelines. Soil profiles were available for 50 to 100m intervals.

A sample of approximately 3000 boreholes covering an area of 15.2km^2 over the suburbs of Altona North, South Kingsville, Yarraville and Newport in the City West Water service region (Figure 4.19) was considered for this primary analysis. The reported depths of basalt rock in each borehole were mapped over the space to identify the rock depth variations in this selected area.

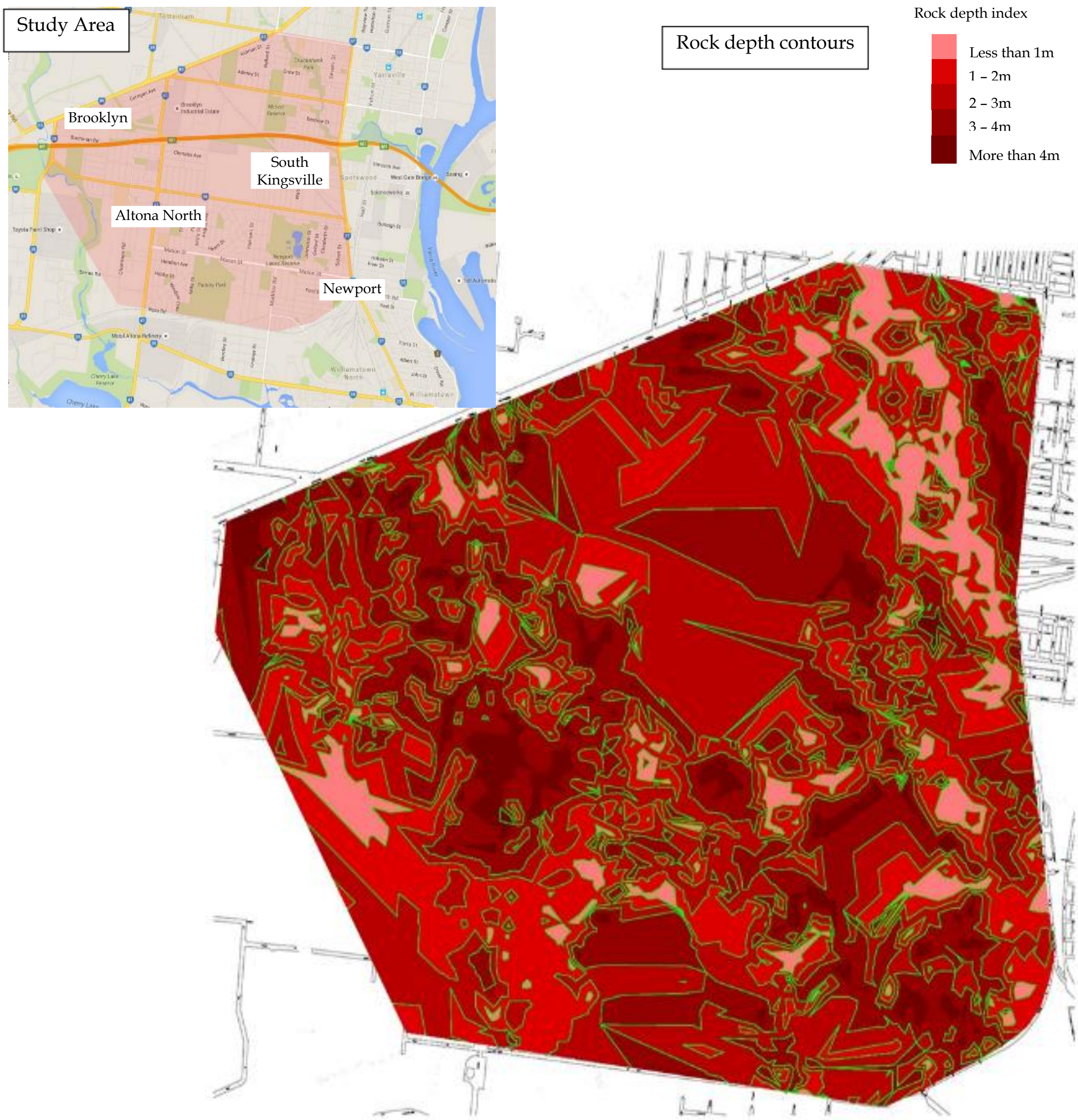

Figure 4.19. Rock depth variations in western suburbs

As can be seen in the contour map (Figure 4.19), the basalt rock depths show a considerable variation from shallower than 1m to deeper than 4m in the region under consideration. These depths were measured relative to the ground surface at the time of borehole investigation. The contours were generated by plotting the surface in the commercial drawing and analytical software, Autocad Civil 3D (Autodesk Inc., 2014).

These contours were then used to generate section views along 15 selected pipelines in the region under study. Significant variation of rock depth and the large number of past pipe failures were factors taken into account in the selection of 15 sections, which are shown in Appendix A. In particular, two selected sections with higher rock depth variations are shown in Figure 4.20. Note that rock profile variations below the moisture variation depth, which is 2.3m for the study area (Section 2.5.2), do not appreciably affect the pipes as ground movement is not significant below that depth. In addition, the minimum gap between pipe and rock was assumed to be 150mm according to the construction guidelines used at the time (Section 2.2.4).

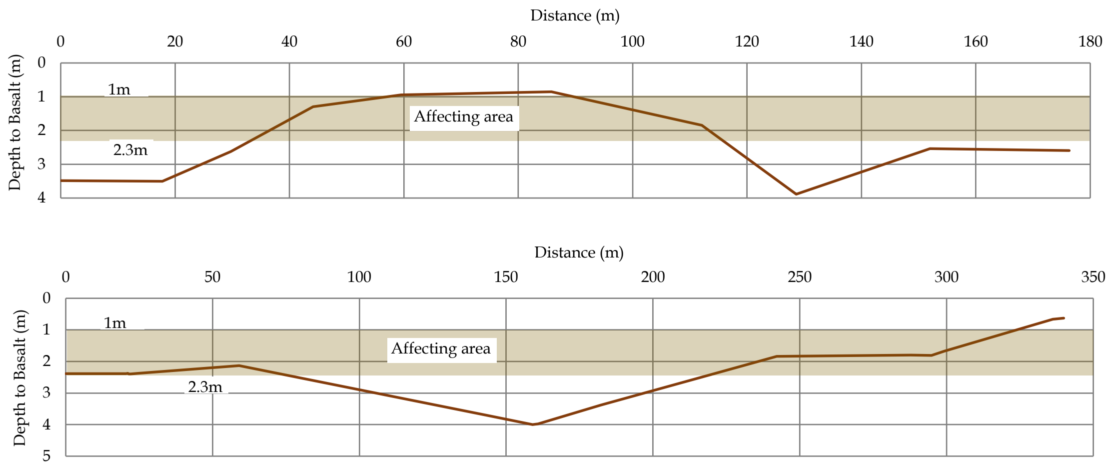

Figure 4.20. Basalt rock profile section views

As can be seen in Figure 4.20, the rock depth varies between 1m and 2.3m along the pipelines within the area under study. However, the characteristics of these rock slopes were studied prior to quantifying their effects on the pipes. The following rock slope characteristics, also illustrated in Figure 4.21, identified for each section are listed in Table 4.4:

- Minimum depth from the ground surface;
- Vertical dip, measured from top of the slope to the bottom of the slope or to the end of the moisture variation depth;
- Horizontal length; the horizontal run of the slope;
- Dip angle and the slope gradient; and
- Crest shape; flat or sharp.

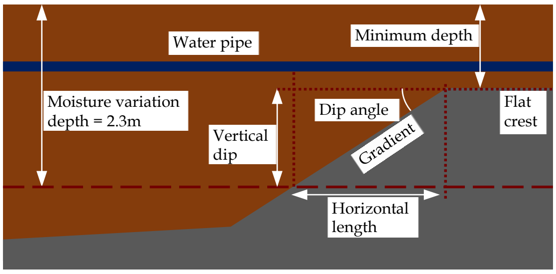

Figure 4.21. Rock slope characteristics

Table 4.4. Characteristics of 15 rock sections

Section no.	Minimum depth (m)	Vertical dip (m)	Horizontal length (m)	Gradient (%)	Dip angle (^{0})	Crest shape
1	1.0	1.3	19.8	6.5	3.7	Flat
2	1.2	1.1	23.7	4.6	2.7	Flat
3	1.0	0.8	30.1	2.6	1.5	Flat
4	Rock is below the moisture variation depth (2.3m)					
5	1.4	0.9	78.8	1.1	0.6	Sharp
6	1.0	1.3	38.0	3.4	2.0	Flat
7	2.0	0.3	16.6	1.8	1.0	Sharp
8	1.0	1.3	45.1	2.9	1.7	Sharp
9	1.7	0.6	15.1	4.0	2.3	Sharp
10	1.7	0.6	19.9	3.0	1.7	Sharp
11	Rock is below the moisture variation depth (2.3m)					
12	Rock is below the moisture variation depth (2.3m)					
13	Rock is below the moisture variation depth (2.3m)					
14	1.4	0.9	14.4	6.2	3.6	Sharp
15	1.3	1.0	36.5	2.7	1.6	Sharp

As Table 4.4 shows, the maximum rock slope dip angles are in the range of 3 to 4 degrees and some rock profiles are very close to the pipe depth (0.75m). In addition, both flat and relatively sharp rock protrusions are identified near the pipe. The influence of critical rock profiles was studied by analysing finite element models, as discussed in Section 4.5.2.1.

However, it is to be noted that these rock profiles were determined by interpolating borehole information at 50 to 100m intervals. Therefore, the precision of the intermediate rock depth information cannot be refined as rapid rock depth variations were not captured in the linear interpolation over long distances.

4.5.1.2 Borehole information – set 2

A second set of boreholes, provided by Golder Associates Pty Ltd (Gniel, 2017), was used for further analysis of rock depth variations in the western suburbs. This dataset consists of borehole information along a 900m distance at 3m intervals. As the information is available at closer intervals, this dataset was used to identify the possible fine variations of the bedrock which were not captured in the previous dataset.

The rock depth variation relative to the ground surface was analysed and the results are shown in Figure 4.22. The highlighted zone in the figure shows a critical variation when considered with an approximate pipe depth of 0.75m and the moisture variation depth of 2.3m. However, there was no record of a pipe along this borehole series and the marked depth is for an imaginary pipe.

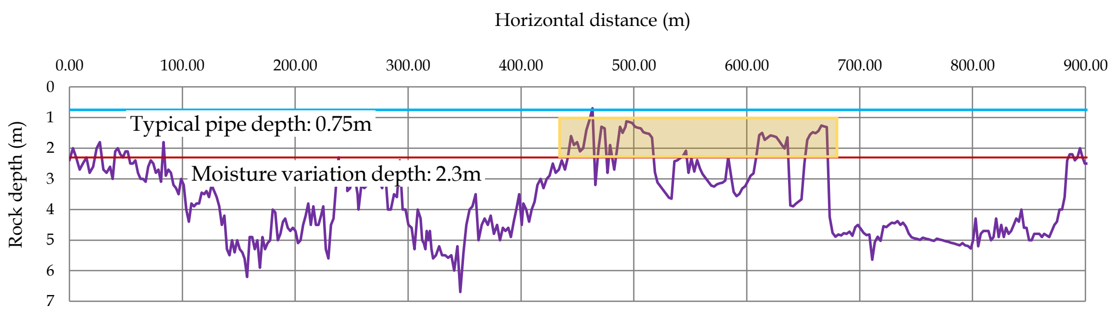

Figure 4.22. Rock depth variation – borehole set 2

It was observed that the rock slopes at some locations are as steep as the dip angles (calculated from slope gradients) are more than 50 degrees, which is considerably larger than the dip angles of borehole set 1 (Table 4.4). This highlights that this section was suspected to generate significant stresses on the pipe. A numerical simulation was performed on this section to study the possible stresses on the pipe and the results are presented in Section 4.5.2.2.

This borehole data analysis verifies the existence of significant rock protrusions close to the pipe burial region. However, a more refined data set is required to detect such close variations of the rock profile.

4.5.1.3 Ground Penetration Radar surveys

In an alternative approach, a ground penetration radar (GPR) survey was carried out to verify the rock depth along the pipelines. GPR is a common method of investigating the sub-surface properties of soil and rock (Davis and Annan, 1989). This method was also considered a convenient method to investigate rock profiles near pipes as no excavation is involved. This study was collaboratively carried out with the School of Earth Atmosphere and Environment, Monash University. McIntosh Road, Altona North was selected for this survey which was completed on the 25th and the 31st of May, 2016. GPR instruments with radar frequencies of 250 and 100MHz were used, as shown in Figure 4.23. The survey and the analysis of the results were carried out by a commercial company (Hunter Geophysics).

Figure 4.23. GPR surveying at McIntosh road, Altona North

The final outcome of the survey is shown in Figure 4.24 as a colour map of rock depth variations. These data represent the results of the 250MHz radar survey. The rock depths were determined by analysing the subsurface layers identified from filtered (to remove extraneous noise) GPR data. The locations of the primary borehole information presented in Figure 4.17 are also indicated in this figure for comparison of the rock depth measurements.

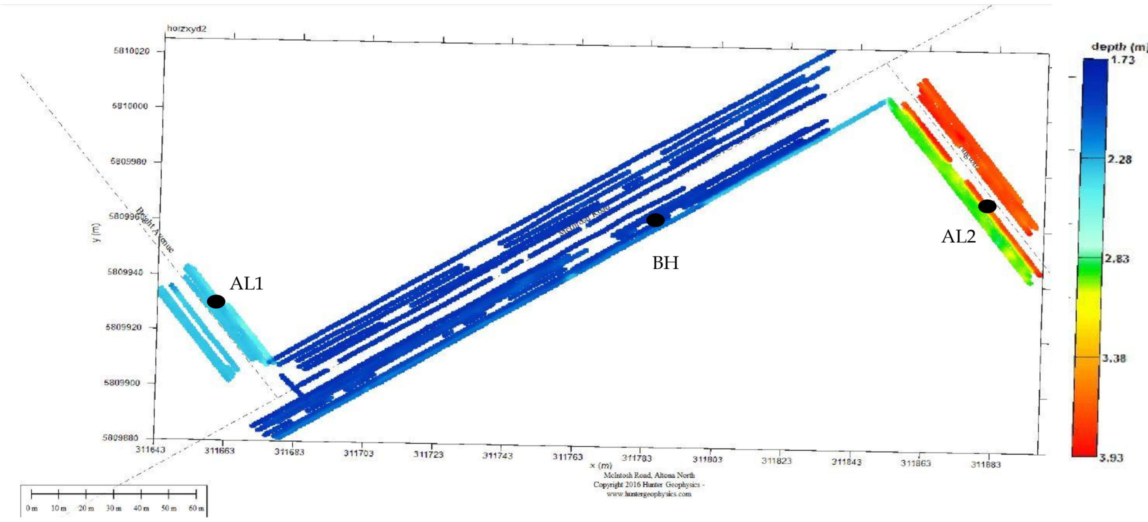

Figure 4.24. Bedrock depths from the 250MHz GPR survey

It can be seen that the bedrock depths from the GPR survey show good agreement with the measured bedrock depths, which are 2.5m at AL1, 2m at BH and beyond 3m at AL2. Therefore, the use of GPR to investigate bedrock depth information is a sufficiently accurate technique to be considered for further studies. However, more research is needed to improve the accuracy of the produced results.

4.5.2 Finite element simulations of the effect of rock protrusions near the pipe

The possible influence of these rock profile variations on pipe deformations and the resultant bending stresses were studied by analysing several finite element models. Natural rock slopes that were observed in the field data as well as in some assumed rock slopes were considered in this analysis. The outcomes of these simulations are explained below.

4.5.2.1 Analysis of natural rock slopes – borehole set 1

Considering the rock depth analysis of borehole set 1 and the slope characteristic data in Table 4.4, section number 1 was selected for finite element simulation as it contains a slope with a maximum dip angle of 3.7^{0}.

The stress variations of a 100mm diameter cast iron pipe at 0.75m depth were analysed with the selected rock profile section as shown in Figure 4.25. A 0.05 moisture change was applied to the pipe depth with linear variations for both wetting and drying analyses, as shown in Figure 4.13.

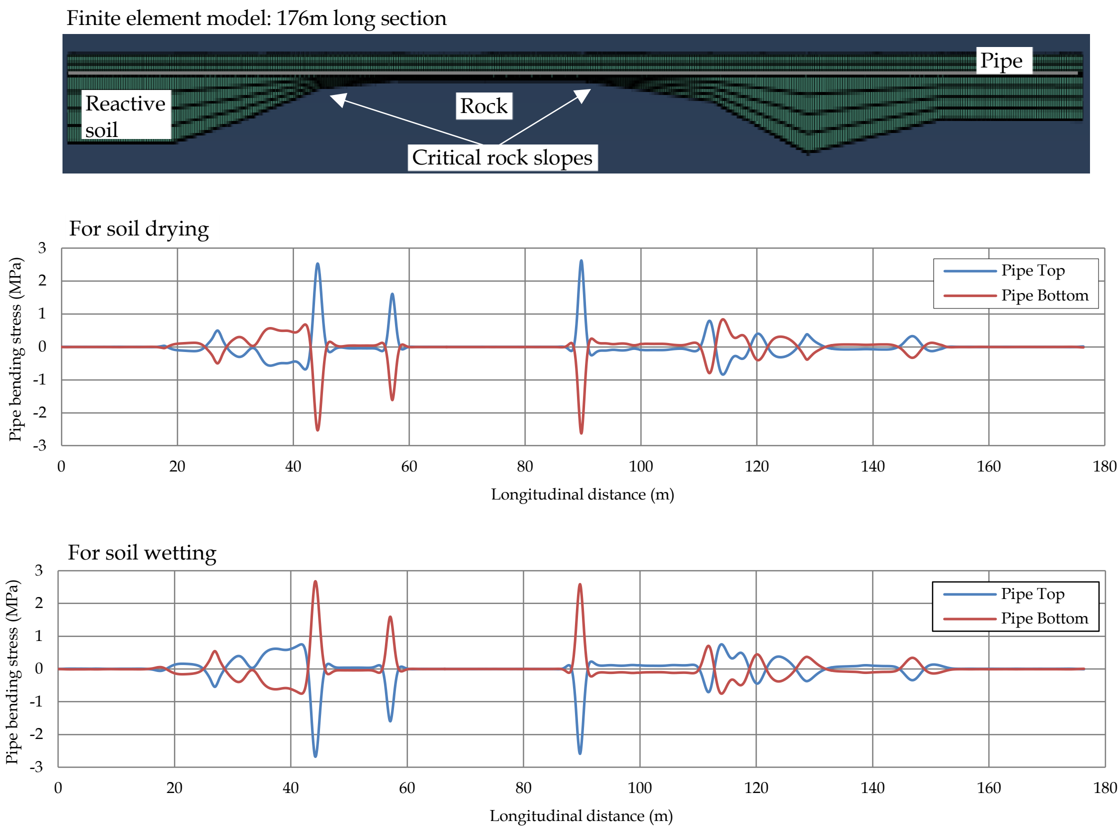

Figure 4.25. Pipe bending stress variation due to natural rock slopes of borehole set 1

As can be seen in the above figure, the highest tensile pipe stresses (longitudinal bending stresses) at critical rock slopes are about 2.7 MPa for the applied soil moisture change. The reason for these relatively low stresses can be explained by the lower gradients of the natural rock slopes of borehole set 1. However, this analysis shows that the stresses are high at critical slopes. The pipe top is subjected to the highest stress when the soil is drying and the pipe bottom is subjected to the highest stress for soil wetting.

Also, it is noted that any rock depth variation significantly deep from the pipe level is not caused appreciable effects on the pipe. This is due to the insignificant differential ground movements since the influence of moisture variation at significant depths is marginal.

4.5.2.2 Analysis of natural rock slopes - borehole set 2

The critical section of the borehole set 2 (highlighted section in Figure 4.22) was also analysed assuming a 100mm diameter cast iron pipe at 0.75m depth. A similar moisture change to the analysis in borehole set 1 rock slope was applied to this analysis for both wetting and drying cases and the pipe stress variations are shown in Figure 4.26.

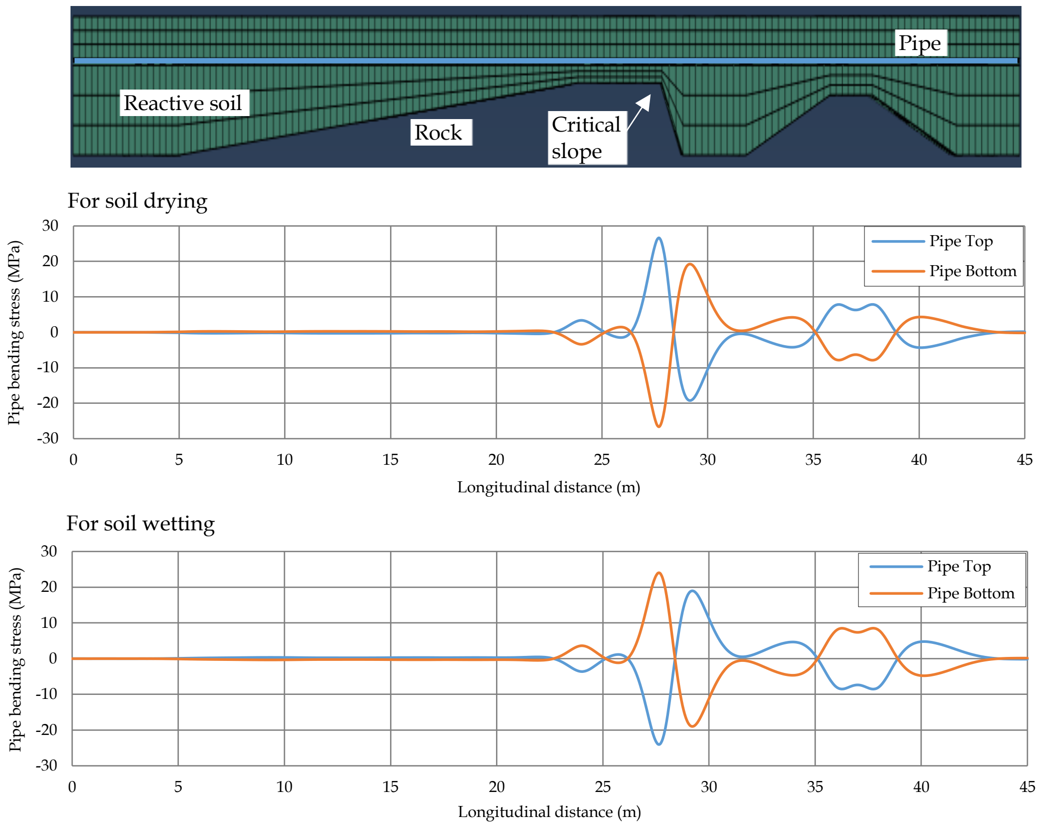

Figure 4.26. Pipe bending stress variation due to natural rock slopes of borehole set 2

This analysis shows that the maximum pipe tensile stresses are very high at the critical rock slope. The characteristics of this slope are shown in Table 4.5 with the maximum pipe stress results. Note that these stresses are sufficient to break a corroded pipe with a reduced strength as shown in Section 2.2.5.2.

The reason for the relatively similar maximum bending stresses for soil wetting and soil drying cases can be explained as the similarity differential ground movement profiles for both swell and shrink conditions. As the total length of the pipe, including the section above the rock hump, is surrounded by reactive soils, the pipe is simply moving with the ground and reduces the effects of bending against the hard rock when soil drying. However, greater differences in pipe stresses between wetting and drying conditions were observed when the pipe is directly placed on the rock, which is unrealistic according to the information in Section 2.2.4.

Table 4.5. Evaluation of maximum pipe stresses due to critical rock slope of borehole set 2

Characteristic	Value
Minimum depth	1m
Slope gradient	130%
Dip angle	52.4^0
Maximum tensile stress - drying	26.6 MPa (pipe top)
Maximum tensile stress - wetting	24.0 MPa (pipe bottom)

Since the pipe stresses are significant when the dip angle of the rock slope is relatively high and the rock is close to the pipe, as in this natural rock profile (Figure 4.22), it can be concluded that the presence of such rock profile variations in the field is a considerable factor for pipe stress analysis. However, more data should be used in the future to find similar rock slopes underneath the pipe network which critically affect the pipes.

4.5.2.3 Analysis of assumed rock slopes

In addition to the natural rock slope analyses, some assumed rock slope profiles were analysed to study the effects of variation of the rock slope characteristics illustrated in Figure 4.21 on pipe bending stresses. The results are shown in Figure 4.27.

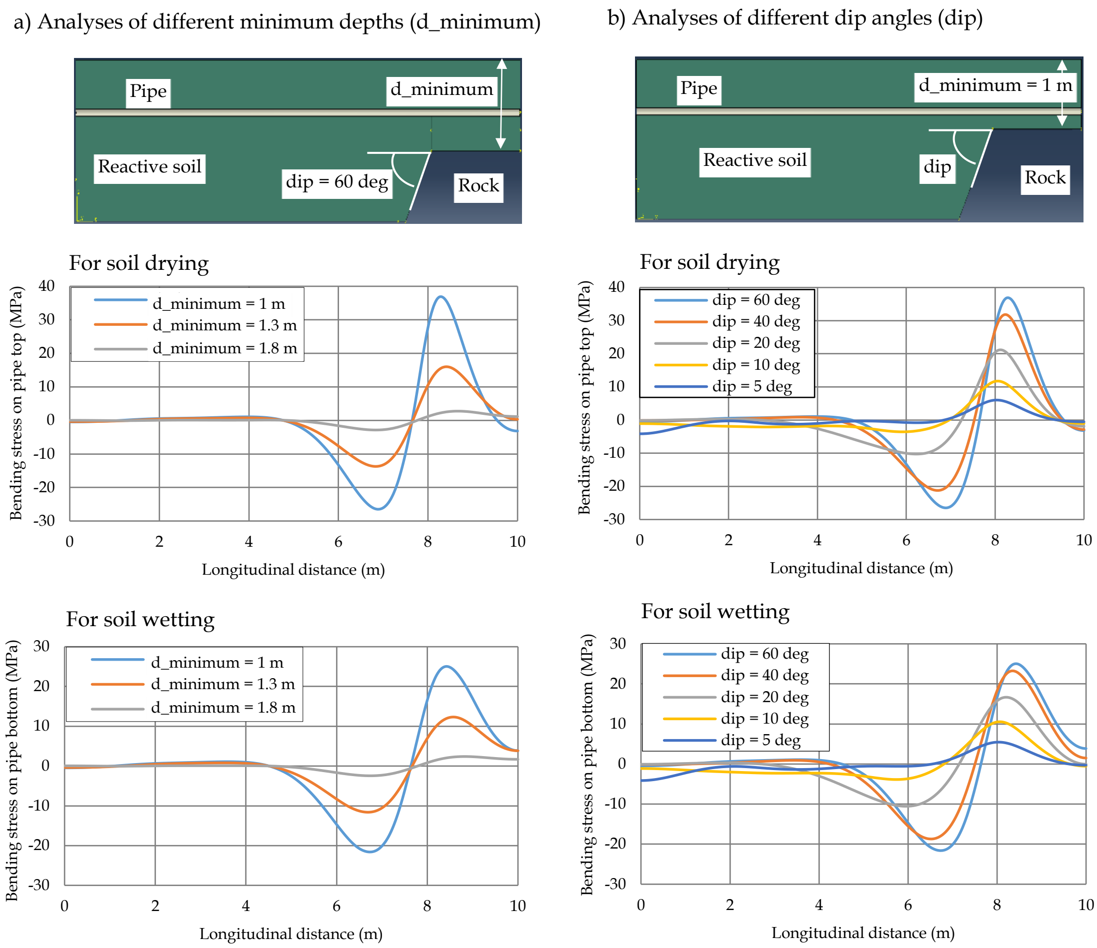

Figure 4.27. Results of analyses of assumed rock slopes

A 100mm diameter cast iron pipe at 0.75m depth was analysed with assumed rock slopes of different minimum depths (d_minimum) and different dip angles (dip). Similar to the previous analyses, a moisture change of 0.05 was applied to the pipe depth (with the linear depth variation shown in Figure 4.13) for both drying and wetting. The results depicted in Figure 4.27 show that the pipe bending stresses (tensile) are maximum for shallower minimum depths (d_minimum) and steeper dip angles. The maximum tensile stresses were observed in the range of 30 to 40 MPa for soil drying and 20 to 30 MPa for soil wetting. Note that the stresses on the pipe top are plotted for soil drying and the pipe bottom stresses are plotted for soil wetting with the maximum stress observations in Figure 4.25 and Figure 4.26.

Based on these results, the effect of rock slope variation on pipe stress is significant when the variation is steep and the rock is close to the pipe. The field example of borehole set 2 data (Table 4.5) shows the presence of such critical rock profiles in natural rock.

4.6 Soil Boundaries

Previously, uniform ground movement along a pipeline was assumed when both soil properties and moisture variations were considered uniform along the pipeline section. However, these uniform conditions may alter at a soil boundary that separates two different soils. As a result, these variations were assumed to cause differential ground movements at the soil boundaries. Such distinct boundaries are hard to be expected in natural soil property variations such as at the boundary of geological formations, whereas man-made soil boundaries may be present. For example, the boundary of a newly backfilled soil or a deep road base can cause pipe bending if the soil reactivity is different in the filled soil. Therefore, such soil boundaries were also identified as potential stress hotspots and the possible pipe bending is illustrated in Figure 4.28. However, such identifiable soil boundaries are not found in the field as commonly as other stress hotspots.

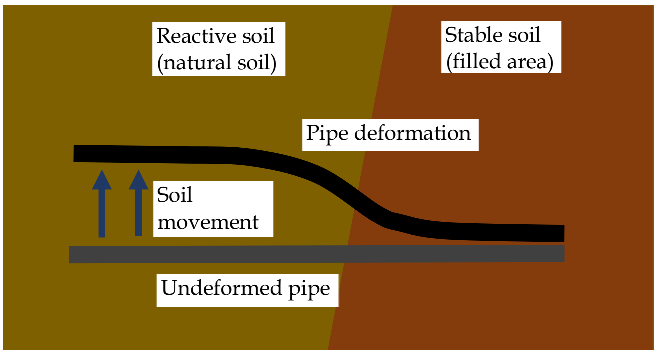

Figure 4.28. Pipe bending at soil boundaries

4.6.1 Finite element simulations

The results of a finite element simulation of pipe behaviour at a reactive and non-reactive soil boundary are shown in Figure 4.29.

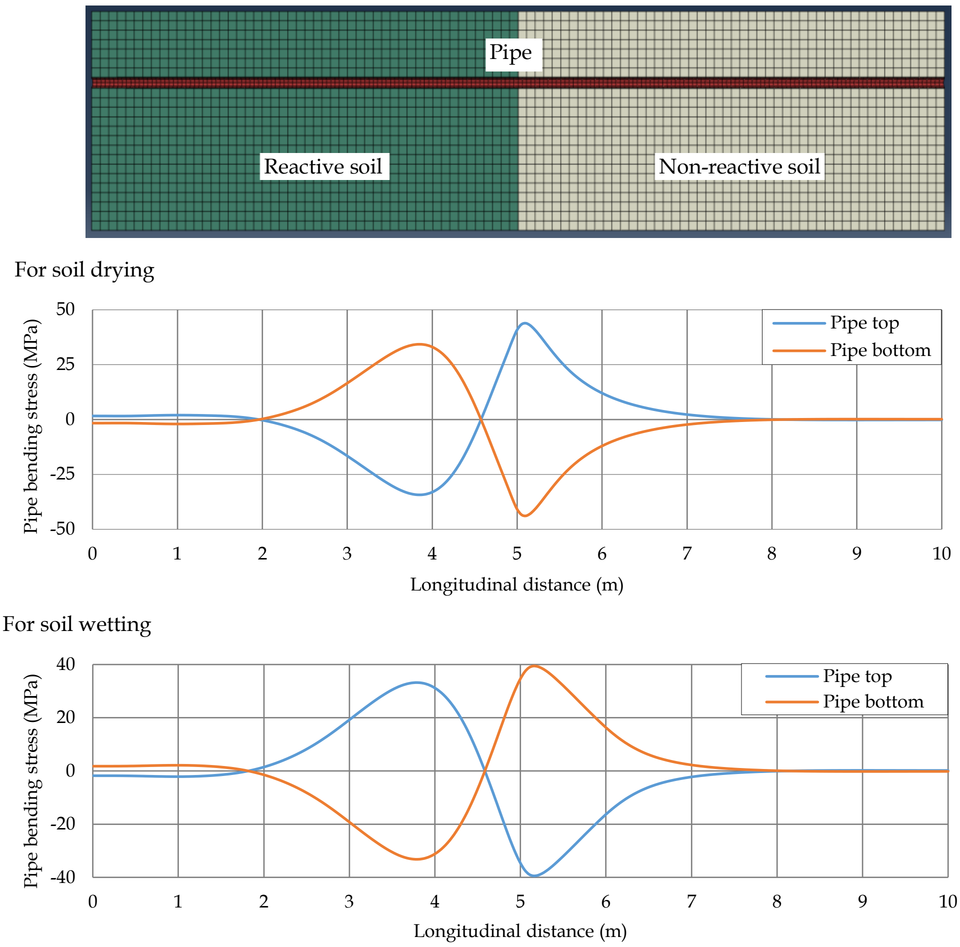

Figure 4.29. Pipe bending stress variation at soil boundaries

A 100mm diameter cast iron pipe was analysed for 5% moisture change (for both drying and wetting) at a pipe depth of 0.75 m from the surface. Reactive soil was modelled with similar soil properties to the other simulations in this chapter and the non-reactive soil was modelled without the moisture swelling component of the soil model.

According to the results (Figure 4.29), the maximum stresses were observed at the soil boundary, as the pipe section in reactive soils moves with ground swell and shrinkage while non-reactive soil holds the pipe against vertical movement. The highest tensile pipe stresses observed in this analysis, which are in the range of 40 to 45 MPa, may be a slight over-estimation of field pipe stresses as such distinct soil boundaries are not commonly found in the field. However, this analysis shows that reactive soil property variations along the pipe can generate significant stresses on pipes, especially at their boundaries.

4.7 Water Leaks

In general, seasonal or weather-affected soil moisture changes of open land (in nature strips) were assumed to be uniform along the pipe as the environmental conditions are uniform. However, these uniform moisture conditions can change when water leaks from a pipe. Concentrated wetting can create localised swelling and uplift of the pipe locally. This effect creates another stress hotspot along the pipe as the deformation pattern is expected to be as shown in Figure 4.30.

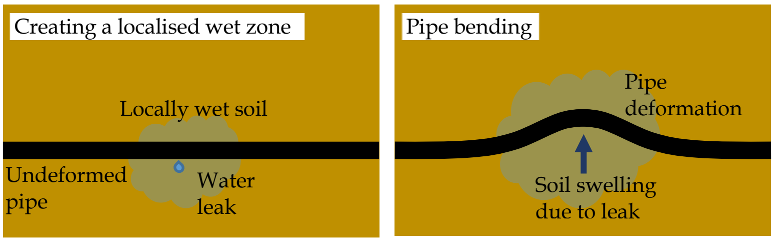

Figure 4.30. Possible pipe bending at water leaks

4.7.1 Possible water leaks in a pipe network

Depending on the pipe conditions, water leaks can occur anywhere along the pipe. The main reasons for water leaks have been identified as through-wall corrosion patches and manufacturing defects in the pipe wall (Shannon et al., 2016b; Rathnayaka et al., 2017). In addition to through-wall water leaks, faulty connections or past repair clamps can also cause water leaks in a pipe network. Such water leaks were consistently identified during the field case studies presented in Chapter 5. The identified potential leak locations can be listed as follows:

- Through-wall corrosion patches

- Manufacturing defects
- Loosened clamps of old repairs
- Leaking at house connections
- Pipe connections or joints

Therefore, any of the above locations can be assumed to be a potential pipe stress hotspot.

4.7.2 Finite element simulations of water leak effects

A finite element model of a leaking pipe was analysed by simulating an assumed locally-wetted soil region around the pipe. The soil moisture in the wetted region was increased to full saturation while the soil moisture in the remaining area was unchanged. A small wetted region 300mm wide and 400mm deep (below the pipe) was assumed for this analysis, as shown in Figure 4.31. However, the extent of such locally wetted regions due to leaks can widely vary in the field as it depends on the soil properties as well as the duration of the leak. This simulation is only an example of such a water leak.

Similar to the previous cases, a 100mm diameter cast iron pipe at 0.75m depth was modelled to study the response of the pipe. Three different models were analysed with three initial moisture contents to observe the pipe bending due to water leaks in wet and dry seasons.

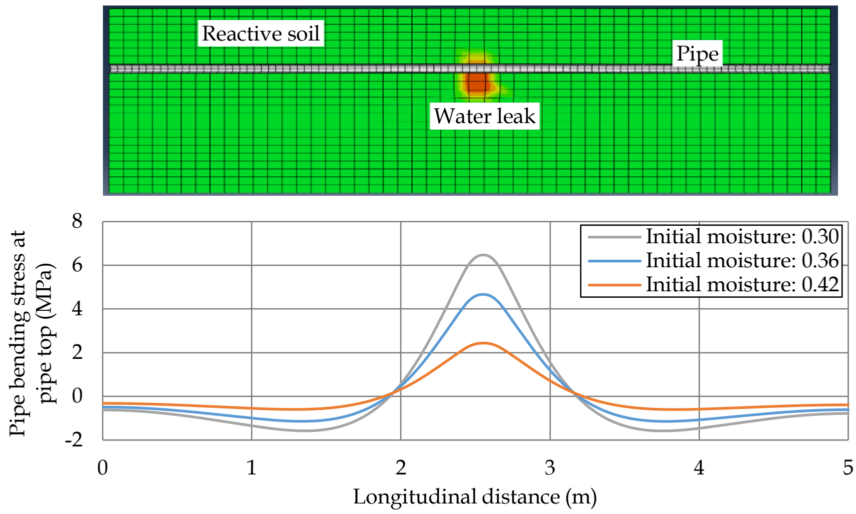

Figure 4.31. Pipe bending stress variation due to water leaks

The results of this analysis shows that the highest tensile stresses at the pipe top (only pipe top stresses are plotted in Figure 4.31 as the maximum tensile stresses were observed at the pipe top) are from the driest initial conditions (volumetric moisture content of 0.30) and the minimum is from the wettest initial conditions (volumetric moisture content of 0.42). The reason was identified as the high soil swelling when wetting from a drier condition than wetting from a wet condition. The estimated stresses in Figure 4.31 may increase when a larger area is wetted due to the leak. Therefore, it can be concluded that pipes are more affected at leak hotspots during dry seasons (summers).

4.8 Tree Roots

Large trees are commonly seen in most nature strips where the pipes are laid. When the roots of these trees grow near pipes, the pipes can be affected in several ways. Mainly, these effects can be categorised into two groups: mechanical constraints and moisture controls. Both scenarios were assumed to affect the ground or pipe movements and to create stress hotspot conditions, as explained below.

4.8.1 Mechanical restraints from tree roots

The movements of tree roots relative to the surrounding soils are expected to be minimum as the roots can grow over a wide range. For most large street trees, the root depth has been found to be as deep as more than 5m, depending on the availability of water and other factors (Crombie et al., 1988). Therefore, reactive soil- induced pipe movement can be restricted when the pipe is in contact or extremely close to a tree root. This restriction was considered to identify the pipe deformation near the tree roots, as shown in Figure 4.32.

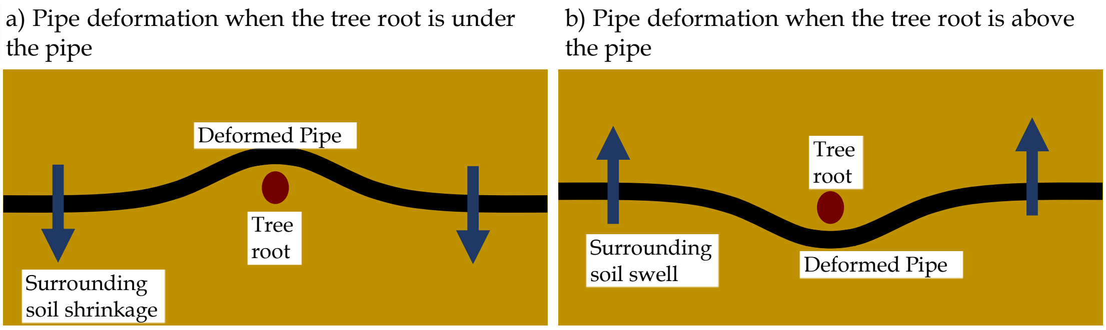

Figure 4.32. Possible reactive soil caused pipe deformation near tree roots

In addition to the above, the gradual growth of tree roots near pipes has been an identified problem for some water utilities (South East Water, 2015) and wind- caused movement of trees observed under certain circumferences (James and Hallam, 2013) has been identified as affecting pipe stresses by either imposing or restricting additional movement with respect to the pipe/soil interaction. However, this type of condition can cause elevated stresses in pipes whether the soil is reactive nor not.

4.8.2 Effect on moisture content changes

In addition to the movement influences coming directly from tree roots as identified above, it is also possible to induce additional soil movement due to the elevated suction generated by tree roots (Li et al., 2014; Li and Guo, 2017). However, this moisture effect was not considered in the finite element analyses in the present study.

The effects of tree roots on shallow foundations for light structures such as houses have been studied in some detail and appropriate methodologies for incorporating them into foundation design have been reported (Cameron et al., 2006).

4.9 Other possible hotspots

In addition to the stress hotspots discussed above, which are mainly created by external features, pipe joints and connections may be considered as hotspots that are created by the pipe network itself. Depending on the fastening method and the dimensions of the method, these spots can cause higher bending stresses on the pipe due to ground movement including that due to reactive soils. Due to time constraints, the pipe behaviour at joints was not considered to be within the scope of the present study. Nonetheless, it should be noted that for small-diameter cast iron pipes, as the joints are significantly stronger than the pipe barrel, direct joint failures are not commonly observed. However, for large-diameter cast iron pipes, it has been observed that joints can fail by developing cracks due to over-stressing (Jiang et al., 2017a). Due to the high moment of inertia in large-diameter pipes, pipe barrels behave mostly as rigid bodies, transferring any ground movement-induced deformations to joints and potentially generating very high stresses.

In addition, pipe bending under the road intersections are also believed to be similar to the pipe behaviour under driveways. However, conditions at the road can be significantly more complicated due to the presence of variable road base material placed during construction, the influence of intermittent traffic loads, changes during road maintenance etc. In addition, pipe elevation can also be changed or sleeves can be put in within roads to protect the pipe. Furthermore, road crossings are not at all common as driveways in reticulation systems.

4.10 Conclusions

This chapter has presented a theoretical analysis of pipe bending mechanisms at certain locations where the stresses were expected to be maximal. These locations were named stress hotspots on the pipe. The major outcomes of this study can be summarised as follows:

- Stress hotspots were theoretically identified at driveways, shallow bedrock profiles, soil boundaries, water leaks and tree roots. At all these locations, reactive ground movement imposes differential movements on the pipe due to the non-uniform conditions in the soil environment;
- Impermeable driveways create differential moisture variations at the centre of the driveway compared with uncovered soil and the rigidity of the driveway partially restrains upward soil movement under the driveway. In addition, more differential conditions were observed for soil drying than for soil wetting. The maximum tensile stresses were identified on the pipe top under the centre of the driveway for soil drying and on the pipe bottom under the edge of the driveway for soil wetting;
- Sharp variations of rock profile near the pipe were identified as creating maximum pipe bending due to the changing reactive soil thickness below the pipe. Analyses of field data confirmed the existence of such critical rock profile variations in the reactive soil areas of Melbourne; and
- The presence of tree roots near the pipe was identified as another stress hotspot due to pipe movement restraints, affecting soil moisture and pushing the pipes.
- The boundaries of different soils (reactive and non-reactive) were identified as another stress hotspot, as differential ground movement creates critical pipe bending.
- Localised soil swelling due to water leaks was also identified as a stress hotspot due to pipe uplift at wetted areas.

In addition to the above conclusions, some similarities have been observed in different hotspot scenarios. For example, similar pipe bending patterns were observed in pipe bending at driveways under drying conditions, near water leaks and near the tree roots under both wetting and drying conditions. Similarly, pipe bending patterns at driveways under wetting conditions, near rock humps under both wetting and drying conditions and at soil boundaries under both wetting and drying conditions were observed to be comparable.

The verification of the existence of such stress hotspots in the field is presented in the next chapter.

CHAPTER 5: SMALL-DIAMETER PIPE FAILURE CASE STUDIES

5.1 Overview

The previous chapter concluded that circumferential (broken-back) failures in reactive soil zones are likely to occur at certain places (stress hotspots) where differential ground movements occur. The small-diameter pipe failure case studies presented in this chapter evaluate the field evidence for these pipe failures at hypothetical stress hotspots and the predicted circumferential failure mechanisms. The aim of these case studies was to gather detailed information about cast iron pipe failure due to ground movement and identify the relevance to stress hotspots. Therefore, cast iron pipe failures in severely reactive soil zones of Melbourne were the focus of these studies. Visual inspections of the pipe failure environment and the failure crack orientation were used to identify the cause and categorise the failures. Samples of the replaced failure sections were brought to the laboratory for further condition assessment. These case studies provide extensive knowledge about field activities related to pipe failures and repair processes in order to enhance practical understanding. This chapter explains all the findings of 21 cases studied over a period of 13 months.

5.2 Planning of Pipe Failure Data Collection

The requirement for a small-diameter pipe failure data collection arose when a comprehensive dataset of pipe failures in reactive soil zones was needed for the verification of the theoretical findings of circumferential failure mechanisms. The existing information about past pipe failures, consisting of failure dates, street addresses of failure locations, pipe specifications and brief facts about failure types (leaks and bursts) are alone insufficient for detailed studies of their failure mechanisms and the failure environment. However, these data have been used in statistical analyses of pipe failure prediction methods as the existing information is sufficient for such analyses (Chik, 2018).

As mechanistic studies are associated with pipe stress and deformation analysis, additional information about the failure environment is necessary to assess failures as listed below:

- Accurate location

Accurate failure location is important as it provides information on nearby features such as driveways, trees, rocks etc. that may directly affect failures.

- Failure type (circumferential or longitudinal split)

Detailed information on the failure type is necessary to compare the effects of stress hotspots on different failure types. As the primary analyses of stress hotspots were limited to circumferential failures, observations of longitudinal splits can be used to verify any effects of identified stress hotspots on longitudinal split failures.

- Crack orientation (pipe top, bottom or side)

As the location of crack initiation on the pipe determines the orientation of the highest stress, this information can be used to identify the pipe bending that caused circumferential failure. In the case of longitudinal split failure, information on the crack location can be used to evaluate the crack initiation associated with the current condition of the pipe.

- Corrosion level

The observation of corrosion in the pipe is important, as corrosion patches increase the stresses to the failure level and the distribution of corrosion patches affects crack initiation (see Section 2.2.5). When pipe samples were not available for laboratory inspections, visual evidence of corrosion (Mohebbi and Li, 2011), including yellowish-brown patches on the pipe wall and soil colour change around the pipe, was sought to determine corrosion in the field.

Since this information was not recorded on past pipe failure data sheets, the data collection was specifically planned to collect field pipe failure data for mechanistic studies of small-diameter pipe failure.

5.2.1 Study area

The selected study area for these case studies is shown in Figure 5.1. This area was selected on the basis of the soil properties and the travel time from Monash University, Clayton campus. As circumferential failures due to reactive ground movement are frequently reported in the western suburbs of Melbourne, a total of 12 western suburbs shown in Figure 5.1 were selected for these studies.

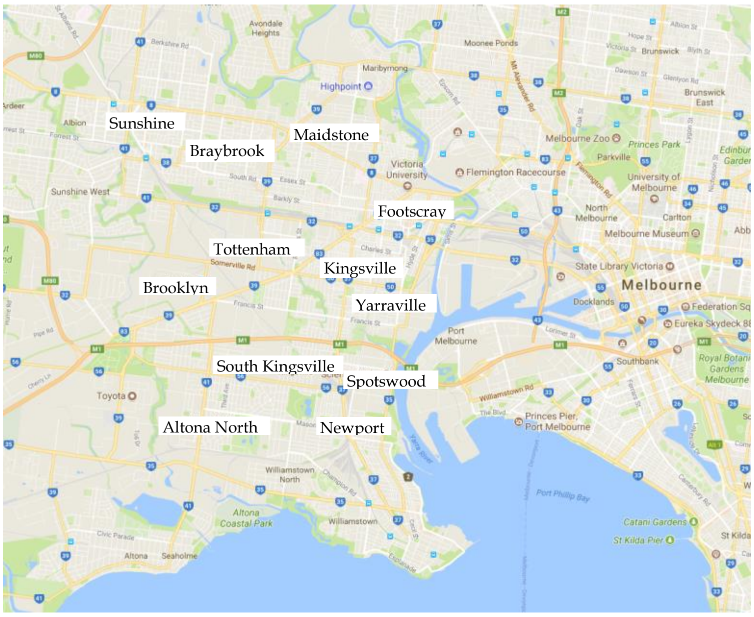

Figure 5.1. Study area of the case study (Google Maps, 2017)

Prompt arrival at the repair location during repairs was necessary as the required information can only be collected during the repair process. Therefore, a manageable travel time was also considered when selecting this area for the daily data collection. As scheduled failure repairs are generally carried out in the morning, the approximate travel time in the mornings (off-peak) was estimated to be 45 minutes from the university to these suburbs. However, pipe failures in neighbouring suburbs were also visited on some occasions, depending on availability.

The water distribution and pipe asset management of this area is regulated by City West Water Ltd. Therefore, the pipe failure data collection in this area was organised with the support of the asset management division of City West Water Ltd.

5.2.2 Target group of pipe failures

Since the most problematic pipe group in reactive soil zones in Melbourne has been identified as small-diameter (less than 300mm) cast iron pipes, the same pipe group was the focus of these studies. The relevant repair locations were identified and selected from the daily repair schedules of City West Water Ltd., before accessing the repair sites.

5.3 Climate during the Case Studies

The study started in May 2016 and continued until June 2017. A thirteen-month period was selected as both winter and summer failures needed to be monitored. Therefore, the climate of the selected study area during the study period was considered to distinguish the winter and summer failures. Generally, the Australian winter is in mid-year, from June to August and summer at the end of the year from December to February the following year. However, these months may vary slightly in some years, depending on the monthly climate. Therefore, monthly rainfall, temperature and soil moisture content data were obtained to analyse the climate during the year.

These climate data were obtained from the online database of the Bureau of Meteorology (BOM), Australia (Bureau of Meteorology, 2017c). Monthly rainfall data and monthly average temperature data are presented in Figure 5.2 and Figure 5.3 respectively.

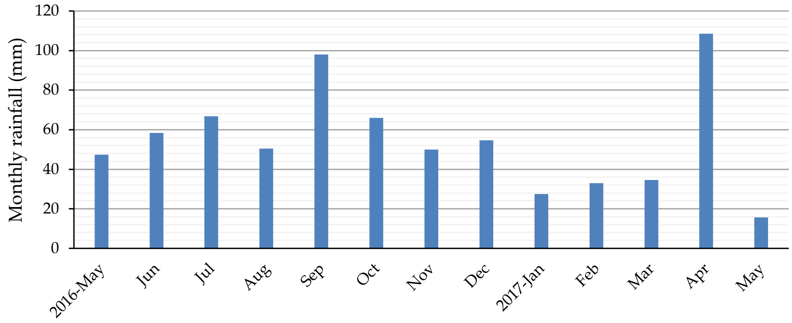

Figure 5.2. Monthly rainfall in study area (Bureau of Meteorology, 2017c)

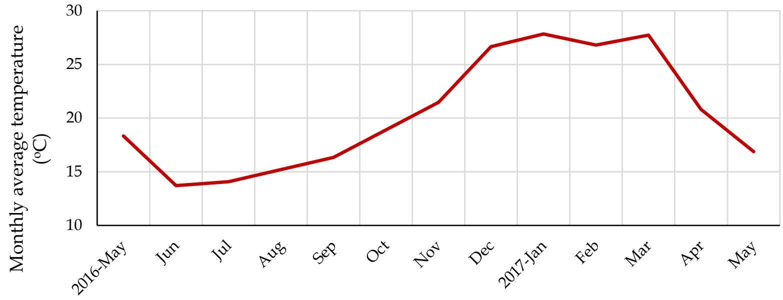

Figure 5.3. Monthly average temperature of study area (Bureau of Meteorology, 2017c)

Soil moisture data were obtained from the Australian landscape water balance database of the Bureau of Meteorology, Australia (Bureau of Meteorology, 2017b). These soil moisture data are presented in Figure 5.4.

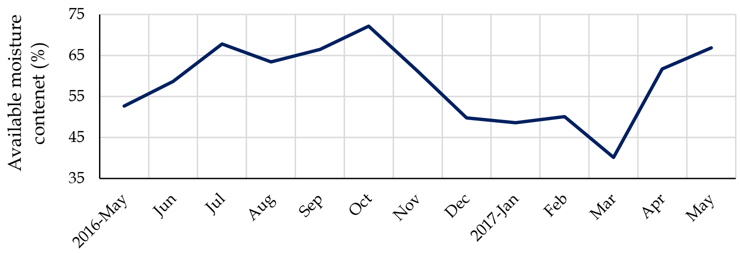

Figure 5.4. Soil moisture data at pipe depth in the study area (Bureau of Meteorology, 2017b)

These soil moisture data are presented as a percentage of available water content for crops (Bureau of Meteorology, 2017b), and represent the fluctuation of field soil moisture content.

The climate data indicate that the soil was in a wetting state from May 2016 to October 2016 and also from March 2017 to June 2017. Drying conditions were apparent from October 2016 to March 2017. Therefore, pipe failures were categorised as due to either soil drying (shrinkage) or soil wetting (swelling), as shown in Table 5.1.

Table 5.1. Climate during study period

Time period	Failure climate category
May 2016 to October 2016	Due to soil wetting (winter failures)
October 2016 to March 2017	Due to soil drying (summer failures)
March 2017 to June 2017	Due to soil wetting (winter failures)

5.4 Cases Studied

The case studies started on 13th May, 2016. During the period of study, a total of 21 cast iron reticulation pipe failures were investigated. However, in that twelve-month period, there were some unattended time periods due to unavoidable reasons.

The uncertainty of finding a cast iron pipe failure at each repair site attended also reduced the total number of relevant cases. Generally, pipe repairs are scheduled after noticing water leaks at the ground surface, which may be attended due to attended reticulation main failures or service pipe failures. Therefore, the exact reason for the leak is unidentifiable until the soil cover is excavated.

5.4.1 Case studies summary

A summary of these 21 cases is given in Table 5.2. The failures were categorised into summer or winter failures based on the failure date, the applicable climate (Table 5.1), and the crack orientation. Knowledge gained from the stress hotspot analysis was used to identify the failure category and the possible cause: soil shrinkage or soil swelling. Also, in Table 5.2, the failures observed during soil wetting periods are indicated in blue colour and the failures in soil drying periods are indicated in orange colour.

Table 5.2. Summary of cases studied

Case no.	Failure date	Location	Failure category	Soil type
1	13 – 05 - 2016	70 Severn St., Yarraville	Circumferential - Tree root	Silty clay
2	24 – 05 – 2016	27 Stewart St., Williamstown	Circumferential - Tree root	Silty / sandy clay
3	27 – 05 - 2016	19 Schutt St., Newport	Circumferential - Driveway (due to soil wetting)	Silty clay
4	03 – 06 – 2016	32 Baldwin Rd., Altona North	Longitudinal split	Silty clay
5	17 – 06 – 2016	33 Stooke St., Yarraville	Circumferential - Driveway (due to soil wetting)	Silty clay
6	15 – 02 – 2017	14 Boyd St., Altona	Longitudinal split	Sandy / silty clay
7	21 – 02 – 2017	131 Millers Rd., Altona North	Longitudinal split	Silty clay, some gravel
8	28 – 02 – 2017	19 (10) Buckingham St., Footscray	Longitudinal split	Silty clay below the road base
9	01 – 03 – 2017	57 Swan St., Keilor Park	Circumferential - due to water leak	Silty clay
10	01 – 03 – 2017	111 Westmoreland Rd., Sunshine North	Circumferential - Driveway (due to soil drying)	Silty clay
11	07 – 03 – 2017	39, McCoubrie Ave., Sunshine West	Longitudinal split	Silty clay
12	07 – 03 – 2017	6, Aviation Road, Laverton	Longitudinal split	Gravelly road base
13	08 – 03 – 2017	58 Civic Parade, Altona	Longitudinal split	Sandy clay
14	14 – 03 – 2017	24 Bromyard St., Yarraville	Circumferential - Driveway (due to soil drying)	Silty clay, some gravel
15	15 – 03 – 2017	18 Thomas St., St Albans	Circumferential - due to water leak	Silty clay
16	15 – 03 – 2017	30 Simpson St., Sunshine North	Circumferential - Road (due to soil drying)	Silty clay below the road base
17	04 – 04 – 2017	11 Jubilee St., Newport	Circumferential - Driveway (due to soil drying)	Silty / sandy clay
18	11 – 04 – 2017	63 Driscolls Rd., Kealba	Circumferential – Nature strip	Silty / sandy clay
19	12 – 04 – 2017	18 Nixon St., Sunshine	Longitudinal split	Clay, organic matters
20	23 – 05 – 2017	28, Morrison Crescent, Sunshine West	Longitudinal split	Silty clay, some gravel
21	21 – 06 - 2017	5, Chorley Avenue, Altona	Circumferential - Tree root	Silty clay

A summary of these case studies shows that the majority of these failures were circumferential failures. There were 12 circumferential failures out of 21 total failures observed during these case studies. In addition, 12 failures out of the total of 21 failures occurred in summer. The overall distribution of these failures is shown in the following flow chart (Figure 5.5).

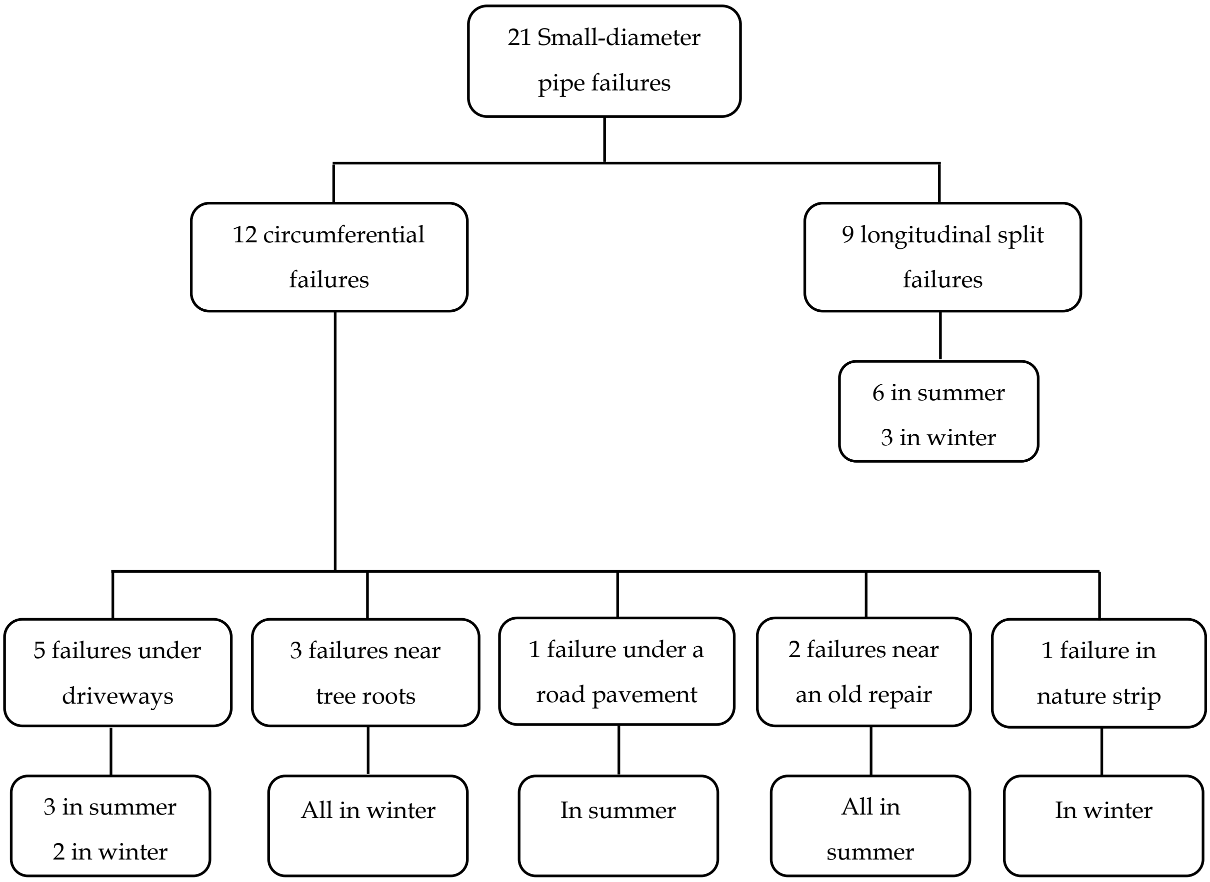

Figure 5.5. Distribution of pipe failure types

It can be seen that all circumferential failures, except one failure at nature strip (Case 18), occurred at locations where stress hotspots were identified. Unique failure mechanisms were observed for each failure category. These similarities and their correspondence to the hypothetical findings of relevant stress hotspots were evaluated based on field observations. This evaluation showed that the pipe cracks in the observed circumferential failures were consistent with the failure mechanisms of stress hotspots. The field data sheets for these 21 cases are attached in Appendix B.

5.4.2 Circumferential failures near driveways - summer failures

During the study, three examples were found for this failure category, namely Cases 10, 14 and 17 in Table 5.2. According to the finite element analyses undertaken (Section 4.4.3.3), the highest tensile stress in the pipe when soil is drying at driveways was observed to be on the pipe top at the centre of the driveway. Therefore, crack initiation and opening was expected at the pipe top. Confirming this hypothesis, all these three summer pipe failures at driveways were found to have cracked from the top of the pipe under the middle of driveways. Photographic evidence of these failures is shown in Figure 5.6.

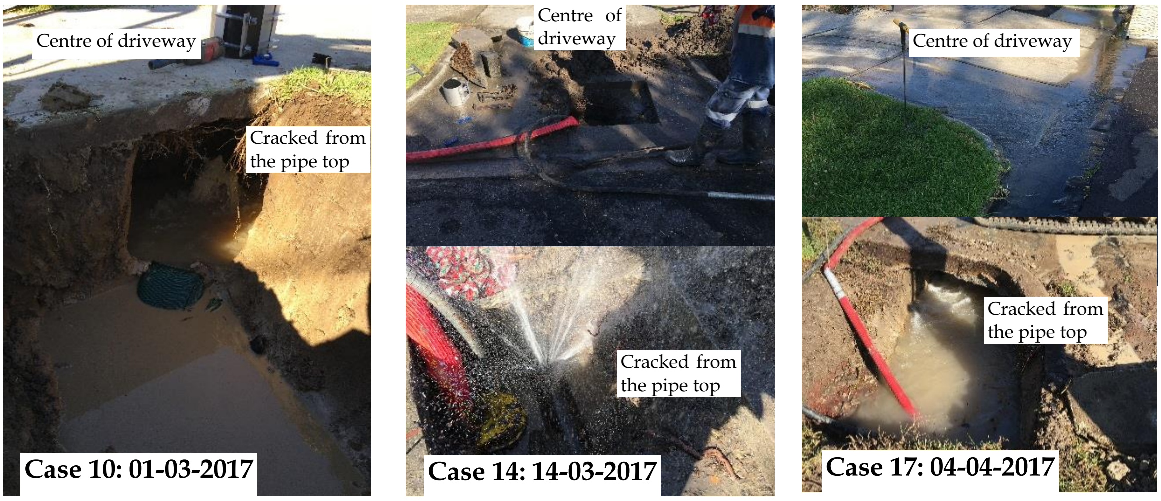

Figure 5.6. Studied circumferential failures under driveways: soil drying in summer

The crack opening at the pipe top can be clearly seen in case 14. In the other two cases, the upward leaking of pressurised water indicates the pipe top crack. However, the crack positions were confirmed after the water was shut off in all three cases.

Failure case 10 was found in a 150mm diameter cast iron cement-lined (CICL) pipe and Cases 14 and 17 were found in 100mm pipes of the same material. These pipes were constructed in 1958, 1960 and 1958 respectively, making them 57 to 59 years old at the time of failure. Pipe corrosion was evidenced by yellowish-brown patches on the pipe and surrounding soil colour changes, as shown in Figure 5.7.

Figure 5.7. Visible corrosion evidence

In addition to these three failures, the only circumferential failure under the road pavement is Case 16 in Table 5.2, which was also determined to be in this category. As the pipe is buried across the road, the differential conditions are similar to the soil drying at an impermeable cover (road pavement). As Figure 5.8 shows, as with other driveway failures, the pipe was broken at the middle of the road and the pipe was cracked from the top.

Figure 5.8. Circumferential failure under the middle of the road

It is summarised that the failure mechanisms applicable to summer pipe failures (circumferential) at driveways or at similar impermeable covers are consistent with the field pipe failures observed, providing validation for further theoretical analysis of circumferential summer failures at driveways (Section 4.4.3.3).

5.4.3 Circumferential failures near driveways - winter failures

As shown in the Table 5.2, two circumferential failures, Cases 3 and 5, were categorised as winter failures at driveways due to seasonal soil swelling. The pipe deformation pattern for this failure category was that the maximum longitudinal tensile stresses were on the pipe bottom at the driveway edge (Section 4.4.3.3). Therefore, circumferential failure was expected at the edge of the driveway with a crack opening from the pipe bottom. Consistent with this hypothesis, similar failures were observed in the field and the associated photographic evidence is shown in Figure 5.9.

Figure 5.9. Circumferential failures under driveways: soil wetting in winter

In the above pictures, the crack initiation at pipe bottom can be seen as the water leaks from the pipe bottom. Failures in both Cases 3 and 5 were found in 100mm diameter cast iron cement-lined (CICL) pipes that were constructed in 1923 and in 1957, respectively. Therefore, the pipe ages were 93 years and 57 years at failure.

In contrast to the distinct circumferential cracks in summer failures, more destructive cracks were observed in these pipe failures. While the main circumferential crack initiated from the pipe bottom, multiple cracks were observed along the pipe wall. In addition, small pieces had blown out due to the water pressure. Therefore, the broken pipe sections were removed from the ground due to this destructive failure mode. These removed pipe sections are shown in Figure 5.10.

Figure 5.10. Cracked pipe sections showing winter failures near driveways

Severe pipe corrosion can be seen in these cracked sections, as coloured corrosion patches are visible along the cracked faces of the pipe wall. Therefore, it was concluded that these cracks were caused by excessive corrosion at the pipe bottom. Further evidence was found for pipe corrosion after the pipe pieces in Figure 5.10 were grit-blasted to identify the remaining cast iron material in the pipe section. These experimental results are presented in Section 5.5.6.

Field observations verified the failure mechanism hypothesised based on finite element modelling for winter pipe failure. This mechanism is further analysed in the following chapters.

5.4.4 Circumferential failures near trees

In this study, three examples were found for this category of circumferential failure near tree roots. These failures were Cases 1, 2 and 21 in Table 5.2. All these failures were reported in the winter (a time of soil wetting). Circumferential failures near tree roots, due to surrounding soil swelling in winter were expected to initiate from the pipe bottom, according to the failure mechanism noted in Section 4.8. However, it was highlighted that gradual pushing of pipes by tree roots also imposes additional longitudinal stresses on pipes. Of the three cases studied, Case 1 was determined to be a failure due to tree root pushing and the other two cases were determined to be failures due to surrounding soil swelling. Photographs of these failures are shown in Figure 5.11.

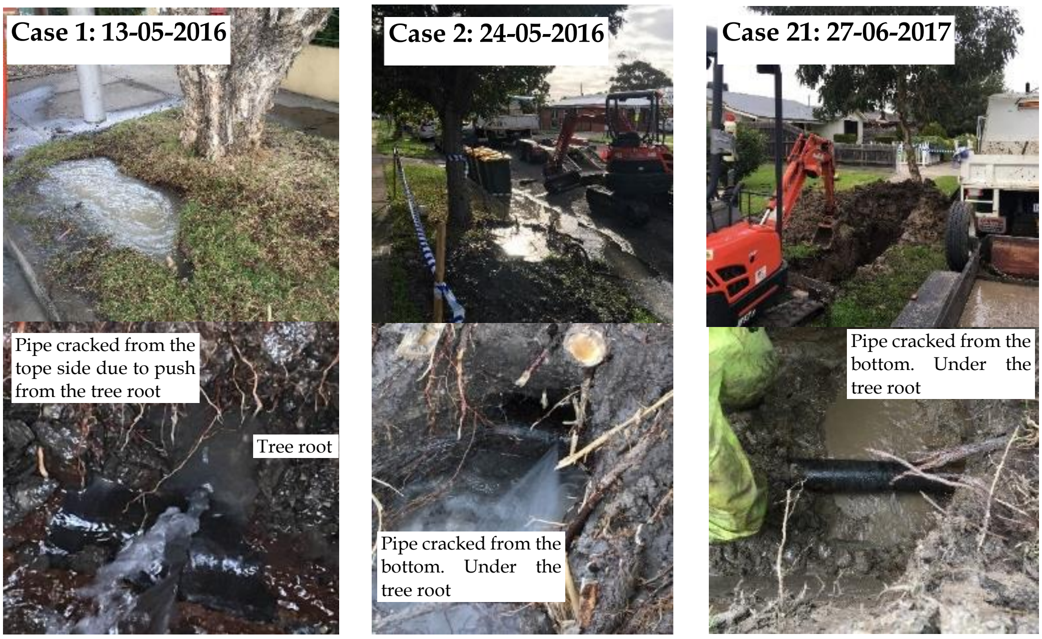

Figure 5.11. Circumferential failures near tree roots

The Case 1 picture shown in Figure 5.11 clearly shows the deflection of the pipe caused directly by the tree roots. As a result, the pipe has bent away from the tree roots and cracked on the side opposite to the tree roots. In the other two cases, the tree roots have grown above the pipes, pushing them down. The circumferential cracks of these two failures were observed to initiate from the bottom of the pipe, as the highest tensile stresses occurred at the pipe bottom. As the overall soil moisture was increasing during the time of failure, it is also possible that the pipe was prevented from upward movement due to surrounding soil swelling soil by the tree roots.

All these three failures were in 100mm diameter CICL pipes and the three pipes were constructed in 1973, 1966 and 1968 respectively. As the pipes were 43 to 50 years old at the time of failure, corrosion was visible on the pipe walls as yellowish- brown patches (Figure 5.12).

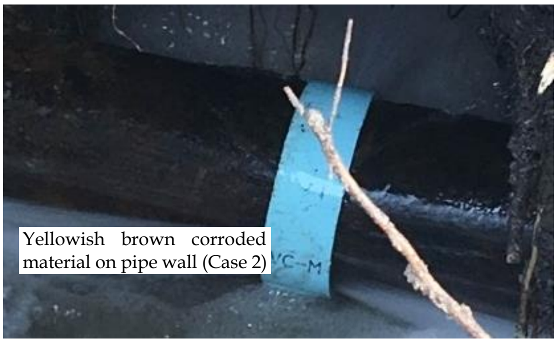

Figure 5.12. Field evidence for pipe corrosion near tree roots

In summary, the influence of tree roots near pipelines is a considerable factor in circumferential failures. In addition, this type of failure can be expected in both reactive and stable (non-reactive) soil zones, as the pipes were observed to be deflected by the growth of tree roots.

5.4.5 Circumferential failures due to possible leaks

The failure mechanism of circumferential failures due to water leaks (localised wetting) was defined as a breakage at the pipe top in Section 4.7. Two failures were identified as being due to possible water leakage. These failures are reported as Cases 9 and 15 in Table 5.2. As both of the failures occurred adjacent to old repairs, small water leaks may have occurred to create soil swelling at these locations. Since these were summer failures, seasonal moisture variation was not responsible for causing any upward movement of the pipes (due to soil shrinkage and downward movements in summer). Photographs of these failures are shown in Figure 5.13.

Figure 5.13. Pipe failures near old repairs

It was observed that the pipe crack opened from the pipe top in Case 9 and from the pipe bottom in Case 15. The failure location of case 9 was at a nature strip where no other possible pipe movement restraint was observed. In contrast, the failure in Case 15 was observed under the edge of a driveway. Based on these observations, the first failure (Case 9) was explained as possibly due to localised soil swelling at the water leak. As a result, the pipe cracked from the pipe top. The effect of the driveway was assumed to be the reason for the pipe bottom crack in Case 15. The effect is similar to pipe deformation caused by soil wetting near driveways.

These 100mm diameter cast iron pipes were constructed in 1973 and 1960 respectively, making them 44 and 57 years old at the time of failure. As two failures (an old repaired failure and the current failure) occurred close together, pipe corrosion was observed to be considerable in the failed pipe sections (as indicated in Figure 5.13).

5.4.6 Circumferential failure under the nature strip

As reported in Table 5.2, Case 18 involved circumferential failure of a 41-year old 150mm diameter cast iron pipe under the nature strip. The pipe showed a crack starting from the pipe top, as shown in the photograph in Figure 5.14.

Figure 5.14. Circumferential failure under nature strip

As no visible evidence of a stress hotspot (tree root, driveway or old repair) was observed near the failure, this failure could not be categorised as a particular type of stress hotspot. However, although not verified in this study, it may have been due to the effects of bedrock depth variations, recently back-filled soil boundaries, or leaking from a through-wall corrosion hole.

5.4.7 Longitudinal split failures

In addition to the twelve circumferential failures observed in these case studies, nine longitudinal split failures were also observed in small-diameter pipes. These failures are noted in Table 5.2 as Cases 4, 6, 7, 8, 11, 12, 13, 19 and 20. Of these nine longitudinal split failures, six failures were reported in summer and the remaining three failures were reported in winter. The main reason for longitudinal split failures was considered to be excessive hoop stresses in the pipe wall resulting from the internal water pressure (Section 2.3.1). This is consistent with the fact that the failure cracks were oriented in the longitudinal direction, as can be seen in Figure 5.15.

Figure 5.15. Longitudinally-cracked pipe sections

Failures of CICL pipes of both 100mm and 150mm diameters were found in these nine cases and they were 44 to 84 years old at failure (see Figure 5.15). In these cases, some common facts were observed, as follows:

- A piece from the pipe wall had blown out in some cases.
- The crack location was the bottom of the pipe for many failures.
- Severe corrosion damage was observed on the pipe wall near the crack.

The main reasons for these observations were assumed to be the nature of the underground corrosion process, which is currently being investigated at Monash University (Azoor et al., 2017). As the hoop stress due to internal water pressure is considerably smaller in small-diameter pipes (Section 2.3.1), significant corrosion damage is required to develop a crack to failure. Therefore, longitudinal split failures are likely to occur at critical corrosion defects on the pipe wall. If the corrosion damage is greater at the pipe bottom, a crack is likely to occur at the pipe bottom and severely corroded pieces may be blown out due to the water pressure.

Another interesting observation was that all these pipes failed away from stress hotspots, such as under nature strips, away from trees and parallel to road pavements. Therefore, it can be assumed that the pipes were not subjected to critical bending deformations at these locations. Under these conditions, hoop stresses become the dominant stress in the pipe wall and cause failure at severely corroded sections. More information about these failure locations is provided in Appendix B.

5.5 Other Information from the Case Studies

In addition to the pipe failure studies, these case studies were utilised to collect more information on aspects that are not explained in detail in the research literature. Pipe depths, pipe repair techniques, service connection failures, current condition of old pipes and water pressure details of the reticulation pipes were collected for each failure case. The collection of this additional information was considered to be useful for future studies of the water reticulation network.

5.5.1 Pipe burial depths

As mentioned in the literature review (Section 2.2.4), a convenient record of pipe burial depth was not available with the pipe asset data. Therefore, pipe depths were measured during the data collection stage while the pipe was exposed for repair. These pipe depths were then compared with the construction year, pipe diameter and the location, and the results are summarised in Table 5.3.

Table 5.3. Pipe burial depth information

Case number	Pipe construction year	Pipe diameter (mm)	Location	Pipe depth (mm)
1	1973	100	Nature strip	950
2	1966	100	Nature strip	900
3	1923	100	Driveway	650
4	1965	150	Nature strip	800
5	1957	100	Driveway	700
6	1961	100	Nature strip	900
7	1958	150	Nature strip	1200
8	1963	100	Road	700
9	1973	100	Nature strip	950
10	1958	150	Driveway	850
11	1973	100	Nature strip	950
12	1933	150	Road	1000
13	1962	100	Road	950
14	1960	100	Driveway	450
15	1960	100	Driveway	850
16	1958	100	Road	600
17	1958	100	Driveway	500
18	1976	150	Nature strip	1300
19	1973	150	Nature strip	950
20	1968	100	Driveway	900
21	1968	100	Nature strip	900
Average				855

The table shows that the burial depths of these reticulation pipes vary in a range of 450 to 1300mm, irrespective of the pipe diameter, location or year of construction. Although there were burial depth guidelines (refer to Section 2.2.4) at the time of construction (40 to 90 years ago), the topology of the ground surface as the pipes were buried may be a reason for the variation of pipe depths. These depth measurements can be used for further studies as the measurements are relative to the current ground level.

5.5.2 Repair methods

The knowledge gathered about the repair techniques for small-diameter reticulation pipes was another valuable outcome of the data collection phase of the present study. As frequent failures of old cast iron pipes interrupt the asset owner's daily water distribution routines, convenient and efficient repair methods are practised in the pipe industry to avoid further losses due to failures.

Two major repair methods were commonly used in circumferential and longitudinal split failure repairs, these case studies have revealed. As Figure 5.16 shows, either clamping the crack or replacing the cracked section were commonly practised by repair crews.

Figure 5.16. Small-diameter pipe repair methods: clamping and replacing

The repair method appears to have been chosen on the basis of the failure type and the nature of the pipe wall crack. Clamping repairs were observed in pure circumferential crack failures without any longitudinal damage or blown out pieces. Since the stainless steel clamps are tightened around the pipe, they are able to hold the cracked pipe circumference tightly together. However, these clamps are ineffective for fixing lengthy longitudinal cracks, as further crack propagation is unavoidable as these clamp lengths are limited 200 to 300mm. This method is a less time-consuming repair technique that can be implemented without shutting the water main. However, the durability of these repairs is questionable, as leaks from old clamps and subsequent failures near old clamps were frequently observed during this study.

The other repair method, pipe section replacement, was frequently observed for longitudinal split failures with destructive cracks. As damage was propagated and affected by severe pipe wall corrosion, the entire failed section was replaced with a polyvinyl chloride (PVC) pipe section. Compared with clamping, pipe section replacement requires more effort, including shutting the water main, longer excavation and cutting the cast iron pipe. This technique is a relatively durable repair method.

5.5.3 Failure (or leak) detection techniques

Locating the exact failure section of the pipe was one of the most time-consuming activity observed in the pipe repair process. When a leak starts from a cracked section, a wet surface can be seen in an extended area, depending on the severity of the leak. The wetted area may be significant distance away from the exact failure location, if the failure is under an impermeable surface (driveway or road pavement). As excavation of the wrong location is a costly decision, several detection techniques are used to identify the exact leak location before excavation starts.

Field crews practise listening to the sound of leaks as a simple and convenient method to locate leaks. This technique is effective for metal pipes, as metals are good conductors of sound. Steel rods inserted in the ground that are in contact with the pipe (as shown in Figure 5.17) are used to listen to the sound of leaking pipes. In many cases, these leaks are audible to the human ear with sound transmitted through the metal rod and amplifiers are used when the sound is weak. In this manner, the sound can be examined from several locations and the leak location can be successfully identified near the location of the loudest sound.

Figure 5.17. Inserting metal rods to listen for water leaks

5.5.4 Service and connection failures

During the period of study it was observed that failures in the pipe network are not limited to failures of reticulation pipes. Breakages in service pipes and connecting ferrules also frequently interrupt water distribution. These ferrules and service pipes connected to the reticulation mains and individual households are usually made of copper. In many cases, it is not possible to identify the exact reason for these failures, but it is possible that the relative movement between the reticulation and service pipe is the reason for these failures.

Furthermore, it was noted that distinguishing these failures from reticulation pipe failures is difficult without excavating the wetted area. Therefore, some pipe failures were attended which proved to be service and connection failures. Figure 5.18 shows photographs of some of these failures.

Figure 5.18. Service pipe and connection failures

5.5.5 Pipe water pressure

The internal water pressure data for these small-diameter cast iron reticulation pipes were studied to identify the water pressure variations in these pipes. The hourly variations of internal water pressure show the maximum pressure heads are in the range of 60 to 80m (equivalent to 588 to 784 kPa) and these peaks occur around midnight. The hoop stresses in pipe walls generated due to these maximum water pressures ($\sigma_{hoop,w}$) were calculated using Equation 5.1 and the results are shown in Table 5.4.

$$\sigma_{hoop,w} = P_w \frac{D}{2t} \qquad \text{Equation 5.1}$$

where, P_w is the internal water pressure, D is the internal pipe diameter and t is the pipe wall thickness.

Although these stresses are much lower than the failure strength, they can cause failures with extreme corrosion defects on the pipe wall. The observed corrosion levels of some failed pipes are discussed in Section 5.5.6.1.

Table 5.4. Calculated hoop stresses for 784 kPa internal water pressure for selected pipe sizes

Pipe diameter (internal), mm	Wall thickness, mm	Hoop stress, MPa
100	8	4.9
150	10	5.9

5.5.6 Pipe conditions

In these case studies, the serviceability condition of these pipes was also examined while the pipes were exposed for repair. The pipe corrosion level was the main concern in this condition assessment and manufacturing defects were also observed in some pipes. In addition to visual inspections, some pipe samples were further inspected in the laboratory, and these observations are discussed in the following sections.

5.5.6.1 Corrosion

As discussed in the literature review (Section 2.2.5), pipe corrosion is the most common natural deterioration mechanism of old cast iron pipes. It was observed that due to graphitisation, corroded areas on the pipe wall are not directly identifiable unless colour changes are visible. However, a fresh cut on a pipe can expose these graphitised (corroded) areas and the remaining metal (cast iron) on the pipe section, as shown in Figure 5.19.

Figure 5.19. Cut section of a 93 years old pipe

The 93 year-old pipe section shown in Figure 5.19 is from a failed pipe (Case 3 in Table 5.2). The pipe wall is completely graphitised, as no remaining metal is visible in some places. Therefore, it is possible that relatively low stresses could initiate failure in this section. In addition, corrosion has affected the pipe section both inside and outside the pipe wall. A better view of these corrosion defects can be obtained if graphitised areas are removed from the pipe section by sand-blasting. Therefore, the entire failed section of this longitudinal split failure (Case 3) was sand-blasted in the laboratory and the intact material in the section was compared, as shown in Figure 5.20.

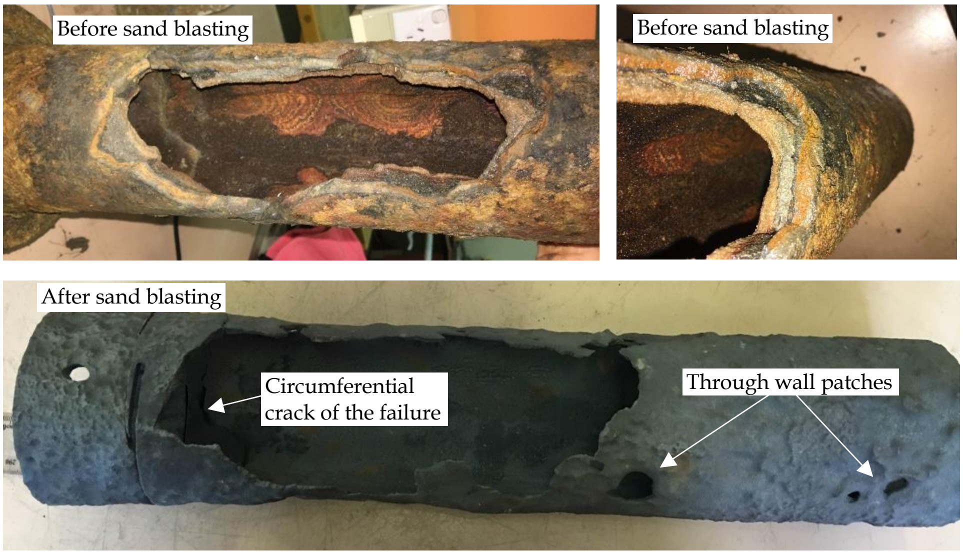

Figure 5.20. Pipe section Case 3 before and after the sand blasting

The images before and after sand-blasting shown above indicate that a pipe may be severely corroded (thickness less than one millimetre), but may appear to be uncorroded due to graphitisation. The several through-wall corrosion holes in the pipe wall also show the extreme corrosion in this pipe, although they may not have contributed to leakage due to plugging by the graphitised material.

However, these relatively small size (30-60mm) corrosion patches can affect the circumferential or longitudinal crack failures by creating concentrated stresses (as explained in Section (2.2.5). Once the crack is initiated due to the concentrated stresses, small pieces can be blown out due to the water pressure, as observed in many failures.

In contrast to the relatively large corrosion patches in large diameter pipes, these patches are not generally large enough to cause blowout holes.

5.5.6.2 Manufacturing defects

Other possible defects in these old pipes are due to manufacturing defects. Such a weak pipe section was found during this study (Case 12, Table 5.2), as shown in Figure 5.21. This 83-year old 150mm diameter cast iron pipe section shows multiple air bubbles throughout its circumference and in the longitudinal direction. These air bubbles are trapped in the pipe wall during the process of casting and weaken the section's strength.

Figure 5.21. Pipe section with manufacturing defects

5.6 Conclusion

This chapter has presented and analysed the observations that were made during the small-diameter pipe failure case studies. The major outcomes can be summarised as follows:

- The observed circumferential failures and their failure mechanisms at different locations (driveways, near tree roots and near old repairs) corroborate the theories of potential stress hotspots presented in Chapter 4. However, some stress hotspots (bedrock profile and soil boundaries) were not verified as examples were not found during these case studies;
- The observed longitudinal split failures show that this kind of failure is likely to occur away from stress hotspots where the bending stress is minimal. Hoop stress is lower in small-diameter pipes, but may become the dominant stress on the pipe wall when the bending stress is insignificant and corrosion is extensive. Therefore, a high corrosion level possibly over a large patch is required to initiate longitudinal cracks;
- A certain level of corrosion is necessary for both failure types. However, it was observed that corrosion is more severe at longitudinal failures than at circumferential failures. Therefore, it can be concluded that circumferential failures are caused by higher bending stresses at stress hotspots with relatively low corrosion, whereas longitudinal split failures are caused by smaller hoop stresses and relatively high corrosion.

In addition to the above conclusions, these case studies show the importance of collecting this information for the mechanistic analysis of pipe failure. Therefore, the continuous collection of such detailed data is recommended for further advancement of knowledge.

CHAPTER 6: AN ANALYTICAL METHOD TO ESTIMATE PIPE STRESSES

6.1 Overview

The use of finite element simulations to estimate pipe stresses due to reactive ground movement and its application in the identification of stress hotspots were discussed in Chapters 3 and 4 respectively. The theoretical findings were verified based on field observations in Chapter 5. In this chapter, the new knowledge of these studies is combined to develop an analytical method for the estimation of reactive soil- induced pipe stress. This analytical method provides a set of mathematical equations for the analysis of longitudinal pipe stresses for different pipe bending scenarios. These equations are derived according to the pipe bending patterns, and the equations are calibrated and verified using finite element simulations. The main purpose of developing this analytical method is to utilise the findings of the research in a wide range of applications. Since these analytical equations are programmable in simple computer applications, these stress estimations can be efficiently integrated with any pipe failure assessment model. Although the equations presented in this chapter are specifically calibrated for Melbourne reactive soils, the methodology is applicable elsewhere.

6.2 Methodology

An analytical method of pipe bending stress calculation was developed to combine ground movement and pipe stress calculations. The basic steps of the overall procedure are as follows:

- Calculation of free ground movement at pipe depth;

  The stress in the pipe is a variable of the amount of ground swell or shrinkage at pipe depth (as seen in the analyses in Chapter 3 and 4). Therefore, the free ground movement at pipe depth for a given soil moisture variation is first calculated, without considering the surrounding environment (presence of driveways, rock, trees etc.). In addition to the soil moisture variation data corresponding to pipe depth, the reactive properties of the soil and the reactive zone depths are considered in this calculation.
- Determination of differential ground movement;

  Differential ground movements, which cause pipe bending at different stress hotspots (as explained in Chapter 4), are determined in the second step to identify the potential pipe bending shape due to different conditions. The geometric parameters of the shape of pipe bending are considered in this step.
- Pipe stress calculation.

  As the final step, the maximum tensile bending stress in the pipe wall is calculated by considering the section and material properties of the pipe as well as the stiffness due to the soil-pipe interaction. An approach similar to the pipe stress estimation method developed for settling soils (Wols and Thienen, 2014) is followed in this pipe stress estimation model, with appropriate modifications.

The method calculates pipe stresses for an undamaged pipe section that has not deteriorated due to underground corrosion. Hence, potential corrosion defects must be considered before the calculated stresses are used in failure analyses. The complete procedure is illustrated in the schematic diagram shown in Figure 6.1.

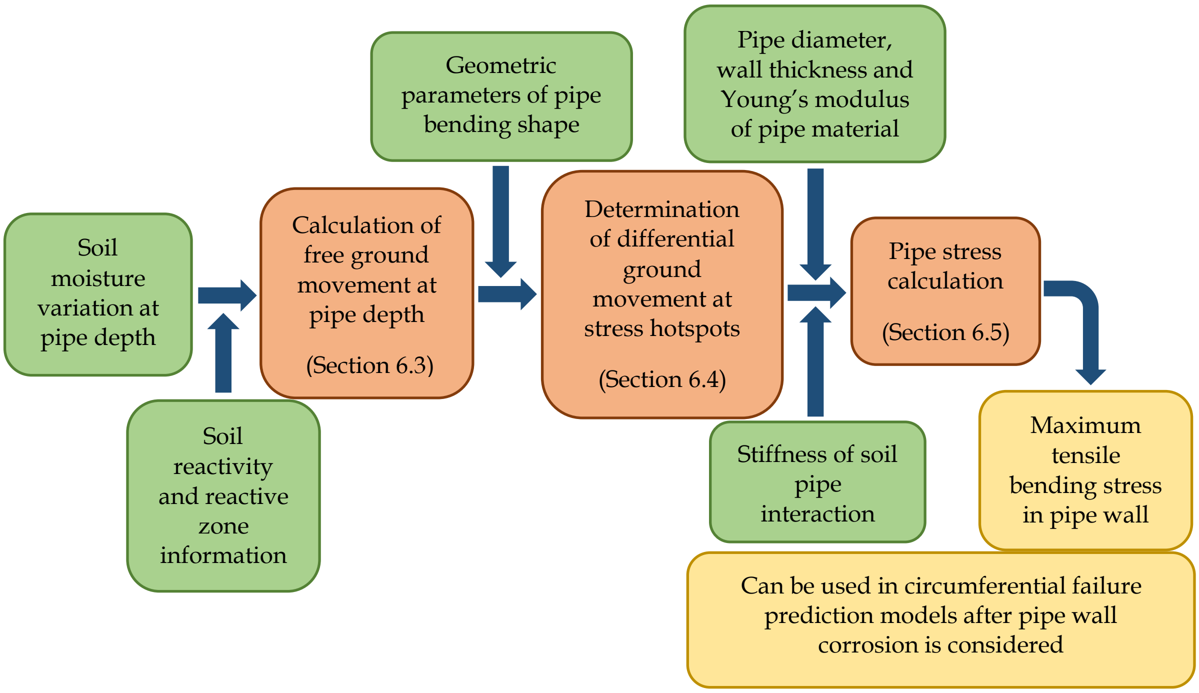

Figure 6.1. Pipe stress estimation methodology

The main steps involved in this methodology are explained in Sections 6.3, 6.4 and 6.5.

6.3 Estimation of Free Ground Movements at Pipe Depth (ΔH)

In this calculation, the free ground movement at pipe depth (ΔH) is defined as the ground displacement at the pre-defined pipe depth that is unaffected by the changing conditions in the surroundings, such as driveways, trees or the pipe itself. Therefore, the variation of moisture content at the pipe depth, soil reactive properties and the soil profile are the only considerations in this calculation. This calculation is similar to the calculation of characteristic ground movement (y_s) in AS2870 (Australian Standards, 2011). However, y_s is calculated for a fixed soil moisture change (for a maximum suction change), whereas ΔH is calculated for various moisture changes.

6.3.1 Calculating ΔH

The methodology presented in AS2870 (Australian Standards, 2011) to calculate characteristic ground movement (y_s) (Section 2.4.4.1) was considered for calculating ΔH in this study. However, instead of soil suction change, the volumetric soil moisture content (θ_v) is used as the major variable. A new soil strain index (I_{θ_v}) is defined for the vertical strain (in decimals) per unit volumetric moisture content change ($\Delta\theta_v$) to substitute for the stability index, I_{pt} in the AS2870 method.

The following facts were considered when selecting the new soil strain index (I_{θ_v}).

- The volumetric strain change of the tested Altona North reactive clays (as presented in Table 3.5) showed a linear variation with the volumetric moisture content of the soil for the tested moisture variation range, which is also the expected moisture change in the field at pipe depths. This data is presented in Figure 6.3. Therefore, a single value of I_{θ_v} can be selected for the entire moisture change considered in the present work.
- Unrestrained conditions were assumed for the entire moisture variation depth as the basaltic expansive clays in western Melbourne areas are known to have deep cracked zones, extending to 2-3m (Morris et al., 1992; Wijesooriya and Kodikara, 2012). However, when necessary, the restrained conditions can be considered for the deeper soils by introducing a factor as in AS2870 method (Clause 2.3.2) (Australian Standards, 2011).

The reactive zone depth (H_s) of 2.3m is used for reactive soil regions in Melbourne (refer to Section 2.4.4.1) when the bedrock or water table is not in this region and the effect of bedrock and water table are considered similarly. Although the field moisture profiles indicate some non-linear variations over the depth (as mentioned in Section 2.5.1, Figure 2.32), a linearly-varying moisture content profile similar to the moisture profiles of the analyses in Chapter 4 (Figure 4.13) is assumed for simplicity, as shown in Figure 6.2.

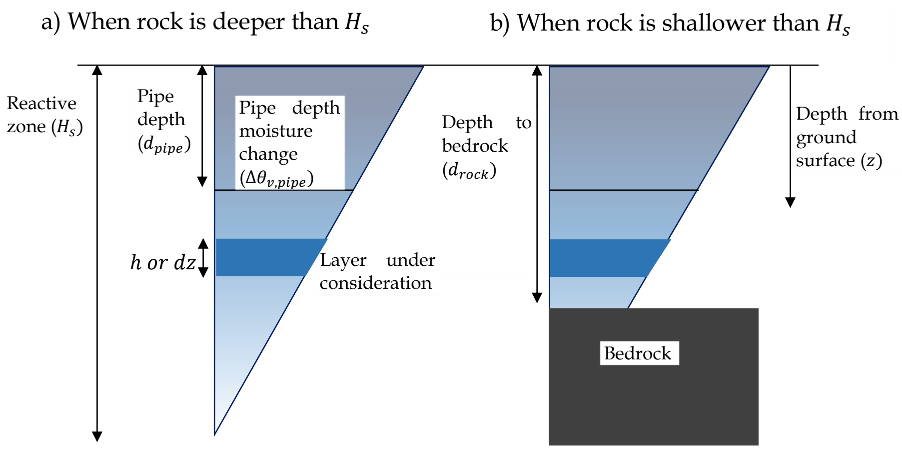

Figure 6.2. Soil moisture profile for ground movement calculation

Considering the above soil moisture profile, the free ground movement at pipe depth (ΔH) is calculated following the methods proposed in AS2870 (Australian Standards, 2011) and for moisture-based ground movement calculations (Fityus, 1999), as shown in Equation 6.1.

$$\Delta H = \sum_{n=1}^{N} \left(I_{\theta_v}\, \Delta\theta_v\, h\right)_n \qquad \text{Equation 6.1}$$

where, h is the thickness of the layer under consideration and N is the number of layers in the design depth. If uniform soil reactivity properties are assumed for the total design depth, Equation 6.1 can be rearranged by integrating over the design depth (as in Equations 6.2 and 6.3). For the case of deeper bedrocks, this design depth is the difference between the reactive zone depth and the pipe depth ($H_s - d_{pipe}$) and for shallow bedrocks, it is the difference between the rock depth and the pipe depth ($d_{rock} - d_{pipe}$).

When $H_s \leq d_{rock}$,

$$\Delta H = I_{\theta_v} \int_{d_{pipe}}^{H_s} \Delta\theta_v(z)\, dz \qquad \text{Equation 6.2}$$

When $H_s > d_{rock}$,

$$\Delta H = I_{\theta_v} \int_{d_{pipe}}^{d_{rock}} \Delta\theta_v(z)\, dz \qquad \text{Equation 6.3}$$

In the above equations, z is the depth measured from the ground surface and dz is the thickness of the layer under consideration. The assumed linearly-varying vertical soil moisture variation ($\Delta\theta_v(z)$) can be formulated as shown in Equation 6.4 for integration purposes:

$$\Delta\theta_v(y) = \Delta\theta_{v,pipe}\frac{H_s - z}{H_s - d_{pipe}} \quad \text{Equation 6.4}$$

Then the integrated solutions for ΔH can be presented, as shown in Equations 6.5 and 6.6.

When $H_s \leq d_{rock}$,

$$\Delta H = \frac{I_{\theta_v}\,\Delta\theta_{v,pipe}}{2}\left(H_s - d_{pipe}\right) \quad \text{Equation 6.5}$$

When $H_s > d_{rock}$,

$$\Delta H = \frac{I_{\theta_v}\,\Delta\theta_{v,pipe}}{2\left(H_s - d_{pipe}\right)}\left(2H_s - d_{pipe} - d_{rock}\right)\left(d_{rock} - d_{pipe}\right) \quad \text{Equation 6.6}$$

The required parameters and their availability to calculate ΔH from the above equations are listed in Table 6.1.

Table 6.1. Required parameters for ΔH calculation

Parameter		Availability
Reactive zone depth	H_s	Constant for a climate region as in AS2870; 2.3m for temperate climate zones (Australian Standards, 2011)
Pipe depth	d_{pipe}	Can be measured or can be assumed to be an average value if sufficient data are not available
Depth to bedrock	d_{rock}	Can be measured or can be assumed to be greater than the reactive zone depth when data are not available
Volumetric moisture change at pipe depth	$\Delta\theta_{v,pipe}$	Can be obtained from soil moisture data
Vertical strain index	I_{θ_v}	Can be determined experimentally

For the reactive soils tested in the present research (in Section 3.4.3.2), the strain index, I_{θ_v} was calculated from the measured volumetric strain variations. In this definition, the vertical strain component (ε_z) is assumed to be one third of the total volumetric strain (ε_v) of the soil due to the assumed unrestrained conditions (Equation 6.7).

$$\varepsilon_z = \frac{1}{3}\varepsilon_v \qquad \text{Equation 6.7}$$

Therefore, the strain index was calculated as 0.52 (vertical strain per unit volumetric moisture change) for the tested Altona North soil (data from Table 3.5), considering one third of the gradient of volumetric strain variation, which is shown as 1.57 in Figure 6.3.

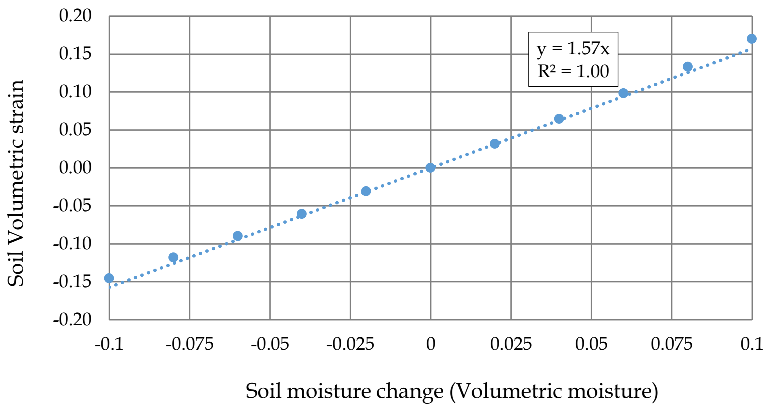

Figure 6.3. Volumetric strain behaviour of Altona North soil

When a suitable strain index (I_{θ_v}) is determined for the soil, ground movements can be calculated for different soil moisture variations and various rock profiles. The results of an example calculation are shown in Figure 6.4.

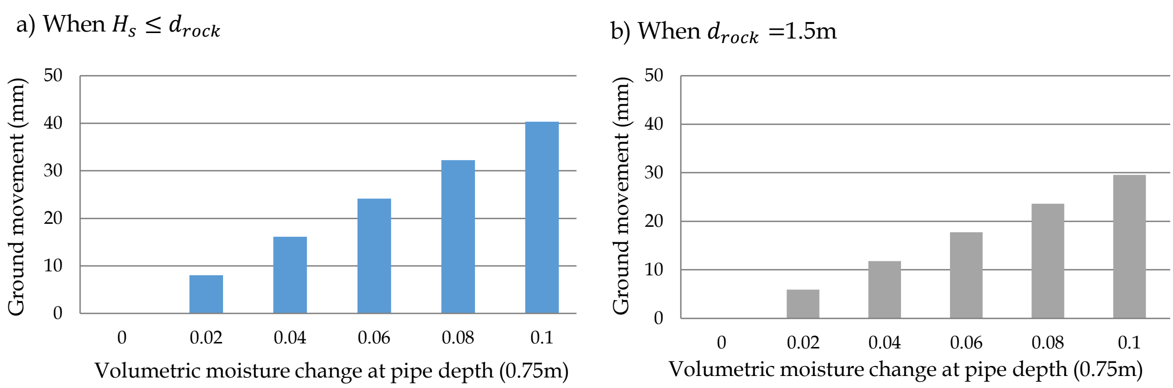

Figure 6.4. Calculated ground movements for different soil moisture changes

Figure 6.4 indicates that the ground movements are greatest when the rock depth is greater than the moisture variation depth ($H_s \leq d_{rock}$), as it provides a full reactive soil layer to generate more soil swelling and shrinkage. As the general soil moisture change observations at the pipe depths are between 0.04 and 0.06 in Altona North (Section 2.5.1), the pipe depth ground movements were estimated to be in the range of 16 to 24mm.

The applicability of these estimations was verified with field measurements and other practical methods.

6.3.2 Comparison and validation

As a validation step, the ground movement calculations of the above method were compared with the available ground movement measurements measured at Altona North and Braybrook (Section 2.4.4.2). Both data sets were available with the measured soil moisture contents and the vertical ground movements. The soil properties at the two locations were assumed to be similar as both suburbs are located in highly expansive soil zones in Melbourne (as identified in Section 2.4.4). Therefore, a similar strain index (I_{θ_v}) was used to calculate the ground movements of both locations. However, the Altona North comparison was made for ground movement at 0.4m depth (measurements at 0.4m depth, (Chan, 2013)) and the Braybrook comparison was made for movement at the surface (total ground movement measurements (Karunarathne et al., 2014)). In addition, on the basis of field observations, the rock depth was (d_{rock}) assumed to be 2m for Altona North and 1m for Braybrook in the ground movement calculations. These comparisons can be seen in Figure 6.6 and Figure 6.5.

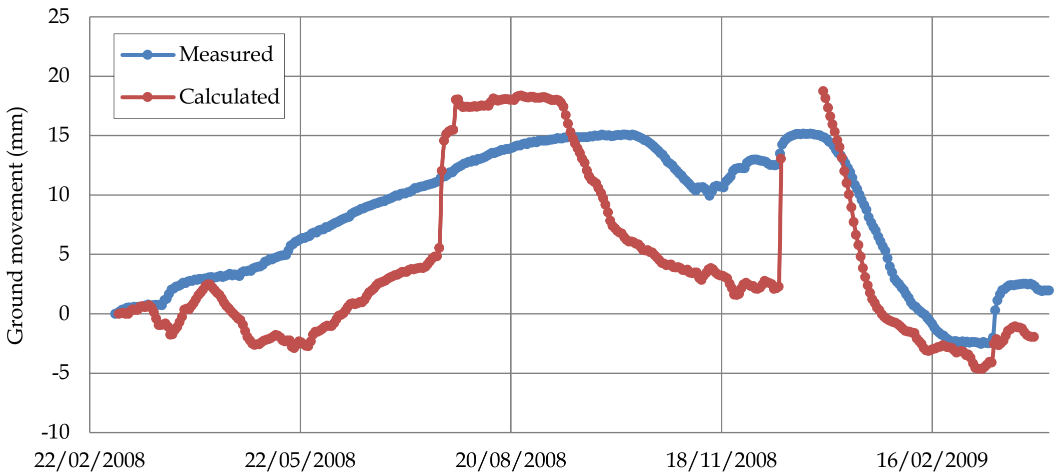

Figure 6.6. Measured and calculated ground movements of Altona North site (0.4m depth)

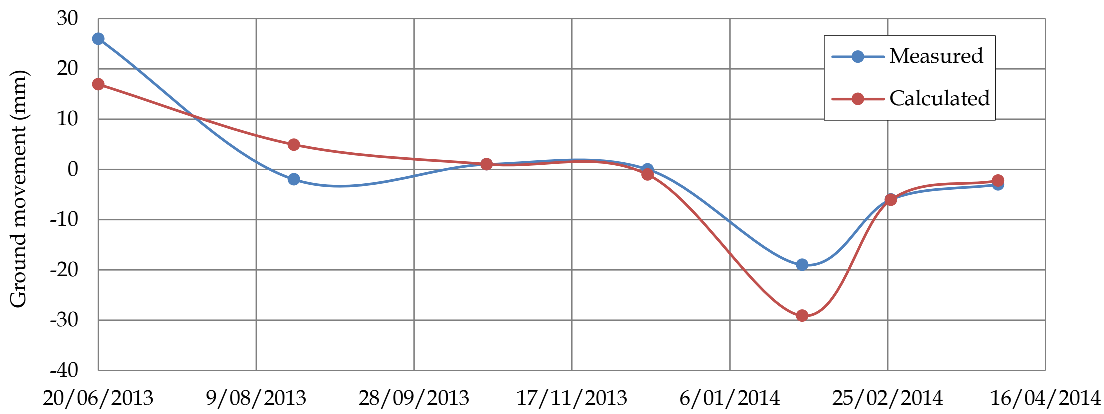

Figure 6.5. Measured and calculated ground movements of Braybrook site

Note that the positive ground movements in the above figures represent upward (swelling) movements and the negative movements are downward (shrinkage) ground movements. As the comparisons show, the calculated ground movements closely follow the variations of the measured ground movements at the Braybrook site. However, some deviations can be observed in the Altona North comparison, which can be assumed to be due to the assumptions (such as the linear moisture profiles) in the calculations and/or errors in field measurement.

6.3.2.1 Comparison of strain index (I_{θ_v})

In addition to the ground movement estimations, the suitability of the use of strain indices was also validated by comparing the results with those for the other methods. As the most common method of ground movement estimation in practice is the AS2870 (Australian Standards, 2011) method, this strain index (I_{θ_v}) was compared with the instability index (I_{pt}) in the AS2870 method.

For unrestrained swelling and shrinkage, this instability index (I_{pt}) is the same as the shrink-swell index (I_{ss}) (in percentage strain per pF) of the soil. Therefore, the strain index (I_{θ_v}) can be converted into the shrink-swell index (I_{ss}), as shown in Equation 6.8:

$$I_{ss} = I_{\theta_v} \frac{\Delta\theta_v}{\Delta u} \times 100\% \qquad \text{Equation 6.8}$$

The ratio between the soil moisture change ($\Delta\theta_v$) and the suction change (Δu) can be obtained from the applicable soil-water characteristic curve. For the Altona North soil (based on Figure 3.4)), this ratio was found to be 0.122 (moisture change per suction (in pF) change) for the considered moisture variation range. The substitution of the above value in Equation 6.8 shows that the shrink-swell index (I_{ss}) for the strain index ($I_{\theta_v} = 0.52$) is 6.3%. The calculated I_{ss} was compared with the typical I_{ss} values suggested by other researchers (as shown in Table 6.2) for Melbourne reactive soils.

Table 6.2. Comparison of shrink-swell indices (in strain % per pF)

AS2870 Site classification	I_{ss} (Peck et al., 1992)	I_{ss} (Li et al., 2014)
Class S (slightly reactive)	0.8 – 1.7	
Class M (moderately reactive)	1.7 – 3.3	
Class H (highly reactive)	3.3 – 5.8	5 – 6
Class E (extremely reactive)	Greater than 5.8	6 - 8

This comparison shows that the calculated shrink swell index (I_{ss} = 6.3%) for Altona North clay is in an acceptable range as Altona North is located in an extremely reactive soil zone (see Figure 2.26). On this basis, it is argued that the strain index (I_{θ_v} = 0.52) and the present methodology are an alternative approach for ground movement calculation at extremely reactive soil sites in Melbourne. The advantage of this method is that frequently updates of soil moisture content data are commonly available in contrast to soil suction data.

Considering the typical I_{ss} values (Table 6.2), the relevant strain indices (I_{θ_v}) were calculated for different reactive soil sites and the results are shown in Table 6.3. Equation 6.8 was used for the calculation with a similar soil water characteristic curve gradient, assuming that all these reactive clays show similar water retention properties.

Table 6.3. Suggested strain indices for different reactive clay sites

AS2870 Site classification	I_{θ_v}
Class S (slightly reactive)	0.07 – 0.14
Class M (moderately reactive)	0.14 – 0.27
Class H (highly reactive)	0.27 – 0.46
Class E (extremely reactive)	Greater than 0.46

These suggested strain indices can be used for ground movement calculations when the required data are not available for the site under consideration.

6.4 Determination of Differential Ground Movement

After the free ground movement is estimated, the next step involves the determination of differential ground movement causing pipe bending. Therefore, the possible shapes of differential ground movement profiles were studied for different pipe bending environments (stress hotspots) by examining the results of finite element analyses.

6.4.1 Differential ground movement profiles

In order to obtain differential ground movement profiles at different hotspot locations, a finite element model for each hotspot was analysed without considering the presence of a pipe. Therefore, this differential ground movement is independent of the soil-pipe interaction, or it can be explained as a bending profile of a fully flexible pipe that exactly follows the ground movement, as stated in the methodology proposed by (Wols and Thienen, 2014).

Figure 6.7 shows an example ground movement profile for soil drying under a driveway. The ground movement results from the differential moisture variation under the driveway (as explained in Section 4.4.1).

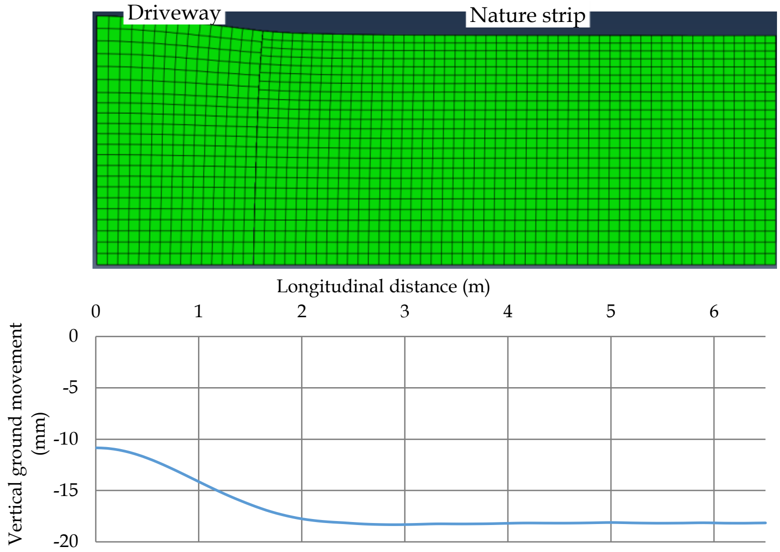

Figure 6.7. Example of ground movement profile under driveway – for soil drying

The figure shows that the shrinkage movement increases towards the nature strip, while the smallest movement is under the centre of the driveway. Therefore, the maximum curvature of the profile is located under the centre of the driveway. In contrast to this behaviour, the ground movement profile for soil wetting under driveways shows a relatively flat movement under the centre of the driveway, while the curvature is shifted towards the edge of the driveway (as can be seen in Figure 6.8).

In addition to the differential moisture variation under the driveway, the rigidity of the driveway causes this profile shape (as explained in Section 4.4.2).

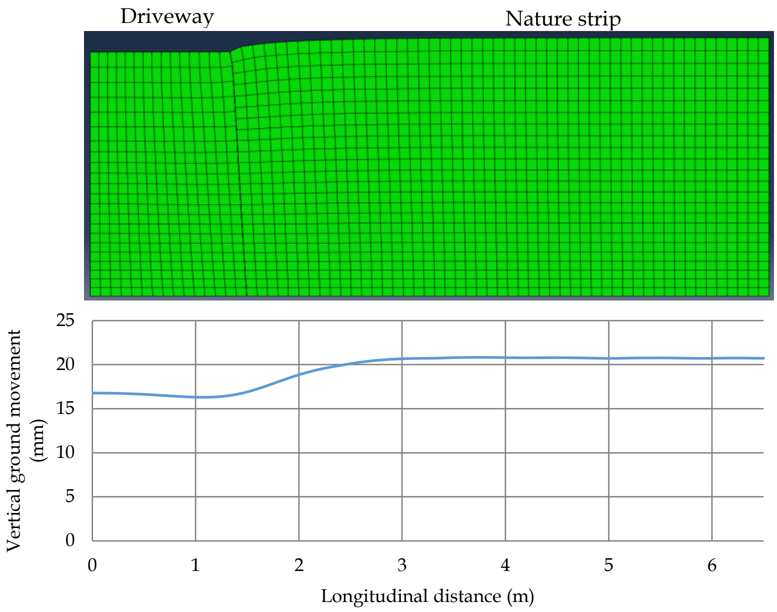

Figure 6.8. Example of ground movement profile under driveway – for soil wetting

Examples of ground movement profiles for stress hotspots with varying bedrock profiles and water leaks were also analysed and the profiles are shown in Figure 6.9 and Figure 6.10. The ground movement with varying rock profiles (Figure 6.9) shows that ground movement above flatter parts of the rock surface produces a more uniform pattern whereas the curvature of the ground movement is heightened at rock slopes. In the case of a water leak, swelling is observed to be localised at the leak location, creating the highest curvature of the ground movement profile there, as shown in Figure 6.10.

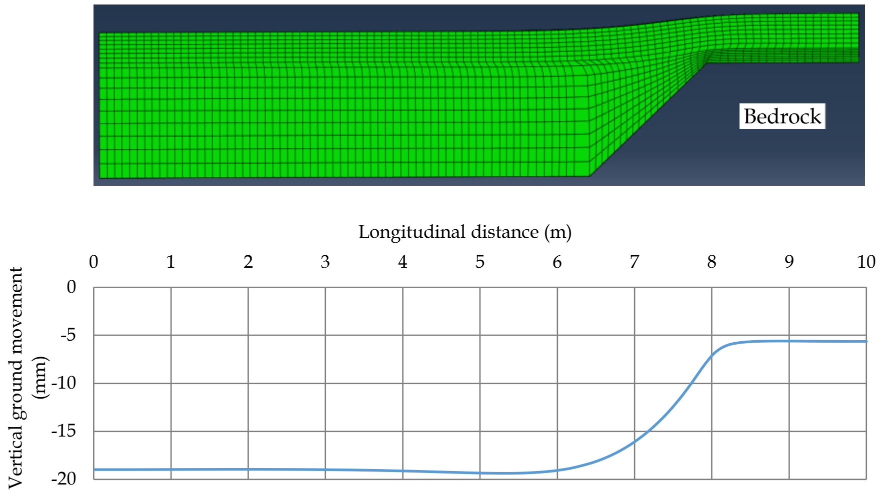

Figure 6.9. Example of ground surface movement due to varying bedrocks

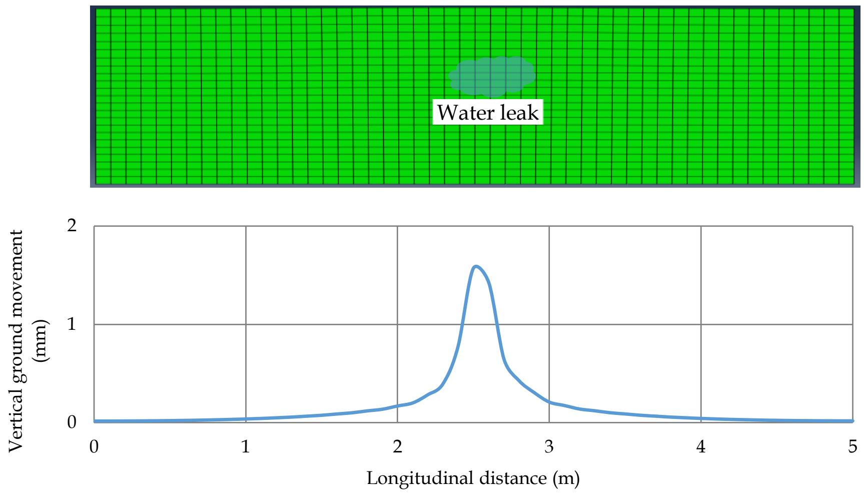

Figure 6.10. Example of ground movement profile at a water leak

For use in pipe stress estimation, it is necessary to mathematically characterise these ground profiles. Therefore, all identified ground movement profiles were categorised into the two different equivalent shapes shown in Figure 6.11 based on their general shapes. The applicability of these two shapes in the ground movement profiles of different pipe stress hotspots is highlighted in Table 6.4.

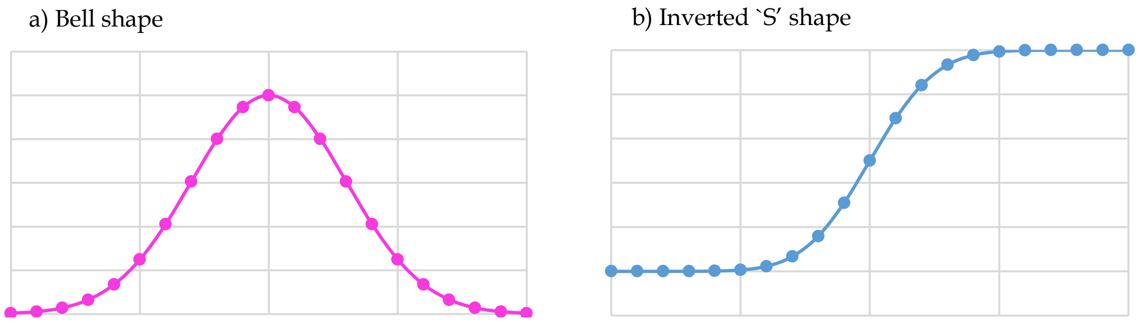

Figure 6.11. Identified general ground movement profile shapes

Table 6.4. Applicability of general ground profile shapes to stress hotspots

	Bell shape	Inverted `S' shape
Applicable field stress hotspots:	Driveway-soil drying Water leaks Tree roots.	Driveway-soil wetting Varying rock profiles Soil boundary

These two shapes can be identified as well-established curves in normal probability distribution analyses (Ahsanullah et al., 2014). Therefore, available mathematical expressions can be used for these two shapes in the rest of the analyses presented in this chapter, as described in the following sections.

It is to be noticed that these two differential ground displacement shapes have been commonly used in different soil-pipe interaction analyses. For example, the bell shape has been used to simulate the pipe deformation due to tunnelling effects (Klar et al., 2005) and the inverted 'S' shape has been used to simulate pipe deformations due to ground settlements (Wols and Thienen, 2014). Considering their appropriateness to represent the shapes of differential ground movement profiles presented in Figures 6.7 to 6.10 and the previous uses for different analyses, these two ground displacement shapes can be expected to produce convenient results in the present analysis.

6.4.1.1 Bell shape

It was identified that this bell shape can be designated as the shape of the probability density function of a normal distribution. Hence, this shape can be mathematically expressed as shown in Equation 6.9.

$$f(x) = \frac{1}{\sigma^* \sqrt{2\pi}} e_N^{-\frac{(x-\mu)^2}{2\sigma^2}} \qquad \text{Equation 6.9}$$

where, μ is the mean of the distribution, σ^* is the standard deviation and e_N is the natural logarithm.

6.4.1.2 Inverted 'S' shape

The other shape, an inverted 'S', was identified as the shape of the cumulative density function, which is the area under the probability density function of the normal distribution. Therefore, this shape can be mathematically expressed as shown in Equation 6.10:

$$F(x) = \frac{1}{2}\left[1 + erf\left(\frac{x-\mu}{\sigma^* \sqrt{2}}\right)\right] \qquad \text{Equation 6.10}$$

where, the Gaussian error function is denoted as $erf(.)$.

The above expressions for the two identified differential ground movement shapes were modified using the ground movement parameters, as explained in the following section.

6.4.2 Characteristic parameters of differential ground movement shapes (S_{max} and i)

In order to use Equations 6.9 and 6.10 in ground movement calculations, the constants in those equations need to be recognised as the characteristics of differential ground movement patterns. As understood from the literature review (Section 2.7.2), such characteristic parameters have been denoted as S_{max} and i in pipe deformation shape determinations of soil settlement problems (Wols and Thienen, 2014). Therefore, similar parameters are used in the present study and the physical meanings of these two parameters are illustrated in Figure 6.12.

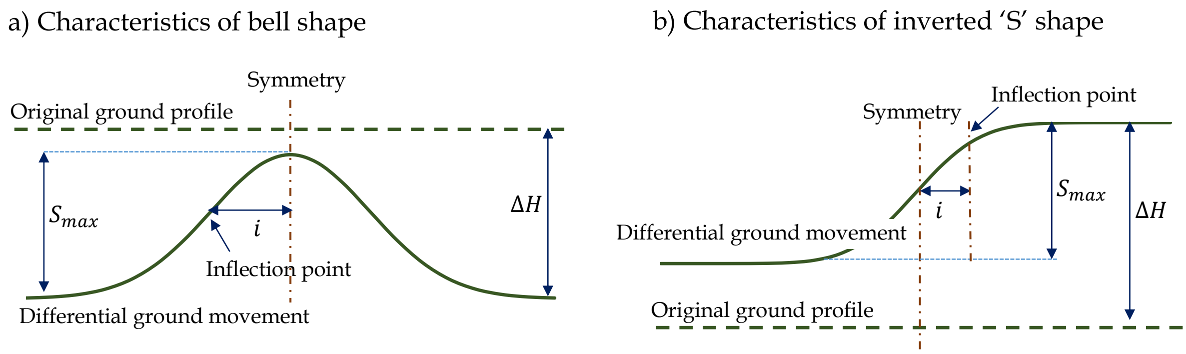

Figure 6.12. Characteristics of ground movement shapes

As the above figure indicates, S_{max} is the maximum differential ground movement with reference to the smallest movement. S_{max} can be defined as a fraction of free ground movement (ΔH). i is a function of the geometry of the problem and it can be identified as the distance from the mean position to the inflection point of the curve.

The Australian standard for the design of slabs in reactive soil environments (Australian Standards, 2011) also refers to specifications similar to S_{max} and i in the structural definitions of slab mound shapes. It can be seen in Figure 6.13 that the differential mound movement of the slab (y_m) is equivalent to the differential movement S_{max}, while the edge distance (e_d) is equivalent to the characteristic horizontal length of the curvature i.

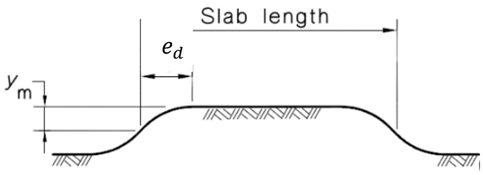

Figure 6.13. Idealised mound shape as in AS2870 (Australian Standards, 2011)

With the use of S_{max} and i, Equations 6.9 and 6.10 were modified as shown in Equations 6.11 and 6.12, respectively.

$$S_v(x) = S_{max}\, e_N^{-\frac{(x-x_0)^2}{2i^2}} \qquad \text{Equation 6.11}$$

$$S_v(x) = \frac{1}{2} S_{max} \left[1 + erf\left(\frac{-(x-x_0)}{i\sqrt{2}}\right)\right] \quad \text{Equation 6.12}$$

In the above equations, $S_v(x)$ is the vertical soil movement along the pipe direction (x) and x_0 is the point of symmetry of the differential movement (see Figure 6.12).

The numerically-analysed ground movement profiles using the FE method (as in Figure 6.7 to Figure 6.10) were used to assess the applicability of these equations and to determine the characteristic parameters (S_{max} and i). A comparison of differential ground movement profiles under driveways is shown in Figure 6.14.

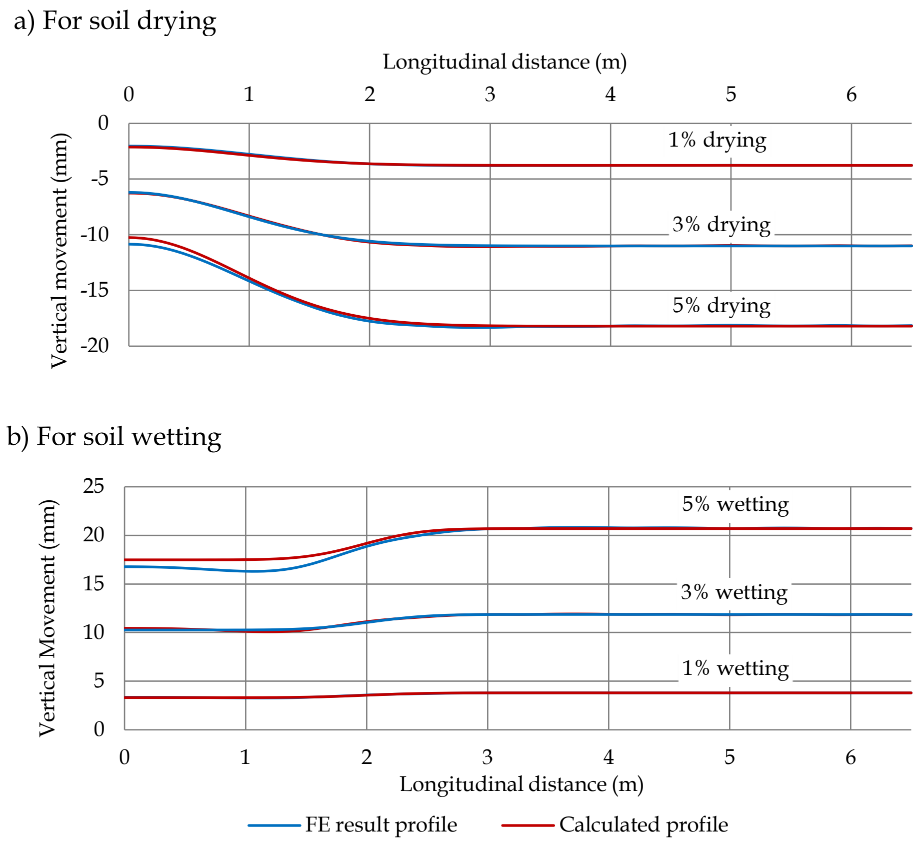

Figure 6.14. Calculated and FE ground movement profiles under driveways

The ground movement profiles in the above figure were calculated by determining the characteristic parameters, S_{max} and i as shown in Table 6.5. Since it was observed that the S_{max} is proportional to the free ground movement at pipe depth (ΔH), the proportional factors in Table 6.5 were determined by considering several finite element simulations under different dying and wetting conditions. The other parameter, , was observed to be two constant values for soil drying and wetting profiles. These values were defined for a 3m wide driveway.

Table 6.5. Characteristic parameters for differential ground movement under driveways

	S_{max}	i
For soil drying	0.44 ΔH	907 mm
For soil wetting	0.16 ΔH	484 mm

Similarly, the differential ground movements due to rock depth variations were determined by simulating ground movements with several arbitrary rock slopes. For example, comparisons of calculated and finite element result profiles of four simulations are shown in Figure 6.15.

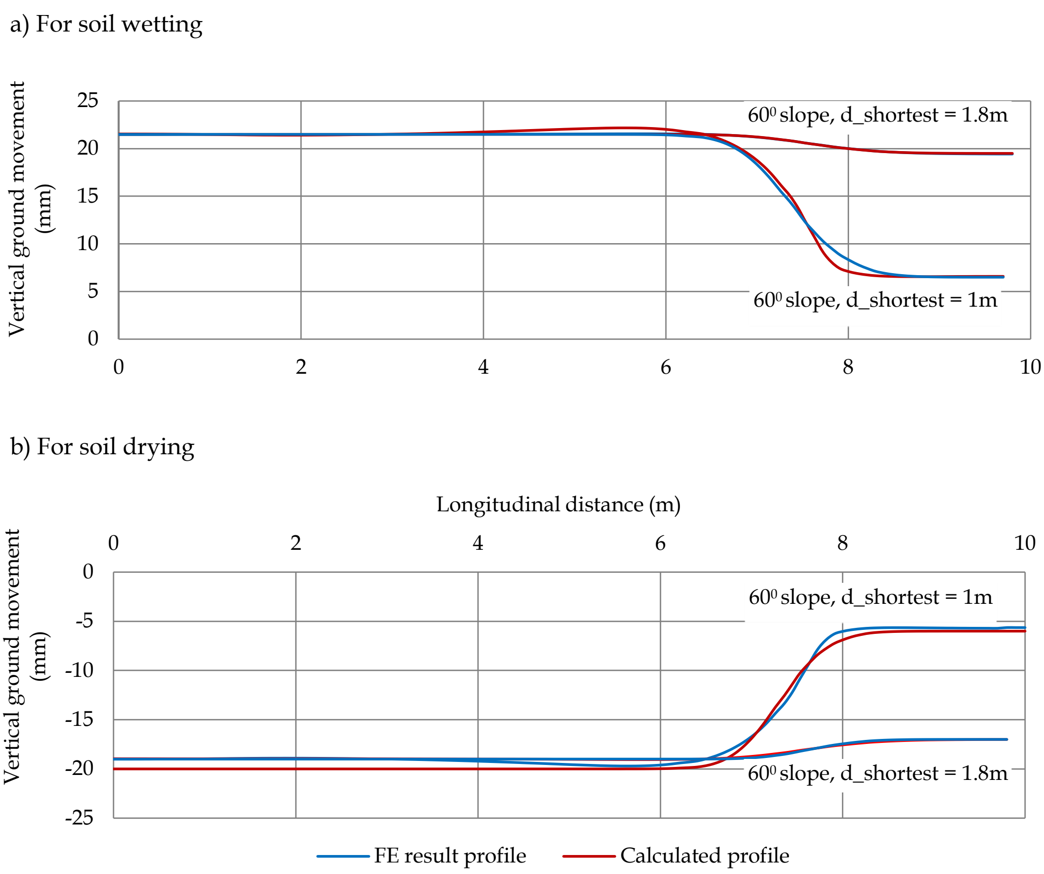

Figure 6.15. Calculated and FE ground movement profiles near bedrock variations

In this comparison, the characteristic parameters S_{max} and i were determined, as explained in Table 6.6. These definitions are based on the results of several finite element analyses (as shown in Figure 6.15). From the results, S_{max} was simply identified as the difference in free ground movement at pipe depth (ΔH) between the shallowest and deepest rock depths in soil reactive zones (down to 2.3m depth). The other parameter, , was identified as a function of the horizontal pitch (explained in Figure 4.21) of the rock slope in soil reactive zones, as shown in Table 6.6.

Table 6.6. Characteristic parameters for differential ground movement near rock slopes

	S_{max}	i (mm)
For soil drying	Difference of ΔH at shallowest and deepest rock depths. (Equation 6.5 and/or 6.6)	$0.17\ (horizontal\ pitch\ of\ the\ slope) + 380$
For soil wetting		

However, the determination of the S_{max} and i parameters for other cases (differential movements at soil boundaries, tree roots and water leaks) was not as simple as in the driveway and rock slope cases. The main reason for that is the difficulty of defining an affected area for these stress hotspots. For instance, in a case of a water leak, the differential ground movement is dependent on the wetted area. If the wetted area is widely spread, the curvature may be low with a greater i. However, Table 6.7 shows some approximate estimations for S_{max} and i parameters based on the finite element simulations. These estimations are based on assumptions for the worst possible scenarios (as stated in Table 6.7).

Table 6.7. S_{max} and i parameters for other cases

Stress hotspot	S_{max}	i	Worst case assumptions
At soil boundary	ΔH at the reactive soil side	500 – 600 mm	Reactive soil-non-reactive soil boundary
Tree root	ΔH at the far side of the tree root	100 – 300 mm	Pipe movement is completely restricted by tree root
Water leak	$\Delta\theta_v I_{\theta_v} H$ ($\Delta\theta_v$ is moisture change by the leak and H is the affected depth)	150 - 300 mm	Pipe movement is limited to the leak location

After defining the curvature parameters of differential ground movements, the next step involves the estimation of pipe bending stresses.

6.5 Pipe Stress Calculation

This section explains the procedure to determine the maximum bending stress in a pipe due to differential ground movement. According to the method of pipe stress estimation for settling ground (Wols and Thienen, 2014) (Section 2.7.2), the second derivative of the ground movement profile ($S_v(x)$) with respect to longitudinal pipe length (x) is used to determine the bending movement of a flexible pipe (Section 2.7.2). Equations 6.13 and 6.14 determine these bending moment profiles ($M_G(x)$) for both bell-shaped and inverted 'S'-shaped ground movement profiles.

For the bell-shaped differential ground movement profile:

$$M_G(x) = -EI\ \frac{S_{max}}{i^4}\ e_N^{\frac{-(x-x_0)^2}{2i^2}}[(x-x_0)^2 - i^2] \qquad \text{Equation 6.13}$$

For the inverted 'S'-shaped differential ground movement profile:

$$M_G(x) = -EI\,\frac{S_{max}}{i^3\sqrt{2\pi}}\,(x - x_0)\,e_N^{-\frac{(x-x_0)^2}{2i^2}} \qquad \text{Equation 6.14}$$

where, E is the Young's modulus of the pipe material and I is the second moment of area about the neutral axis of the pipe cross-section.

Since the highest pipe bending stress is determined using this methodology, the maxima of the above bending moment profiles ($M_{G,max}$) were considered by differentiating again with respect to longitudinal pipe length (x). These maximum bending moments are expressed in Equations 6.15 and 6.16.

For the bell-shaped differential ground movement profile, the maximum bending moment obtained at $x = x_0$ is given as:

$$M_{G,max} = EI\,\frac{S_{max}}{i^2} \qquad \text{Equation 6.15}$$

For the inverted 'S'-shaped differential ground movement profile, the maximum bending moment is obtained when $x = (x_0 \pm i)$. Therefore, the maximum bending moment is given by:

$$M_{G,max} = \pm EI\,\frac{S_{max}}{i^2\sqrt{2\pi}}\,e_N^{-\frac{1}{2}} \qquad \text{Equation 6.16}$$

The pipe bending stress is then calculated using the stiffness factor (M_{norm}) to convert the flexible pipe bending moment ($M_{G,max}$) to the actual pipe bending moment ($M_{p,max}$), as expressed in Equation 6.17.

$$M_{p,max} = M_{norm} \times M_{G,max} \qquad \text{Equation 6.17}$$

This stiffness factor, M_{norm} has been used as a function of the stiffness properties of both soil (K – soil subgrade modulus) and pipe (E and I) (Wols and Thienen, 2014) (Equation 6.18).

$$M_{norm} = \frac{1+b_1\left(\frac{EI}{Ki^4}\right)^{c_1}}{1+b_2\left(\frac{EI}{Ki^4}\right)^{c_2}} \qquad \text{Equation 6.18}$$

However, it is simplified in the present study and uses fewer parameters by considering a constant E/K ratio for the whole pipe network, as explained in Section 6.5.1.

After the pipe bending moment is calculated, the maximum tensile bending stress at the outer wall of the pipe is calculated using Equation 6.19:

$$\sigma_{p,max} = \frac{M_{p,max}}{I}\left(\frac{D+2t}{2}\right) \qquad \text{Equation 6.19}$$

where, D is the internal diameter of the pipe and t is the wall thickness.

6.5.1 Soil-pipe stiffness factor (M_{norm})

This soil-pipe stiffness factor is defined as a function of differential ground movement characteristic parameter i and the second moment of area of the pipe section I. The determination of this dimensionless parameter is expressed by the following Equation 6.20:

$$M_{norm} = \frac{1+b_1\left(\frac{I}{i^4}\right)^{c_1}}{1+b_2\left(\frac{I}{i^4}\right)^{c_2}} \qquad \text{Equation 6.20}$$

where, b_1, c_1, b_2 and c_2 are fitting parameters.

These fitting parameters were determined from the results of the finite element model. The results of a series of different pipe deformation cases (under driveways and near rock slopes) were considered in this work.

6.5.2 Finite element analyses to find fitting parameters

The procedure followed to determine the fitting parameters of the stiffness factor calculation can be explained as follows:

- For each analysed case, the highest pipe bending stress was obtained from the finite element results.

- The same bending stress was then calculated by considering a set of assumed fitting parameters for the stiffness factor.
- Finally, the assumed fitting parameters were optimised to minimise the error between the analytical and numerical bending stresses based on finite element analysis of the same pipe.
- This procedure was followed separately for each different pipe bending case, such as soil drying and wetting under driveways, at rock slopes etc.

The optimised fitting parameters of each different analysis are shown in Table 6.8. The complete details of all variables considered for each optimisation analysis (pipe diameter, wall thickness, Young's modulus of pipe material, soil moisture change and differential movement characteristics) are listed for analytical and numerical pipe stresses based on finite element analyses in Appendix C.

Table 6.8. Optimised fitting parameters for stiffness factor calculations

Pipe bending case	b_1	c_1	b_2	c_2
Bell-shaped bending	0	3.64	463	0.51
Inverted 'S'-shaped bending (except at bedrock)	0	3.64	665	0.69
Soil drying at rock slopes	0	3.64	889369	1.45
Soil wetting at rock slopes	0	3.64	27126780	1.71

A comparison of finite element results and bending stresses calculated from optimised fitting parameters is shown in Figure 6.16. The figure shows good agreement between the finite element results and the analytically-estimated stresses, as the results are close to the 1:1 line. This shows that the simplified analytical equation proposed is sufficiently accurate to estimate pipe stresses estimated by finite element models. However, it is to be mentioned that the presented methodology can be improved in the future with more validations and verifications when more pipe deformation and stress data are available.

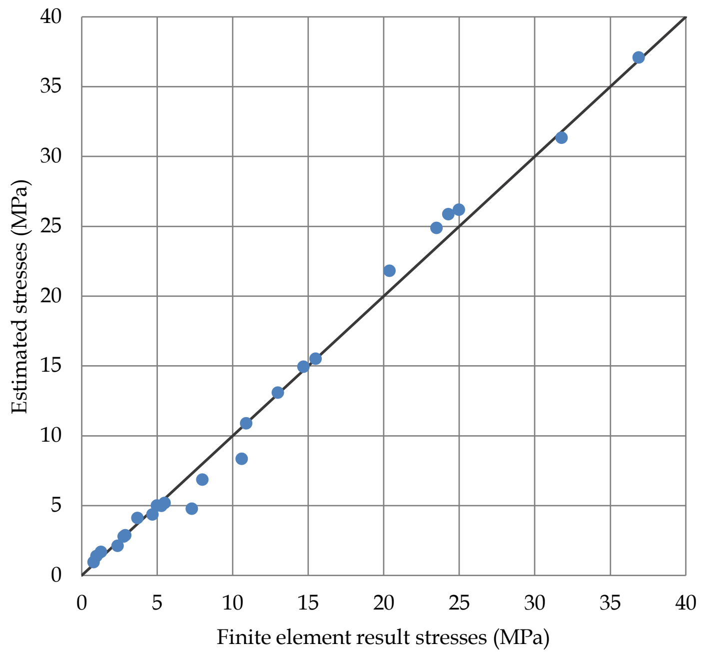

Figure 6.16. Comparison of finite element results and calculated pipe stresses: Optimisation stage

6.5.3 Pipe stress equations

As given in Equations 6.21 and 6.22, the final versions of the equations to calculate pipe bending stresses were derived by substituting Equations 6.15, 6.16 and 6.17 into Equation 6.19.

For the bell-shaped differential ground movement profile,

$$\sigma_{p,max} = EM_{norm}\frac{S_{max}}{i^2}\left(\frac{D+2t}{2}\right) \qquad \text{Equation 6.21}$$

For the inverted 'S'-shaped differential ground movement profile,

$$\sigma_{p,max} = EM_{norm}\frac{S_{max}}{i^2}\frac{e_N^{-\frac{1}{2}}}{\sqrt{2\pi}}\left(\frac{D+2t}{2}\right) \qquad \text{Equation 6.22}$$

Henceforth, these two equations are used in all pipe stress calculations, with the appropriate soil-pipe stiffness factor (M_{norm}) being calculated based on Equation 6.19 and the parameters given in Table 6.8.

6.5.4 Comparison and Validation

In addition to the comparison made in the model optimisation stage (as shown in Figure 6.16), another comparison was made by analysing a new set of pipe bending configurations to validate the applicability of the analytical stress calculation equation for general use. Since these stress estimations are independent of the model optimisation analyses, this comparison indicates the appropriateness of this analytical equation and its fitting parameters for general practice. In this step, the finite element results were used only for comparative purposes, as shown in Figure 6.17.

As can be seen in Figure 6.17, the analytically-calculated pipe bending stresses show good agreement with the finite element results. The majority of the analytical and finite element pipe stresses are close to the 1:1 line. In addition, the resultant bending stresses of these analyses are in the range of 0 to 25 MPa, with the exception of three extreme analyses. Since the estimated stresses are within the range of field pipe responses (in Chapter 3), these analytical equations can be reasonably utilised for field pipe stress estimation. However, with more information related to the pipe deformations at each hotspots locations, the current assumptions and hence the validity of these results can be improved in the future.

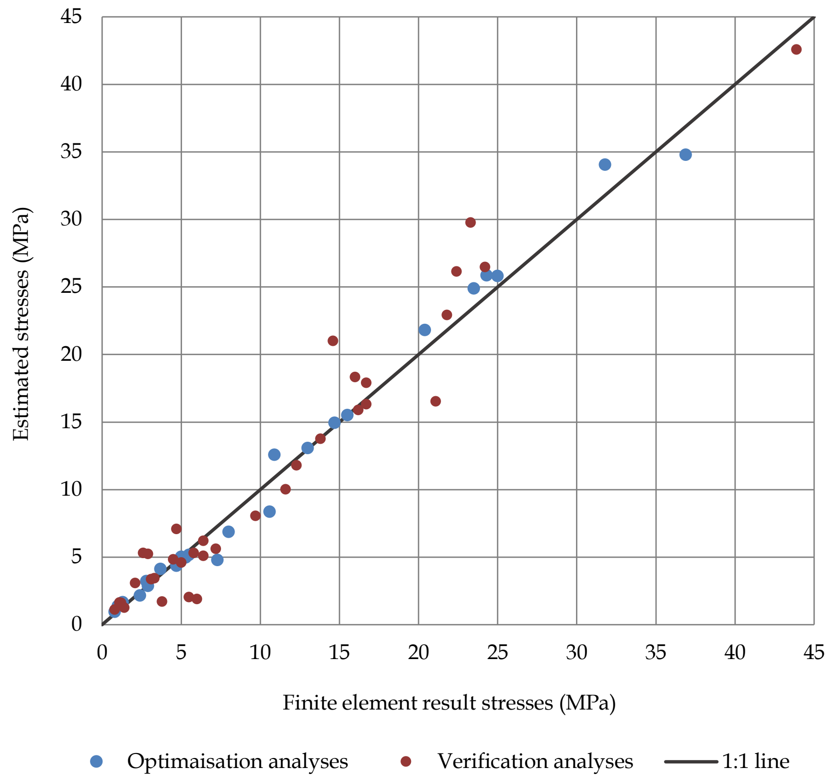

Figure 6.17. Comparison of finite element results and calculated pipe stresses: Verification stage

Note that the 60 analyses related to the results in the above figure were conducted considering different soil moisture changes, pipe sizes and material properties (Young's moduli). A complete description of each analysis is provided in Appendix C.

6.6 General Behaviour of the Model

As the last step, the behaviour of these pipe stress estimation equations with the main input parameters was tested to identify the general response of the equations. The main input parameters were identified as the soil moisture variation, soil type, pipe size and material. The variations in the calculated pipe stresses for these input parameters are discussed in the following sections.

6.6.1 Responses to different soil moisture changes

In these pipe stress estimation equations (Equations 6.21 and 6.22), soil moisture change is incorporated in the differential ground movement characteristic parameter S_{max}. Since S_{max} is a linear function of free ground movement ΔH (Section 6.4.2), S_{max} shows a linear relationship with pipe level soil moisture variations (according to Equations 6.5 and 6.6 for calculating ΔH). Therefore, linearly varying pipe stresses are observed for different soil moisture changes when the other parameters (bending location, pipe size pipe material) are unchanged. An example of this analysis is shown in Figure 6.18.

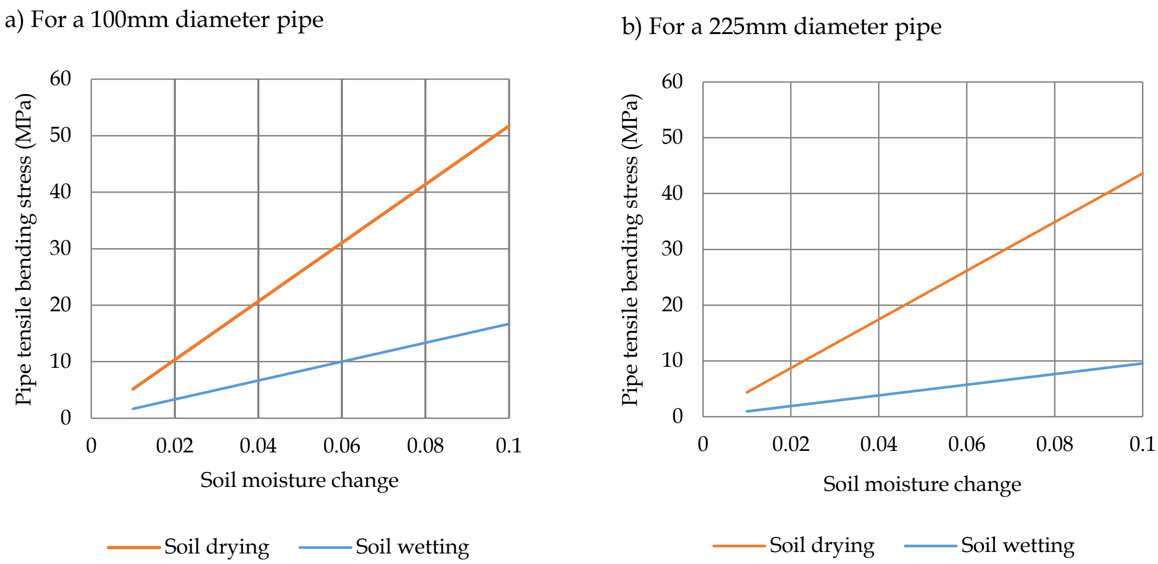

Figure 6.18. Estimated pipe stress variations for different soil moisture changes at driveways

6.6.2 Response to different soil types

The variation of estimated stresses with soil type was similar to the variation in the previous example given in Figure 6.18. In Equations 6.5 and 6.6, the soil type determines the strain index I_{θ_v} (as in Table 6.3). Therefore, the free ground movement ΔH, and hence S_{max} , becomes smaller for less reactive soils. As a result, a similar linear relationship is observed with a smaller gradient. The results of calculations of pipe bending stresses at driveways of four different reactive soil classes are shown in Figure 6.19.

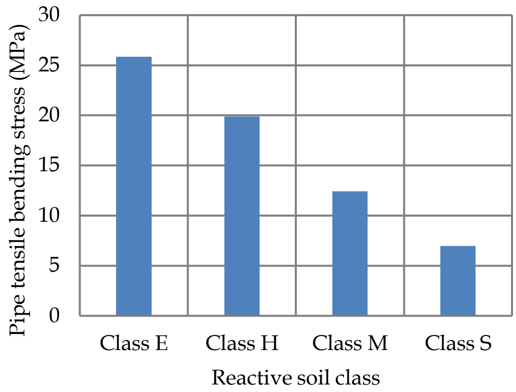

Figure 6.19. Estimated pipe stress variations for different reactive soil classes of AS2870: for soil drying at driveways

As can be seen in the above figure, due to the change of strain indices (I_{θ_v}), the maximum tensile bending stress in the pipe decreases significantly from extremely reactive soils (Class E) to slightly reactive soils (Class S). Although this example is for 0.05 moisture variation (drying) and a 100mm diameter pipe buried at 750mm depth, a similar trend was observed for all other cases.

6.6.3 Response to different pipe depths

Since the free ground movement (ΔH) was calculated for the pipe burial depth, the calculated pipe stress is considerably affected by the variation of the burial depth. As expressed in Equations 6.5 and 6.6, the vertical distance between the pipe and the reactive soil zone depth ($H_s - d_{pipe}$) decreases when the pipe is buried at deeper depths. Furthermore, the moisture variations of deep soil layers are generally smaller than those of shallow soils. Figure 6.20 shows that the calculated pipe stresses decrease with the pipe burial depth. Eventually, these pipe stresses are expected to become zero if the pipe is buried deeper than the reactive soil depth (H_s).

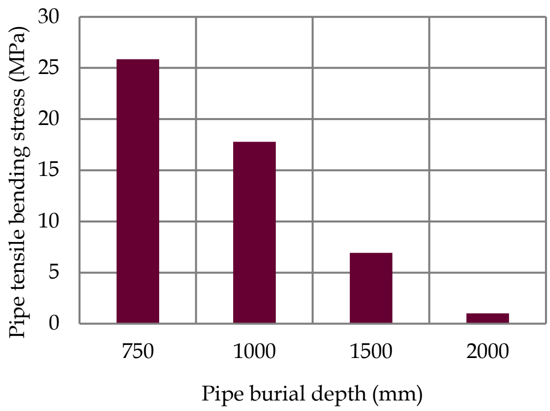

Figure 6.20. Estimated pipe stress variations for different burial depths for soil drying at driveways

The results shown in the above figure were calculated for a 100mm pipe and a linear vertical variation of soil moisture change (as in Figure 6.2) with 0.05 moisture change at 750mm depth.

6.6.4 Response to different pipe sizes

The pipe size is another key input parameter of this model. Generally, the pipe diameter and its wall thickness are considered as the pipe size. Since the pipe network contains pipe sizes from 100mm diameter small pipes to 600mm diameter large pipes, the model response to different pipe diameters was analysed. The variation of the soil-pipe stiffness factor (M_{norm}) for different pipe diameters was studied, as it is a key parameter for stress calculation and is dependent on the pipe size. The variation of M_{norm} for soil drying at a driveway is shown in Figure 6.21.

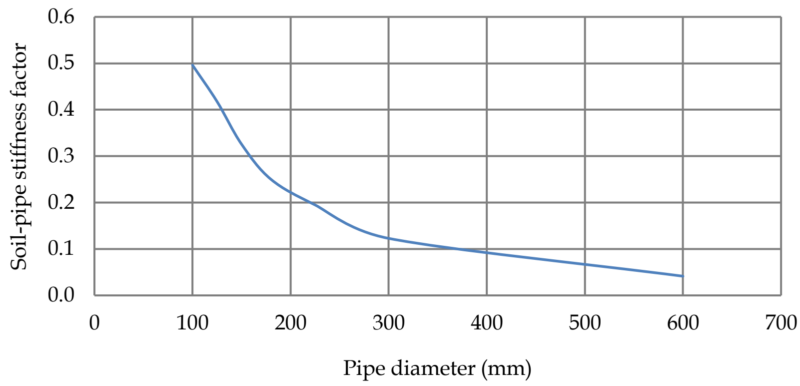

Figure 6.21. Variation of soil-pipe stiffness factor (M_{norm}) with different pipe diameters

As the above figure indicates, the soil-pipe stiffness factor (M_{norm}) rapidly decreases with increasing pipe diameter. This indicates that the bending resistance of large-diameter pipes results in smaller bending moments for the same ground movement. However, as expressed in the stress estimation equations (Equations 6.21 and 6.22), the bending stress is also proportional to the pipe dimeter (D). Therefore, the calculated stress is affected by both effects (decreasing M_{norm} and increasing D) and their combined effect can be seen in Figure 6.22.

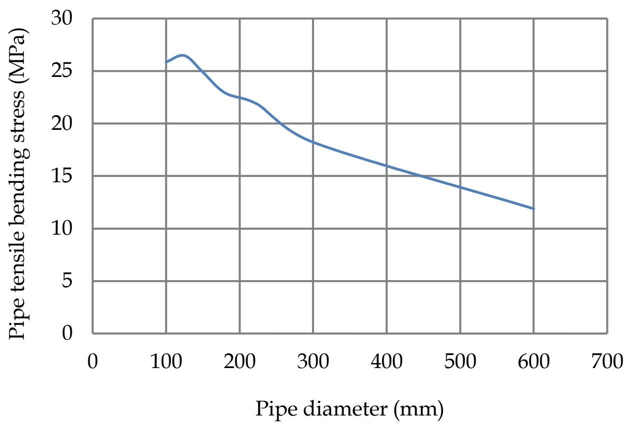

Figure 6.22. Estimated pipe stress variations for different pipe diameters for soil drying at driveways

As can be seen in the above figure, the overall effect of increasing pipe diameter is a stress decrease. For the case of 0.05 moisture change (drying) at a driveway, the estimated pipe stress decreases from 26 MPa to 12 MPa when the pipe size changes from 100mm to 600mm. All these pipes were assumed to be buried at 750mm depth.

6.6.5 Response to different pipe material properties

As expressed in the stress estimation equations (Equations 6.21 and 6.22), the pipe bending stress is proportional to the pipe material's Young's modulus (E). Therefore, a linear relationship is expected between the calculated pipe stresses and the material's Young's modulus. Figure 6.23 shows the variation of pipe bending stress with the Young's modulus of the cast iron pipe.

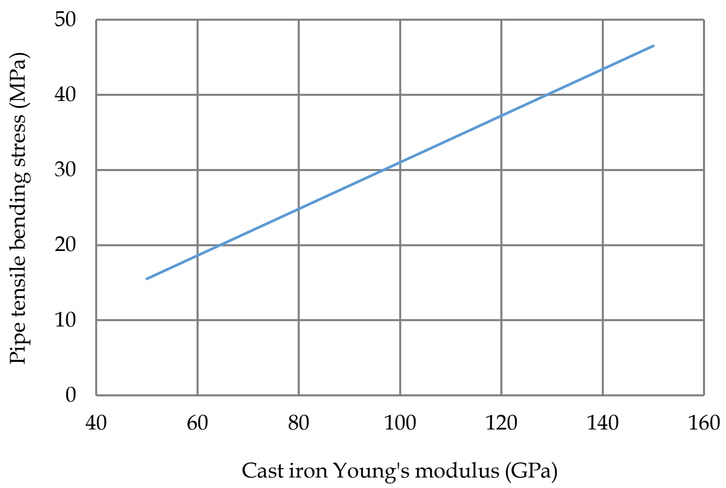

Figure 6.23. Estimated pipe stress variations for different cast iron Young's moduli: for soil drying at driveways

6.7 Conclusions

This chapter has presented a simple analytical method to estimate pipe bending stresses due to ground movement at pre-identified stress hotspots. This simplified method was developed based on existing methods of pipe stress estimation for settling ground (Wols and Thienen, 2014) and considering theoretical explanations for pipe bending patterns in Chapter 4 and further finite element simulations. The major outcomes of this chapter can be summarised as follows:

- The proposed analytical model estimates the pipe stresses based on the differential ground movement at each stress hotspot and the material and section properties of the pipe.
- The differential ground movement is defined by two characteristic parameters (S_{max} and i) which are determined by considering the curvature of differential ground movement profiles.
- A soil-pipe stiffness factor (M_{norm}) is used in the stress estimation equations to incorporate the stiffness of different diameter pipes. The fitting parameters required to calculate this stiffness factor were determined by optimising the analytically-estimated stresses to be matched with the results of the finite element simulation.
- This pipe stress estimation model requires only a limited number of input parameters: soil moisture change, soil reactivity data, pipe depth, pipe diameter and wall thickness and pipe material Young's modulus.
- The estimated stresses show good agreement with the finite element results.
- A sensitivity analysis of the input parameters of the model shows that the model results are reasonably consistent with the expected pipe behaviour, as identified in the literature review.

The practical application of the stress estimation model to field pipe failure analysis is presented in the next chapter.

CHAPTER 7: APPLICATION OF PIPE STRESS ESTIMATION EQUATIONS TO FIELD PIPE FAILURE ANALYSIS

7.1 Overview

This chapter presents an application of the pipe stress estimation equations presented in Chapter 6 to field pipe failure analysis for asset management purposes. This work has also contributed to other pipe failure prediction models developed in the Smart Water Fund project, `An Innovative Integrated Algorithm for Cost-Effective Management of Water Pipe Networks' (Smart Water Fund, 2017b). The estimations of pipe bending stresses due to seasonal soil moisture variations are integrated with predictions of circumferential (broken-back) failure. For instance, this chapter explains the use of estimated stresses in the Monash Pipe-failure Prediction (MPP) model. In this model, the input parameters of the stress estimation equations are used according to the field conditions. Appropriate variations of soil moisture contents, soil and pipe properties are considered. The stress estimations are verified by comparing the seasonal variations of the estimated stresses with past pipe failure records. Before the stress estimations are applied to failure predictions, the effects of corrosion patches are included they reduce the nominal strength of the pipe material (cast iron).

7.2 Input Data for Field Pipe Stress Analysis

The basic input parameters which are required for pipe stress estimations were identified in Chapter 6. These parameters can be categorised into soil moisture information and soil and pipe properties, as listed in Table 7.1.

Table 7.1. Input data for pipe stress estimation

Moisture properties	Soil Properties	Pipe properties
Soil moisture changes at pipe depth	Soil reactivity indices	Diameter
	Thickness of reactive clay layer	Wall thickness
		Young's modulus

As was concluded in Chapter 6, final stress estimations are notably sensitive to these input parameters. Therefore, the selection of appropriate data for these input parameters is an important step in field application as the output stress estimations must be reliable for pipe failure analyses. However, in a large-scale analysis, the uncertainty of the input parameters is unavoidable due to the limited availability of data. In this work, the available data are utilized in the stress estimation equations with reasonable assumptions and simplifications, where necessary. The nature of the available data and their limitations are explained in the following sections.

7.2.1 Soil moisture

The variation of estimated stresses with time is primarily dependent on the moisture variation. In addition, the geographical variations of soil moisture content are important, as the soil moisture content varies spatially, depending on the climate and the soil properties. Therefore, a large-scale soil moisture database that is regularly updated is required for the convenient stress analysis of the entire pipe network.

The moisture data available from the Bureau of Meteorology, Australia (Bureau of Meteorology, 2017b) were considered in this analysis, as this database includes daily updated soil moisture data for the whole of Australia (see Section 2.5.2). Soil moisture variations of 0.1 to 1m depths applicable to the pipe buried region were considered for pipe stress analysis.

The moisture content percentages were converted into volumetric moisture contents by considering the water storage capacities of relevant soils (Armstrong et al., 2001). This derivation is presented below.

The raw information in the database, which is the percentage of available water content ($\theta_{Available,\%}$), is calculated as follows:

$$\theta_{Available,\%} = \frac{\theta_v - \theta_{PWP}}{\theta_{FC} - \theta_{PWP}} \times 100 \qquad \text{Equation 7.1}$$

where, θ_v is the volumetric water content of the soil and θ_{FC} and θ_{PWP} are the soil moisture contents corresponding to the field capacity and permanent wilting point, respectively.

The field capacity and permanent wilting points represent the upper and lower limits of soil water availability for crops, respectively. When these limiting moisture contents are known, the moisture information in the database is convertible to the volumetric moisture content (θ_v) using Equation 7.1. In this conversion, field capacities and permanent wilting points are used, as shown Table 7.2.

Table 7.2. Field capacity and permanent wilting point moisture contents (Armstrong et al., 2001)

Soil type	θ_{FC}	θ_{PWP}
Light clay	0.39	0.24
Medium to heavy clay	0.39	0.25

An example of the conversion of available water content ($\theta_{Available,\%}$) to volumetric soil moisture content (θ_v) for Altona North moisture data is shown in Figure 7.1.

a) Available water contents ($\theta_{Available,\%}$) (%)

b) Converted volumetric moisture contents (θ_v)

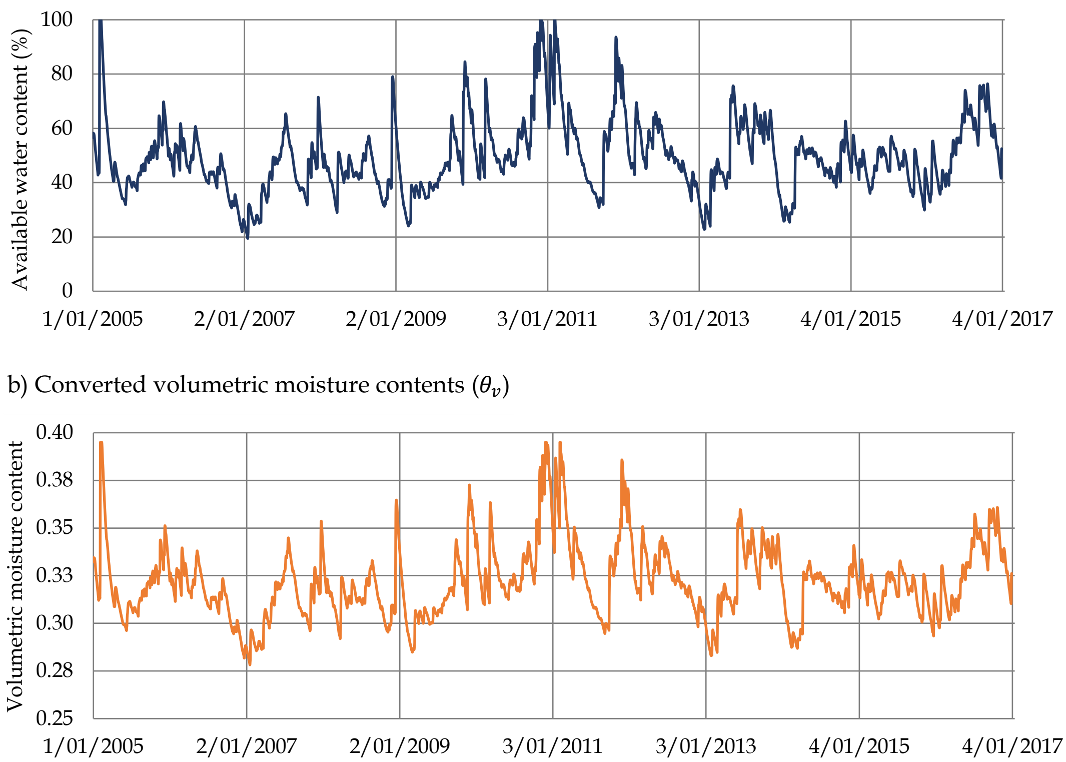

Figure 7.1. Converted volumetric soil moisture contents for Altona North

The figure shows that the converted volumetric moisture contents at the considered soil depth (0.1 to 1m) vary in the range of 0.28 to 0.40, whereas the original available water contents fluctuate between 20% and 100%. This soil moisture (θ_v) range can be compared with the average soil moisture variations of neutron probe measurements (as noted in Section 2.5.1) at pipe depths to study the suitability of these converted moisture values for soil moisture applications.

A comparison of the measured and converted moisture values of two selected suburbs (Altona North and Sunshine) is shown in Figure 7.2. It is evident that the measured moisture data vary in a similar range to the moisture data of both Altona North and Sunshine.

Some discrepancies between measured and converted data are visible, possibly due to errors in the estimation and conversion methodologies. For instance, the conversions of soil moisture estimations determined for a large area (25km^2 grid size, see Section 2.5.2) can be expected not to match exactly the discretely measured neutron probe data (see Section 2.5.1). In addition, averaging over the pipe depth region may also contribute to these errors. Notwithstanding these limitations, the proposed procedure making use of the BOM soil moisture data set and the conversion method for the pipe stress analyses was adopted as a practical approach, as described below.

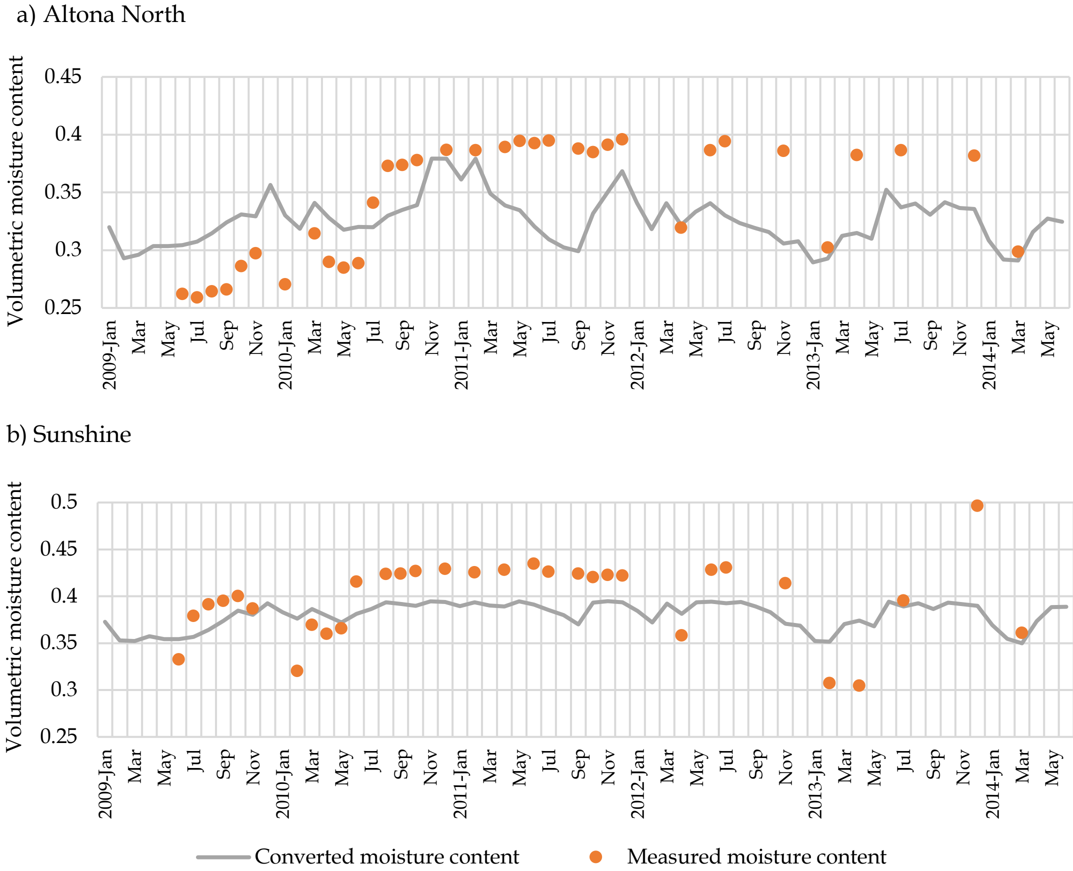

Figure 7.2. Comparison of measured and converted soil moisture contents

7.2.2 Soil moisture data for future pipe failure analyses

As the soil moisture data presented above are only available for current and past pipe stress analyses, a prediction method is required for future pipe stress or failure analyses. This requirement may be achieved either by simply adopting soil moisture variations from the past years to the next year with or without some adjustments, or by estimating future soil moisture contents based on climate forecasts. The implementation of soil moisture estimation models is a convenient method (in contrast to suction), as the yearly variation of soil moisture contents due to climate changes can be incorporated, and they are based on Australia-wide modelling and field-validated satellite monitoring (Yee et al., 2016). In particular, a soil moisture estimation model for Melbourne that is capable of being extended to future soil moisture predictions has been developed at Monash University as part of the Smart Water Fund project (Smart Water Fund, 2017a).

7.2.3 Reactive soil properties around pipe assets

Reactive soil information for Melbourne's water reticulation network area is available from several sources, as noted in Sections 2.2.2 and 2.2.3. Since the reactive soil site classification method of AS2870 (Australian Standards, 2011) is commonly practised in Australia, the same site classifications can be conveniently adopted for pipe assessment purposes. Therefore, an appropriate reactive soil class can be selected for each pipe in the network.

The thickness of the reactive soil layer is assumed to be the reactive soil zone depth (2.3m for Melbourne) when the bedrock information is not available. However, it can be modified for areas where the bedrock depths are found to be shallower.

When the reactive soil class and the soil layer thickness data are determined for a pipe, the resultant ground movement can be determined from the equations in Chapter 6 to estimate the pipe stresses.

7.2.4 Pipe material and section properties

The other important input parameters for the model are pipe section (size) and material data. Pipe section properties can be found from the pipe asset data sheets of each water authority as the records are available for asset management purposes. Therefore, each of the pipes in the network can be recognised with its diameter (internal or external) and nominal wall thickness. Here, the nominal wall thickness is defined as the original pipe wall thickness before any material deterioration (mostly due to corrosion). If the pipe wall thickness information is not available for each pipe, a typical value can be selected, as suggested in the literature review (see Section 2.2.3).

The main pipe material properties required for pipe stress estimation and subsequent pipe failure analysis are the Young's modulus and the tensile strength. These properties of cast iron have been identified as dependent on the manufacturing method and the time of manufacturing (Rajani, 2000; Gould, 2011). Therefore, the selection of suitable material properties for each pipe in the network is important for precise stress estimation.

As a possible solution, a research group at Monash University has initiated a cast iron pipe cohort investigation by testing several samples of Australian cast iron pipes (Shannon et al., 2016a; Jiang et al., 2017b). The main purpose of this work is to identify the material properties and categorise Australian cast iron pipes into groups of similarities. Then the cohort properties can be used in pipe stress and failure analyses of the same cohort. The information in Table 7.3 shows the main material properties identified for each pipe cohort.

Table 7.3. Major cast iron mechanical properties of pipe cohorts (Shannon et al., 2016a)

Pipe cohort	PIT-H	PIT-V	SPUN-I	SPUN-D	SPUN-S	SPUN-Y
Average Young's modulus (GPa)	85	85	115	117	107	127
Average tensile strength (MPa)	100	103	130	127	156	214

The methodology for the identification of cast iron pipes for each cohort is defined as shown in Figure 7.3. When the pipe manufacturing year and the manufacturing type are known, this procedure can be followed to identify the most appropriate cohort of the pipe.

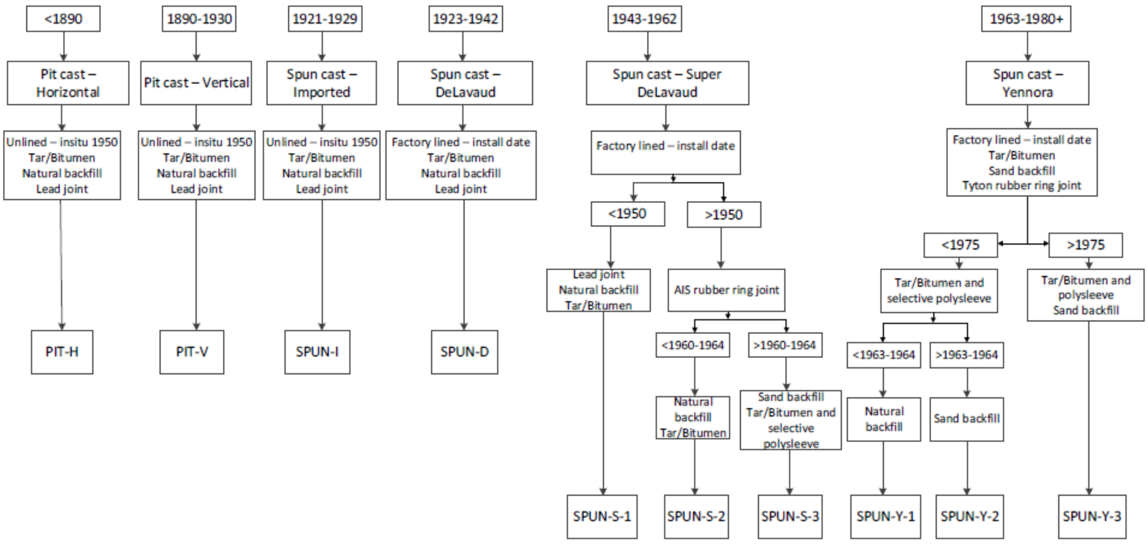

Figure 7.3. Definition of pipe cohorts (Shannon et al., 2016a)

As explained in the above sections, all required input information (as in Table 7.1) for pipe stress estimation can be conveniently found for the application of field pipe stress analyses. The following section further explains the application of the model explained in Chapter 6 to field pipes.

7.3 Field Pipe Stress Analysis

The suggested methodology of applying the simple pipe stress estimation model to field pipes was tested in five selected suburbs around Melbourne. These suburbs were selected by considering both very expansive and slightly expansive soil sites in Melbourne (site classifications according to Figure 2.26), as listed in Table 7.4.

Table 7.4. Selected areas and soil reactivity classes (according to Figure 2.26) for pipe stress estimations

Suburb or Municipality	Soil reactivity	Land area (km^2)	Failures per km^2 per year
Altona North	Very expansive	14.1	2.6
Sunshine	Very expansive	4.9	5.6
Yarraville	Very expansive	5.6	5
Bayside	Slightly expansive	36	0.6
Frankston	Slightly expansive	131	0.1

Since the effect of reactive ground movement is at its maximum in very expansive sites, three suburbs where very expansive soil sites are commonly present were selected for this application. The other two sites were selected as a control application to examine the model outcomes for less reactive soil sites.

7.3.1 Pipe stress calculation

The following steps were used in estimating the critical tensile bending stresses of pipes in the selected regions.

- Soil moisture changes: monthly average volumetric soil moisture contents at each location from January 2005 to May 2013 were obtained by following the procedure outlined in Section 7.2.1. Next, the long-term average soil moisture content was used as the mean neutral moisture content at each site. Finally, the moisture change ($\Delta\theta_v$) was determined with reference to the mean neutral moisture content, assuming that moisture contents above the mean (positive changes) represent wet conditions and those below the mean (negative changes) represent dry conditions.
- Ground movements: the calculated soil moisture changes were used to determine the free ground movements (ΔH) for each month at each site. The strain indices (I_{θ_v}) were chosen according to the site classification.
- Pipe bending stress: finally, the bending stresses were determined for each month at each site by considering the most critical bending configurations corresponding to stress hotspots.

In this pipe stress calculation, the most critical bending stresses were determined on the basis of the following assumptions:

- Pipe stress at the mean neutral soil moisture content (long-term average moisture content) was assumed to be zero.
- Bedrock depth was assumed to be deeper than the reactive depth of 2.3m, as it produces the highest possible ground movement at the region under consideration.

- Stresses were calculated for pipe bending at driveways, since driveways are the most common stress hotspots identified in any suburb or municipality.
- Since the highest bending stresses were observed for small pipe sizes, 100mm diameter cast iron pipes (E = 85 GPa)) were considered.

Using this methodology and these assumptions, the calculated pipe stresses represent the maximum tensile bending stresses in 100mm diameter cast iron pipes at any driveway in the particular suburb or municipality. The calculated monthly pipe stresses are shown in the following section.

7.3.2 Comparison with past pipe failures

The calculated pipe stresses were compared with the reported past pipe failures in the same suburb or municipality to examine the relationship between pipe stress and reported failures. The reported circumferential pipe failures of 100mm diameter cast iron pipes were used for this comparison. The results for three suburbs with very expansive soil are presented in Figure 7.6 to Figure 7.4 and the results for two slightly expansive soil areas are presented in Figure 7.7 and Figure 7.8.

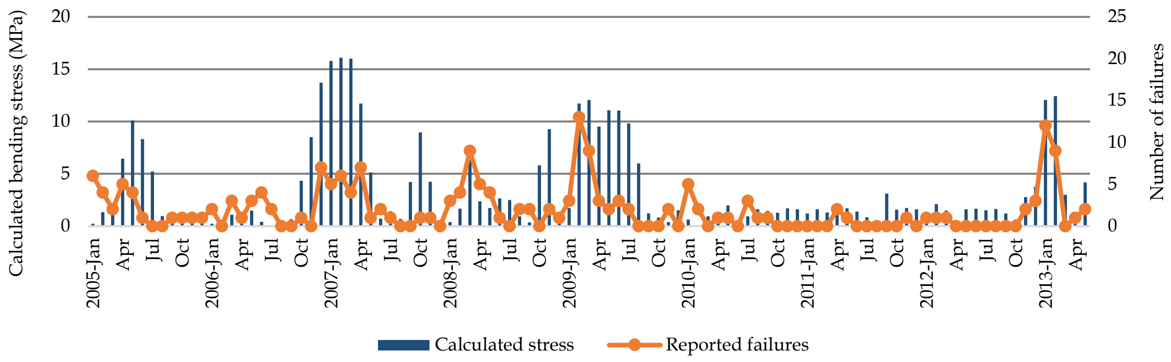

Figure 7.6. Comparison of calculated pipe stresses and reported past failures: Sunshine

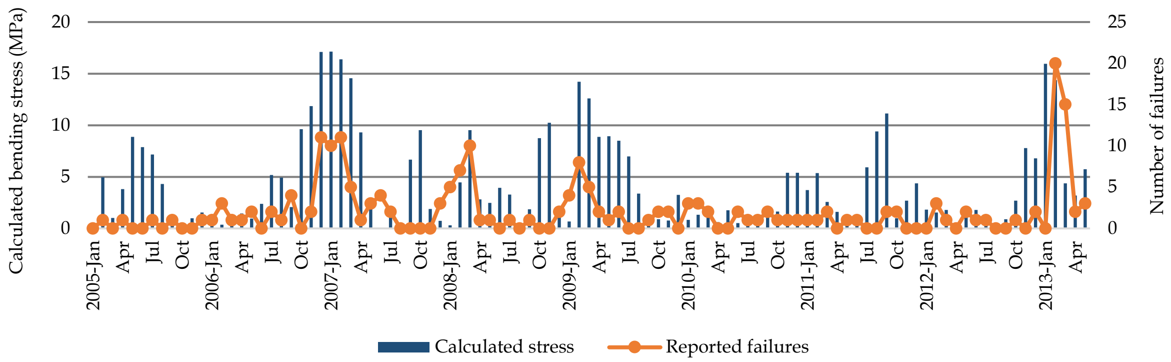

Figure 7.5. Comparison of calculated pipe stresses and reported past failures: Altona North

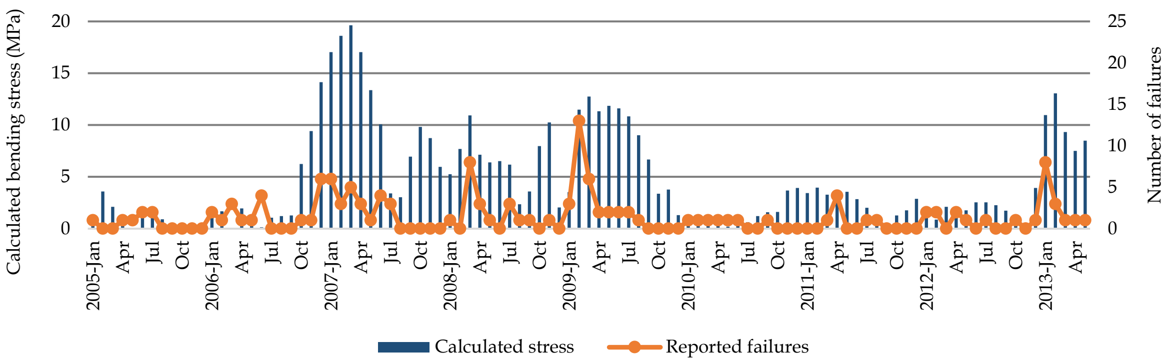

Figure 7.4. Comparison of calculated pipe stresses and reported past failures: Yarraville

The comparison of calculated pipe stresses and reported past failures in very expansive soil areas shows a consistent relationship between stresses and past failures. The figures show that higher numbers of pipe failure are reported for months with higher estimated pipe stresses. This verifies the link between calculated pipe stresses and their influence on circumferential failures.

The comparison of calculated pipe stresses and reported past failures in slightly expansive soil areas shows a relatively weak relationship between stresses and past failures, as the estimated bending stresses are very low compared to those corresponding to extremely reactive soils. In addition, the number of failures is less and more random in different months of the year. This confirms that the effect of seasonal reactive soil movements on pipe failures is negligible in less reactive soil regions, and the reported circumferential failures might have occurred with small stresses and excessive corrosion.

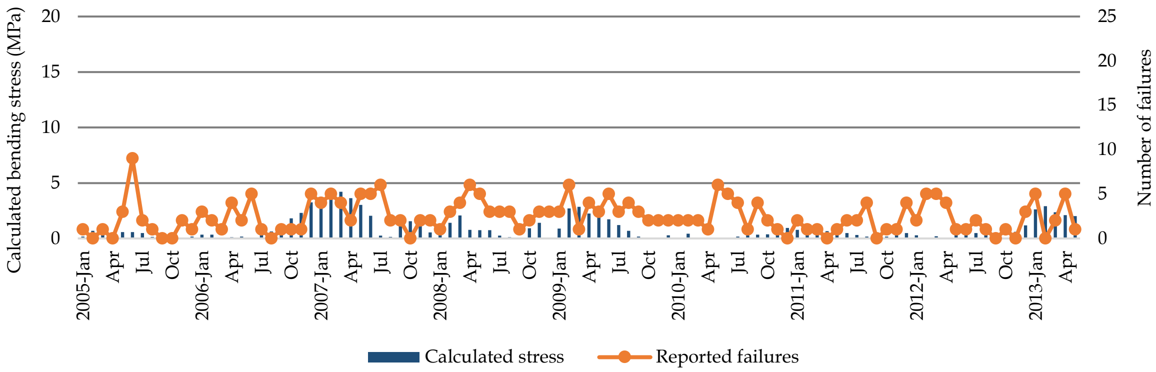

Figure 7.7. Comparison of calculated pipe stresses and reported past failures at Bayside

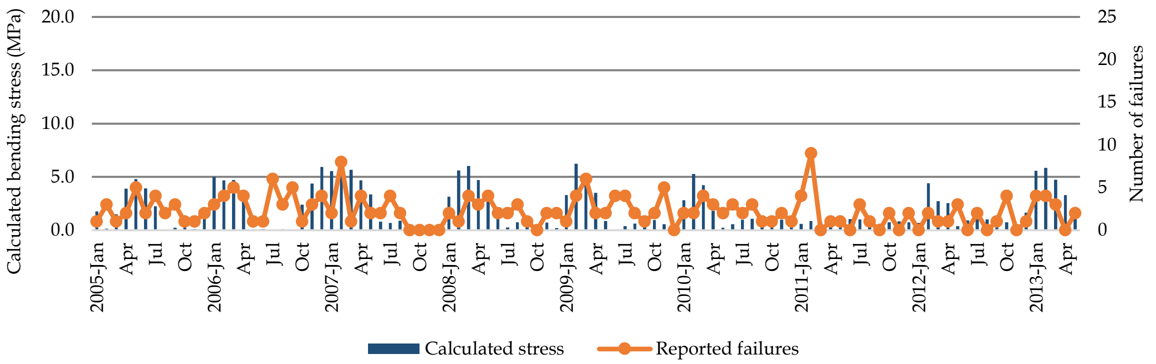

Figure 7.8. Comparison of calculated pipe stresses and reported past failures at Frankston

However, all five comparisons were made without considering the possible corrosion on the pipe wall, which is an essential factor in pipe failure, as noted in Section 2.2.5. As the calculated stresses are in the range of 0 to 20 MPa and the tensile strength of the material is about 100 MPa (see Table 7.3), the effect of pipe wall corrosion is identified as the bridging factor between stress and strength causing failure. Therefore, the incorporation of this influence is important for accurate pipe failure analysis and an appropriate methodology is explained in the following section.

7.4 Inclusion of Corrosion Defects

It was identified that the formation of corrosion patches on the pipe wall affects the thickness of the load-carrying cast iron of the pipe wall due to graphitisation (refer to Section 2.2.5). As a result, the load-carrying capacity of the pipe section becomes lower and creates weaker sections. When these weakened sections are exposed to sufficient bending stresses, the first crack is to initiate causing failure, which may, in some cases, manifest first as a leak.

This phenomenon has been treated in a different way for large-diameter pipes by considering a stress concentration factor to elevate the calculated stresses to higher values at corrosion patches (Ji et al., 2015). This method has been successfully applied to large-diameter pipes which are affected by relatively large corrosion patches, most commonly about 100mm x 100mm in size.

Since small-diameter pipes are the main priority of the present study, relatively smaller corrosion defects on narrow pipe circumferences are the focus of this analysis. Therefore, strength reduction is applied instead of stress concentration. Applying a strength reduction factor (SRF) to incorporate the effect due to cast iron wall thinning has been a common method in the pipe industry (Antaki, 2003) and this method is sometimes referred to as net section collapse (Gould, 2011). The formulation of SRF for wall thinning in circumferential direction (Antaki, 2003) can be expressed as in Equation 7.2:

$$SRF = 1 - \frac{d_{eff}}{t} \quad \text{Equation 7.2}$$

where, t is the nominal (original) wall thickness and d_{eff} is calculated as follows:

$$d_{eff} = \frac{d\left(1-\frac{1}{f}\right)}{1-\frac{d}{tf}}$$ Equation 7.3

where, d is the depth of the corrosion patch and the size factor, f, can be calculated as follows:

$$f = \sqrt{1 + 0.5\left(\frac{b}{t}\right)^2}$$ Equation 7.4

where, b is the circumferential width of the corrosion patch. The physical presence of these parameters of a corrosion patch on a pipe section is illustrated in Figure 7.9.

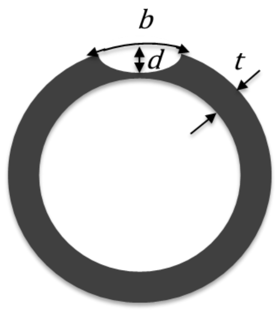

Figure 7.9. Parameters to determine corrosion defects

When these three parameters are known for a corrosion patch, the strength reduction factor (SRF) can be calculated and the reduced strength ($S_{reduced}$) of the pipe can be calculated using the following equation:

$$S_{reduced} = S_{tensile,CI} \times SRF$$ Equation 7.5

where, $S_{tensile,CI}$ is the nominal tensile strength of the pipe cohort.

An example of the calculation of strength reduction due to assumed corrosion patch configuration are shown in Figure 7.10. The strength reduction is shown as a percentage value for different patch depth-to-wall thickness (d/t) ratios. Three corrosion patches are considered with three circumferential width (b) values.

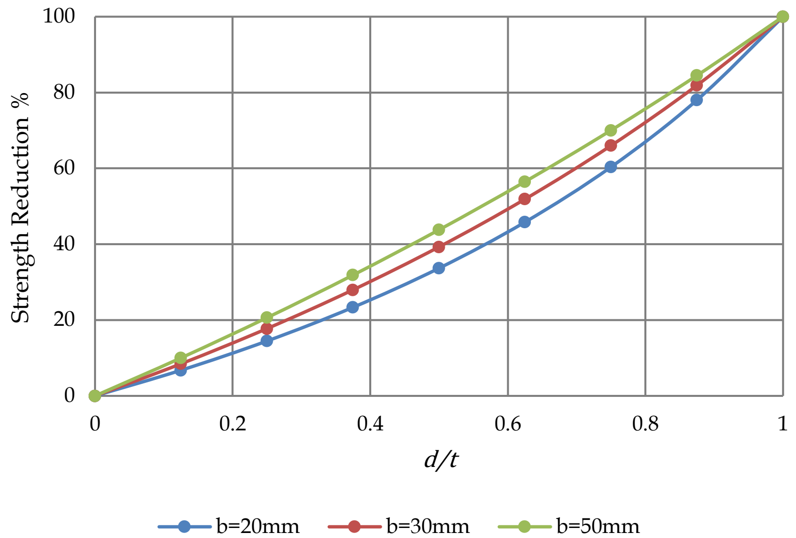

Figure 7.10. Percentage of strength reduction due to different corrosion patch configurations

The figure indicates that the strength is considerably reduced when the corrosion patch depth (represented by the d/t ratio) is increased. As illustrated in Figure 7.10, the nominal strength of the pipe material is reduced by 75% when the d/t ratio approaches 0.8. For example, for a cast iron pipe with a nominal tensile strength of 100 MPa, the reduced strength is 25 MPa ($SRF = 0.25$) when 80% ($d/t = 0.8$) of the pipe wall thickness is affected by a corrosion patch. This is a significant strength reduction compared with the estimated pipe stresses, as the maximum stresses were observed to be 20 to 25 MPa.

However, the determination of corrosion patch size is a complicated process, as corrosion damage is dependent on several parameters, including pipe age, soil type, and the air and moisture contents of the soil. The use of empirically-determined corrosion rates to estimate patch growth according to the pipe age and the surrounding environment is a common method currently used to determine corrosion patch sizes (Petersen and Melchers, 2012; Petersen et al., 2013). Long-term corrosion (steady-state corrosion) loss or the pit depth (d) of old cast iron pipes can be calculated according to the empirical model shown in Figure 7.11 as given by Equation 7.6:

$$d = C_s + r_s T_{years} \qquad \text{Equation 7.6}$$

where, C_s is the intersection of the steady-state corrosion line with the pit depth axis (in mm), r_s is the steady-state (long-term) corrosion rate (mm/year) and T_{years} is the exposure time of the pipe (in years). C_s and r_s can be determined by calibrating the model using measured pit sizes.

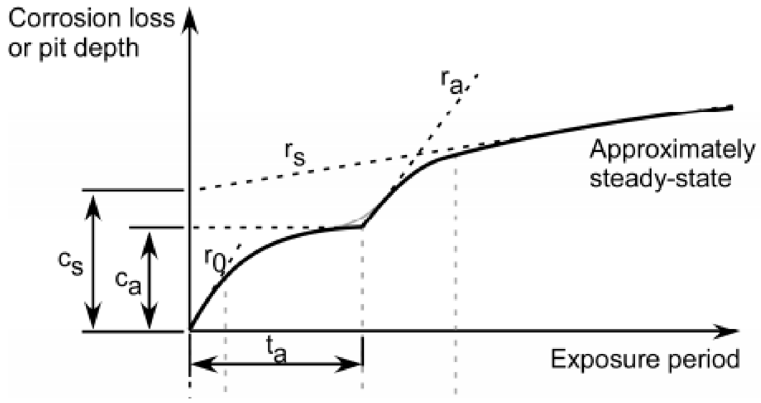

Figure 7.11. Explanation of corrosion parameters (Petersen and Melchers, 2012)

In addition to the above method, research on an innovative and robust way of determining corrosion patches at specific locations in a pipeline is currently underway at Monash University (Azoor et al., 2017). This work focuses on identifying possible corrosion hotspots on a buried pipeline due to specific corrosion- favouring soil-pipe environments along a pipe and involves the use of finite element simulations of underground corrosion. Therefore, in future, such novel techniques can be incorporated in the determination of corrosion defects for pipe failure analysis.

After the corrosion defects are incorporated, the calculated maximum pipe tensile bending stresses ($\sigma_{p,max}$) and the reduced tensile strengths ($S_{reduced}$) are combined for pipe failure analysis. A pipe failure prediction model that has been developed at Monash University using the pipe stress estimation of the present study is briefly explained in the following section.

7.5 Monash Pipe-Failure Prediction (MPP) Model

MPP is a recently introduced pipe failure prediction model that has been developed by integrating physical models with statistical records of past pipe failures as part of another PhD study at Monash University (Chik, 2018). The novelty of this model compared with other statistical pipe failure prediction models (the non-homogeneous Poisson process (NHPP) and the Bayesian simple model (BSM) (Chik, 2018)), lies in the incorporation of pipe physical conditions such as loads and the corrosion level. Currently, this model is being tested for both circumferential and longitudinal failures. This model's procedure of analysing pipe failures can be summarised as follows:

- The stress on the pipe is calculated using the available stress estimation models. For circumferential failures, the stresses are estimated using the analytical model presented in Chapter 6.
- The current corrosion level is determined using the updated corrosion parameters shown in Figure 7.11. The appropriate corrosion parameters are selected by training the model to capture past pipe failures.
- Finally the damage factors (as expressed in Equation 7.7) are calculated for each pipe based on the current or future condition of the pipe.

$$Damage\ Factor\ (DF)_{broken\ back} = \frac{Estimated\ bending\ stress\ (\sigma_{p,max})}{Reduced\ strength\ due\ to\ corrosion\ (S_{reduced})} \qquad \text{Equation 7.7}$$

As the above equation indicates, when the damage factor reaches unity, the pipe becomes unsafe as the stresses in pipe wall become closer to the reduced strength of the pipe section. In contrast, damage factors significantly less than 1 suggest that the pipe is safe, since the stresses are less than the strength. Therefore, these calculated damage factors have been identified as a convenient indicator of possible pipe failure. When the damage factors are calculated for future conditions (stresses and reduced strengths), this model can be simply utilised as a prediction tool to analyse future pipe failures.

7.6 Applicability in Global Information Systems (GISs) and Other Visual Interfaces

Visual presentation of the analytical results is one concern of the final stage of the Smart Water Fund project (Smart Water Fund, 2017a) which is the parent project of this PhD study. Therefore, the applicability of the outcomes of this work to such visualisation platforms was a main research aim of the study.

As explained in the previous section, the estimated pipe bending stresses of this work are integrated with pipe failure analyses using the Monash Pipe failure Prediction (MPP) model. In this model, the damage factors are calculated for each pipe in the network based on the physical properties as well as the past pipe failure data. Therefore, the spatial distribution of the pipe assets and past pipe failure records are important for the calculation of damage factors.

Generally, GIS software applications are efficiently used by water service providers to visualise and store the spatially-distributed pipe asset data and past failure records. Therefore, a similar visualisation platform was selected for visualising the results of pipe failure analysis. The final version of this planned GIS-based software is to be developed for the analysis and display of both statistical (such as NHPP and BSM) and physical (MPP) pipe failure predictions (Smart Water Fund, 2017a).

The outcomes of the pipe failure analyses have been developed for use in common visualisation platforms such as Google Earth. This will make the use of pipe failure prediction information open to any user. Figure 7.12 shows an example view of such failure analysis. All pipe asset information and the analysed failure data are displayed for the selected pipe in the figure. The predicted damage factor can be observed as 1, as a past pipe failure in the same pipe is marked as a pin.

Figure 7.12. Visualisation of pipe failure analyses in Google Earth (Smart Water Fund, 2017a)

This prediction tool is currently being extended for both longitudinal and circumferential pipe failure analysis, as the stress estimation models have been completed for both failure modes.

7.7 Conclusions

This chapter has presented the application of the pipe stress estimations presented in the previous chapter. The application process includes the selection of input parameters for the model, the estimation of pipe stresses for field pipes and the extension of the estimated pipe stresses to the failure prediction models. The major outcomes of this chapter can be summarised as follows:

- The main input variable of the pipe stress estimation, soil moisture data, are easily obtained from the online database of the Bureau of Meteorology which is updated daily. As data are available for the entire water supply area, this data can be used to determine the moisture changes near each pipe in the network.
- Pipe section and material properties are available for the different pipe cohorts defined by researchers at Monash University. Each pipe in the network can be assigned to a relevant cohort as the cohorts are identified based on the date of manufacture and the manufacturing process of the pipe.
- The comparison of estimated pipe stresses and past pipe failures shows a consistent relationship in extremely reactive (very expansive) soil areas. Greater numbers of past failures were observed for the months with high pipe stresses. This pattern verifies the field application of the pipe stress estimation equations.
- For pipe failure analysis, the current pipe corrosion level is incorporated in the model by introducing a strength reduction factor to the deteriorated pipe wall. Knowledge from existing and ongoing research on pipe corrosion was applied for the determination of the corrosion patch size.
- The final outcomes of this work are to be integrated with the Monash Pipe-failure Prediction (MPP) tool which provides the possibility of pipe failure by calculating a damage factor for each pipe.

The Smart Water Fund project for an innovative integrated algorithm for cost-effective management of water pipe networks is to be completed with the development of a

GIS-based software package to visualise pipe failure predictions with the incorporation of the outcomes of the current PhD project.

CHAPTER 8: CONCLUSIONS AND RECOMMENDATIONS

8.1 Conclusions

The major aim of this PhD research was to develop a convenient methodology to quantify pipe-bending stresses due to reactive soil movement. A stress estimation method was required in the form of simple analytical equations as the outcome of this research was to be integrated with pipe failure prediction models. This aim was achieved by developing pipe stress estimation equations for identified stress hotspot locations on pipelines. The finite element method was used as the main analysis tool and the results of finite element models were used to optimise the stress estimated by the equations. Field pipe failure data collected from case studies verified the theoretical predictions of pipe bending at stress hotspots.

The major conclusions of the research can be listed as follows:

- The finite element analysis method is a robust way to analyse structural deformations in reactive ground movements. In this study, the simulation of reactive ground movements and the interaction with pipes was successfully utilised in pipe deformation and pipe stress determinations. In addition, this method is a user-friendly modelling technique as a common finite element analysis commercial software package and its in-built features were used to simulate reactive soil behaviour. The calculated pipe strains were found to be in a similar range (200 to 300 $\mu\varepsilon$) to the limited field measurements.

- Bending deformations and stresses in a pipe are not critical at any location in reactive soil zones, unless appreciable differential ground movements occur. Such critical locations were identified as non-uniform pipe-soil environments, where changes in soil properties, moisture profiles and boundary restraints are present along the pipe. For example, driveways, elevated bedrock profiles, soil boundaries, water leaks and tree roots were recognised as leading to these “stress hotspots”. This knowledge provided insight into the potential locations of circumferential failures in a pipe network.

- The analysis of differential ground movements at stress hotspots revealed that differential conditions are more severe under soil drying conditions and create higher curvatures of pipe bending than those due to soil wetting conditions. This observation provides a reasonable explanation for the higher small-diameter pipe failure rates reported during summer in Melbourne than in winter. Therefore, the mechanism of differential ground or/and pipe movements at stress hotspot locations is recognised as the reason for seasonal variations of pipe failure rates.

- Observations made at field pipe failures confirm the concept of stress hotspots by proving that the circumferential failures of small-diameter pipes frequently occur at driveways and near tree roots. These two hotspots were identified as the most common stress hotspots in the pipe network analysed. These field observations also confirmed that the failure mechanisms are similar to the predicted pipe bending mechanisms in hotspots analyses.

- The theoretical and finite element analyses of pipe deformations due to reactive ground movements have been successfully combined to develop simple analytical equations to estimate pipe bending stresses. This simplified pipe stress estimation model requires soil reactive properties, soil moisture changes, pipe burial depth information and pipe material and size as the input parameters. They can be used to produce the maximum tensile stress on the pipe wall for the pipe bending configurations (hotspots) under consideration. In addition, the equations can be readily applied using any commonly available computer program such as Microsoft Excel or Matlab.

- The application of stress estimation equations in field pipe stress analyses shows that the maximum bending stresses are in the range of 20 to 30 MPa, which is significantly below the material strength. This highlights that corrosion defects are required to initiate failure. In addition, corroded pipe wall sections were a major focus of the field pipe failure case studies. Therefore, the consideration of corrosion defects is recognised as an important feature for failure analyses. In this study, the application of a strength reduction factor is suggested for corroded pipe wall sections prior to pipe failure analysis.

As the suggested analytical method of pipe stress estimation method is currently being integrated with the Monash Pipe-failure Prediction (MPP) model, it can be stated that the aims and objectives of this PhD research have been achieved.

The following recommendations are proposed to improve the use of the methods and models suggested in this work.

8.2 Recommendations

1. Gathering of more pipe deformation data: Validation of the finite element models of soil-pipe interactions and pipe deformation was a challenging task, as the available field data are limited. Instrumental measurements of reactive soil-induced pipe deformations at some more locations will provide a sufficient dataset for researchers analysing pipe deformations in reactive soils.

2. Studies of pipe joints: The scope of this study was circumferential failures in pipe barrels. Pipe deformation at or due to rigidly- or flexibly-connected pipe joints was not considered. This gap can be filled in the future by studying experimentally or

numerically pipe failure modes at joints especially in large-diameter pipes since it is expected that large-diameter pipes joints are more stressed.

3. More adequate pipe failure data collection: The current method of pipe failure data collection by water utilities was identified as ineffective for mechanistic studies of pipe failures. Important failure characteristics, such as crack location (at pipe top or bottom), crack orientation (circumferential or longitudinal), the exact location of the failure (driveway edge or middle, nature strip, near trees) and corrosion levels are missing from existing databases. Therefore, an efficient way of collecting all this information is essential for future work, and will be useful for the identification of more pipe failure hotspots.

4. Pipe corrosion information: Convenient ways of identifying pipe corrosion patches are essential for pipe failure analysis. As knowledge of the corrosion patch size is required to determine the reduction of pipe wall strength, efficient techniques are required to determine the current corrosion level of the pipe. The outcomes of ongoing pipe corrosion research at Monash University may be implemented in pipe failure analysis models to improve the current models.

These recommendations may lead to future studies and improve the current knowledge and practice of small-diameter pipe failure analysis and eventually proactive pipe asset management.

In addition, the applicability of the finite element model developed in this work to other reactive soil-structure interactions can be tested. Finite element analyses of footings and road pavement designs on reactive soils are used by researchers. Since the modelling technique proposed in this study is disengaged with user-defined sub-routines, this technique can be easily used in other related research.

REFERENCES

AHSANULLAH, M., KIBRIA, B. M. G. & SHAKIL, M. 2014. *Normal and Student´s t Distributions and Their Applications,* Paris, France, Atlantis Press.

AIS 1941. Cast Iron Pipes, Centrifugally Cast by the Super DeLavaud Process. . Port Kembla: Australian Iron & Steel.

ALONSO, E., VAUNAT, J. & GENS, A. 1999. Modelling the mechanical behaviour of expansive clays. *Engineering geology,* 54 (1)**,** pp. 173-183.

ALONSO, E. E., GENS, A. & JOSA, A. 1990. A constitutive model for partially saturated soils. *Géotechnique,* 40 (3)**,** pp. 405-430.

ANTAKI, G. A. 2003. *Piping and Pipeline Engineering: Design, Construction, Maintenance, Integrity, and Repair,* New York, USA, Marcel Dekker Inc.

ARMSTRONG, D., COTCHING, W. E. & BASTICK, C. 2001. *Assessing your soil resources for irrigation, Wise Watering Irrigation Management Course notes* [Online]. Tasmanian Department of Primary Industries, Water and Environment. Available: http://www.dpipwe.tas.gov.au/inter.nsf/WebPages/JMUY-5FJVP7?open#CourseMaterial [Accessed 19/09/2017.

ASCE 2014. Soil Parameters for Assessing Axial and Transverse Behavior of Restrained Pipelines; Part 1: Axial Behavior. *Pipelines 2014: From Underground to the Forefront of Innovation and Sustainability.* American Society of Civil Engineers Portland, Oregon. pp.

ASTM INTERNATIONAL 2003a. D 4829 – 03 Standard test method for expansion index of soils. West Conshohocken, PA.

ASTM INTERNATIONAL 2003b. Standard Test Method for Measurement of Soil Potential (Suction) Using Filter Paper. West Conshohocken, PA: ASTM International.

ASTM INTERNATIONAL 2006. D 2487-06 Standard Practice for Classification of Soils for Engineering Purposes (Unified Soil Classification System). West Conshohocken, PA.

ATKINSON, K., WHITER, J. T., SMITH, P. A. & MULHERON, M. 2002. Failure of small diameter cast iron pipes. *Urban Water,* 4 (3)**,** pp. 263-271.

AUSTRALIAN STANDARDS 2003a. AS 1289 Methods of testing soils for engineering purposes. *Method 7.1.1: Soil reactivity tests – Determination of the shrinkage index of a soil – Shrink-swell index.* Sydney, Australia: SAI Global.

AUSTRALIAN STANDARDS 2003b. AS 1289 Methods of testing soils for engineering purposes. *Method 3.6.3: Soil classification tests - Determination of the particle size distribution of a soil - Standard method of fine analysis using a hydrometer.* Sydney, Australia: SAI Global.

AUSTRALIAN STANDARDS 2005. AS 1289 Methods of testing soils for engineering purposes. *Method 2.1.1: Soil moisture content tests – Determination of the moisture content of a soil – Oven drying method (standard method).* Sydney, Australia: SAI Global.

AUSTRALIAN STANDARDS 2006. AS 1289 Methods of testing soils for engineering purposes. *Method 3.5.1: Soil classification tests - Determination of the soil particle density of a soil - Standard method.* Sydney, Australia: SAI Global.

AUSTRALIAN STANDARDS 2008. AS 1289 Methods of testing soils for engineering purposes. *Method 3.4.1: Soil classification tests - Determination of the linear shrinkage of a soil - Standard method.* Sydney, Australia: SAI Global.

AUSTRALIAN STANDARDS 2009a. AS 1289 Methods of testing soils for engineering purposes. *Method 3.2.1: Soil classification tests - Determination of the plastic limit of a soil - Standard method.* Sydney, Australia: SAI Global.

AUSTRALIAN STANDARDS 2009b. AS 1289 Methods of testing soils for engineering purposes. *Method 3.3.1: Soil classification tests - Calculation of the plasticity index of a soil.* Sydney, Australia: SAI Global.

AUSTRALIAN STANDARDS 2009c. AS 1289 Methods of testing soils for engineering purposes. *Method 3.1.1: Soil classification tests - Determination of the liquid limit of a soil - Four point Casagrande method.* Sydney, Australia: SAI Global.

AUSTRALIAN STANDARDS 2011. AS 2870 Residential slabs and footings. Sydney, N.S.W.: SAI Global Limited

AUSTRALIAN STANDARDS 2015. AS 1289 Methods of testing soils for engineering purposes. *Method 1.3.1: Sampling and preparation of soils – Undisturbed samples – Standard method.* Sydney, Australia: SAI Global.

AUTODESK INC. 2014. Autodesk AutoCAD Civil 3D 2015

AWWA C101–67 1977. American national standard for thickness design of cast-iron pipe. . Denver, CO: American Water Works Association.

AZOOR, R. M., DEO, R. N., BIRBILIS, N. & KODIKARA, J. K. 2017. Modelling the Influence of Differential Aeration in Underground Corrosion. Proceedings of the 2017 COMSOL Conference, Boston, USA.

BARSHAD, I. 1955. Adsorptive and swelling properties of clay-water system. *Clays Clay Technol. Bull,* 169**,** pp. 225-238.

BELL, F. G. & CULSHAW, M. G. 2001. Problem Soils: A review from a British perspective. *In:* JEFFERSON, I., MURRAY, E. J., FARAGHER, E. & FLEMING, P. R., eds. Problematic soils symposium, Nottingham pp. 1-35.

BEST, M., PRYOR, M., CLARK, D., ROONEY, G., ESSERY, R., MÉNARD, C., EDWARDS, J., HENDRY, M., PORSON, A. & GEDNEY, N. 2011. The Joint UK Land Environment Simulator (JULES), model description–Part 1: energy and water fluxes. *Geoscientific Model Development,* 4 (3)**,** pp. 677-699.

BISHOP, A. W. 1959. The principle of effective stress. *Teknisk Ukeblad,* 106 (39)**,** pp. 859–863.

BISHOP, A. W. & BLIGHT, G. E. 1963. Someaspectsofeffectivestress insaturated and unsaturated soil. *Geotechnique,* 13 (3)**,** pp. 177-197.

BUREAU OF INDIAN STANDARDS 1977. IS 2720 Method of Test for Soils. *Part 40 :Determination of free swell index of soils* New Delhi: BIS.

BUREAU OF METEOROLOGY. 2017a. Available: http://www.bom.gov.au/water/nwa/2014/melbourne/contextual/physicalinformation.shtml [Accessed 10-12-2017.

BUREAU OF METEOROLOGY. 2017b. *Australian Landscape Water Balance* [Online]. Available: http://www.bom.gov.au/climate/data/ [Accessed 20/07/2017.

BUREAU OF METEOROLOGY. 2017c. *Climate Data Online* [Online]. Available: http://www.bom.gov.au/climate/data/ [Accessed 04/08/2017.

CAMERON, D., JAKSA, M. B., POTTER, W. & O'MALLEY, A. 2006. The influence of trees on expansive soils in southern Australia. *In:* AL-RAWAS, A. A. & GOOSEN, M. F. A. (eds.) *Expansive soils: recent advances in characterization and treatment, .* Taylor & Francis London, UK. pp. 295-314

CAMERON, D. A. & WALSH, P. F. 1984. Damage to buildings on clay soils. Melbourne, Australia: Australian Council of National Trusts.

CAST IRON PIPE RESEARCH ASSOCIATION 1952. *Handbook of Cast Iron Pipe for Water, Gas, Sewage and Industrial Services.,* Chicago, Illinois.

CHAN, D. 2008. *Performance of water and gas pipes buried in reactive soil.* MSc thesis, Monash University.

CHAN, D. 2013. *Study of Pipe-Soil-Climate Interaction of Buried Water and Gas Pipes.* PhD thesis, Monash University.

CHAN, D., GALLAGE, C. P. K., RAJEEV, P. & KODIKARA, J. 2015. Field performance of in-service cast iron water reticulation pipe buried in reactive clay. *Canadian Geotechnical Journal,* 52 (11)**,** pp. 1861-1873.

CHAN, D., KODIKARA, J., GOULD, S., RANJITH, P., CHOI, X. & DAVIS, P. 2007. Data analysis and laboratory investigation of the behaviour of pipes buried in reactive clay. *In:* AMERATUNGA, J., TAYLOR, B. & PATTEN, M., eds. Common Ground - Proceedings of the 10th Australia New Zealand Conference on Geomechanics 21-24 October 2007 Queensland, Australia. Carillon Conf. Management Pty Ltd for the AGS, Australia,pp. 206 - 211.

CHAN, D., SHANNON, B. & KODIKARA, J. 2016. Relative importance of external factors on pipe performance. Ozwater'16, 10-12 May 2016 Melbourne, Australia.

CHEN, F. 1973. The basic physical property of expansive soils. *Proc. 3rd ICES, Haifa***,** pp. 17-25.

CHIK, L. 2018. *Water Main Failure Prediction by Integration of Statistical Data and Physical Processes (in preparation)* PhD thesis, Monash University.

CITY OF MELBOURNE. 2017. Available: http://www.melbourne.vic.gov.au/about-melbourne/melbourne-heritage/history/Pages/history.aspx [Accessed 10-12-2017.

CLARK, D., MERCADO, L., SITCH, S., JONES, C., GEDNEY, N., BEST, M., PRYOR, M., ROONEY, G., ESSERY, R. & BLYTH, E. 2011. The Joint UK Land Environment Simulator (JULES), model description-Part 2: carbon fluxes and vegetation dynamics. *Geoscientific Model Development,* 4 (3)**,** pp. 701-722.

COLE, I. S. & MARNEY, D. 2012. The science of pipe corrosion: A review of the literature on the corrosion of ferrous metals in soils. *Corrosion Science,* 56**,** pp. 5-16.

COLIN, R. & BAKER, T. 1991. Application of fracture mechanics to the failure of buried cast iron mains. *Contractor report.* United Kingdom: Ground Engineering Division, Structures Group, Transport and Road Research Laboratory.

COSTELLO, S. B., CHAPMAN, D. N., ROGERS, C. D. F. & METJE, N. 2007. Underground asset location and condition assessment technologies. *Tunnelling and Underground Space Technology,* 22 (5)**,** pp. 524-542.

COVAR, A. P. & LYTTON, R. L. 2001. Estimating soil swelling behavior using soil classification properties. *Expansive Clay Soils and Vegetative Influence on Shallow Foundations.* pp. 44-63

CROMBIE, D., TIPPETT, J. & HILL, T. 1988. Dawn Water Potential and Root Depth of Trees and Understorey Species in Southwestern Australia. *Australian Journal of Botany,* 36 (6), pp. 621-631.
CROSSLAND, B. & DEARDEN, W. H. 1958. The Plastic Flow and Fracture of a 'Brittle' Material (Grey Cast Iron) with Particular Reference to the Effect of Fluid Pressure. *Proceedings of the Institution of Mechanical Engineers,* 172 (1), pp. 805-820.
DAHLHAUS, P. & O'ROURKE, M. 1992. The Newer Volcanics. *In:* PECK, W. A., NEILSON, J. L., OLDS, R. J. & SEDDON, K. D., eds. Engineering Geology of Melbourne: Proceedings of the Seminar on Engineering Geology of Melbourne, Editors pp. 205-212.
DASSAULT SYSTÈMES 2014. Abaqus 6.14 Online Documentation.
DAVIS, J. L. & ANNAN, A. P. 1989. Ground-penetrating radar for high-resolution mapping of soil and rock stratigraphy1. *Geophysical Prospecting,* 37 (5), pp. 531-551.
DIF, A. & BLUEMEL, W. 1991. Expansive soils under cyclic drying and wetting. *Geotechnical Testing Journal,* 14 (1), pp. 96-102.
FITYUS, S., WELLS, T. & HUANG, W. 2011. Water Content Measurement in Expansive Soils Using the Neutron Probe. *Geotechnical Testing Journal,* 34 (3), pp. 255-264.
FITYUS, S. G. 1999. A soil moisture based method of estimating ys. *In:* VITHARANA, N. D. & COLMAN, R., eds. 8th Australia New Zealand Conference on Geomechanics: Consolidating Knowledge, Barton, ACT. Australian Geomechanics Society,pp. 809-815.
FITYUS, S. G., CAMERON, D. A. & WALSH, P. F. 2005. The shrink swell test. *Geotechnical Testing Journal,* 28 (1), pp. 92-101.
FREDLUND, D. & MORGENSTERN, N. 1976. Constitutive relations for volume change in unsaturated soils. *Canadian Geotechnical Journal,* 13 (3), pp. 261-276.
FREDLUND, D. G. & VU, H. Q. 2003. Numerical Modelling of Swelling and Shrinking soils around slabs-on-ground. Post-Tensioning Institute Annual Technical Conference, Huntington Beach, CA, USA.
GALLAGE, C. P. K., KODIKARA, J. & CHAN, D. 2011. Response of a plastic pipe buried in expansive clay. *Proceedings of the ICE-Geotechnical Engineering,* 165 (1), pp. 45-57.
GENS, A. & ALONSO, E. E. 1992. A framework for the behaviour of unsaturated expansive clays. *Canadian Geotechnical Journal,* 29 (6), pp. 1013-1032.
GEOLOGICAL SURVEY OF VICTORIA. 1974. *Melbourne. 1 mile to 1 inch geological map.* Department of Mines, Victoria.
GNIEL, J. 2017. *RE: Basalt rock depths.* Personal Communication to KODIKARA, J. on 18-09-2017. Golder Associates Pty Ltd.
GOOGLE MAPS. 2017. *Map of Altona North* [Online]. Available: https://www.google.com.au/maps/place/Altona+North+VIC+3025/@-37.8383358,144.7910979,14683m/data=!3m1!1e3!4m5!3m4!1s0x6ad66106e65c1f11:0x5045675218cd910!8m2!3d-37.841!4d144.849 [Accessed 05-09-2017.
GOULD, S. 2011. *A Study of the Failure of Buried Reticulation Pipes in Reactive Soils.* PhD thesis, Monash University.

GOULD, S., BOULAIRE, F., BURN, S., ZHAO, X.-L. & KODIKARA, J. 2011a. Seasonal factors influencing the failure of buried water reticulation pipes. *Water Science and Technology,* 63 (11), pp. 2692-2699.

GOULD, S. & KODIKARA, J. 2008. Exploratory Statistical Analysis of Water Reticulation Main Failures (Melbourne, Australia). Monash University.

GOULD, S. J. F., KODIKARA, J., RAJEEV, P., ZHAO, X.-L. & BURN, S. 2011b. A void ratio – water content – net stress model for environmentally stabilized expansive soils. *Canadian Geotechnical Journal,* 48 (6), pp. 867-877.

GRANT, K. 1972. *Terrain classication for engineering purposes of the Melbourne area, Victoria,* Melbourne, Victoria, Australia., CSIRO.

GRIM, R. E. 1953. *Clay mineralogy*, Mcgraw-Hill Book Company, Inc; New York; Toronto; London.

HABIBIAN, A. 1994. Effect of temperature changes on water-main breaks. *Journal of transportation engineering,* 120 (2), pp. 312-321.

HAFEEZ, F., FROST, A., VAZE, J., DUTTA, D., SMITH, A. & ELMAHDI, A. 2015. A new integrated continental hydrological simulation system. *Water: Journal of the Australian Water Association,* 42 (3), pp. 75-82.

HAMILTON, J. J. 1969. Effects of natural and man-made environments on the performance of shallow foandations. *Canadian Geotechnical Journal,* 6 (1), pp. 65-80.

HOLLAND, J. & WALSH, P. 1980. Behaviour and design of residential slabs on the expansive clays of Melbourne. Advances in concrete slab technology: proceedings of the International Conference on Concrete Slabs, 3–6 April 1979 Dundee University, UK. Pergamon,pp. 344–355.

HOLLAND, J. E. 1978. The behaviour and design of lightly loaded foundations in the Quaternary basaltic clays. Seminar on Basalt and Basaltic Soils, October 1978 Australian Geomechanic Society, Victoria Group, Melbourne.

HOLTZ, W. G. & GIBBS, H. J. 1956. Engineering properties of expansive clays. *Transactions of the American Society of Civil Engineers,* 121 (1), pp. 641-663.

HUDAK, P., SADLER, B. & HUNTER, B. 1998. Analyzing underground water-pipe breaks in residual soils. *Water Engineering and Management,* 145 (12), pp. 15-20.

IBRAHIMI, F. 2005. Seasonal variations in water main breaks due to climate variability and ground movement. Ozwater'05, 8-12 May 2005 Brisbane, Australia

JAMES, K. R. & HALLAM, C. 2013. Stability of urban trees in high winds. *Arboricultural Journal,* 35 (1), pp. 28-35.

JENNINGS, J. & BURLAND, J. 1962. Limitations to the use of effective stresses in partly saturated soils. *Géotechnique,* 12 (2), pp. 125-144.

JI, J., ROBERT, D. J., ZHANG, C., ZHANG, D. & KODIKARA, J. 2017. Probabilistic physical modelling of corroded cast iron pipes for lifetime prediction. *Structural Safety,* 64, pp. 62-75.

JI, J., ZHANG, C., KODIKARA, J. & YANG, S.-Q. 2015. Prediction of stress concentration factor of corrosion pits on buried pipes by least squares support vector machine. *Engineering Failure Analysis,* 55, pp. 131-138.

JIANG, R., ROBERT, D., HUTCHINSON, C. R., ZHAO, X. L. & KODIKARA, J. 2017a. Leak-before-break in cast iron mains: a failure analysis of a catastrophic pipe burst on Harris Street, Sydney. *Water Practice and Technology,* 12 (2), pp. 487-494.

JIANG, R., SHANNON, B., DEO, R. N., RATHNAYAKA, S., HUTCHINSON, C. R., ZHAO, X.-L. & KODIKARA, J. 2017b. Classification of major cohorts of Australian pressurised cast iron water mains for pipe renewal. *Australasian Journal of Water Resources,* Nov 2017**,** pp. 1-12.

JONES, H. S. 1941. The development of cement lining of water mains. *Journal (American Water Works Association),* 33 (10)**,** pp. 1695-1699.

JONES, L. D. & JEFFERSON, I. 2012. *Expansive soils*, ICE Publishing.

KARUNARATHNE, A., SIVANER, S., GAD, E., DISFANI, M., RAJEEV, P., WILSON, J. & LI, J. 2014. Field and laboratory investigation of an expansive soil site in Melbourne. *Australian Geomechanics Journal,* 49 (2)**,** pp. 85-93.

KARUNARATHNE, A. N. 2016. *Investigation of Expansive Soil for Design of Light Residential Footings in Melbourne.* PhD thesis, Swinburne University of Technology.

KETTLER, A. & GOULTER, I. 1985. An analysis of pipe breakage in urban water distribution networks. *Canadian Journal of Civil Engineering,* 12 (2)**,** pp. 286-293.

KHALILI, N. & KHABBAZ, M. 2002. A unique relationship for chi for the determination of the shear strength of unsaturated soils. *Geotechnique,* 52 (1)**,** pp. 76-77.

KIM, S. B., ZYL, J. J. V., JOHNSON, J. T., MOGHADDAM, M., TSANG, L., COLLIANDER, A., DUNBAR, R. S., JACKSON, T. J., JARUWATANADILOK, S., WEST, R., BERG, A., CALDWELL, T., COSH, M. H., GOODRICH, D. C., LIVINGSTON, S., LÓPEZ-BAEZA, E., ROWLANDSON, T., THIBEAULT, M., WALKER, J. P., ENTEKHABI, D., NJOKU, E. G., O'NEILL, P. E. & YUEH, S. H. 2017. Surface Soil Moisture Retrieval Using the L-Band Synthetic Aperture Radar Onboard the Soil Moisture Active–Passive Satellite and Evaluation at Core Validation Sites. *IEEE Transactions on Geoscience and Remote Sensing,* 55 (4)**,** pp. 1897-1914.

KLAR, A., VORSTER, T. E. B., SOGA, K. & MAIR, R. J. 2005. Soil—pipe interaction due to tunnelling: comparison between Winkler and elastic continuum solutions. *Géotechnique,* 55 (6)**,** pp. 461-466.

KLEINER, Y. & RAJANI, B. 2002. Forecasting variations and trends in water-main breaks. *Journal of Infrastructure Systems,* 8 (4)**,** pp. 122-131.

KODIKARA, J. 2012. New framework for volumetric constitutive behaviour of compacted unsaturated soils. *Canadian Geotechnical Journal,* 49 (11)**,** pp. 1227-1243.

KODIKARA, J., RAJEEV, P., CHAN, D. & GALLAGE, C. 2013. Soil moisture monitoring at the field scale using neutron probe. *Canadian Geotechnical Journal,* 51 (3)**,** pp. 332-345.

KODIKARA, J., RAJEEV, P., ROBERT, D. & ZEMAN, P. 2012. Critical review of historical information on large diameter pipe failure, Report No. CPP-A1-R1, ACAPFP project-Activity1. Melbourne, Australia.

LEEDOM, L. M. 1946. Graphitic Corrosion of Cast Iron. *Journal (American Water Works Association),* 38 (12)**,** pp. 1392-1397.

LI, J., CAMERON, D. A. & MILLS, K. G. 1996. Numerical Modelling of Covers and Slabs Subject to Seasonal Surface Suction Variations. *In:* JAKSA, M., KAGGWA, W. & CAMERON, D., eds. 7th Australia New Zealand Conference on

Geomechanics: Geomechanics in a Changing World, Barton, ACT. Institution of Engineers, Australia,pp. 424-429.
LI, J. & GUO, L. 2017. Field Investigation and Numerical Analysis of Residential Building Damaged by Expansive Soil Movement Caused by Tree Root Drying. *Journal of Performance of Constructed Facilities,* 31 (1), pp. 1-10 (ID D4016003).
LI, J. & REN, G. 2010. Monitoring in situ soil moisture variations of expansive clay using neutron probes. *In:* LIANG, R., ZHANG, F. & YANG, K., eds. Proceedings of Geoshanghai 2010: Deep Foundations and Geotechnical In Situ Testing, 3-5 June 2010 China. The American Society of Civil Engineers,pp. 341-346.
LI, J., ZHOU, Y., GUO, L. & TOKHI, H. 2014. The establishment of a field site for reactive soil and tree monitoring in Melbourne. *Australian Geomechanics Journal,* 49 (2), pp. 63-72.
LIU, X. & BUZZI, O. 2014. Use of Hand-Spray Plaster as a Coating for Soil Bulk Volume Measurement. *Geotechnical Testing Journal,* 37 (3), pp. 522-528.
LORET, B. & KHALILI, N. 2002. An effective stress elastic–plastic model for unsaturated porous media. *Mechanics of Materials,* 34 (2), pp. 97-116.
MAKAR, J., DESNOYERS, R. & MCDONALD, S. 2001. Failure modes and mechanisms in gray cast iron pipe. Underground Infrastructure Research, 10-13 June 2001 Ontario.
MAKAR, J. M. 2000. A preliminary analysis of failures in grey cast iron water pipes. *Engineering Failure Analysis,* 7 (1), pp. 43-53.
MAKAR, J. M. & RAJANI, B. 2000. Gray Cast-Iron Water Pipe Metallurgy. *Journal of Materials in Civil Engineering,* 12 (3), pp. 245-253.
MELBOURNE WATER. 2017. Available: https://www.melbournewater.com.au/ [Accessed 10-12-2017.
MIRO, J. V., RAJALINGAM, J., VIDAL-CALLEJA, T., BRUIJN, F. D., WOOD, R., VITANAGE, D., ULAPANE, N., WIJERATHNA, B. & SU, D. 2013. A live test-bed for the advancement of condition assessment and failure prediction research on critical pipes. Strategic Asset Management of Water and Wastewater Infrastructure: Leading Edge Strategic Asset Management (LESAM13), 9 – 12 September 2013 Sydney, Australia.
MOHEBBI, H. & LI, C. Q. 2011. Experimental Investigation on Corrosion of Cast Iron Pipes. *International Journal of Corrosion,* 2011 (2011), pp. 1-17 (ID 506501).
MORRIS, P. H., GRAHAM, J. & WILLIAMS, D. J. 1992. Cracking in drying soils. *Canadian Geotechnical Journal,* 29 (2), pp. 263-277.
MOSER, A. P. & FOLKMAN, S. L. 2001. *Buried pipe design*, McGraw-Hill New York.
MRWA 2013. Specification 04-03.2: Backfill Specification. Melbourne, Australia: Melbourne Retail Water Agencies.
NELSON, J. & MILLER, D. J. 1997. *Expansive soils: problems and practice in foundation and pavement engineering*, John Wiley & Sons.
NELSON, J. D., CHAO, K. C. G., OVERTON, D. D. & NELSON, E. J. 2015. Nature of Expansive Soils. *Foundation Engineering for Expansive Soils.* John Wiley & Sons, Inc Hoboken, NJ, USA. pp. 9-58

PECK, W. A., NEILSON, J. L., OLDS, R. J. & SEDDON, K. D. 1992. *Engineering Geology of Melbourne : Proceedings of the Seminar on Engineering Geology of Melbourne, Victoria, Australia,* Rotterdam, Netherlands, A A Balkema Publishers.

PETERSEN, R. B., DAFTER, M. & MELCHERS, R. E. 2013. Long-term corrosion of buried cast iron water mains: field data collection and model calibration. Strategic Asset Management of Water and Wastewater Infrastructure: Leading Edge Strategic Asset Management (LESAM13), 9 – 12 September 2013 Sydney, Australia. International Water Association (IWA)

PETERSEN, R. B. & MELCHERS, R. E. 2012. Long-term corrosion of cast iron cement lined pipes. Annual Conference of the Australasian Corrosion Association 11 – 14 November 2012 Melbourne, Australia.

RAJANI, B. 2000. *Investigation of grey cast iron water mains to develop a methodology for estimating service life,* Denver, CO, AWWA Research Foundation and American Water Works Association.

RAJANI, B. & KLEINER, Y. 2001. Comprehensive review of structural deterioration of water mains: physically based models. *Urban Water,* 3 (3), pp. 151-164.

RAJANI, B. & KLEINER, Y. 2004. Non-destructive inspection techniques to determine structural distress indicators in water mains. *Evaluation and Control of Water Loss in Urban Water Networks*, pp. 21-25.

RAJANI, B., KLEINER, Y. & SINK, J.-E. 2012. Exploration of the relationship between water main breaks and temperature covariates. *Urban Water Journal,* 9 (2), pp. 67-84.

RAJANI, B. & TESFAMARIAM, S. 2004. Uncoupled axial, flexural, and circumferential pipe soil interaction analyses of partially supported jointed water mains. *Canadian geotechnical journal,* 41 (6), pp. 997-1010.

RAJANI, B. & ZHAN, C. 1996. On the estimation of frost loads. *Canadian geotechnical journal,* 33 (4), pp. 629-641.

RAJANI, B., ZHAN, C. & KURAOKA, S. 1996. Pipe soil interaction analysis of jointed water mains. *Canadian Geotechnical Journal,* 33 (3), pp. 393-404.

RAJEEV, P., CHAN, D. & KODIKARA, J. 2012. Ground–atmosphere interaction modelling for long-term prediction of soil moisture and temperature. *Canadian Geotechnical Journal,* 49 (9), pp. 1059-1073.

RAJEEV, P. & KODIKARA, J. 2011. Numerical analysis of an experimental pipe buried in swelling soil. *Computers and Geotechnics,* 38 (7), pp. 897-904.

RAJEEV, P., KODIKARA, J., ROBERT, D., ZEMAN, P. & RAJANI, B. 2014. Factors contributing to large diameter water pipe failure. *Water Asset Management International,* 10 (3), pp. 9-14.

RAO, B. H., VENKATARAMANA, K. & SINGH, D. N. 2011. Studies on the determination of swelling properties of soils from suction measurements. *Canadian Geotechnical Journal,* 48 (3), pp. 375-387.

RATHNAYAKA, S., KELLER, R., KODIKARA, J. & CHIK, L. 2016. Numerical Simulation of Pressure Transients in Water Supply Networks as Applicable to Critical Water Pipe Asset Management. *Journal of Water Resources Planning and Management,* 142 (6), pp. 1-13 (ID 04016006).

RATHNAYAKA, S., SHANNON, B., ZHANG, C. & KODIKARA, J. 2017. Introduction of the leak-before-break (LBB) concept for cast iron water pipes on the basis of laboratory experiments. *Urban Water Journal,* 14 (8), pp. 820-828.

RATHNAYAKA, S. U. P. 2016. *A study of water pressure influence on failure of large diameter water pipelines.* PhD thesis, Monash University.

RIVETTE, C. & MOORE, D. 2015. *RE: Soil cover and underneath bedrock information of Melbourne pipes.* Personal Communication to WEERASINGHE, D. & CHAN, D. on 15-07-2015. City West Water.

ROBERT, D., SOGA, K. & LALOUI, L. 2013. Soil–Pipeline Interaction in Unsaturated Soils. *Mechanics of Unsaturated Geomaterials.* John Wiley & Sons, Inc. pp. 303-325

ROBERT, D. J., JIANG, R., RAJEEV, P. & KODIKARA, J. 2016a. Contribution of cement mortar lining to structural capacity of cast iron water mains. *ACI Materials Journal,* 113 (3), pp. 295-306.

ROBERT, D. J., RAJEEV, P., KODIKARA, J. & RAJANI, B. 2016b. Equation to predict maximum pipe stress incorporating internal and external loadings on buried pipes. *Canadian Geotechnical Journal,* 53 (8), pp. 1315-1331.

SATTLER, P. & FREDLUND, D. 1991. Numerical modelling of vertical ground movements in expansive, soils. *Canadian Geotechnical Journal,* 28 (2), pp. 189-199.

SCHMUGGE, T., JACKSON, T. & MCKIM, H. 1980. Survey of methods for soil moisture determination. *Water Resources Research,* 16 (6), pp. 961-979.

SCHOFIELD, A. & WROTH, P. 1968. *Critical state soil mechanics,* London, McGraw-Hill

SCOTT, R. J. 1990. Water Main Renewal Study: Reticulation Water Mains 1857-1990. Melbourne Water.

SEICA, M. V. & PACKER, J. A. 2004. Mechanical Properties and Strength of Aged Cast Iron Water Pipes. *Journal of Materials in Civil Engineering,* 16 (1), pp. 69-77.

SHAMS, M. A., SHAHIN, M. A. & ISMAIL, M. A. 2017. Analysis and Modelling of Stiffened Slab Foundation on Expansive Soils. *In:* SHEHATA, H. & RASHED, Y. (eds.) *Numerical Analysis of Nonlinear Coupled Problems: Proceedings of the 1st GeoMEast International Congress and Exhibition, Egypt 2017 on Sustainable Civil Infrastructures.* Springer International Publishing Cham. pp. 250-261

SHANNON, B., JIANG, R., JI, J., CHAN, D. & KODIKARA, J. 2016a. Investigation of cohort properties for Australian cast iron water mains. IWA World Water Congress & Exhibition 2016, 9–14 Oct., Brisbane, Australia.:

SHANNON, B., RATHNAYAKA, S., ZHANG, C. & KODIKARA, J. 2016b. Lessons learnt on pipe failure mechanisms from observation of exhumed cast iron pipes. Ozwater'16, 10-12 May 2016 Melbourne, Australia.

SKEMPTON, A. 1953. The colloidal activity of clays. Proceedings of 3rd International Conference of Soil Mechanics and Foundation Engineering, 16th - 27th August 1953 Zurich.

SMART WATER FUND 2015. An innovative integrated algorithm for cost-effective management of water pipe networks: Report for Milestone 4. Monash University.

SMART WATER FUND 2017a. An innovative integrated algorithm for cost-effective management of water pipe networks: Final Report for Milestone 10. Monash University.

SMART WATER FUND. 2017b. *An Innovative Integrated Algorithms for Cost-Effective Management of Water Pipe Networks* [Online]. Melbourne Australia. Available: https://www.waterportal.com.au/swf/projects/item/155-an-innovative-integrated-algorithms-for-cost-effective-management-of-water-pipe-networks [Accessed 7/12/2017.
SMITH, A. B., HAFEEZ, M., RAHMAN, J., BARON-HAY, S. & SHIPMAN, D. 2015. A new web based water information service leveraging the Australian Water Resources Assessment Modelling System. 36th Hydrology and Water Resources Symposium: The art and science of water. Engineers Australia,pp. 1276.
SNETHEN, D. R., JOHNSON, L. D. & PATRICK, D. M. 1977. An evaluation of expedient methodology for identification of potentially expansive soils. United States: Department of Transportation, Federal Highway Administration.
SOUTH EAST WATER. 2015. *Tree roots: a growing problem* [Online]. Available: http://southeastwater.com.au/SiteCollectionDocuments/Residential/HowTo/TreeRootsAGrowingProblem.pdf [Accessed 27/09/2017.
SRIDHARAN, A. & PRAKASH, K. 2000. Classification procedures for expansive soils. *Proceedings of the Institution of Civil Engineers-Geotechnical Engineering,* 143 (4), pp. 235-240.
SRITHAR, S. 2014. Engineering design and earthworks aspects related to basaltic clays in Victoria. *Australian Geomechanics,* 49 (2), pp. 1-12.
TERZAGHI, K. V. 1931. The influence of elasticity and permeability on the swelling of two-phase systems. *Colloid chemistry,* 3, pp. 65-88.
TERZAGHI, K. V. 1936. The shearing resistance of saturated soils and the angle between the planes of shear. Proceedings of the 1st international conference on soil mechanics and foundation engineering. Harvard University Press Cambridge, MA,pp. 54-56.
THOMPSON, R. W. & MCKEEN, R. G. 1995. Heave Prediction Using Soil Suction: A Case Study. *In:* WRAY, W. K. & HOUSTON, S. L., eds. Soil Suction Applications in Geotechnica Engineering Practice: Proceedings of a Session Held in Conjunction with the ASCE Convention, 22–27 October 1995 San Diego, Calif.: American Society of Civil Engineers,pp. 1-13.
TRIPATHY, S., RAO, K. S. & FREDLUND, D. 2002. Water content-void ratio swell-shrink paths of compacted expansive soils. *Canadian geotechnical journal,* 39 (4), pp. 938-959.
VINEY, N., VAZE, J., CROSBIE, R., WANG, B., DAWES, W. & FROST, A. 2014. AWRA-L v4. 5: technical description of model algorithms and inputs. CSIRO, Australia.
VLOERBERGH, I. & BLOKKER, E. 2009. Failure data analysis-a Dutch case study. *In:* ALEGRE, H. & CEU ALMEIDA, M. D. (eds.) *Strategic Asset Management of Water Supply and Wastewater Infrastructures.* IWA Publishing London, UK. pp. 433 - 450
WIGGIN, T. H., ENGER, M. L. & SCHLICK, W. J. 1939. A Proposed New Method for Determining Barrel Thicknesses of Cast Iron Pipe. *Journal (American Water Works Association),* 31 (5), pp. 841-908.

WIJESOORIYA, S. D. & KODIKARA, J. K. 2012. Experimental study of shrinkage and swelling behaviour of a compacted expansive clay soil. *In:* NARSILIO, G., ARULRAJAH, A. & KODIKARA , J., eds. Proceedings of 11th Australia New Zealand Conference on Geomechanics ANZ 2012 Australia. Australian Geomechanics Society,pp. 25 - 30.

WOLS, B. A. & THIENEN, P. V. 2014. Modelling the effect of climate change induced soil settling on drinking water distribution pipes. *Computers and Geotechnics,* 55, pp. 240-247.

YAMAMOTO, K., MIZOGUTI, S., YOSHIMITSU, K. & KAWASAKI, J. 1983. Relation between Graphitic Corrosion and Strength-degradation of Cast Iron Pipe. *CORROSION ENGINEERING,* 32 (3), pp. 157-162.

YEE, M. S., WALKER, J. P., MONERRIS, A., RÜDIGER, C. & JACKSON, T. J. 2016. On the identification of representative in situ soil moisture monitoring stations for the validation of SMAP soil moisture products in Australia. *Journal of Hydrology,* 537, pp. 367-381.

ZHANG, C., JI, J., KODIKARA, J. & RAJANI, B. 2017. Hyperbolic constitutive model to study cast iron pipes in 3-D nonlinear finite element analyses. *Engineering Failure Analysis,* 75, pp. 26-36.

APPENDIX A

LONGITUDINAL SECTIONS OF ROCK SLOPE ANALYSES

Section 1

Location: Marsh Street, Altona North

Pipe: 180mm diameter, polyethylene (PE), reticulation main

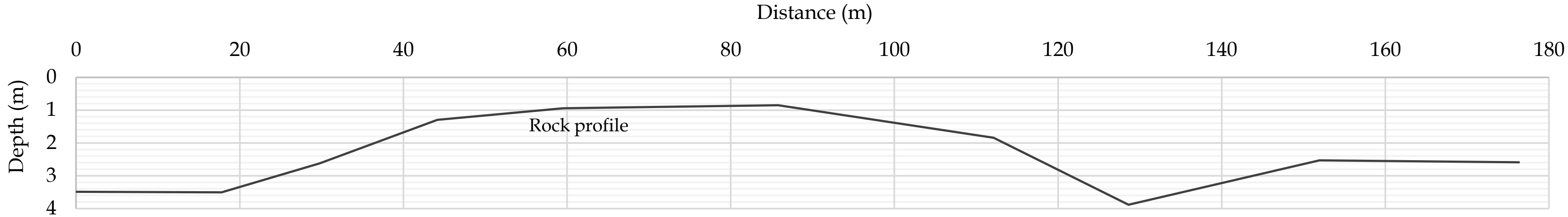

Section 2

Location: Estelle Court, Altona North

Pipe: 100mm diameter, asbestos cement (AC), reticulation main

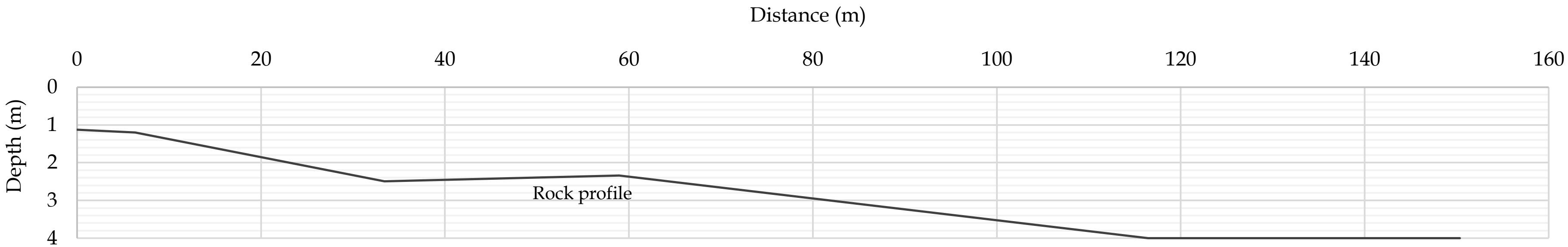

<u>Section 3</u>

Location: Kyle Road, Altona North

Pipe: 150mm diameter, cast iron cement lined (CICL), reticulation main

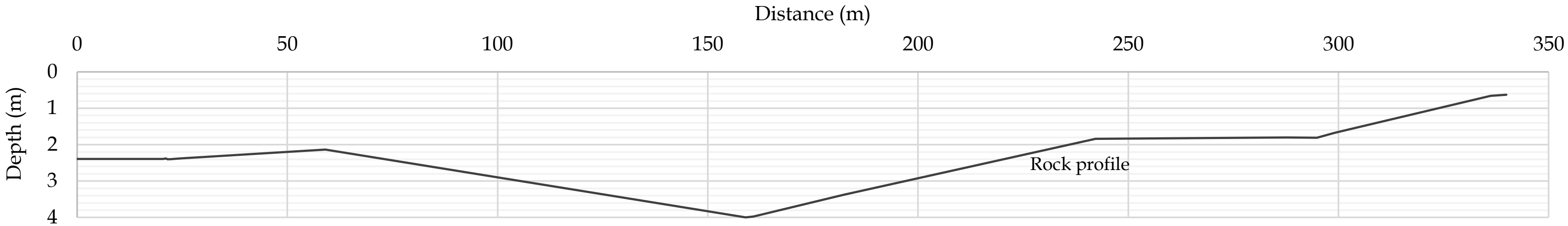

<u>Section 4</u>

Location: Fifth Avenue, Altona North

Pipe: 100mm diameter, cast iron cement lined (CICL), reticulation main

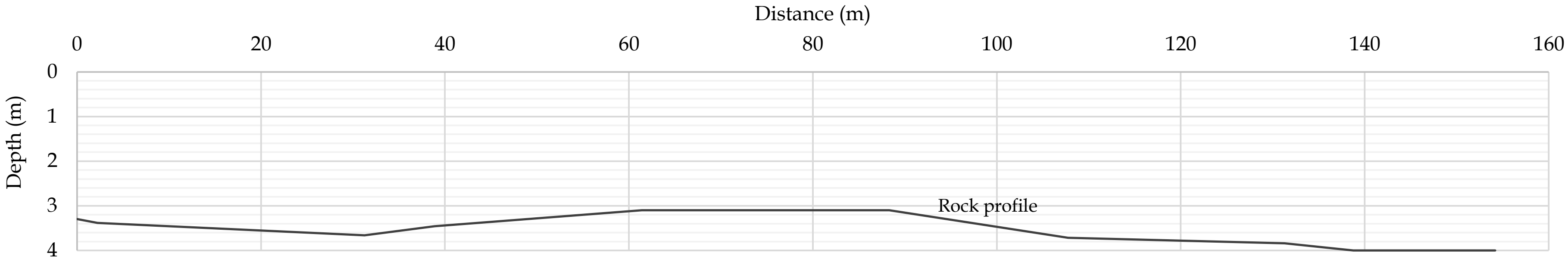

Section 5

Location: Arras Street, Spotswood

Pipe: 100mm diameter, cast iron cement lined (CICL), reticulation main

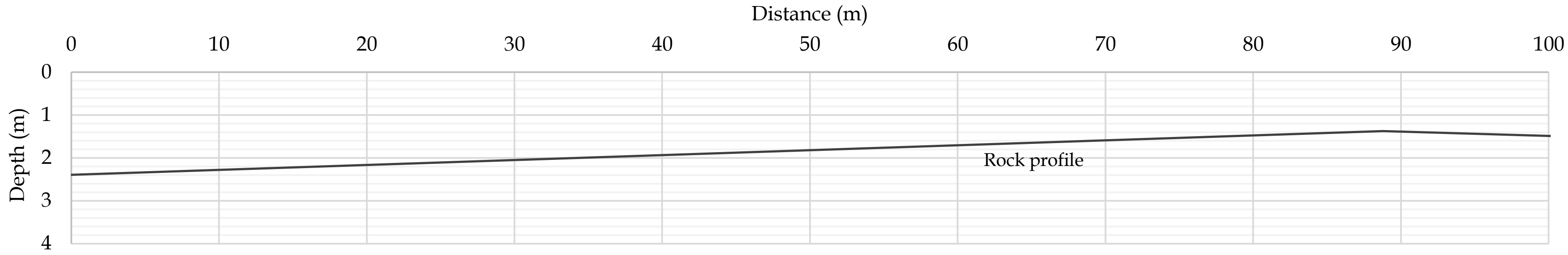

Section 6

Location: Arras Street, Spotswood

Pipe: 100mm diameter, M-PVC, reticulation main

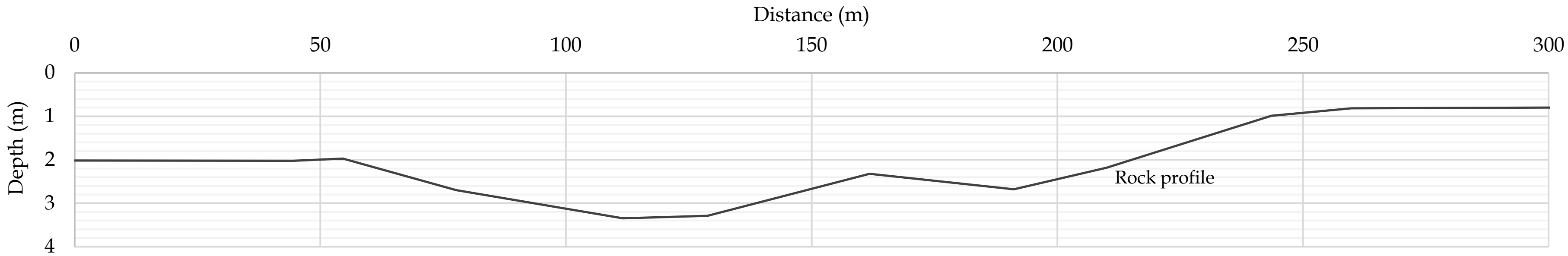

<u>Section 7</u>

Location: Ballard Street, Yarraville

Pipe: 125mm diameter, HD-PE, reticulation main

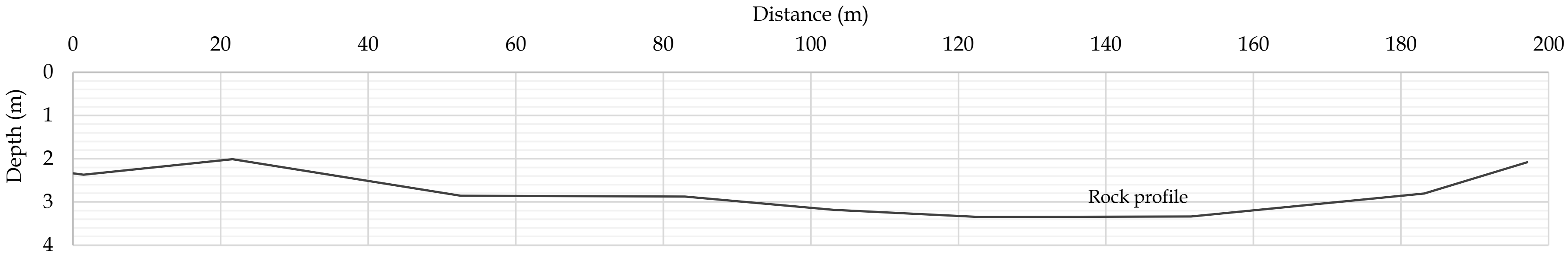

<u>Section 8</u>

Location: Stranger Street, Yarraville

Pipe: 100mm diameter, cast iron cement lined (CICL), reticulation main

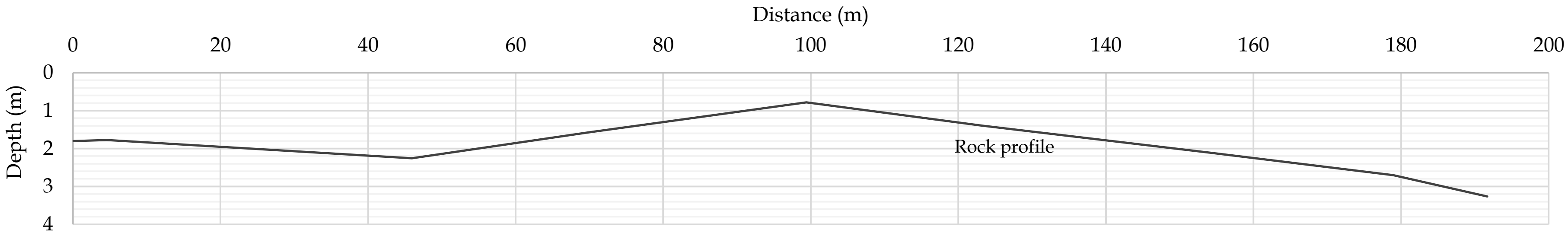

Section 9

Location: Saltley Street, South Kingsville

Pipe: 100mm diameter, cast iron cement lined (CICL), reticulation main

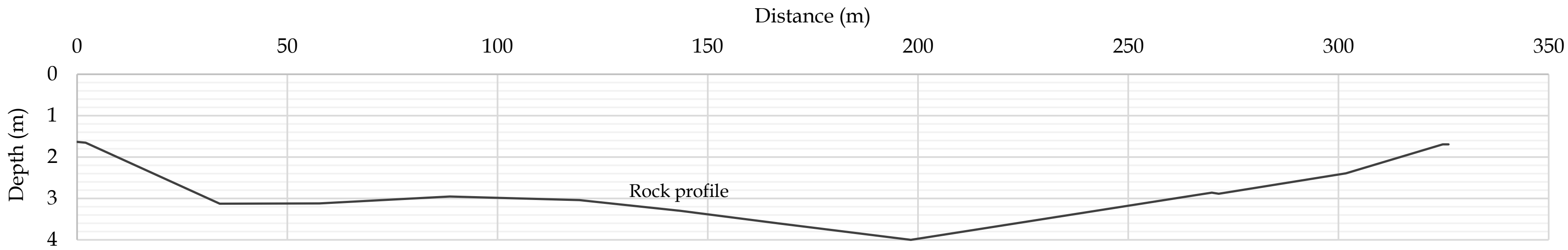

Section 10

Location: Paw Paw Road, Brooklyn

Pipe: 150mm diameter, U-PVC, reticulation main

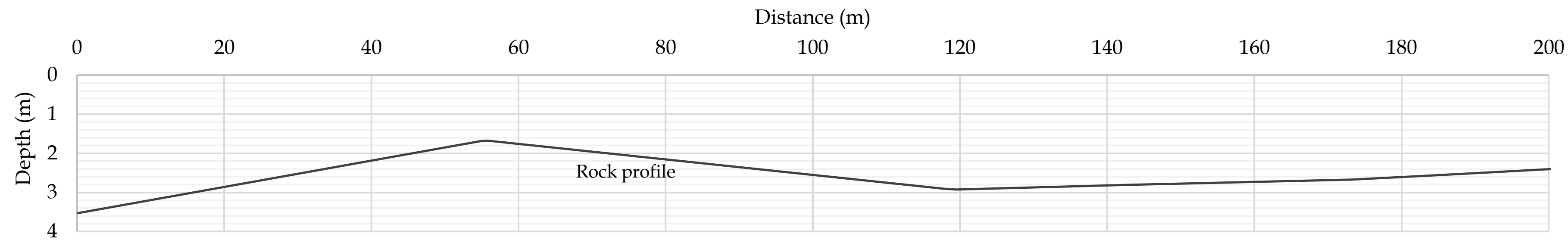

Section 11

Location: Cooper Avenue, Altona North

Pipe: 100mm diameter, cast iron cement lined (CICL), reticulation main

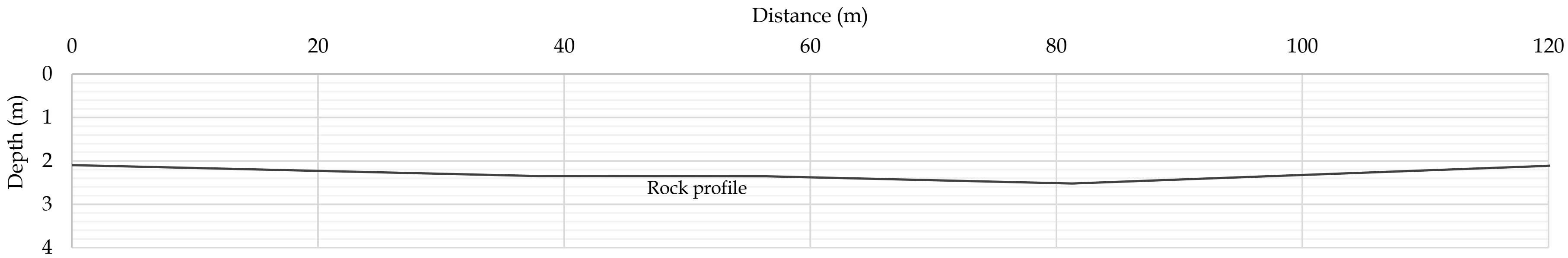

Section 12

Location: Agg Street, Newport

Pipe: 125mm diameter, HD-PE, reticulation main

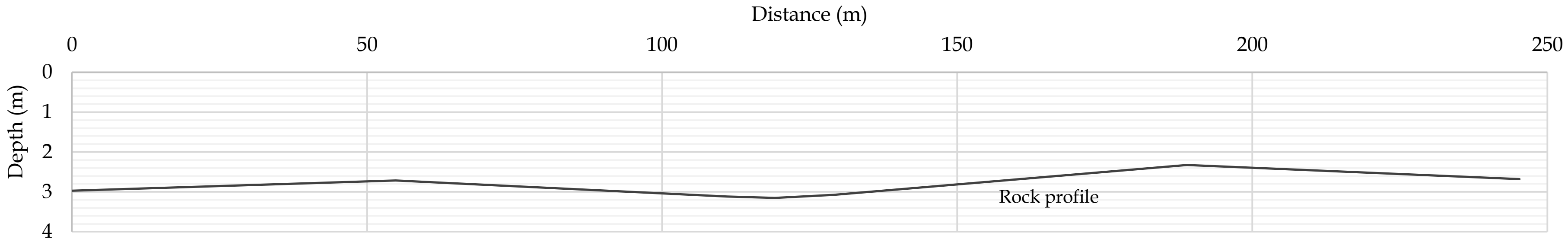

Section 13

Location: McIntosh road, Altona North

Pipe: 180mm diameter, PE, reticulation main

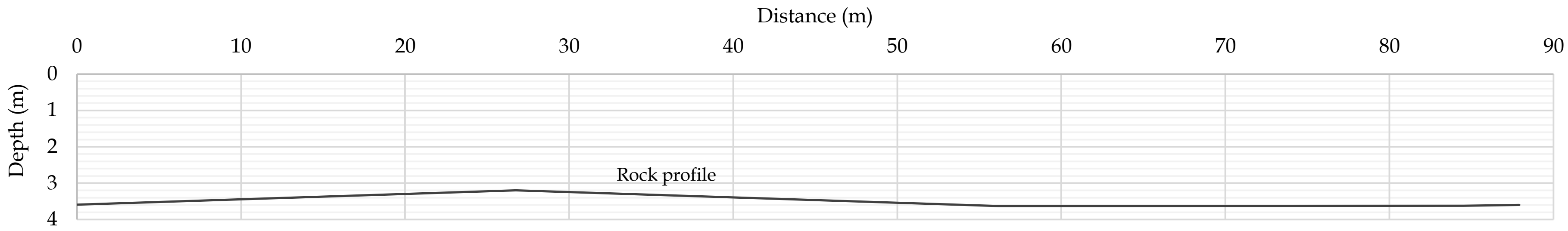

Section 14

Location: Clyde Street, Newport

Pipe: 100mm diameter, cast iron cement lined (CICL), reticulation main

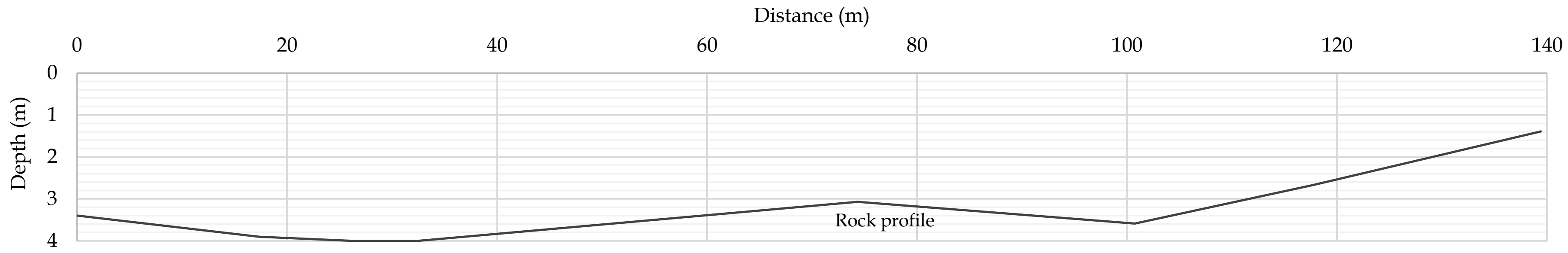

Section 15

Location: Millers Road, Brooklyn

Pipe: 150mm diameter, cast iron cement lined (CICL), reticulation main

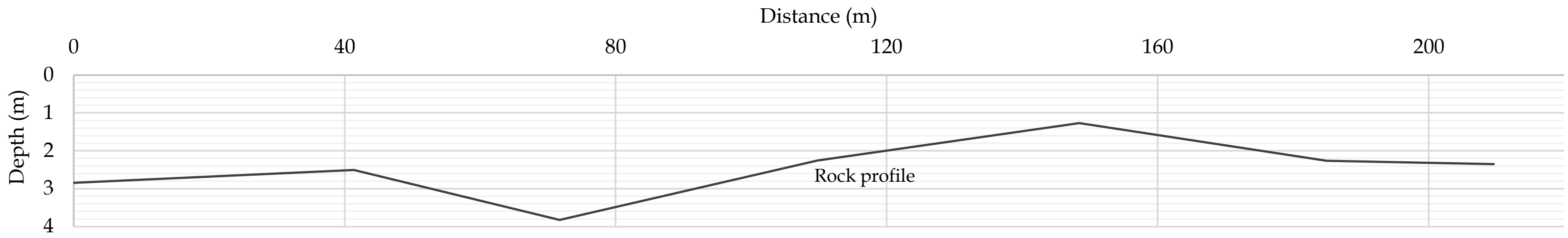

APPENDIX B

FIELD DATA COLLECTION SHEETS OF THE PIPE FAILURE CASE STUDY

Case No.	1
Date and Time (repair time)	13-05-2016 , 10:45 am
Street Address	70, Severn St, Yarraville
Location	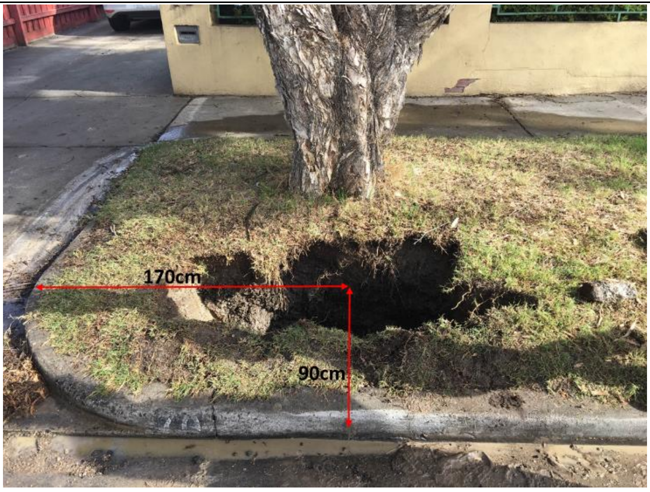
Failure type	Broken back Crack opened from top 
Pipe	100 mm CICL Reticulation main
Pipe age	43 years (Construction date: 9-05-1973)
Pipe depth	95cm
Pipe corrosion	Not visible corrosion
Repair type	Clamped
Pipe sample	No
Soil samples	No
Other measurements	No
General Comments	Pipe bending at the tree root can be the main reason for this failure. Also, the failure is next to the driveway. 

Past Failures	7-03-2008 – Leaking main 31-05-2013 – Burst main 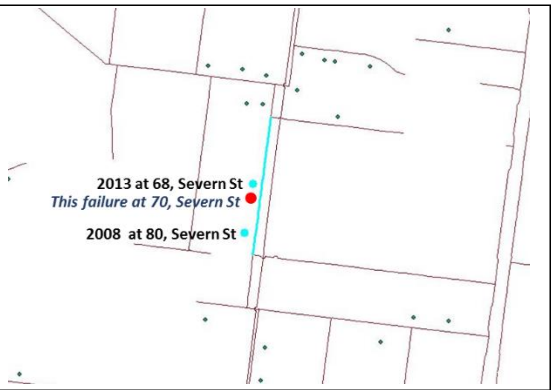

Case No.	2
Date and Time (repair time)	24 – 05 – 2016 , 9:45 am
Street Address	27, Stewart St, Williamstown
Site Details	
Failure type	Broken back Crack opened from bottom About 75% of the circumference is opened 
Pipe	100 mm CICL Reticulation main
Pipe age	50 years (Construction date: 4-06-1966)
Pipe depth	90cm
Pipe corrosion	Some graphitization (No corrosion patches)
Repair type	Clamped
Pipe sample	No
Soil samples	No (Sandy clay soil)
Other measurements	No

General Comments	Failure is underneath a tree at middle of the nature strip Since the crack is opened from bottom, the failure can be due to downward push from the tree roots Or due to the restrain at the tree to the upward pipe movement at nature strip 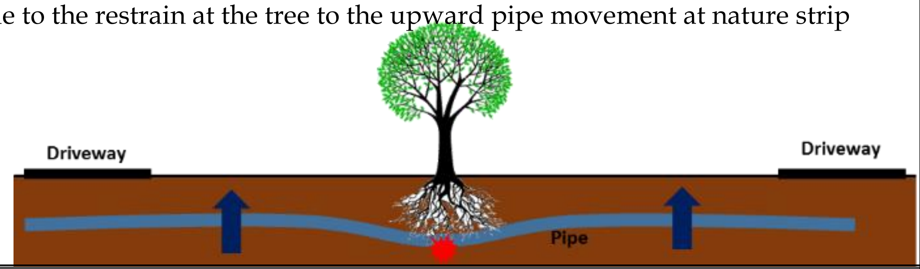
Past Failures	NO

Case No.	3
Date and Time (repair time)	27 – 05 – 2016 , 9:30 am
Street Address	19, Schutt St, Newport
Site Details	
Failure type	Piece blown next to the joint blown from bottom A piece of about 200mm long is blown 
Pipe	100 mm CI(CL75) Reticulation main
Pipe age	93 years (Construction date: 19-05-1923)
Pipe depth	65cm
Pipe corrosion	Some graphitization (can be tested later)
Repair type	replaced
Pipe sample	Yes
Soil samples	Some disturbed samples
Other measurements	No
General Comments	Combination of; soil upward movement in the nature strip, restrain at the driveway, pipe stiffness change at the joint and corrosion can be the reason for this failure. + the restraints from the tree roots and the (PVC) drainage pipe

Past Failures	24-04-2011 – Burst main	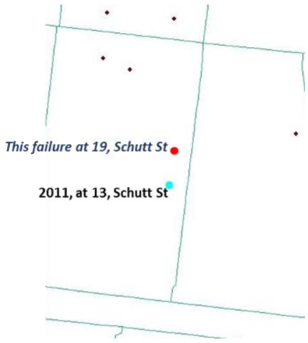

Case No.	4
Date and Time (repair time)	03 – 06 – 2016 , 10:00 am
Street Address	32, Baldwin Rd, Altona North
Site Details	
Failure type	Leak at a crack Main crack is longitudinal (20cm) and some circumferential cracks Failure is under a tree 
Pipe	150 mm CICL75 Reticulation main
Pipe age	51 years (Construction date: 21-06-1965)
Pipe depth	80 cm
Pipe corrosion	Some graphitization (can be tested later)
Repair type	replaced
Pipe sample	Yes
Soil samples	No
Other measurements	No
General Comments	Reason for this failure can be, the movement of pipe against the tree roots Or the pressure on the pipe due to the movement of tree roots (The field crew thinks this can be due to wind deflection of the tree)

Past Failures	3-06-2008 – Burst main	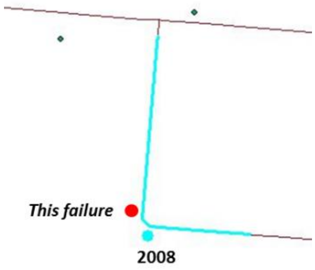

Case No.	5
Date and Time (repair time)	17 – 06 – 2016 , 09:45 am
Street Address	33, Stooke St, Yarraville
Site Details	This failure has occurred at edge of a driveway that is 3m wide and towards 9.2m nature strip. 
Failure type	A broken back failure that has cracked from the bottom of the pipe. A small piece was blown away from the bottom due to the water pressure. 
Pipe	100 mm CICL Reticulation main
Pipe age	59 years (Construction date: 25-11-1957)
Pipe depth	70 cm
Pipe corrosion	
Repair type	replaced
Pipe sample	Yes
Soil samples	No
Other measurements	No
General Comments	This failure mode is exactly similar to the way of broken back failures that is predicted for at the driveways in wetting seasons, in the early research. The swollen nature strip has lifted the pipe while it was held at the driveway. Therefore the crack was opened from the bottom of the pipe at the driveway edge.

<table>
<tr><td>Case No.</td><td>6</td></tr>
<tr><td>Date and Time (repair time)</td><td>15 – 02 – 2017 , Morning, (Sunny day)</td></tr>
<tr><td>Street Address</td><td>14, Boyd St, Altona</td></tr>
<tr><td>Site Details</td><td>Failure was in middle of the nature strip, next to the power pole


</td></tr>
<tr><td>Failure type</td><td>Piece blown from the bottom of the pipe. Longitudinally spread defect (about 10-15cm).
 </td></tr>
<tr><td>Pipe</td><td>100 mm CICL Reticulation main</td></tr>
<tr><td>Pipe age</td><td>56 years (Construction date: 05-09-1961)</td></tr>
<tr><td>Pipe depth</td><td>90 cm</td></tr>
</table>

Pipe corrosion	Visual inspections: Pipe bottom has been significantly corroded while the other parts were not. 
Repair type	replaced
Pipe sample	
Soil type	Sandy Clay, deep clay layers  Sand (after clay has been washed away)
Other measurements	No
General Comments	Possibly, the internal water pressure has blown out the severely corroded pipe bottom. No evidence for pipe bending or other type of loading on the pipe.
Past Failures	No recorded past failures (between 1997-2013) 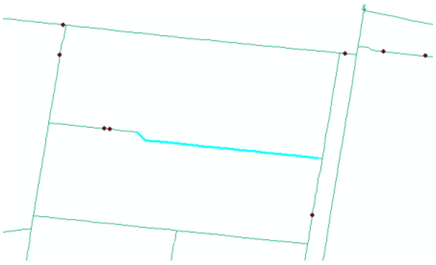

Case No.	7
Date and Time (repair time)	21 – 02 – 2017 , Morning, (Sunny day)
Street Address	131, Millers Rd, Altona North
Site Details	Failure was in middle of the nature strip.  
Failure type	Piece blown from the bottom of the pipe (at about 5' O clock position) Longitudinally spread defect (about 20cm).  
Pipe	150 mm CICL Reticulation main
Pipe age	59 years (Construction date: 30-07-1958)
Pipe depth	120-150 cm

Pipe corrosion	Visual inspections: some sever corrosion was observed near the failure location (bottom of the pipe)  
Repair type	replaced
Pipe sample	To be received later….
Soil type	Clay , mixed gravel 
Other measurements	No
General Comments	Possibly, the internal water pressure caused a longitudinal crack and has blown out the severely corroded pipe bottom. No evidence for pipe bending or other type of loading on the pipe.
Past Failures	3 recorded past failures (between 1997-2013) 19/1/1999 – 133 Millers Rd 8/1/2003 – 129 Millers Rd 16/12/2008 – 133 Millers Rd 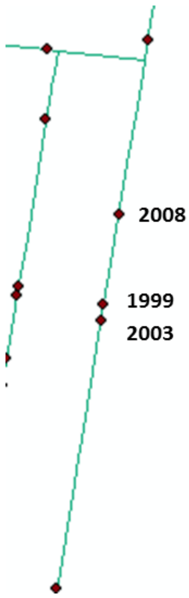

Case No.	8
Date and Time (repair time)	28 – 02 – 2017 , Morning, (Sunny day)
Street Address	19 (10), Buckingham St, Footscray
Site Details	Failure was below the road surface (about 450mm from the road edge)  
Failure type	Longitudinal crack, Bottom of the pipe  
Pipe	100 mm CICL Reticulation main
Pipe age	54 years (Construction date: 25-07-1963)
Pipe depth	70 cm
Pipe corrosion	Visual inspections: some sever corrosion was observed near the crack (bottom of the pipe)  
Repair type	replaced

Pipe sample	To be received later….
Soil type	Clay under the road base 
Other measurements	No
General Comments	Possibly, the internal water pressure caused a longitudinal crack at severely corroded pipe bottom.
Past Failures	1 recorded past failures (between 1997-2013) 22/12/2003 – 13 Buckingham St 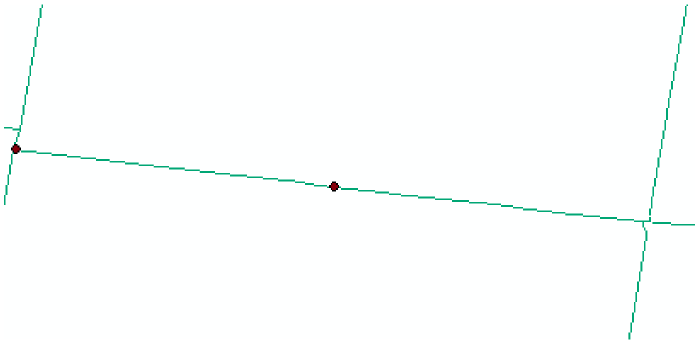

Case No.	9
Date and Time (repair time)	01 – 03 – 2017 , Morning, (Sunny day)
Street Address	57, Swan St, Keilor Park
Site Details	Failure was in middle of the nature strip.  
Failure type	Broken back Opened from top Pipe broken in to two pieces There was a clamped old repair next to the failure 
Pipe	100 mm CICL Reticulation main
Pipe age	44 years (Construction date: 13-04-1973)
Pipe depth	95 cm
Pipe corrosion	Visual inspections: The whole section seems significantly corroded as several failures has occurred in the pipe section 
Repair type	replaced

Pipe sample	To be received later….
Soil type	Clayey soil 
Other measurements	No
General Comments	This broken back failure could be resulted by the ground movement. Since the crack is opened up from the top, the possible reason for the failure could be a local swelling due to a leak from the old clamp.
Past Failures	4 recorded past failures (between 1997-2013) 2/08/2006 – 57 Swan St 28/02/2008 – 47 Swan St 20/04/2008 – 41 Swan St 19/03/2009 – 55 Swan St 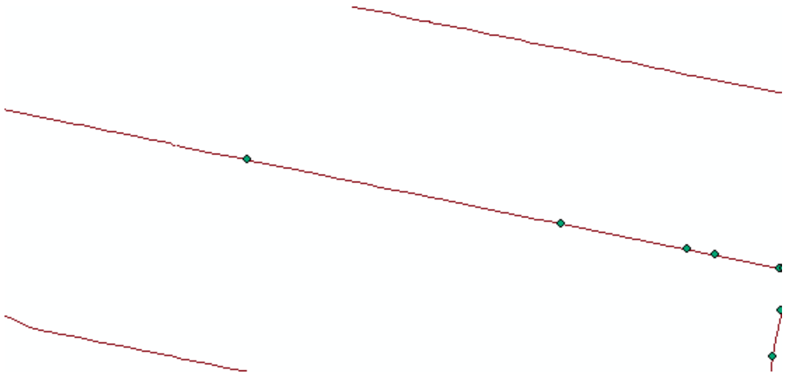

Case No.	10
Date and Time (repair time)	01 – 03 – 2017 , Morning, (Sunny day)
Street Address	111, Westmoreland Rd, Sunshine North
Site Details	Failure was under a newly constructed concrete walkway (1.5m wide, 10cm thick) at the corner of two roads.  
Failure type	Broken back Opened from top 
Pipe	150 mm CICL Reticulation main
Pipe age	59 years (Construction date: 27-12-1958)
Pipe depth	85 cm
Pipe corrosion	No observation Pipe was covered with water
Repair type	Clamped
Pipe sample	No

Soil type	Clayey soil 
Other measurements	No
General Comments	This broken back failure could be due to the movement associated with soil shrinkage in the long nature strip opposite and the restriction from the concrete walkway and the road. The soil swell near the failure and the cracks on the walkway indicate this pipe could have been cracked some time ago and kept leaking until the burst  
Past Failures	1 recorded past failures (between 1997-2013) 10/09/2012 – Swan St 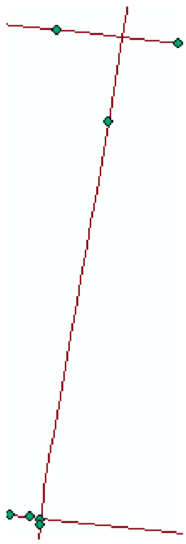

Case No.	11
Date and Time (repair time)	07 – 03 – 2017 , Morning, (Sunny day)
Street Address	39, Mccoubrie Ave, Sunshine West
Site Details	Failure was in middle of the nature strip.  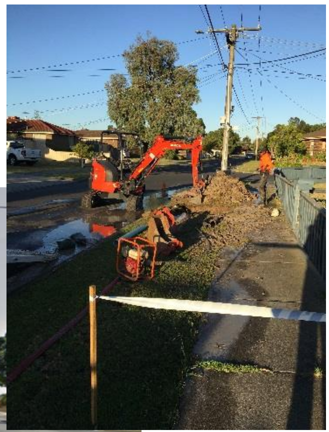
Failure type	Longitudinal Crack Piece blown Opened from side (house side) 
Pipe	100 mm CICL Reticulation main
Pipe age	44 years (Construction date: 04-07-1973)
Pipe depth	95 cm
Pipe corrosion	Crack area is severely corroded However, the cut end of the pipe shows a good amount of metal  
Repair type	Replaced
Pipe sample	To be received later

Soil type	Clayey soil 
Other measurements	No
General Comments	Possibly, the internal water pressure caused a longitudinal crack at severely corroded pipe side. Some small plant roots were observed near the pipe at one end of the pit. 
Past Failures	1 recorded past failures (between 1997-2013) 11/01/2007 – 26 Mccoubrie Ave 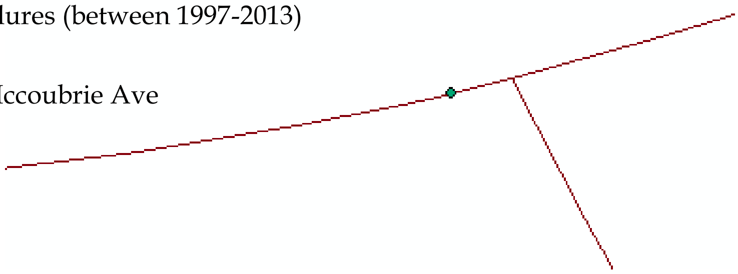

Case No.	12
Date and Time (repair time)	07 – 03 – 2017 , Morning, (Sunny day)
Street Address	6, Aviation Road, Laverton
Site Details	Failure was under a r/f concrete walkway next to the road. 
Failure type	Longitudinal Crack (about 80cm long) Bottom of the pipe 
Pipe	150 mm CI(CL83) Reticulation main
Pipe age	84 years (Construction date: 1933), in-situ cement lining: 1983
Pipe depth	100cm
Pipe corrosion	Crack area is severely corroded Bottom shows more corrosion Internal surface shows uniform corrosion (maybe due to weak cement lining) 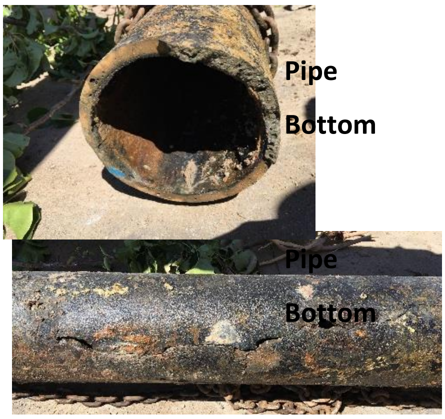

Repair type	Replaced
Pipe sample	To be received later
Soil type	Soil is mixed with road base materials Pipe was under the r/f concrete pavement and an old asphalt road pavement 
Other measurements	No
General Comments	Possibly, the internal water pressure caused a longitudinal crack at severely corroded pipe bottom. Pipe section shows significant manufacturing defects (trapped air bubbles). 
Past Failures	no recorded past failures (between 1997-2013)

Case No.	13
Date and Time (repair time)	08 – 03 – 2017 , Morning, (Sunny day)
Street Address	58, Civic Parade, Altona
Site Details	Failure was under a carpark (asphalt paved)  
Failure type	Longitudinal Crack (about 25cm long) Small piece blown Top of the pipe 
Pipe	100 mm CICL Reticulation main
Pipe age	55 years (Construction date: 11-09-1962)
Pipe depth	95cm
Pipe corrosion	Some corrosion is observed on pipe top  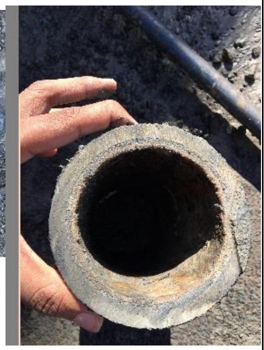

Repair type	Replaced
Pipe sample	To be received later
Soil type	Sandy clay 
Other measurements	No
General Comments	Possibly, the internal water pressure caused a longitudinal crack on corroded pipe top No evidence of pipe bending
Past Failures	1 recorded past failures (between 1997-2013) 11-11-2009 47 Civic Parade 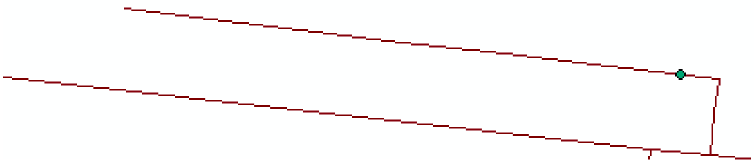

Case No.	14
Date and Time (repair time)	14 – 03 – 2017 , Morning, (Sunny day)
Street Address	24, Bromyard St, Yarraville
Site Details	Failure was under a driveway (middle of the driveway – 2.75m wide, 0.1m thick). 
Failure type	Broken back Opened from top 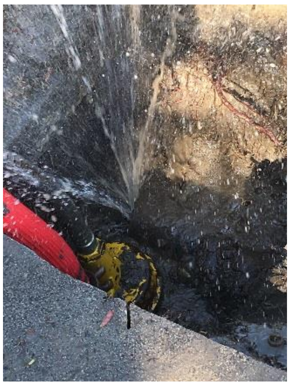 
Pipe	100 mm CICL Reticulation main
Pipe age	57 years (Construction date: 30-11-1960)
Pipe depth	45cm

Pipe corrosion	Not direct observations. However, pipe must have some significant corrosion as the colour change (yelowish) of the surrounding materials. 
Repair type	Clamped
Pipe sample	No
Soil type	Clayey soil. Some gravel material under the driveway.
Other measurements	No
General Comments	Possibly, the restraint of the driveway to the downward ground movement (shrink) in the nature strip caused this broken back. Soil under the driveway looks different to the natural soil in the driveway (more gravel particles) Strong driveway – no water was coming out from the driveway (no driveway cracks)
Past Failures	2 recorded past failures (between 1997-2013) 04-03-2009 26 Bromyard St 09-06-2010 38 Bromyard St

Case No.	15
Date and Time (repair time)	15 – 03 – 2017 , Morning, (Sunny day)
Street Address	18, Thomas St, St Albans
Site Details	Failure was under a driveway (near the edge – 3m wide, 0.15m thick).  
Failure type	Broken back Opened from bottom 
Pipe	100 mm CICL Reticulation main
Pipe age	57 years (Construction date: 08-09-1960)
Pipe depth	85cm
Pipe corrosion	Not direct observations. However, pipe must have some significant corrosion as the colour change (yelowish) of the surrounding materials. 

Repair type	Clamped
Pipe sample	No
Soil type	Clay, Silty Clay 
Other measurements	No
General Comments	As the crack is opened from the bottom and near the edge of the driveway, this failure can be explained with two possibilities. 1. Tensile stress (minor to the highest tensile stress at top of the pipe in the e middle of driveway) the bottom of the pipe due to downward ground movement in the nature strip triggered the failure with possible high corrosion at the bottom of the pipe near the driveway edge 2. As the pipe has experienced several failures in the past, leaks through the old repairs or weak pipe sections in the nature strip could cause the ground swelling and results tensile stress at the bottom of the pipe Strong driveway – no water was coming out from the driveway (no driveway cracks)
Past Failures	13 recorded past failures (between 1997-2013) 20-01-1998 18 Thomas St (broken back at same place) 28-12-2002 12 Thomas St 08-02-2003 16 Thomas St 09-03-2003 24 Thomas St 09-04-2006 28 Thomas St 19-01-2007 5 Thomas St 27-06-2007 18 Thomas St (circumferential failure N/S) 14-03-2008 18 Thomas St (circumferential failure N/S) 09-05-2008 2 Thomas St 11-08-2008 10 Thomas St 31-08-2009 16 Thomas St 24-05-2011 16 Thomas St 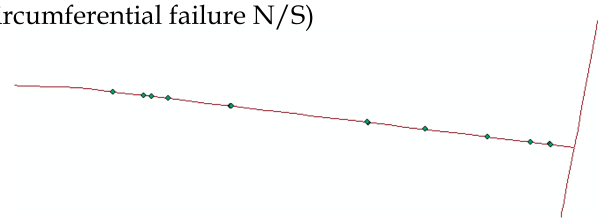

Case No.	16
Date and Time (repair time)	15 – 03 – 2017 , Morning, (Sunny day)
Street Address	30, Simpson St, Sunshine North
Site Details	Failure was under road pavement (middle of the road).  
Failure type	Broken back Opened from top Pipe bending is clearly visible 
Pipe	100 mm CICL Reticulation main
Pipe age	59 years (Construction date: 11-07-1958)
Pipe depth	60cm
Pipe corrosion	Not enough observations 

Repair type	Clamped
Pipe sample	No
Soil type	Clay below the road base 
Other measurements	No
General Comments	This failure is possibly due to the restraint at the road surface to the downward ground movement in the adjacent nature strips. High tensile stresses at the pipe top in middle of the road. Leaking water was not seen on the road surface until drilling the surface. This indicates the resistance to moisture transferring. 
Past Failures	2 recorded past failures (between 1997-2013) 02-09-2008 34 Simpson St 25-11-2012 36 Simpson St 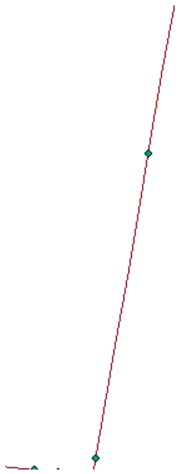

Case No.	17
Date and Time (repair time)	04 – 04 – 2017 , Morning, (Sunny day)
Street Address	11 Jubilee St, Newport
Site Details	Failure was under (middle of) driveway.  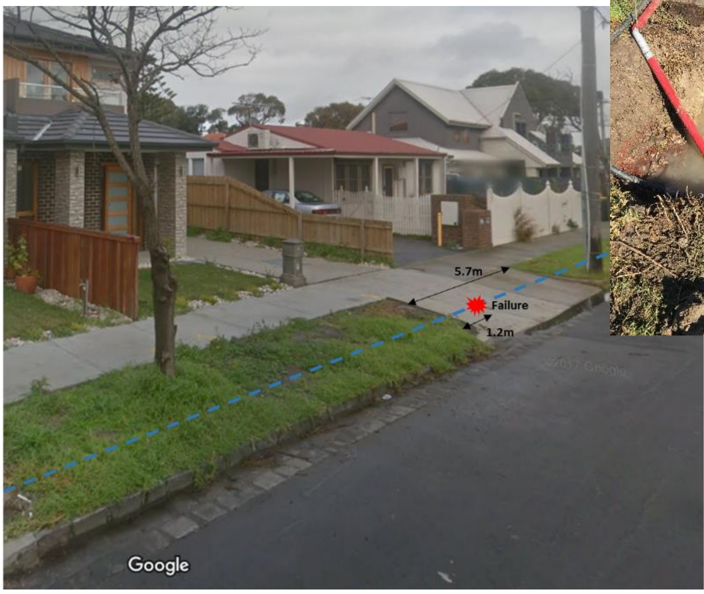
Failure type	Broken back Opened from top 
Pipe	100 mm CICL Reticulation main
Pipe age	59 years (Construction date: 22-01-1958)
Pipe depth	80cm
Pipe corrosion	Colour changes (yellowish brown) in pipe and surrounding soils indicate some corrosion 

Repair type	Clamped
Pipe sample	No
Soil type	Caly + sandy clay soil Plenty of plant (grass) roots through soil 
Other measurements	No
General Comments	This failure is possibly due to the restraint at the driveway to the downward ground movement in the adjacent nature strips. High tensile stresses at the pipe top in middle of the driveway.
Past Failures	5 recorded past failures (between 1997-2013) 16-07-2007 15 Jubilee St 30-04-2009 15 Jubilee St 09-10-2009 9 Jubilee St 17-06-2011 9 Jubilee St 16-11-2011 11 Jubilee St 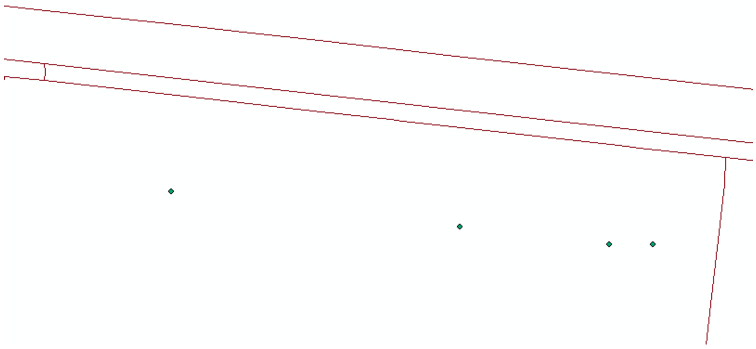

Case No.	18
Date and Time (repair time)	11 – 04 – 2017 , Morning, (Sunny day)
Street Address	63 Driscolls Road, Kealba
Site Details	Failure was at middle of the nature strip 
Failure type	Broken back About 90% of the pipe circumference is cracked 
Pipe	150 mm CICL Reticulation main
Pipe age	41 years (Construction date: 14-05-1976)
Pipe depth	130cm
Pipe corrosion	Colour changes (yellowish brown) in pipe and surrounding soils indicate some corrosion 

Repair type	Clamped
Pipe sample	No
Soil type	Caly + sandy clay soil Plenty of plant (grass) roots through soil 
Other measurements	No
General Comments	Pipe is in a relatively deep level. A clear evidence of an effect of surrounding features were not found. It could be due to an uninspected effect such as bedrock.
Past Failures	5 recorded past failures (between 1997-2013) 13-12-2006 61 Driscolls Rd 06-07-2007 49 Driscolls Rd 01-09-2008 51 Driscolls Rd 27-02-2009 59 Driscolls Rd 30-12-2011 51 Driscolls Rd 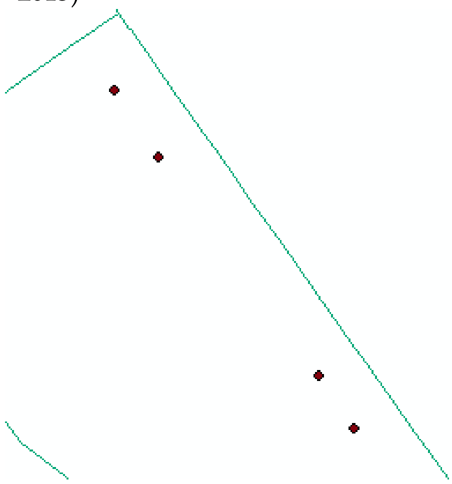

Case No.	19	
Date and Time (repair time)	12 – 04 – 2017 , Morning, (Sunny day)	
Street Address	18 Nixon Street, Sunshine	
Site Details	Failure was at middle of the nature strip 	
Failure type	Longitudinal crack Bottom of the pipe	
Pipe	100 mm CICL Reticulation main	
Pipe age	49 years (Construction date: 11-06-1968)	
Pipe depth	90cm	
Pipe corrosion	Colour changes (yellowish brown) in pipe and surrounding soils indicate some corrosion 	
Repair type	Replaced	

Pipe sample	Yes
Soil type	Surrounding soil was observed to be black colour. Smelly soil (due to organinc matters) 
Other measurements	No
General Comments	A small leak from a small crack. Pipe section was weak due to corrosion 
Past Failures	1 recorded past failures (between 1997-2013) 07-04-2009 18 Nixon St 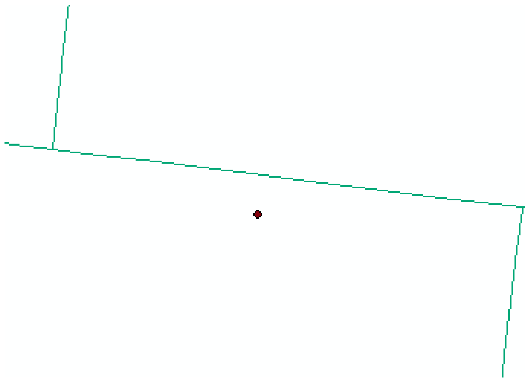

Case No.	20
Date and Time (repair time)	23 – 05 – 2017 , Morning,
Street Address	18 Nixon Street, Sunshine
Site Details	Failure was under a driveway (middle of the 6.5m wide driveway) 
Failure type	Longitudinal crack Piece blown About 40 cm long crack Bottom of the pipe 
Pipe	150 mm DICL Reticulation main
Pipe age	44 years (Construction date: 04-07-1973)
Pipe depth	95cm

Pipe corrosion	Colour changes (brown) in pipe and surrounding soils indicate some corrosion 
Repair type	Replaced
Pipe sample	
Soil type	Clayly soil Some granular material under the driveway 
Other measurements	No
General Comments	No pipe bending was observed. (no bending stresses are expected under middle of the driveway in winters)
Past Failures	No recorded past failures (between 1997-2013) 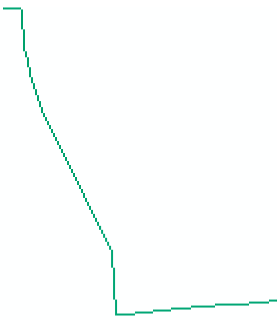

Case No.	21
Date and Time (repair time)	27 – 06 – 2017 , Morning,
Street Address	5 Chorley Avenue, Altona
Site Details	Failure at a nature strip. Near a tree 
Failure type	Broken back failure Bottom of the pipe 
Pipe	100 mm CICL Reticulation main
Pipe age	49 years (Construction date: 15-07-1968)
Pipe depth	90cm
Pipe corrosion	Colour changes (brown) in pipe and surrounding soils indicate some corrosion 

Repair type	Clamped
Pipe sample	No
Soil type	Clayly soil
Other measurements	No
General Comments	Pipe bending due to tree was considered as the reason for this failure
Past Failures	4 recorded past failures (between 1997-2013) 20-12-2006 7 Chorley Ave 02-05-2011 7 Chorley Ave 15-04-2012 5 Chorley Ave 17-04-2012 1 Chorley Ave 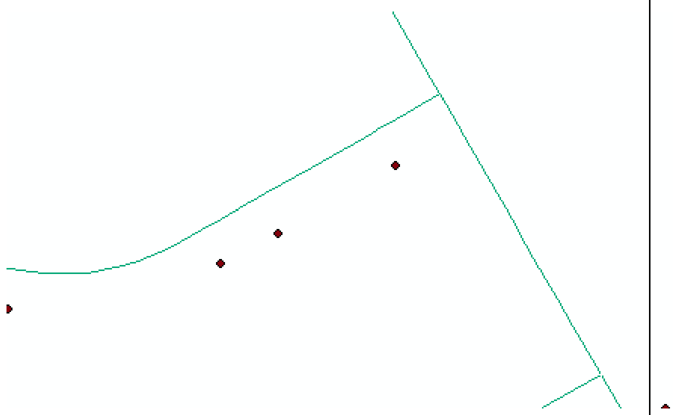

APPENDIX C

DETAILS OF THE OPTIMISATION AND VERIFICATION ANALYSES OF PIPE STRESS ESTIMATION MODEL

Table C.1. Details of model optimisation analyses of Chapter 6

No.	Hotspot case	Moisture change at pipe depth	ΔH (mm)	S_{max} (mm)	i (mm)	Pipe internal diameter (D) (mm)	Wall thickness (t) (mm)	E (GPa)	$M_{G,max}$ (Nmm)	M_{norm}	Estimated stress ($\sigma_{p,max}$) (MPa)	Stress from FE simulations (MPa)
1	Driveway	1% drying	-4	-1.8	907	100	8	83.4	715330	0.50	5.17	5.5
2	Driveway	3% drying	-12	-5.3	907	100	8	83.4	2145992	0.50	15.5	15.5
3	Driveway	5% drying	-20	-8.9	907	100	8	83.4	3576653	0.50	25.9	24.3
4	Driveway	1% wetting	4	0.64	484	100	8	83.4	221061	0.52	1.67	1.3
5	Driveway	3% wetting	12	1.9	484	100	8	83.4	663184	0.52	5.01	5
6	Driveway	5% wetting	20	3.2	484	100	8	83.4	1105308	0.52	8.35	10.6
7	Driveway	1% drying	-4	-1.8	907	150	10	83.4	2902834	0.33	4.98	5.3
8	Driveway	3% drying	-12	-5.3	907	150	10	83.4	8708502	0.33	14.9	14.7
9	Driveway	5% drying	-20	-8.9	907	150	10	83.4	14514170	0.33	24.9	23.5
10	Driveway	1% wetting	4	0.64	484	150	10	83.4	897074	0.29	1.37	1.00
11	Driveway	3% wetting	12	1.9	484	150	10	83.4	2691225	0.29	4.11	3.70
12	Driveway	5% wetting	20	3.2	484	150	10	83.4	4485375	0.29	6.86	8.00
13	Driveway	1% drying	-4	-1.8	907	225	12	83.4	11305957	0.19	4.36	4.7
14	Driveway	3% drying	-12	-5.3	907	225	12	83.4	33917872	0.19	13.1	13
15	Driveway	5% drying	-20	-8.9	907	225	12	83.4	56529787	0.19	21.8	20.4
16	Driveway	1% wetting	4	0.64	484	225	12	83.4	3493927	0.14	0.95	0.8
17	Driveway	3% wetting	12	1.9	484	225	12	83.4	10481782	0.14	2.86	2.9

18	Driveway	5% wetting	20	3.2	484	225	12	83.4	17469637	0.14	4.77	7.3
19	Rock slope (dip = 40^0 at 1m depth)	5% drying		13.5	646	100	8	83.4	2594226	0.85	32.3	31.8
20	Rock slope (dip = 60^0 at 1m depth)	5% drying		13.5	509	100	8	83.4	4183254	0.60	36.4	36.9
21	Rock slope (dip = 20^0 at 1.3m depth)	5% drying		7.9	853	100	8	83.4	872870	0.97	12.3	10.9
22	Rock slope (dip = 10^0 at 1m depth)	5% wetting		14.5	1648	100	8	83.4	428726	1.00	6.24	10.5
23	Rock slope (dip = 60^0 at 1.8m depth)	5% wetting		2.1	430	100	8	83.4	913617	0.16	2.15	2.4
24	Rock slope (dip = 600 at 1.8m depth)	5% drying		2	430	100	8	83.4	870111	0.35	4.52	2.8
25	Rock slope (dip = 10^0 at 1m depth)	5% drying		13.5	1648	100	8	83.4	399159	1.00	5.81	11.8
26	Rock slope (dip = 60^0 at 1m depth)	5% wetting		15.0	509	100	8	83.4	4648060	0.38	25.8	25

Table C.2. Details of model verification analyses of Chapter 6

No.	Hotspot case	Moisture change at pipe depth	ΔH (mm)	S_{max} (mm)	i (mm)	Pipe internal diameter (D) (mm)	Wall thickness (t) (mm)	E (GPa)	$M_{G,max}$ (Nmm)	M_{norm}	Estimated stress ($\sigma_{p,max}$) (MPa)	Stress from FE simulations (MPa)
1	Driveway	1% drying	-4	-1.8	907	125	8	83.4		0.42	5.29	5.8
2	Driveway	3% drying	-12	-5.3	907	125	8	83.4		0.42	15.9	16.2
3	Driveway	5% drying	-20	-8.9	907	125	8	83.4		0.42	26.5	24.2
4	Driveway	1% wetting	4	0.64	484	125	8	83.4		0.41	1.61	1.2
5	Driveway	3% wetting	12	1.9	484	125	8	83.4		0.41	4.84	4.5
6	Driveway	5% wetting	20	3.2	484	125	8	83.4		0.41	8.06	9.7
7	Driveway	1% drying	-4	-1.8	907	180	12	83.4		0.25	4.58	5
8	Driveway	3% drying	-12	-5.3	907	180	12	83.4		0.25	13.7	13.8
9	Driveway	5% drying	-20	-8.9	907	180	12	83.4		0.25	22.9	21.8
10	Driveway	1% wetting	4	0.64	484	180	12	83.4		0.20	1.12	0.8
11	Driveway	3% wetting	12	1.9	484	180	12	83.4		0.20	3.37	3.1
12	Driveway	5% wetting	20	3.2	484	180	12	83.4		0.20	5.62	7.2
13	Driveway	1% drying	-4	-1.8	907	100	8	100		0.50	22.9	21.8
14	Driveway	3% drying	-12	-5.3	907	150	10	100		0.33	6.20	6.4
15	Driveway	5% drying	-20	-8.9	907	225	12	100		0.19	17.9	16.7
16	Driveway	1% wetting	4	0.64	484	150	10	100		0.29	1.64	1.1
17	Driveway	3% wetting	12	1.9	484	225	12	100		0.14	3.44	3.3

18	Driveway	5% wetting	20	3.2	484	100	8	100		0.52	10.0	11.6
19	Rock slope (dip = 60^{0} at 1.3m depth)	5% drying		8	479	100	8	83.4		0.51	20.8	16
20	Rock slope (dip = 20^{0} at 1m depth)	5% drying		14	994	100	8	83.4		0.99	16.3	21.1
21	Rock slope (dip = 5^{0} at 1m depth)	5% drying		14	2936	100	8	83.4		1.00	1.90	6
22	Rock slope (dip = 5^{0} at 1.3m depth)	5% drying		8	2346	100	8	83.4		1.00	1.70	3.8
23	Rock slope (dip = 5^{0} at 1.8m depth)	5% drying		2	1363	100	8	83.4		1.00	1.26	1.4
24	Rock slope (dip = 10^{0} at 1.3m depth)	5% drying		8	1355	100	8	83.4		1.00	5.09	6.4
25	Rock slope (dip = 10^{0} at 1.8m depth)	5% drying		2	868	100	8	83.4		0.97	3.01	2.1
26	Rock slope (dip = 20^{0} at 1.8m depth)	5% drying		2	616	100	8	83.4		0.82	5.04	2.6
27	Rock slope (dip = 40^{0} at 1.3m depth)	5% drying		8	585	100	8	83.4		0.77	21.0	14.6
28	Rock slope (dip = 40^{0} at 1.8m depth)	5% drying		2	482	100	8	83.4		0.52	5.22	2.9
29	Rock slope (dip = 60^{0} at 1.3m depth)	5% wetting		8	479	100	8	83.4		0.29	11.8	12.3
30	Rock slope (dip = 40^{0} at 1m depth)	5% wetting		14	646	100	8	83.4		0.76	29.8	23.3
31	Rock slope (dip = 20^{0} at 1m depth)	5% wetting		14	994	100	8	83.4		0.98	16.3	16.7

32	Rock slope (dip = 5^0 at 1m depth)	5% wetting		15	2936	100	8	83.4		1.00	2.04	5.5
33	Water leak			1.5	187	100	8	83.4		0.03	7.09	4.7
34	Soil boundary	5% wetting		20	151	100	8	83.4		0.04	42.6	43.9